Diagenesis and porosity preservation in deepwater oilfield sandstones.

Ann Marchand

PhD
University of Edinburgh
2001

Declaration

This dissertation is entirely my own work except where indicated otherwise.

ABSTRACT

DIAGENESIS AND POROSITY PRESERVATION IN DEEPWATER OILFIELD SANDSTONES

PH.D., UNIVERSITY OF EDINBURGH, 2001

ANN MARCHAND

Currently, a controversy exists as to whether oil charge in reservoirs has an inhibiting effect on quartz cementation. The Brae Formation sandstone reservoirs in the Miller and Kingfisher oilfields display in some areas anomalously high porosity (25-30%) preserved to depths in excess of 4km (~120°C). The high porosity in these sandstones is directly linked to low quartz cement volumes (<5%). In the Miller Field, the crestal areas of the reservoir have porosities of up to 25% and a quartz cement content of <5%. Towards the oil-water contact (OWC), and in the aquifer of this same reservoir, porosity decreases and quartz cement content increases to 14% and 15% respectively. In the Kingfisher Field, two reservoirs separated by a mudstone layer are present. The lower reservoir, which connects with the reservoir in the adjacent Miller Field, displays porosities ~14% and quartz cement contents of ~10%. The upper reservoir is of overall high porosity (25-30%) and exhibits low quartz cement contents (<5%). Combined results from fluid inclusion and basin modelling studies in the Brae Formation reservoirs show that the duration of quartz cement precipitation is linked to hydrocarbon emplacement. In the Miller Field, quartz cementation in the high porosity (up to 25%) parts of the reservoir continued until the sandstones were buried to 95-105°C. This temperature corresponds to the burial depth (3km) and time (40Ma) at which oil entered the reservoir. Results for the Kingfisher Field indicate a similar oil emplacement time in the upper reservoir with 25-30% porosity and <5% quartz cement content, but a more recent (15Ma) oil-fill for the lower reservoir with ~14% porosity and ~10% quartz cement content. Kinetic modelling of the quartz cementation process reveals that quartz cementation rates in the oil-filled parts of reservoirs examined (10^{-22} moles/cm^2.s) are at least two orders of magnitude smaller than in the aquifers (10^{-19} moles/cm^2.s). The quantification of quartz precipitation rates in the presence of oil is directly applicable to different reservoirs in other areas and has the potential of improving reservoir quality predictions in unknown prospects. Calculated oxygen isotopic compositions of pore-fluids indicate that, with increasing burial depth and temperature, quartz cements progressively precipitated from fluids which evolved in composition from a meteoric-type fluid ($\delta^{18}O$ ~–7 ‰) to a basinal-type fluid with $\delta^{18}O$ similar to the present day formation water oxygen isotopic composition (+0.6 ‰). The initial presence of meteoric fluids in the marine Brae Formation sands implies that the sandstones were open to surface water recharge during shallow burial (<1500m) (open-system). The shift towards a basinal-type fluid during deeper burial (>1500m) is the result of increased rock-water interactions when the sandstones became more isolated from through-flow of external fluids (closed-system). Pore-fluid evolution is similar in all three reservoirs studied, indicating that hydrogeologic evolution was similar across the whole Brae Formation sandstone. The main silica-supplying processes for quartz cementation in the sandstones examined are pressure solution and clay mineral reactions in interbedded mudrocks.

ACKNOWLEDGMENTS

I would like to thank my supervisors Stuart Haszeldine and Tony Fallick for their support and for giving me the opportunity to work on such an exciting project over the past years. I would like to thank BP and Shell UK for allowing me access to data and core of the Miller and Kingfisher oilfields. I am also indebted to the academic and technical staff in the Edinburgh Geology and Geophysics Department and the S.U.E.R.C. for their assistance and advice; Paula McDade, John Craven, Mike Hall, Anton Ziolkowski, Ian Main, Jon Turner, Malcolm Rider, Colin Chilcott, Chris Taylor, Andrew Tait, Julie Dougans, Brian Davidson, Terry Donnelly and Adrian Boyce. I would like to thank Craig Smalley and Shelagh Baines from BP for their guidance and suggestions regarding the quartz modelling work.

I would also like to thank my friends for all the coffee-breaks and numerous other distractions they have given me; Kati, Celine, JC, Salima, Paula, Aderson and the rest of the "Old Attic" gang. Finally, special thanks to Calum for his continuous help and support over the past years.

CONTENTS

CHAPTER I

INTRODUCTION

1.1 Introduction

Development of hydrocarbon fields in the North Sea basin provides a wealth of information which can be used to undertake studies of subsurface geological processes. Studies of oilfield reservoirs aim particularly to understand porosity and permeability distributions and the processes which cause changes in these physical parameters in reservoir rocks. Understanding the factors that influence reservoir quality are important for effective development and production of a hydrocarbon field. Diagenesis is acknowledged to be a critical control on porosity and permeability but remains difficult to understand and quantify, and hence to predict. Despite the large variation in physical and chemical conditions during diagenesis, it is striking that calcite and quartz are volumetrically the dominant chemical precipitates in the pore spaces of sandstones (Blatt, 1979). In deeply buried clay-poor clastic reservoirs, which are the subject of this thesis, it is especially authigenic quartz cement that is the most common diagenetic mineral and the principal cause of porosity loss by cementation (e.g. Bjørlykke et al., 1986; Land & Fisher, 1987; McBride, 1989; Bloch et al., 1990; Ehrenberg, 1990). Despite the common occurrence and economic significance of quartz cement, there is not yet a general consensus on the mechanism of the quartz cementation process (Worden & Morad, 2000). This lack of understanding of the quartz cementation process itself, and of other processes that may influence it, limits the predictive capacity of diagenetic models.

1.2 The key controversies

Quartz cement is a major destroyer of porosity and is a critical control on reservoir quality in many sandstones (McBride, 1989). Considerable controversy exists surrounding the source of silica, the transport mechanism of silica from the site of dissolution to the site of quartz precipitation, the influence of hydrocarbon emplacement on quartz cementation and the ways of modelling the quartz cementation process for reservoir quality prediction purposes.

Silica source & transport Sources of silica for quartz cement can be located outside the sandstone or within the sandstone. In this thesis, silica sources located outside the Brae Formation sandstones are referred to as "external sources" whereas silica sources within the Brae Formation sandstones are referred to as "internal sources". External sources of silica and transport mechanisms suggested over the years are circulation of meteoric fluids (e.g. Friedman, 1954), compaction water released from mudrocks (e.g. Land & Dutton, 1978; Blatt, 1979; Boles & Franks, 1979; Sullivan & McBride, 1991), convection fluids (e.g. Haszeldine et al., 1984bis; Wood & Hewett, 1984), up-dip cooling of fluids in equilibrium with dissolved silica (e.g. Leder & Park, 1986; Robinson & Gluyas, 1992) and movement of hot fluids up fault planes (e.g. Jourdan et al., 1987; Scotchman et al., 1989; Burley, 1993). All these external sources require influx of large volumes of silica-rich aqueous fluids into sandstones. Advective fluid flow is driven by pressure gradients which may drive meteoric water down into the basins and force pore-water upwards out of compacting sediments (Bjørlykke, 1993). Such flow of fluids can operate on a km-scale, or tens of km, across sedimentary basins. The problem with large-scale fluid flow is, as demonstrated by Bjørlykke (1993 and 1994), that because of the low silica solubility (pH <9) in the fluids there would be exceptionally high flow rates required in order to mass-balance the silica in solution with the amounts of quartz cement often observed in deeply buried sandstones. Quartz cementation is also considered to increase systematically with burial (e.g. Bjørlykke et al., 1986; Leder & Park, 1986; Schmoker & Gautier, 1988). As a result, flow rates become increasingly restricted with burial as compaction and diagenesis continuously decrease porosity and permeability in the sandstones. Because of these fluid flow problems associated with externally derived silica, emphasis has shifted more and more towards internally derived silica as the main source of quartz cement in sandstones (e.g. Aplin & Warren, 1994; Bjørlykke et al., 1995; Oelkers et al., 1996; Bjørkum et

al., 1998; Giles et al., 2000). In this scenario, silica is transported from areas of high silica concentration (sites of dissolution; e.g. grain-to-grain contacts) to areas of low silica concentration (sites of precipitation, e.g. pore space in between grains) by diffusion. Diffusional transport of silica in aqeous fluid occurs over short length scales, probably on a cm-scale. Possible internal sources for silica are K-feldspar dissolution and kaolinitisation (e.g. Giles et al., 1992; Glassman, 1992; Macaulay et al., 1993; Barclay & Worden, 2000; Hartmann et al., 2000), illitisation of smectite (e.g. Boles & Franks, 1979), dissolution of amorphous silica (e.g. Vagle et al., 1994; Hendry & Trewin, 1995) and pressure solution by either intergranular pressure dissolution of quartz grains (e.g. Tada & Seiver, 1989; Mullis, 1993) or quartz dissolution at stylolites (Heald, 1959; Houseknecht, 1988; Oelkers et al., 1996; Walderhaug, 1996; Bjørkum et al., 1998). The importance of the dissolution of K-feldspar and amorphous silica, and also of illitisation, as silica sources will typically depend on the abundance of these phases in the sandstone studied. There is controversy surrounding pressure solution as to whether it is initiated by lithostatic pressure, temperature, or the presence of clay minerals along grain interfaces or by a combination of these (Worden & Morad, 2000). Increased silica solubility due to pressure was widely thought to be the key control on chemical compaction (Rutter, 1976). However, the critical role of temperature and the negligible role of pressure have recently been emphasized (Bjørkum, 1996). Also, the role of clay and micas as catalysts in inducing pressure solution has been the subject of argument. Oelkers et al. (1996) assert that pressure dissolution of quartz grains occurs exclusively at mica and clay interfaces with quartz. This might explain why large-scale pressure dissolution and stylolite formation is most common in siltstones that are rich in detrital clays and micas.

Based on calculated quartz solubilities for near-neutral pH conditions in the 1 to 6 km depth range, Porter & James (1986) demonstrated that temperature, pressure and salinity are the most important factors affecting quartz solubility and consequently pressure dissolution. Based on their calculations, Porter & James (1986) concluded that temperature is more important than pressure and pore-fluid salinity in increasing quartz solubility. At 4 km depth and 190 °C, quartz solubility is 7 times higher than at 80 °C. Quartz solubility related to increasing grain-contact pressure with depth is 20 times greater at 6 km than at 1 km. Across the depth, temperature and pH range examined by Porter & James (1986) increasing pore-fluid salinity decreases quartz solubility ("salt-out effect") consistent with extrapolation of

experimental data on quartz solubility in H_2O-NaCl fluids from higher temperatures and pressures (Walther & Orville, 1983).

Hydrocarbon emplacement Some studies have described observations of smaller amounts of quartz cement in the oil-filled crestal areas (i.e. structural highs) of oilfields, as compared to the water-filled aquifer beneath. This difference was interpreted to mean that the presence of oil in the pore-space retards or stops quartz cementation (e.g. Dixon et al., 1989; Macaulay et al., 1992, Emery et al., 1993; Gluyas et al., 1993; Souza & McBride, 2000). In contrast, other workers have inferred that oil emplacement has little or no effect on quartz cementation (e.g. Saigal et al., 1992; Bjørkum et al., 1998; Oelkers et al., 1992; Walderhaug, 1996; Midtbø et al., 2000). Their conclusions were drawn from the observation that some reservoirs do not show differences in quartz cement volumes between water and oil legs (e.g. Ramm, 1992); or from the fact that primary oil inclusions are present in quartz cement in the sandstones in their study (e.g. Walderhaug, 1990). The first of these arguments can easily be dismissed because the timing of oil emplacement is crucial. As Worden & Morad (2000) point out, if oil was emplaced following quartz cementation, then there is no reason why rocks in the oil and water zones should have different quantities of quartz cement. The presence of oil inclusions in quartz cement, on the other hand, proves that at least some quartz can precipitate in the presence of oil. However, it does not prove that precipitation occurs at irreducible water saturations (Worden & Morad, 2000). Generally, empirical data are too poorly constrained to understand the degree of inhibition of quartz cemention by oil and a more quantitative approach is needed to help resolve this issue.

Predictive modelling Many efforts aimed at predicting reservoir quality in sedimentary basins have been based on empirical correlations of porosity with one or more independent variable such as mineralogy, texture and burial depth (e.g. Scherer, 1987; Schmoker & Gautier, 1988; Bloch, 1991; Gluyas & Cade, 1997; Primmer et al., 1997). According to Bjørkum (1998), correlation between parameters does not imply causality and therefore empirical models are limited in their application. Over recent years, effort has been put into designing process-oriented predictive models (e.g. Canals & Meunier, 1995; Lemée & Guéguen, 1996; Walderhaug, 1996; Bjørkum et al., 1998; Wangen, 1998; Lander & Walderhaug, 1999; Oelkers et al., 2000). Predictions from these models are based on chemical

and mathematical models of diagenesis and have the potential advantage of being applicable to systems that are significantly different from those with which they were originally calibrated. However, a major limitation to the process-oriented approach for reservoir quality prediction is the inadequate understanding of the thermodynamic and kinetic properties required by the models (Oelkers et al., 2000).

1.3 The objectives of this thesis

The successful prediction of hydrocarbon reservoir quality is a key exploration goal. Also, prediction of aquifer quality is important for accurate assessment of oil production scenarios. Therefore, there are good reasons for trying to understand the controls on the distribution of diagenetic quartz in actual and potential reservoirs and aquifers.

For this project, we deliberately chose to study a sandstone in which differential porosity is known to exist. The Upper Jurassic Brae Formation sandstones, buried at depths >3.8 km, have an overall porosity of about 15 %. In crestal areas of oilfields, which have their reservoir in the Brae Formation sandstones, porosities can be as high as 25 %. Since the reservoir sands appear to be depositionally homogeneous, it is clear that facies changes cannot explain the dramatic loss in porosity. There is a direct link between porosity loss and diagenesis. The reservoir sandstones with high porosity are least affected by quartz cementation, while areas of lower porosity in the reservoir contain larger amounts of quartz cement. Several oilfields have their reservoirs contained in the Brae Formation sandstones. The South Brae, Central Brae, North Brae and East Brae Fields are all located along the western margin of the Viking Graben and were deposited as proximal submarine fans. The Miller Field is located in mid fan deposits, and the Kingfisher Field in outer fan deposits. The Kingfisher oilfield contains two reservoirs, separated by a mudstone layer. The Brae Formation reservoirs in the Miller and Kingfisher Fields are the subject of this thesis. Based upon regional structural mapping and studies of oil geochemistry undertaken by Shell and Marathon, hydrocarbons are believed to have filled the Brae Formation reservoir in the Miller Field first. Subsequently oil spilled from this reservoir into the sandstone reservoir of the South Brae Field and in the lower reservoir into the Kingfisher Field. The reservoirs in the North Brae and East Brae Fields, and also the upper reservoir in the Kingfisher Field, contain compositionally different hydrocarbons. The hydrocarbons in these reservoirs are

believed to originate from a different, deeper, hydrocarbon kitchen area (Shell, Internal report).

The porosity variations and differential quartz cement distributions within, and possibly also between, the Brae Formation sandstone reservoirs in the Miller and Kingfisher Fields, combined with the probability that the reservoirs filled with oil at different times, make the Brae Formation sandstones the ideal location to study some of the key controversies on quartz cementation. This thesis aims to provide a valuable petrographic and geochemical dataset for the Brae Formation in the Miller and Kingfisher Fields. This dataset will allow improved understanding of the silica sources and transport mechanisms of the quartz cements present in the reservoir sandstones. This project also aims to examine the effect of oil emplacement on quartz cementation. The Brae Formation sandstone reservoirs offer a unique time, depth and geographical perspective for such an examination in light of the good empirical evidence for oil interaction with cementation (porosity anomalies) and different hydrocarbon charge times. Finally, an attempt will be made to quantify, for the first time, the impact of hydrocarbons on quartz cementation rates. This will be done by modelling the quartz cementation history in the reservoirs with the process-oriented predictive model (Exemplar™) of Lander & Walderhaug (1999). At the same time, a critical assessment of this reservoir quality predictive tool will be made.

1.4 Thesis Format

After this first Chapter, this thesis contains eight more Chapters which discuss various aspects of the Brae Formation sandstone reservoirs in the Miller and Kingfisher Fields :

Chapter 2 In this Chapter, the geological setting and depositional history of the Brae Formation sandstones is reported. This is important in order to understand the sedimentological link between the different reservoirs studied in the Miller and Kingfisher Fields. An overview and description of facies present in the sandstones is provided to give an insight into the sampling strategy utilized in this project. Finally, the hydrocarbon play for the two oilfields which are the subject of this thesis is discussed.

Chapter 3 In this Chapter, the reservoir quality of the Brae Formation reservoirs in the Miller and Kingfisher Fields is examined. A statistical analysis of porosity distribution, based on core He porosity data provided by BP-Amoco (Miller) and Shell (Kingfisher), is made in order to identify areas of normal and high reservoir quality. Subsequently, a detailed petrographic and textural study of thin sections provides insight into the processes that control the porosity distributions.

Chapter 4 This Chapter deals with the results of microthermometric measurements of fluid inclusions in quartz cement. Such measurements were carried out in order to constrain the temperatures at which quartz cementation commenced, and possibly also halted, in the Brae Formation sandstone reservoirs. Information on the salinity of the fluid from which quartz precipitated is also obtained from the fluid inclusion measurements. This can provide clues about the type of fluid in which silica was dissolved. Finally, the presence (or absence) and significance of petroleum inclusions in quartz is discussed.

Chapter 5 In this Chapter, the burial and thermal histories of the Brae Formation sandstone reservoir rocks, and also of the Kimmeridge Clay source rocks, are reconstructed with a 1D basin modelling package (BasinMod®). The duration of quartz cementation in each Brae Formation reservoir is determined by integrating quartz cement growth temperatures (obtained from microthermometry) with the thermal histories of the reservoir rocks. An approximate insight into oil emplacement time in the reservoirs is obtained by calculating the maturity of the source rocks. The relationship between the time of oil charge and quartz cement abundance in each reservoir is discussed.

Chapter 6 This Chapter aims to quantify the impact of hydrocarbon emplacement on quartz cementation. Quartz cement precipitation rates, for oil and water leg samples from the different reservoirs studied, are calculated by means of Exemplar™. Exemplar™ is a computer package which aims to predict reservoir quality in clastic reservoirs by simulating compaction and quartz cementation (Lander & Walderhaug, 1999). Any difference in quartz precipitation rates between oil and water leg samples, from the time of oil emplacement in the reservoirs onwards, can be regarded as quantitative proof of the effect of oil on quartz

cementation. At the same time, the adequacy of Exemplar™ as a reservoir quality predictive tool will be assessed.

Chapter 7 The aim of this Chapter is to examine the hydrogeologic regime that operated in the Brae Formation sandstones throughout their geological history. The quartz cements present in the sandstones examined imply transport of significant quantities of silica by either advective or diffusive fluid flow. Understanding the origin of these fluids from which authigenic quartz precipitated can provide insight into the transport mechanism of the silica. Oxygen isotope composition of quartz cements is determined in order to place constraints on the origin and evolution of fluids present in the Brae Formation sandstones since time of deposition until the present day. Results from both conventional mineral separation isotope methods and in-situ analysis with the ion microprobe are discussed.

Chapter 8 In this Chapter, the possible sources of silica for quartz cements precipitated in the Brae Formation reservoirs are discussed. Constraints on silica sources are derived mainly from petrographic observations and mass balance methods. Additionally, silicon isotope analyses were carried out on quartz cements by using the ion microprobe. This was done in order to test whether the silicon isotopic composition of authigenic quartz can be used to trace silica sources.

Chapter 9 Chapter 9 provides a summary of the research results presented in this thesis.

CHAPTER II

GEOLOGY & SEDIMENTOLOGY OF THE BRAE FIELDS

In this chapter :

- *In what geological setting are the Brae Fields located ?*
- *What is the depositional model for the Brae Formation sandstones ?*
- *Which facies types can be differentiated in the Brae Formation sandstones ?*
- *What is the hydrocarbon play for the Brae Fields (source rock-reservoir-seal relationships) ?*

2.1 Introduction

The western margin of the South Viking Graben contains a complex of oil and gas condensate reservoirs in the Upper Jurassic Brae Formation sandstones (Fig.1A). The South Brae, Central Brae and North Brae Fields are all located along the graben margin in UK block 16/7a (Fig.1B). The East Brae Field, also located along the graben margin, is located further north in block 16/3a (Fig.1B). The Miller and Kingfisher Fields are situated more basinwards in adjacent blocks 16/7b, 16/8b and 16/8a (Fig.1B).

Exploration in the Brae area began in the early 1970s, and the first exploration well 16/7-1 (Fig.1B) was drilled in 1975 by Pan Ocean on the North Brae structure (Stephenson, 1991; Hardy & Hart, 1994). This well discovered significant amounts of gas condensate, with an estimated 178 MMbll of recoverable hydrocarbons in place (Stephenson, 1991) (Table 1). Central Brae was discovered by well 16/7-3 (Fig.1B), drilled in 1975-6 as an appraisal well to the North Brae discovery (Turner &

Allen, 1991). Well 16/7-3 was sited on an anticline extending southwards from the North Brae domal feature, and tested oil. With recoverable reserves estimated at 65 MMbbl (Table 1), the Central Brae oilfield is considerably smaller than the North Brae gas condensate field (Turner & Allen, 1991). The South Brae discovery well, 16/7a-8 (Fig.1B), was drilled in 1977 at a location near the crest of an anticlinal structure mapped at Base Cretaceous level on 2D seismic data (Roberts, 1991). South Brae was the first of the discovered Brae Fields to go into production in 1983 with an estimated 312 MMbbl of oil to be recovered (Roberts, 1991) (Table 1). Production of the North Brae and Central Brae Fields followed in 1988 and 1989 respectively (Roberts, 1991). The first well spudded in the Miller Field was 16/7b-20 by BP in 1982, shortly followed by Conoco's 16/8b-2 in 1983 (Rooksby, 1991) (Fig.1B). Results indicated a major oil accumulation which was initially regarded as an eastern extension of the South Brae oilfield. However, following the drilling of 16/8b-3, Conoco's view that the pool was separate from the South Brae Field led them to name the accumulation "Miller", in recognition of pioneering contributions to science by the Scottish geologist Hugh Miller (1802-1856) (McClure & Brown, 1990). The Miller Field proved to be the largest hydrocarbon discovery made by BP in the North Sea during the years 1978-88. Miller Field came into production in 1992 with ultimate recovery estimated to be 240 MMbbl (Garland, 1993) (Table 1). The Kingfisher Field is operated by Shell UK and is the smallest of the Brae Fields (Table 1). The first well drilled was 16/8a-1in the south-eastern part of the field (Fig.1B). This well proved the presence of two separate reservoirs in the structure : a shallower gas condensate accumulation and a lower oil accumulation (Shell internal report).

Table 1 General information on North Sea Fields which have their reservoir in the Brae Formation sandstones. Hydrocarbon reservoirs in the Upper Jurassic Brae Formation were discovered in the early 1970s and came into production at the end of the 1980s. The biggest accumulation discovered in the area was the South Brae Field, followed by the Miller and North Brae Fields.

Field	Licence Block	Discovery Year	Discovery Well	Production Start	HC type	Brae Fm. Reservoir Unit	Top Brae Fm. (m TVD)	HWC (m TVD)	Max. Thickness HC Column (m)	Estimated Recoverable Reserves
North Brae	16/7a	1975	7a-1	1988	gas condensate	1	3606	3802	196	178 MMbbl
Central Brae	16/7a	1975-6	7a-3	1989	oil	2	3581	4092	511	65 MMbbl
South Brae	16/7a	1977	7a-8	1983	oil	2	3603	4111	508	312 MMbbl
Miller	16/7b & 16/8b	1983	7b-20	1992	oil	2	3980	4090	110	240 MMbbl
Kingfisher	16/8a	?	8a-1	?	gas condensate	1	3885	3959	74	37 MMbbl
					oil	2	3979	4005 / 4030	51	12 MMbbl

In this chapter, I give a brief overview of the structural setting and location of the Brae Fields. I give a more thorough overview of the depositional history of the Brae

Formation sandstones. This is described in a stratigraphic context because the project involves two fields, Miller and Kingfisher, and it is important to understand how they relate sedimentologically to each other. The depositional setting of the sandstones will influence which facies will be present in each reservoir. Since facies is an important control on reservoir quality, I also discuss the distribution of facies in the Brae Formation sandstone reservoirs in the Miller and Kingfisher Fields. All depths are given as true vertical depths (TVD) in meters (m) or kilometers (km) subsea.

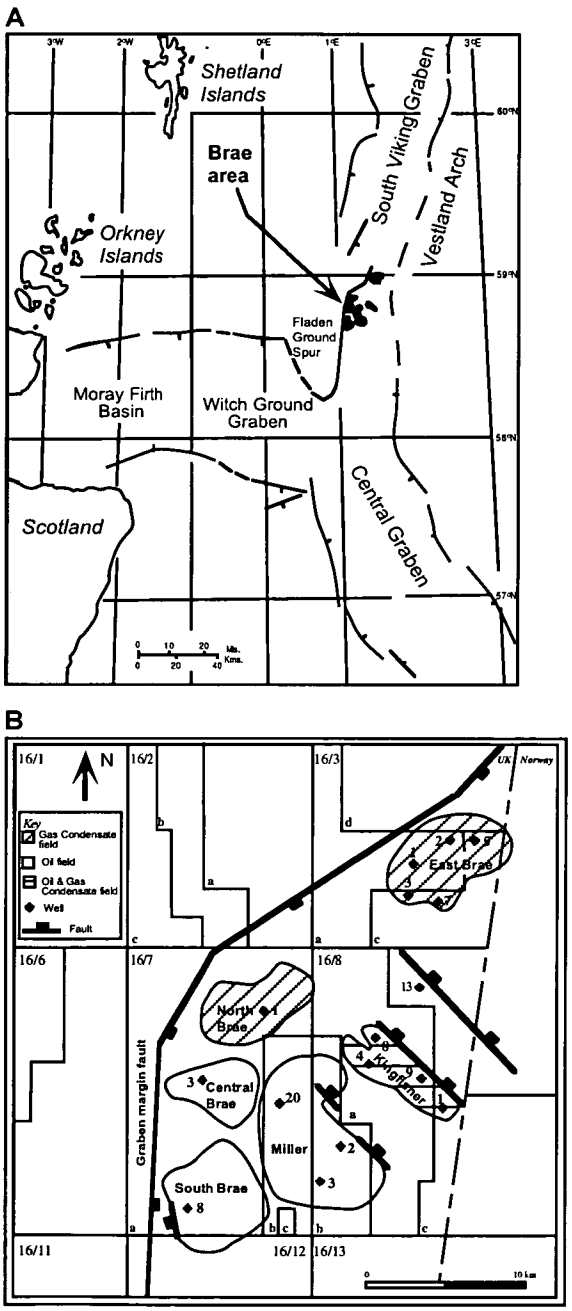

Fig.1 Location map of the Brae Formation reservoirs in the North Sea (**A**). The South, Central, North and East Brae Fields are located along the western margin of the South Viking Graben fault (**B**). The Miller and Kingfisher Fields are located further basinward (**B**).

2.2 Structural setting

The Brae Formation sandstone reservoirs lie in the southern part of the South Viking Graben, which is a north-south trending half-graben that is fault bounded to the west against the Devonian Fladen Ground Spur basement (Fig.1A). The graben floor rises gently eastward to the Vestland arch and is cut by several deep-seated northwest-southeast trending faults oblique to the main boundary fault (Fig.1B) (McClure & Brown, 1990). The South Viking Graben was probably initiated in the early Permian and rifting was active from at least the early Jurassic (Glennie, 1984). Extensional movement continued intermittently on the western boundary fault until the Tertiary, when there was a brief phase of inversion before activity ceased (McClure & Brown, 1990). Over 3 km of Late Jurassic and Cretaceous sediments are estimated to be present at the graben margin, approximately half of which form the Brae Formation. Beneath this is a further thick sequence, probably including mid Jurassic-Permian sediments, resting on Devonian. This contrasts with a relatively thin sequence of about 300m of Mesozoic sediments overlying Devonian basement on the Fladen Ground Spur (Turner et al., 1987).

2.3 Stratigraphy

The regional stratigraphy of the South Viking Graben is summarized by the stratigraphic column in Fig.2. The lithostratigraphic nomenclature used in Fig.2 follows the recommendations of the joint Norway/UK Lithostratigraphic Nomenclature Committee (Deegan & Scull, 1977). The Brae Formation is Upper Jurassic in age and was deposited from Oxfordian to Volgian times (157-143 Ma). On a regional scale the formation is both overlain and underlain by, and interdigitates with, the Kimmeridge Clay Formation (Stoker & Brown, 1986).

The Brae Formation has been chronostratigraphically subdivided into three members (McClure & Brown, 1990; Rooksby, 1991; Garland, 1993). These chronostratigraphic members also relate broadly to the three lithostratigraphic reservoir units (Rooksby, 1991). Unit 3 comprises the lowermost unit of the Brae Formation and ranges from Oxfordian to Late Kimmeridgian in age. Unit 2 ranges from early Volgian to earliest middle Volgian in age and Unit 1 is early to mid middle Volgian.

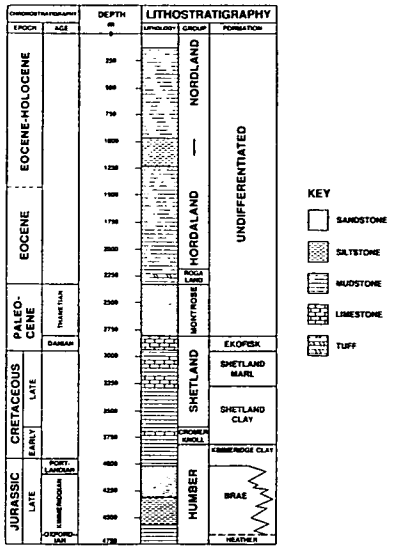

Fig.2 Regional stratigraphy of the South Viking Graben. The Brae Formation is Upper Jurassic in age and was deposited from Oxfordian to Volgian times. It is overlain and interdigitates with the Kimmeridge Clay Formation. (From McClure & Brown, 1990)

2.4 Depositional model

During the development of the Brae Fields, concepts of a depositional model for the Brae Formation continued to evolve from early ideas based on exploration and appraisal drilling (Turner et al., 1987). Initially, it was suggested that the reservoir sandstones were deposited on the subaerial and marginal marine portions of coalescing fan deltas (Harms et al., 1981). Stow et al. (1982) proposed a submarine fan origin for the Brae Formation sandstones. Their model for the South Brae Field suggests that small slope-apron fans developed along the graben margin fault and sediment influx into the basin was fault controlled. Since then, wells drilled to the east of fields located along the graben margin made it clear that the model needed some adaptation to incorporate the newly found Miller and Kingfisher Field deposits. Today the generally accepted depositional model for the Brae Formation is that the sandstones are a system of tectonically controlled extensive submarine fans (Turner et al., 1987; McClure & Brown, 1990). Sediments were derived from the Fladen Ground Spur to the west, which existed at the time of deposition as a shallow marine to subaerial shelf area (Fig.3). The proximity of sediment source to receiving basin, together with active extensional tectonics, provided the ideal setting for the development of submarine fans. Proximal submarine fans at the edge of the marine basin at the foot of the fault scarp received the coarse-grained sediments (East, North, Central and South Brae Fields). These gravel-rich fans are confined to

a narrow belt (5 to 10 km wide) along the basin's actively faulted margin (McClure & Brown, 1990). Interbedded mudstones represent the hemipelagic background sedimentation preserved during periods of quiescence and low clastic input (McClure & Brown, 1990). The basin floor east of the slope apron was the depositional axis of the Miller and Kingfisher Field medium-grained deposits (Fig.3) (Garland, 1993).

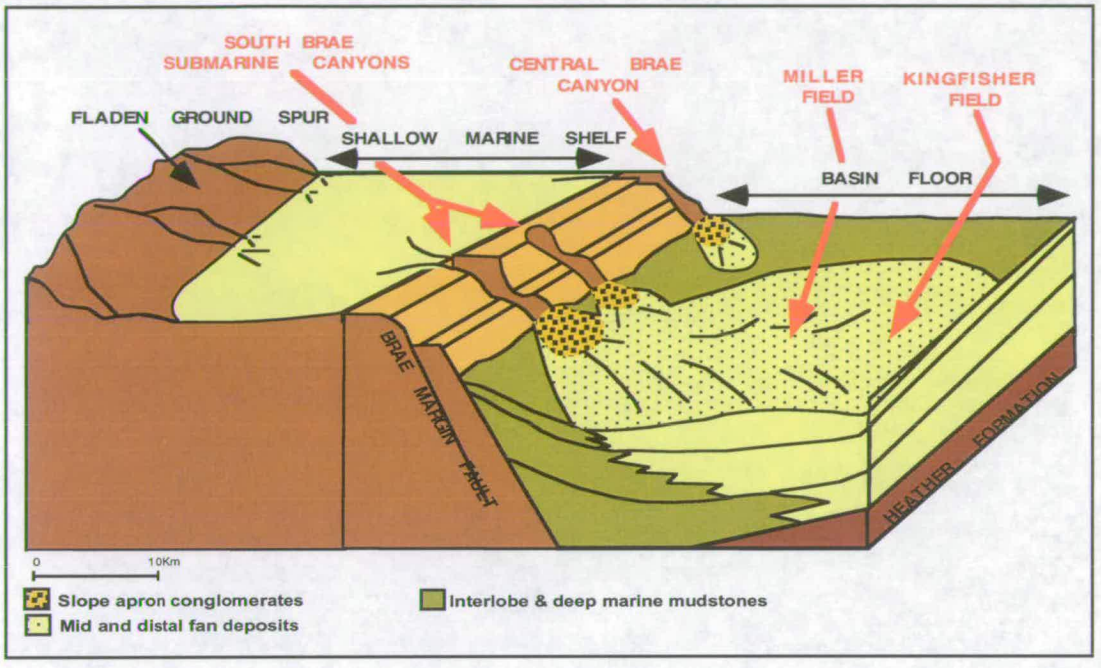

Fig.3 Depositional model for the Brae Formation sandstones. The sandstones were deposited as a system of tectonically controlled extensive submarine fans. Sediments were derived from the Fladen Ground Spur to the west. The area at the foot of the fault scarp received the coarse-grained sediments of the proximal submarine fans (South, Central, North and East Brae Fields). Sands in the mid and distal fan areas are medium-grained and moderately sorted (Miller and Kingfisher Fields). Net:gross decreases from west to east across the area (proximal to distal deposits). (After Garland, 1993)

2.5 Depositional history

The depositional history of the Brae Formation sandstones is discussed for each chronostratigraphic unit separately. All information below is summarized from an internal Shell report, unless noted otherwise.

Unit 3 - Oxfordian to Kimmeridgian The Oxfordian to Kimmeridgian interval represents the progradation of the earliest coarse clastic wedges into the South Viking Graben in response to movements along the graben margin fault zone.

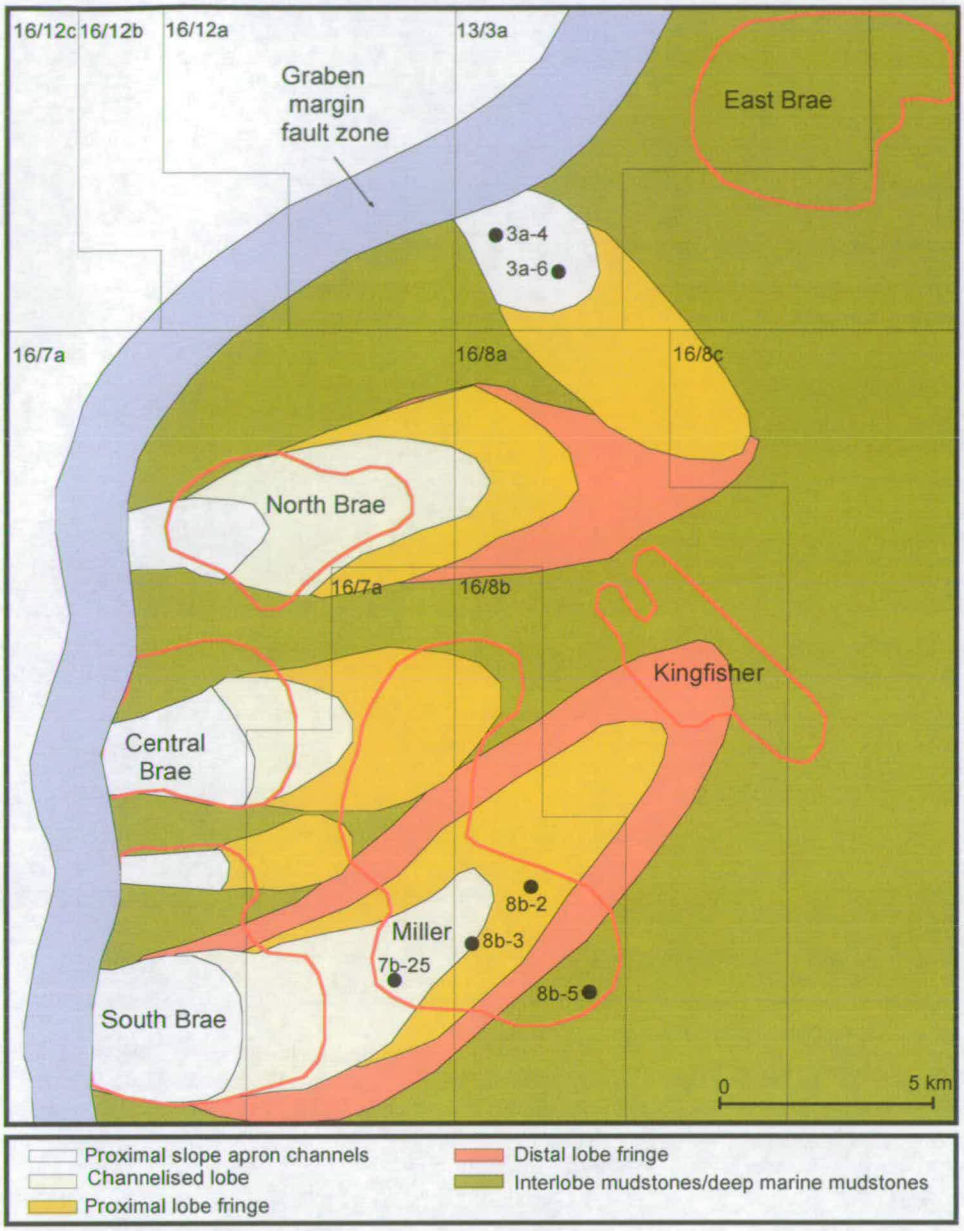

Fig.4A Depositional model for the Brae Unit 3 sandstones during the Late Kimmeridgian. Small slope apron fans developed in the South, Central and North Brae areas and around wells 16/3a-4 and 6. (After Shell Internal Report)

Sediment input was via entry points located in the South, Central and North Brae areas and around wells 16/3a-4 and 6 (Turner & Connell, 1991). Small slope apron fans developed, separated by slope mudstones (Fig.4A). The largest of the slope apron fans was in the South Brae Field and consists of highly channelised proximal fan conglomeratic sandbodies. Passing eastwards towards the Miller Field (i.e. wells 16/7b-25 and 16/8b-3), a transition into medium- to fine-grained mid fan channelised sandbodies occurs (Fig.4A) (Turner & Connell, 1991). This easterly

progradation of the South Brae fan system is also recorded in the Kingfisher Field by the occurrence of a gradual upwards coarsening sequence of thin distal, basinal sheet sands (Fig.4A). The top of the Unit 3 sequence is a maximum flooding surface which represents the temporary abandonment of the fan systems.

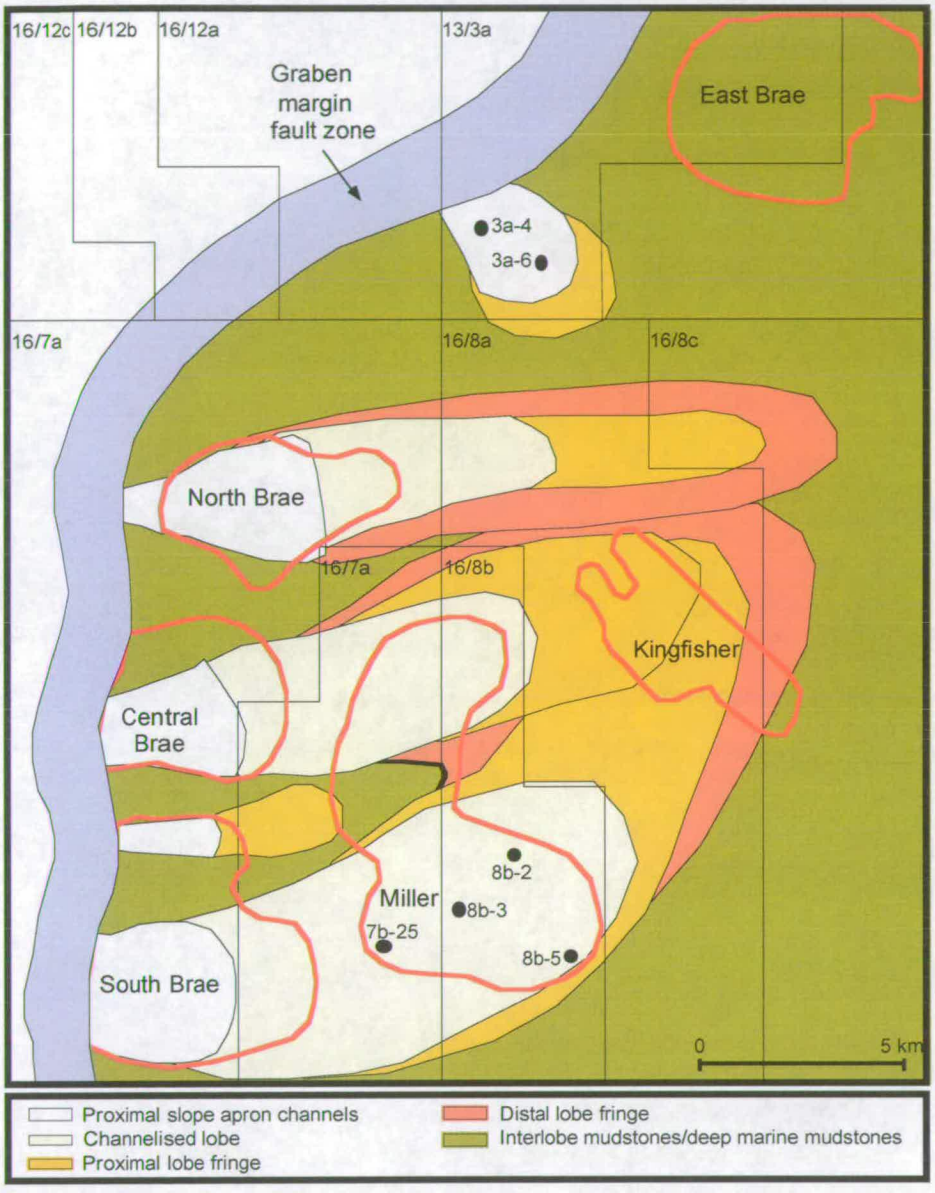

Fig.4B Depositional model for the Lower Brae Unit 2 sandstones during the Lower Volgian. South Brae, Central Brae and North Brae fans were active, as was the system close to wells 16/3a-4 and 6. (After Shell Internal Report)

Lower Unit 2 - Lower Volgian Biostratigraphic data indicate that the South Brae, Central Brae and North Brae fans were active, as was the system close to wells 16/3a-4 and 6 (Fig.4B). The depositional model is similar to that for Unit 3, the main difference being the more basinward extent of the frontal fan lobes (Fig.4B). This is evident from the occurrence of much thicker sheet sands (proximal fan fringe) in the Kingfisher Field. Overlapping of the South Brae and Central Brae fan systems in the more distal fan fringe areas is a likely possibility.

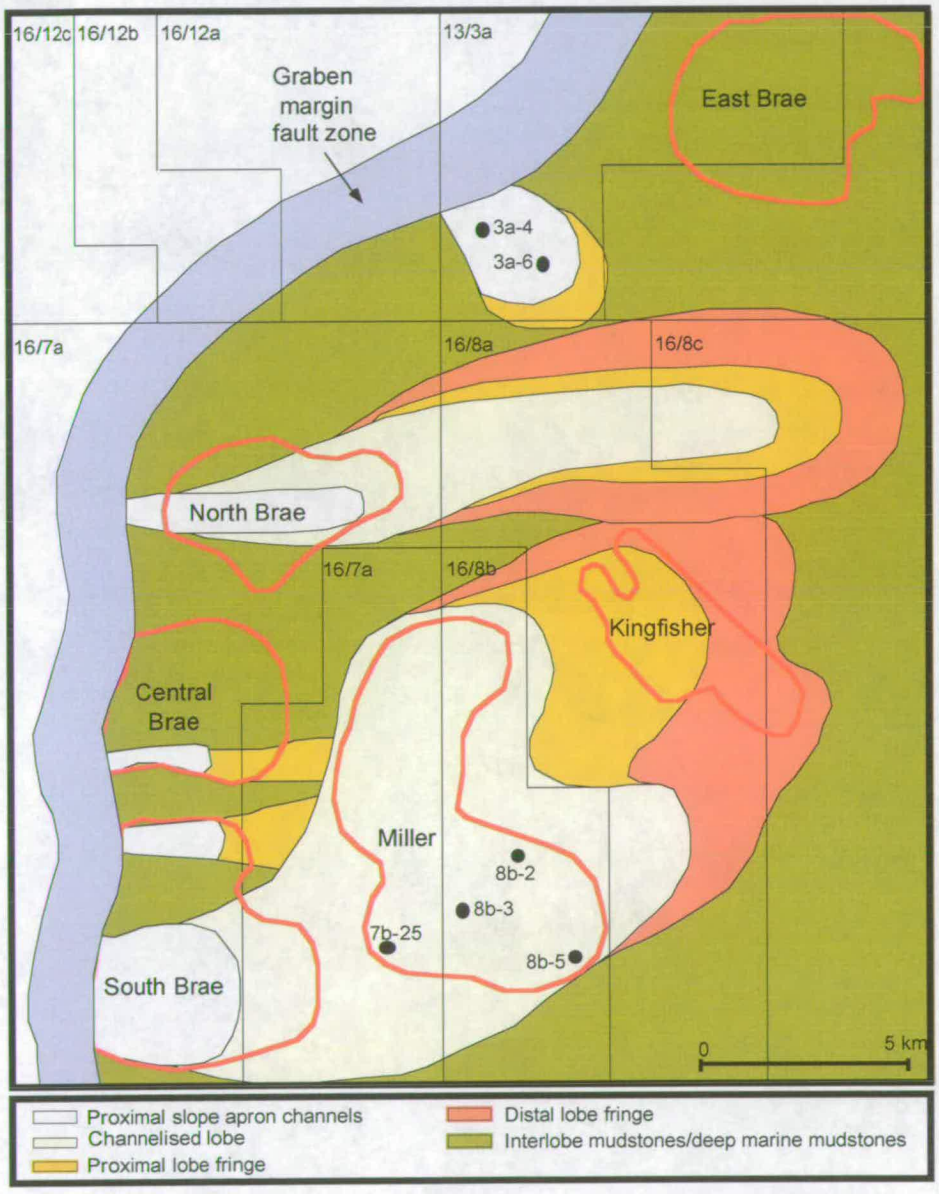

Fig.4C Depositional model for the Upper Brae Unit 2 sandstones during the early Middle Volgian. The South Brae system provided the mid fan sediments for the Miller Field and frontal channelised lobe sediments of the Kingfisher Field. (After Shell Internal Report)

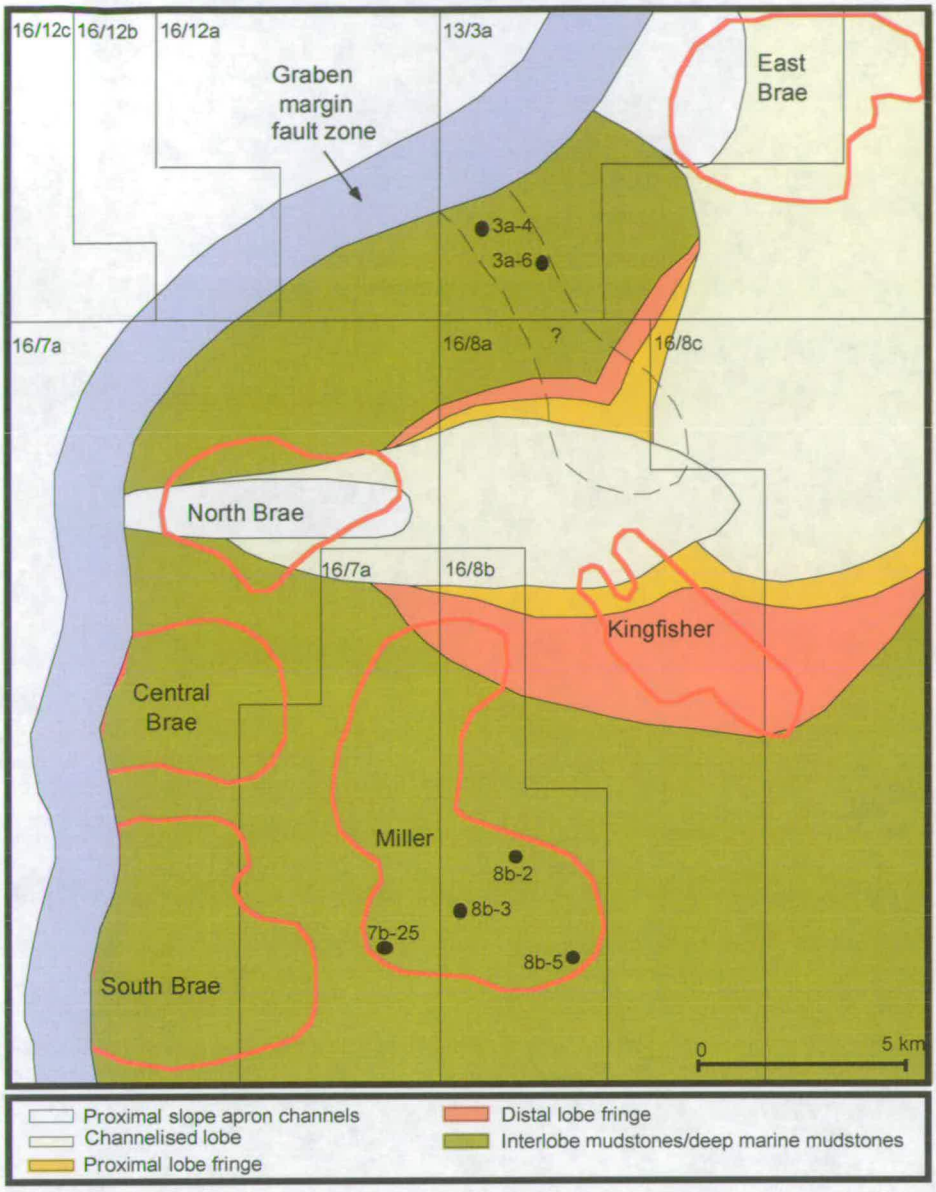

Fig.4D Depositional model for the Brae Unit 1 sandstones during the mid Middle Volgian. Sediment input from the South Brae fan had ceased and this and the southern part of the Miller Field were blanketed by Kimmeridge Clay. The main sources of sediment supply into the basin were now the North Brae and East Brae fan systems. Unit 1 in the Miller Field is present only in the northern part of the field as thin sandstones interbedded with shales. (After Shell Internal Report)

Upper Unit 2 - Early Middle Volgian Biostratigraphic data suggest that by early Middle Volgian times sediment input through the Central Brae fan system either had ceased or was much reduced (Fig.4C). According to the model of Turner & Connell (1991) all the mid fan sediments for the Miller Field and frontal channelised lobe sediments of the Kingfisher Field were supplied via the South Brae system (Fig.4C). In the South Brae Field, a radial pattern of highly channelised conglomerates

passes basinward into the mid fan channelised lobes of the Miller Field and proximal lobe fringe of the Kingfisher Field (Fig.4C). Pressure data suggest that the Unit 2 sands in the South Brae, Miller and Kingfisher Fields are in communication. The North Brae fan system was also active and is seen as the source for stacked channel sands further eastward in the graben (Fig.4C). The top of Unit 2 is a maximum flooding surface which represents the cessation of sand supply from the South Brae system.

Unit 1 - Mid Middle Volgian Sediment input from the South Brae fan had ceased and this and the southern part of the Miller Field were blanketed by Kimmeridge Clay (Fig.4D). The main sources of sediment supply into the basin were now the North Brae and East Brae fan systems (McClure & Brown, 1990) (Fig.4D). Deposits in the North and East Brae Fields are typically proximal fan conglomeratic channel fill complexes. Pressure depletion in wells through Unit 1 sandstones suggests that the sands in the Kingfisher Field were sourced via both North and East Brae and are in communication. This is in agreement with seismic data which indicate that sediment input into the Kingfisher Field area comes from both these sources. Unit 1 in the Miller Field is present only in the northern part of the field as thin sandstones interbedded with shales (Fig.4D) (McClure & Brown, 1990). The top of Unit 1 is also a maximum flooding surface, which represents the start of deposition of the Upper Kimmeridge Clay Formation in the Kingfisher-North Brae area.

2.6 Brae Formation sandstone reservoirs

The Brae Formation Unit 3 sands are oil-bearing in the South Brae and Central Brae Fields (McClure & Brown, 1990). These reservoirs are the oldest in the Brae area and are composed of coarse-grained proximal fan deposits. Unit 3 thins eastward and is represented by thin sandstones interbedded with mudstones in the Miller Field and by thin distal basinal sheet sands in the Kingfisher area (Garland, 1993). Oil was found in wells 16/8b-2, 16/8b-3 and 16/8b-5 in the Miller Field.

Brae Formation Unit 2 sandstones are reservoir to the main oil accumulation in the Central Brae, South Brae, Miller and Kingfisher Fields (Garland et al., 1999). Unit 2 is composed of sandstone and conglomerate in the South, Central and North Brae Fields, but thickens and becomes finer-grained eastwards towards the Miller Field area (Turner et al., 1987). Unit 2 sands in the Miller Field are medium-grained and form the main oil bearing reservoir with net:gross ratios typically greater than 0.75.

The Unit 2 succession in the Kingfisher Field is of a lower net:gross ratio (0.48) due to the distal fringe setting made up of isolated sheet sands (Garland et al., 1999).

Unit 1 comprises the gas condensate reservoirs in the North Brae, East Brae and Kingfisher Fields. In the North and East Brae Fields the sands are coarse-grained proximal deposits, while in the Kingfisher Field they are medium-grained more distal deposits (McClure & Brown, 1990). The gas condensate reservoir in the Kingfisher Field has a net:gross ratio of 0.75. Over most of the Miller Field, Unit 1 is predominantly shaly, although interbedded turbidite sands sourced via the North Brae Field were deposited over the northern part of the field. Unit 1 is not present in the South and Central Brae Fields (Turner et al., 1987).

2.7 Facies descriptions

Turner et al. (1987) have described 5 major lithological facies in the Brae area. These are summarized below.

Facies 1 : Sand matrix conglomerate

The conglomerates have a disorganized appearance and are either clast or matrix supported. The conglomerate matrix is composed of fine- to coarse-grained sandstone. Transport of the conglomeratic facies was by high-density, sand- and gravel-rich, debris flows. This facies was deposited in the proximal parts of the fans, close to the Graben margin fault (Fig.5).

Facies 2 : Mud matrix breccia

This facies is composed of breccia deposited in a matrix composed of variably sandy mudstone. Clasts are poorly sorted and are almost exclusively angular quartzo-feldspathic sandstones of pebble-boulder size. Deposition was from debris flows generated by the avalanche of fault scarp debris onto a muddy substrate with subsequent remobilization, mixing and flow. This facies occurs in the proximal parts of the submarine fans.

Facies 3 : Medium- to thick-bedded sandstone

This facies comprises beds 10 to >30 cm in thickness of fine- to very coarse-grained sandstone, in places containing granules and small pebbles. Internally these beds

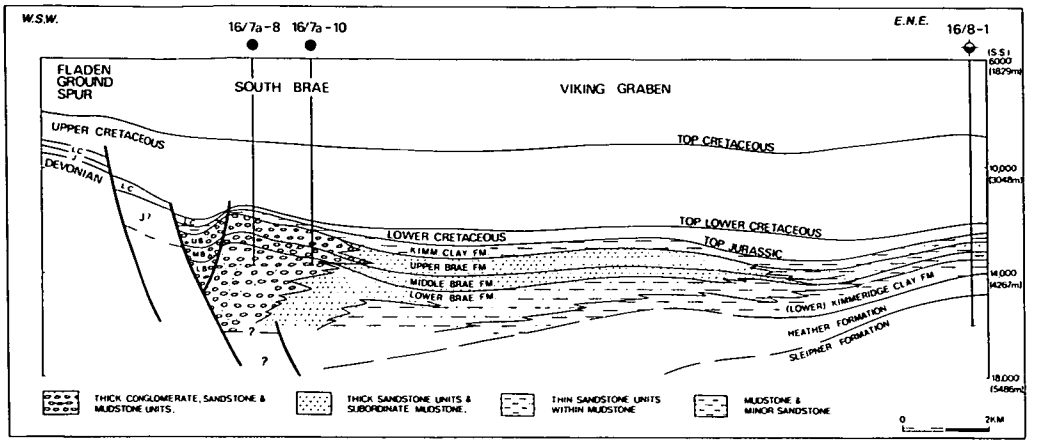

Fig.5 Approximate distribution of lithofacies in the Brae Formation. Conglomerates are deposited in the proximal parts of the fan, close to the graben margin fault. Thick beds of medium-grained sandstones are present in the mid fan area. In regions between fan lobes, and in mid and distal fan areas, interbedded sandstones and mudstone layers occur. Mudstone layers are present in distal fan and basin floor settings. (From Turner et al., 1987)

are commonly structureless, but parallel lamination occurs in places. Some coarser beds display grading. Cross stratification is also occasionally evident. Mudstone laminae are present but make up less than 20 % of facies intervals. Deposition was from high-density turbidity currents. This facies was deposited in the mid areas of the submarine fans (Fig.5).

Facies 4 : Interbedded sandstone-mudstone

This facies contains sandstone as laminae (1-10 mm) and thin beds (1-10 cm) interbedded with mudstone. Sandstones are fine- to medium-grained and are tabular or lenticular. They show a massive to laminated internal structure, and less common cross-lamination. The sandstones were deposited from dilute turbidity currents of varying magnitude. Bed boundaries are generally sharp, indicating that the mudstones were deposited by hemipelagic settling between turbidity flows. This facies was deposited on mid to distal regions of the submarine fan or into regions between fan lobes (Fig.5).

Facies 5: Laminated mudstone

Laminated mudstone is dominated by non-bioturbated dark grey-black, micaceous, carbonaceous mudstone. The mudstone was deposited from hemipelagic settling, with rare sand laminae and graded silts deposited from very dilute turbidity flows. This facies was deposited in distal fan and basin floor settings (Fig.5).

Within the Miller and Kingfisher Fields, which are the subject of this thesis, three of the above 5 facies are recognized. The lithofacies present in the reservoirs in the Miller and Kingfisher Fields have also been described by Garland (1993) and by Prosser et al. (1995).

The first lithofacies consists of clean, fine- to medium-grained sandstone packages of up to 30 m in thickness (Fig.6). This lithofacies in the Miller and Kingfisher Fields corresponds with the medium- to thick-bedded sandstones of Facies 3 described above. The second lithofacies consists of thinly bedded alternations of sandstone and mudstone (Facies 4) (Fig.6). This facies occurs interbedded with the sandstone packages of Facies 3. The interbedded sandstone and mudstone alternations in the Miller and Kingfisher Fields are up to 20 cm and 0.1-5 cm thick respectively. The third lithofacies comprises isolated mudstone layers which are 20-50 cm in thickness. This facies corresponds with the laminated mudstone deposits of Facies 5 described above.

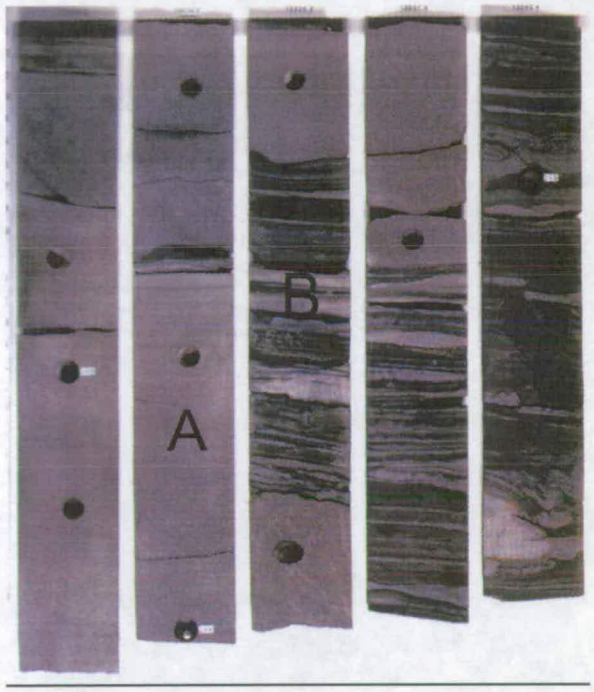

Fig.6 Core photograph from interval 13230-13243ft DD (4022-4026m TVD) in the Brae Unit 2 reservoir (well 8a-4) in the Kingfisher Field. Fine to medium grained sandstone packages make up the actual reservoir rock (A). Interbedded with these packages are intervals of sandstone-mudstone alternations (B) and also isolated mudstone layers (not on photograph). (photograph from Shell UK)

2.8 Hydrocarbon play

The areal extent of the oil and gas condensate reservoirs in the Brae Formation sandstones in the Miller and Kingfisher Fields is defined by a combination of structural and stratigraphic trapping. Both Miller and Kingfisher have anticlinal field structures, and are separated from each other by a syncline (Fig.7 & Fig.8).

The Brae Unit 2 oil reservoir in the Miller Field is isolated by dip closure at the intersection of the oil-water contact (OWC) with the anticlinal structure (McClure & Brown, 1990). In the southwest, the Miller Field is structurally separated from the South Brae Field by a gentle north-south trending syncline (Fig.7) (McClure & Brown, 1990). Closure to the northwest of the field is also stratigraphically related to deterioration of reservoir quality near the margins of the fan (Garland, 1993). The main reservoir in the Miller Field is the southern part of the field which is a fairly low-relief four-way dipping domal anticline feature with an oil-water contact (OWC) at 4090 m and a maximum hydrocarbon column of about 110 m (McClure & Brown, 1990).

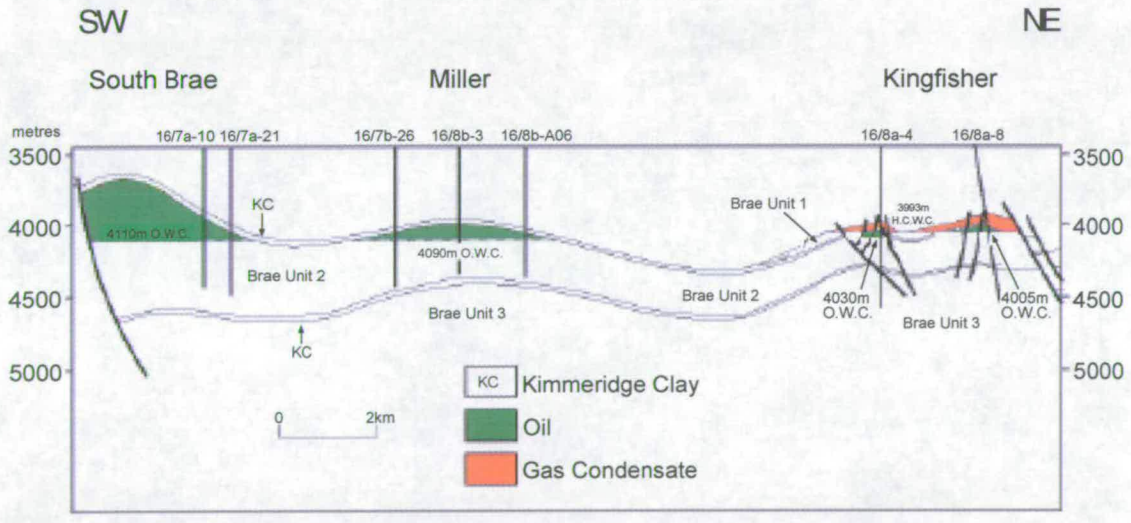

Fig.7 Structural profile across the South Brae-Miller-Kingfisher Fields (SW-NE). South Brae, Miller and Kingfisher all have anticlinal field structures. The fields are separated from each other by synclines. The Brae Unit 2 reservoir in the Miller Field is isolated by dip closure of the intersection of the oil-water contact (OWC) with the anticlinal structure. Also the Brae Unit 2 and Brae Unit 1 reservoirs in the Kingfisher Field are confined by dip closure to the southeast and northwest. The OWC in Kingfisher Field varies due to faulting.

The Kingfisher Field is a southwest dipping dome intersected by faults. The Brae Formation Unit 2 oil reservoir is confined by dip closure to the southwest and northwest (Fig.7 & Fig.8). Stratigraphic pinch-out of these sands towards the

southeast and east completes the hydrocarbon trap (Fig.8). The OWC in the Brae Unit 2 reservoir varies across the field due to lateral reservoir compartmentalisation by faulting (Fig.7). In the northeastern structure the OWC is at 4005 m, with a maximum hydrocarbon column of 26 m (Fig.7). To the southwest in the structure drilled by well 8a-4, the OWC is at 4030 m, creating 44 m of maximum hydrocarbon column (Fig.7). The Brae Unit 1 reservoir in the Kingfisher Field is separated from the Brae Unit 2 reservoir by a sealing layer of shale (Fig.7 & Fig.8). A syncline separates the Unit 1 reservoir from the age equivalent gas condensate reservoirs in the North Brae (Fig.8) and East Brae Fields. The extent of the gas condensate reservoir in the Kingfisher Field is, again, defined by a combination of dip closure and stratigraphic pinch-out of sands (Fig.7 & Fig.8). The gas-water contact (GWC) is located at 3993 m, creating a maximum hydrocarbon column of 108 m.

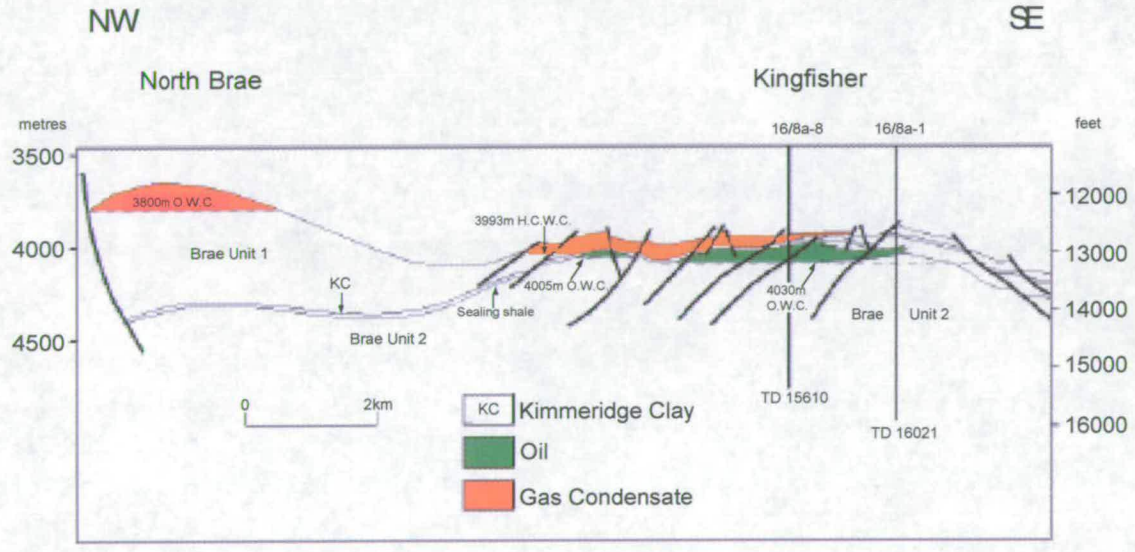

Fig.8 Structural profile across the North Brae-Kingfisher Fields (NW-SE). A syncline separates the Brae Unit 1 reservoirs in the North Brae and Kingfisher Fields. The extent of this gas condensate reservoir in the Kingfisher Field is defined by dip closure to the northwest and stratigraphic pinch-out to the southeast. Reservoir quality in the underlying Brae Unit 2 oil reservoir also deteriorates towards the southeast due to stratigraphic pinch-out.

The Kimmeridge Clay Formation acts as both source rock and seal for the hydrocarbon accumulations in the Brae area (Cornford et al., 1983; MacKenzie et al., 1987). In the Miller and Kingfisher Fields, the Brae Formation is overlain and underlain by, and interdigitates with, these organic-rich clays (Rooksby, 1991). Studies on the geochemistry of the two types of hydrocarbons (oil and gas condensate) present in the Brae area were published by Reitsema (1983) and

Mackenzie et al. (1987). Both studies concluded that the hydrocarbons in the Brae Formation Unit 2 oil reservoirs are locally derived from Kimmeridge Clay mudstones in the vicinity of the reservoirs. The gas condensate in the Brae Formation Unit 1 reservoirs is believed to be the result of a longer migration pathway. The gas condensate is thought to have been generated in deeper parts of the graben to the east of the Kingfisher Field (Reitsema, 1983). From there, it could have migrated through the submarine fan sequence into the reservoir structures of the North and East Brae Fields, and also the Kingfisher Field (Stephenson, 1991).

2.9 Summary

1 The Miller and Kingfisher Fields are located along the fault-bounded western margin of the South Viking Graben in blocks 16/7b, 16/8b and 16/8a of the UK North Sea sector.

2 The reservoir sequence in both fields comprises Upper Jurassic sandstones of the Brae Formation. These sandstones were deposited as a complex of submarine fans from Oxfordian to Volgian times (157-143 Ma). Near the Graben margin (South, Central, North and East Brae Fields), the Brae Formation sandstones consist of thick units of mud- and sand-supported conglomerates and coarse-grained sandstones. Further eastwards in the Miller and Kingfisher Fields, these sandstones prograde into medium- to fine-grained mid- and distal-fan deposits.

3 The Brae Formation has been chronostratigraphically subdivided into three members which also relate to the three lithostratigraphic reservoir units. Unit 3, deposited from Oxfordian to Kimmeridgian, represents the progradation of the earliest coarse clastic wedges into the South Viking Graben. Unit 3 sands present in the Miller and Kingfisher Fields were sourced from the South Brae Field graben entry point. In the Miller Field, Unit 3 is present as medium- to fine-grained channelised sandbodies. In the Kingfisher Field, it is represented by thin distal basinal sheet sands. The early Volgian to mid Middle Volgian, when Unit 2 was deposited, was the main period of progradation of the South Brae submarine fan. In the Miller Field, this period is represented by the deposition of mid fan channelised lobes. In the Kingfisher Field, thicker sheet sands (proximal fan fringe) occur. These were possibly partly sourced from the Central Brae fan. When deposition of Unit 1 started from North and East Brae graben entry points in the Middle Volgian, the southern part of the Miller Field was blanketed by

Kimmeridge Clay. In the Kingfisher Field, Unit 1 deposits are present as medium-grained mid-fan deposits and as thin proximal fan fringe sandstone deposits interbedded with shales.

4 Three lithofacies types are recognised in the Miller and Kingfisher Field areas. The first lithofacies comprises fine- to medium-grained sandstone packages of up to 30 m thickness. The second lithofacies consists of thinly bedded alternations of sandstone and mudstone. Isolated mudstone layers are the third lithofacies type present.

5 The areal extent of the reservoirs in the Brae Formation Unit 2 and Unit 1 sandstones in the Miller and Kingfisher Fields is defined by a combination of structural and stratigraphic trapping. Kimmeridge Clay Formation mudstones act as source and seal for the hydrocarbons trapped in the anticlinal reservoir structures. The Unit 2 sandstones contain oil, sourced from Kimmeridge Clay in the vicinity of the reservoirs. The Unit 1 sandstones in the Kingfisher Field, which are not present in the Miller Field, contain a gas condensate. This was generated from Kimmeridge Clay in deeper parts of the graben east of the field structure.

6 The main oil reservoirs (Unit 2) in the Miller and Kingfisher Fields are in pressure communication. Both accumulations are isolated from each other by a syncline. OWC in the Miller Field is at 4090 m (110 m below the crest of the anticline). In the Kingfisher Field, the OWC varies laterally across the field due to faults. In well 8a-8 OWC occurs at 4005 m (26 m below top reservoir), and in well 8a-4 it occurs at 4030 m (44 m below top reservoir).

7 The Brae Unit 1 reservoir in the Kingfisher Field is in pressure communication with the Brae 1 reservoirs in the North and East Brae Fields. The gas condensate accumulation in the Kingfisher Field is isolated by dip closure of the intersection of the GWC with the anticlinal field structure. The GWC in the Kingfisher Field is located at 3993 m. This is 108 m below the top of the reservoir.

CHAPTER III

RESERVOIR QUALITY

In this chapter :

- *How good is the reservoir quality in the reservoirs examined ?*
- *What controls the reservoir quality ?*

3.1 Introduction

The quality of a reservoir is defined by its porosity and permeability. These physical rock parameters are critical to the economics of any oil and gas exploration and production event. Porosity has a major effect on petroleum in-place calculations. Permeability is essential for production flow rates of hydrocarbons and injection fluids (Worden et al., 2000). Reservoir quality in sandstones is the result of often long and commonly complex geologic evolution histories. The combined influence of preburial mineralogy and texture, pressure and temperature gradients, age, diagenesis and timing of petroleum emplacement results in reservoirs which today have widely varying permeability-porosity characteristics (Ramm & Bjørlykke, 1994).
In this chapter, I examine the reservoir quality distribution in the Miller and Kingfisher Fields by means of porosity and permeability data provided by BP-Amoco and Shell. Subsequently, I identify the factors which control poroperm in the Brae Formation reservoirs. To achieve this, I carried out a detailed petrographic study to determine mineralogy, texture and the diagenetic history of the sandstones. In the discussion I draw conclusions as to what processes control poroperm in the Miller and Kingfisher Fields.

3.2 Methods & samples

Initial reservoir quality assessment of the Brae Formation sandstones was based upon porosity and permeability data from 11 different wells in the Miller Field (5446 datapoints) and porosity data from 2 wells in the Kingfisher Field (642 datapoints) (Fig.9). All porosity values are core He data and were provided by BP-Amoco (Miller) and Shell (Kingfisher). No permeability data for the Kingfisher Field were available.

Mineralogy, texture and diagenesis in the Brae Formation sandstones were examined in thin sections using a standard petrographic microscope. Mineralogical sandstone composition was determined by pointcounting (500 counts/thin section). K-feldspar abundances were verified by image analysis of SEM backscatter images (Appendix A). Mean grain size was estimated by measuring the apparent long axis of 100 randomly selected monocrystalline quartz grains per thin section (Houseknecht, 1988). The standard deviation on the grainsize measurements was used as a measure of the sorting of the sediment. Due to difficulties recognising quartz cement in thin section, all quartz cement abundances were verified under SEM-CL combined with image analysis (Appendix A).

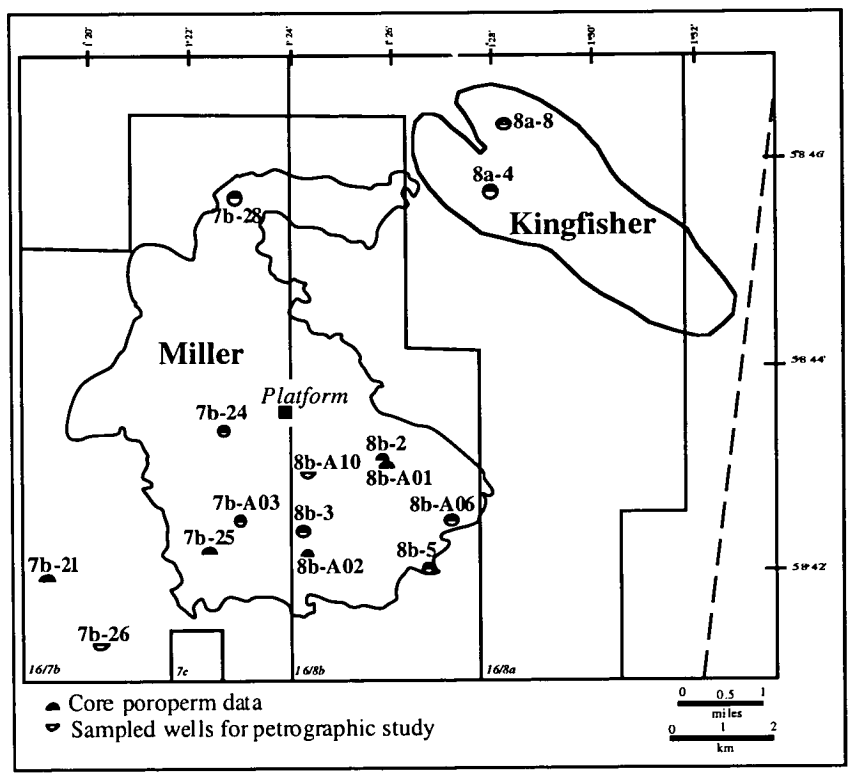

Fig.9 Location of the wells from which core material for thin section analysis was sampled in the Miller and Kingfisher Fields. Wells from which porosity and permeability data were provided by BP-Amoco and Shell UK are also indicated.

For the Miller Field, a total of 74 thin sections from 8 different wells (Fig.9) were examined. The thin sections cover a depth range from 3990 m to 4300 m TVD (Brae Formation Unit 2). This depth range spans from the top of the reservoir in crestal well 16/8b-3, to deep in the reservoir's water leg (OWC at 4090 m). For the Unit 1 Brae Formation sandstones in the Kingfisher Field, 27 thin sections from well 16/8a-8 were studied. Sample depths range from top to bottom in the reservoir (3885 to 3959 m). No water leg samples were available because this well penetrates only oil leg (Fig.7). The Brae Formation Unit 2 sandstones in the Kingfisher Field were sampled (16 thin sections) in well 16/8a-4. Sample depths range from the top of the reservoir (3986 m) down to 4141 m which is in the water leg (OWC at 4030 m).

3.3 Reservoir quality

The poroperm data from the Miller and Kingfisher Fields are analysed in this section. Permeability data were available only for wells in the Miller Field and show good correlation with the porosity data (Fig.10). For this reason, the reservoir quality analysis below is described in terms of porosity only.

In the North Sea hydrocarbon provinces, porosity in most arenitic sandstone reservoirs appears to follow a linear porosity versus depth trend that can be expressed as $\phi=\phi_0$ - G.Z, where ϕ_0 is the porosity at the time of deposition, G is the porosity depth gradient, and Z is burial depth (Ramm et al., 1997). Across the range of burial depths at which North Sea petroleum reservoirs are usually found (ca. 1.5-5.5 km), the porosity loss gradient G ranges from 6 %/km (Bjørlykke et al., 1989) up to 9 %/km (Selley, 1978; Bjørlykke et al., 1989). Overall, a regional North Sea porosity loss gradient of about 8 %/km provides a good estimate (Emery et al. 1993).

According to this gradient, porosity in the Brae Formation reservoir in the Miller Field is expected to range from 13 % in the top of the reservoir (3990 m) to 12 % at the OWC (4090 m) (Fig.11). The core He-porosity data from the Miller Field (Fig.11) range from these normal expected values to exceptionally high porosities of up to 22 %. Detailed analysis indicates that most high porosities are found in the oil leg of the reservoir (3980-4090 m) (Table 4; Fig.12). Overall, the oil leg in the Miller Field has a higher average porosity value (19.1±1.4 %) than the water leg (14.3±0.5 %). Water leg porosities are in agreement with values expected at around 4 kilometres burial.

In the Brae Unit 1 (3885 to 3959 m) and Unit 2 (3986 m to OWC at 4030 m) reservoirs in the Kingfisher Field, porosities expected according to the North Sea trend are between 14 and 13 % (Fig.11). The Unit 1 gas condensate reservoir in the Kingfisher Field appears overall anomalously porous (22.1±4.3 %) (Fig.11 & 13). Note that no water leg data are available from this reservoir. The Unit 2 oil reservoir

shows little reservoir quality variation across the OWC (Fig.11 & 13). Oil and water leg average porosities are 14.4±1.4 % and 13.2±0.6 % respectively.

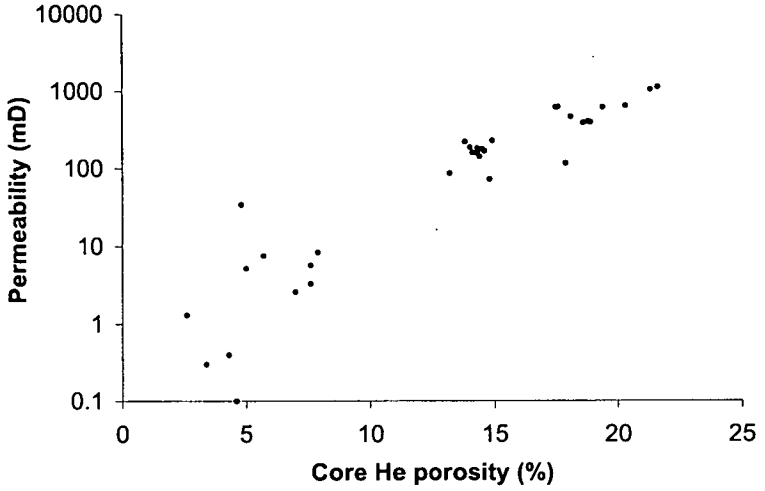

Fig.10 Porosity versus permeability plotted for thin sections examined from the Miller Field. The correlation coefficient between the datasets is 0.8 (25 samples; >99.9% significant). All data come from core plug analyses carried out by BP-Amoco.

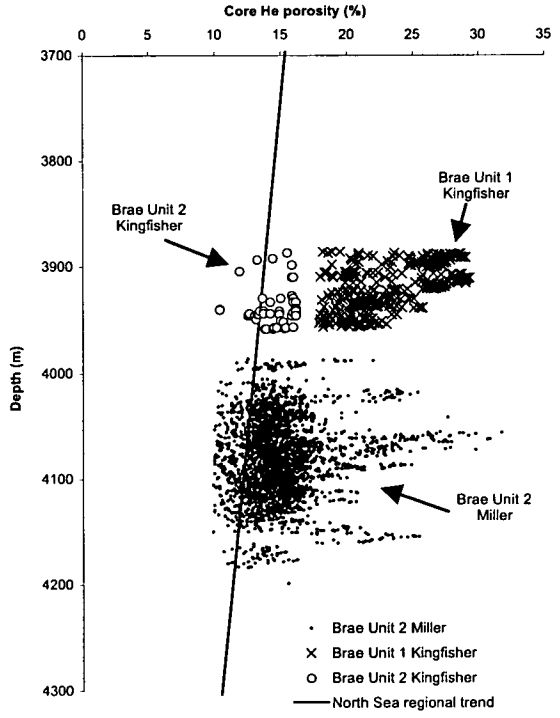

Fig.11 Porosity in the Brae Formation reservoirs in the Miller and Kingfisher Fields in comparison to the regional North Sea trend. This shows a range from high to normal porosity in the reservoir in the Miller Field, anomalously high porosity in the Brae 1 reservoir in the Kingfisher Field, and normal porosity in the Brae 2 reservoir in the Kingfisher Field.

The porosity data from all reservoirs were split into three different reservoir quality groups. The normal reservoir quality group contains data with porosity values between 10 and 15 %. All rocks with porosity values below or above these normal expected porosity values were categorised in a low and high reservoir quality group respectively. In Table 2, average porosity and permeability data from the different reservoir quality groups are listed for each well examined. From examination of well logs it is clear that low poroperm intervals correspond in the reservoirs with interbedded clay or silt layers, or localised carbonate cemented horizons. The normal and high poroperm rocks correspond to the actual reservoir sandstones.

Table 2 Well average porosity and permeability values of high, normal and low reservoir quality groups in the Brae Formation sandstones in the Miller and Kingfisher Fields. Normal reservoir quality is defined as being within the expected range of porosity values for a specific burial depth according to the regional North Sea porosity trend. At 4 km burial (Miller and Kingfisher Fields), this is around 13 to 14 %. Porosities above or below these values were categorised in a high and normal reservoir quality group of rocks respectively. All porosity values are core He-porosity values (n=number of measurements). Data from the Miller Field were provided by BP-Amoco. Data from the Kingfisher Field came from Shell UK.

Field/Reservoir	Well	Depth interval (m TVD)	High reservoir quality group			Normal reservoir quality group			Low reservoir quality group		
			Porosity (%)	Permeability (mD)	n	Porosity (%)	Permeability (mD)	n	Porosity (%)	Permeability (mD)	n
Miller-Brae 2	7b-21	4010-4095	17.9 ± 0.6	119 ± 97	3	13.2 ± 1.7	88 ± 114	57	5.0 ± 2.9	5 ± 25	70
	7b-24	4036-4114	18.8 ± 1.5	417 ± 211	34	14.4 ± 1.5	145 ± 136	208	7.6 ± 2.2	3 ± 1	5
	7b-25	4086-4132	21.3 ± 2.5	1070 ± 948	26	14.3 ± 1.3	186 ± 161	125	7.9 ± 1.3	8 ± 13	6
	7b-28	4075-4175	18.9 ± 2.3	404 ± 488	19	14.8 ± 1.7	74 ± 136	37	4.6 ± 2.7	0 ± 0	15
	8b-2	4027-4073	17.6 ± 0.5	640 ± 244	4	14.0 ± 1.5	191 ±164	124	4.8 ± 3.4	35 ± 96	15
	8b-3	3988-4081	21.6 ± 2.4	1149 ± 791	35	13.8 ± 1.2	227 ± 242	238	7.0 ± 3.4	3 ± 6	23
	8b-5	4082-4158	20.3 ± 2.4	660 ± 453	63	14.3 ± 1.6	163 ± 202	93	4.3 ± 2.8	0 ± 1	44
	8b-A01	4021-4092	18.6 ± 1.5	396 ± 202	41	14.6 ± 1.3	172 ± 138	197	7.6 ± 2.3	6 ± 13	20
	8b-A02	3986-4124	18.1 ± 1.3	478 ± 341	25	14.5 ± 1.5	182 ± 165	434	3.4 ± 3.9	0 ± 1	55
	7b-A03	4022-4134	19.4 ± 2.8	634 ± 730	15	14.1 ± 1.4	162 ± 134	403	5.7 § 3.9	8 ± 40	58
	8b-A06	4065-4113	17.5 ± 0.5	631 ± 256	31	14.9 ± 1.6	233 ± 216	162	2.6 ± 3.7	1 ± 4	38
Kingfisher-Brae 1	8a-8	3885-3959	22.7 ± 3.9	no data	415	13.5 ± 1.1	no data	28	4.5 ± 3.9	no data	71
Kingfisher-Brae 2	8a-4	3986-4048	18.3 ± 1.3	no data	19	13.4 ± 1.0	no data	62	5.1 ± 2.0	no data	47

The abundance of normal, high and low reservoir quality groups in each reservoir is quite different (Table 3). In the Brae Unit 2 reservoir in the Miller Field, normal reservoir quality is the dominant group making up 76 % of the total reservoir. In the same reservoir, 11 % of the rocks are anomalously porous and net:gross is reduced by 13 % by low reservoir quality rocks (Facies 4 and 5) (Table 3). The Brae Unit 1 reservoir in the Kingfisher Field is almost entirely made up of very high quality sandstones (68 %) with only 5 % of the sands displaying normal poroperm values. Net:gross is here reduced by 27 % rocks of Facies 4 and 5. Also, in the Brae Unit 2 reservoir in the Kingfisher Field more mud interbedding occurs. Net:gross is reduced by 48 %. Of the actual reservoir sandstones, 46 % display normal porosity, while 6 % display high porosities. The higher abundance of low reservoir quality rocks in the Kingfisher Field is due to the distal fan depositional setting of the Brae Formation sandstones.

Table 3 Abundance of high, normal and low reservoir quality rocks throughout the examined Brae Formation reservoirs. Net:gross by low reservoir quality mudrocks (or calcite cemented sandstones) is reduced by 13 % in the Brae Unit 2 reservoir in the Miller Field, and by 27 and 48 % respectively in the Brae Unit 1 and Brae Unit 2 reservoirs in the Kingfisher Field. High reservoir quality rocks comprise maximum 11 % of the Brae Unit 2 sandstones in the Miller Field, but are hardly present in the age equivalent reservoir in the Kingfisher Field (6 %). In contrast, high reservoir quality rocks make up the bulk (68 %) of the Brae Unit 1 reservoir in the Kingfisher Field.

Field/Reservoir	High reservoir quality	Normal reservoir quality	Low reservoir quality
Miller-Brae 2	11%	76%	13%
Kingfisher-Brae 1	68%	5%	27%
Kingfisher-Brae 2	6%	46%	48%

The distribution of normal, low and high reservoir quality rocks in the reservoirs was examined. According to Smalley et al. (1993), the Brae Unit 2 reservoir in the Miller Field can be subdivided into several zones : J, K, L, M and N (Fig.12). These zones are separated from each other by shale layers (low reservoir quality rocks). In Fig.12 it can be seen that the K-L boundary shale extends over most of the south part of Miller Field and is regionally an important barrier to vertical fluid communication. The J-K boundary shale is a local barrier in the field crestal area, but is not continuous down the SW flank of the field. The L-M boundary shale forms a barrier in the crestal area. Numerous smaller shale barriers have been identified between and within zones in single wells. These may act as baffles during production from those wells, but are not likely to inhibit the vertical movement of fluids at the field scale (Smalley et al. 1993). High reservoir quality sandstone occurrences in the Miller Field are listed in Table 4. In almost every well a high poroperm sandstone layer occurs at the top of the reservoir. Along the crest of the field, this high poroperm layer appears to be laterally continuous (Fig.12) and reaches a maximum thickness of 13 m in crestal well 8b-3. High reservoir quality occurrences in other parts of the field are mainly located directly underneath shale barriers (Fig.12) and range in thickness between 0.6 and 10 m (Table 4).

The Brae Unit 1 reservoir in the Kingfisher Field (well 8a-8) is almost entirely composed of high reservoir quality rocks (Fig.13). Interbedded shale layers or carbonate cemented sandstone make up 27 % of the reservoir (Table 3). The normal reservoir quality sandstones appear to be located towards the bottom of the reservoir (Fig.13).

In the Brae Unit 2 reservoir in the Kingfisher Field, reservoir quality is much reduced by interbedded mudstone layers (Fig.13). The bulk of the reservoir is composed of normal poroperm sandstones. No layers or zones of high reservoir quality rocks could be differentiated.

Table 4 Occurrence of high porosity layers in the examined wells in the Brae Formation reservoirs. High porosity in the Miller Field occurs mainly along the reservoir top. Other high porosity intervals in this reservoir are mainly located directly underneath shale barriers (data from BP). In the Brae Unit 1 reservoir in the Kingfisher Field, the high porosity intervals are almost continuous throughout the reservoir. They are interrupted only by small layers (max. 3.7 m) of interbedded shale or carbonate cemented sandstone. High porosity layers are not present in the examined well in the Brae 2 reservoir in the Kingfisher Field. High porosity rocks, which comprise 15 % of the bulk reservoir, are scattered throughout the reservoir interval.

Field/Reservoir	Well	Top reservoir (m TVD)	High porosity intervals (m TVD)	Thickness (m)	Average Porosity (%)
Miller-Brae Unit 2	7b-21	?	none		
	7b-24	4036.9	4036.9 - 4046.0	9.1	19.5
			4091.2 - 4096.2	5.0	17.7
	7b-25	approx. 4060.0	no info on 4060 - 4064		
			4064.0 - 4071.7	7.7	21.4
	7b-28	4075.0	4075.0 - 4078.2	3.2	18.0
			4131.2 - 4136.2	5.0	18.0
			4142.2 - 4145.4	3.2	16.8
	8b-2	approx. 4027.0	none		
	8b-3	3988.1	3988.1 - 4001.2	13.1	21.1
			4014.3 - 4015.5	1.2	15.4
			4023.1 - 4026.5	3.4	16.3
	8b-5	4082.2	4082.2 - 4087.7	5.5	19.4
			4119.1 - 4121.2	2.1	20.1
			4122.1 - 4123.7	1.5	18.9
			4125.2 - 4135.2	10.0	21.8
	8b-A01	4021.2	4021.2 - 4022.7	1.5	17.3
			4054.8 - 4055.2	0.4	18.6
			4056.5 - 4057.4	0.9	18.9
			4060.8 - 4064.3	3.5	19.5
			4064.9 - 4065.5	0.6	18.0
	8b-A02	3986.5	3986.5 - 3989.1	2.6	19.1
			4050.3 - 4057.8	7.5	15.7
	7b-A03	4022.2	4022.2 - 4026.3	4.1	22.5
	8b-A06	4065.3	4065.3 - 4067.7	2.4	16.6
			4083.3 - 4084.3	1.0	17.3
Kingfisher-Brae Unit 1	8a-8	3885.3	3885.3 - 3886.3	1	17.8
			3887.0 - 3892.1	5.1	25.8
			3893.5 - 3900.4	6.9	24.9
			3904.1 - 3924.3	20.2	24.4
			3927.0 - 3939.2	12.2	21.2
			3940.2 - 3941.2	1	19.1
			3941.9 - 3942.6	0.7	19.2
			3944.6 - 3945.3	0.7	20.5
			3945.7 - 3949.1	3.4	18.9
			3950.4 - 3956.6	6.2	19.6
Kingfisher-Brae Unit 2	8a-4	3986.2	none		

Rock samples for thin section preparation were taken mainly from sandstones of the normal and high reservoir quality groups. In the following paragraphs, the factors that may control high and normal reservoir quality in the Brae Formation sandstones are examined petrographically. An understanding of the factors that control poroperm in the reservoirs will allow insight into the distribution of the high poroperm layers. These high porosity-permeability layers could indicate hydrocarbon migration routes and are also important in terms of reservoir production planning strategy. Abnormally high porosities have been explained previously in published literature by retarded compaction in highly overpressured reservoirs (Ramm, 1992; Ramm & Bjorlykke, 1994). That mechanism however would result in overall high porosity throughout the reservoirs. Moreover, the Miller and Kingfisher Fields are not significantly overpressured (50 MPa) so this explanation can be rejected. The

porosity differences between sandstones of high and normal reservoir quality groups must therefore be linked to either textural or diagenetic differences.

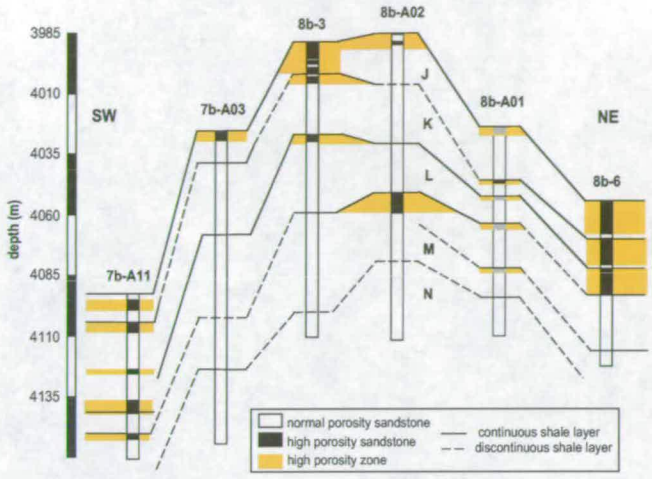

Fig.12 Distribution of normal, high and low reservoir quality rocks in some wells in the Miller Field. Low reservoir quality mudrocks form laterally extensive (solid lines) or local barriers (dashed lines) in the reservoir. The K-L boundary is regionally important. The L-M boundary forms a barrier in the crestal area. Numerous other smaller shale barriers can be identified. A continuous high porosity layer is present in the top of the reservoir, directly underneath the Kimmeridge Clay. Other high porosity zones are difficult to correlate. Throughout the reservoir, high porosity layers are positioned underneath shale layers. (After Smalley et al., 1993).

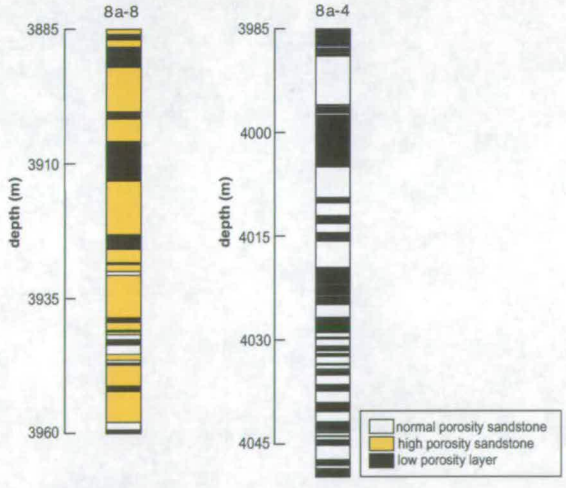

Fig.13 Interpretation of normal, high and low reservoir quality rock distribution in wells 8a-8 and 8a-4 in the Kingfisher Field based on core photograph books from Shell. Well 8a-8 (Brae Unit 1 reservoir 3885-3959 m) displays overall high porosity, interrupted by several low reservoir quality layers (mudrocks or carbonate cemented sandstone). Normal reservoir quality rocks appear occasionally within the high reservoir quality ones, and are located in the bottom half of the reservoir. Well 8a-4 (Brae 2 reservoir 3985-4048 m) displays an abundance of interbedded shales and is of poor reservoir quality. The good reservoir sandstone intervals are typically of normal reservoir quality. The high reservoir quality rocks never form clear high porosity zones or layers and therefore can not be indicated on the well interpretation figure.

3.4 Reservoir sandstone composition

Pointcount results are presented in Table 5. The mineralogical composition of the sandstones was plotted following the scheme of McBride (1963). The thin sections examined plot within the arenite, subarkose and sublith-arenite compositional areas of the plot (Fig.14). Mineral abundances mentioned below are all percentages calculated as for detrital framework mineralogy.

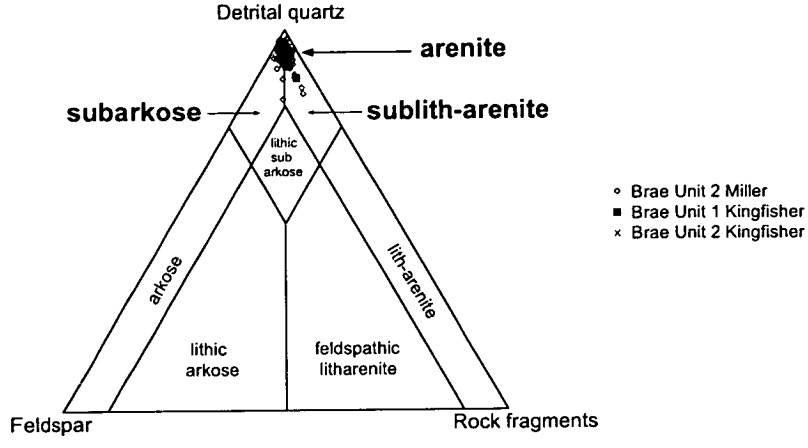

Fig.14 Mineralogical data of the Brae Formation sandstones plotted on the scheme of McBride (1963). All data presented are percentages as calculated for depositional detrital framework mineralogy. Data from all three reservoirs plot within the arenite, subarkose or sublith-arenite area.

In all reservoirs, quartz is the most abundant component comprising 87.9±4.4 % of the detrital framework mineralogy in the Unit 2 reservoir in the Miller Field, 82.5±3.7 % and 82.2±2.1 % in the Brae Unit 1 and Unit 2 reservoirs respectively in the Kingfisher Field (Fig.15). Most quartz is monocrystalline, but composite or polycrystalline quartz is common.

Detrital clay is the second most abundant component of the Brae Formation sandstone reservoirs (Fig.15). This clay does not appear crystalline under the SEM and occurs mainly at grain contacts or as pore filling patches. In the Miller Field, abundance is generally around 3.2±2.3 %. In some thin sections detrital clay abundance can be up to 25 %. Such thin sections come from small interbedded mudstone layers in-between the main reservoir sandstone. They are therefore not representative of the bulk of the reservoir rock. More detrital clay is found in the Brae Formation sandstones in the Kingfisher Field, compared to the Miller Field. Since these sands are distal fan deposits this is hardly surprising. Clay abundance in the Unit 1 reservoir in Kingfisher Field is 6.3±2.2 %. The Unit 2 reservoir contains slightly more detrital clay (7.0±1.9 %) (Fig.15).

Table 5 Thin section point-count results (500 counts/thin section) for the Brae Formation sandstones in the Miller and Kingfisher Fields. K-feldspar abundances were verified by image analysis of SEM backscatter images. All quartz cement abundances were determined by means of SEM-CL and image analysis. Porosity is locally reduced to zero by calcite cementation (calcite cemented samples are shaded grey in the Table).

Field/ Reservoir	Well	Depth	Detrital Minerals					Authigenic Minerals				Organic Material			Porosity		
			Quartz	K-feldspar	Rock Fragments	Clay	Mica	Quartz Cement	Calcite	Clay	Pyrite	Organic Material	Sponge Spicules	Shell Fragments	Primary Porosity	Secondary Porosity	Total Porosity
		TVD ss (m)															
Miller-Brae 2	7b-AO3	4022.7	61.0	2.6	3.2	2.6	0.8	4.8	0.4	1.6	0.4	0.4			17.0	5.2	22.2
		4022.9	57.8	2.4	4.2	2.2	0.4	4.4	0.2	1.6	0.2	1.2			19.8	5.6	25.4
		4023.1	58.6	2.2	4.2	3.4	1.2	5.2	1.6	2.2	0.4	1.6			15.4	4.0	19.4
		4024.8	71.2	2.8	3.4	1.2	0.6	6.0		1.8	0.2	3.2			8.6	1.0	9.6
		4025.0	60.4	2.6	3.4	2.6		5.4	0.2	2.2	0.4	1.6			18.6	2.6	21.2
		4025.3	59.2	2.2	2.0	0.6		6.0	0.4	1.2	0.8	1.6			19.8	6.2	26.0
		4026.2	67.5	1.6	3.0	5.4		4.9			0.6	0.0			16.0	1.0	17.0
		4027.6	48.6	1.4	1.0	27.2	2.4	5.6		0.6	0.2	10.0			3.0		3.0
		4029.4	74.0	2.4	1.6	2.0	0.2	5.8		0.6		1.0			12.2	0.2	12.4
		4031.8	66.4	2.4	2.2	1.2	0.6	7.6	0.2	4.2	0.2	0.6			13.8	0.6	14.4
		4034.0	67.2	2.6	3.4	1.0		8.2		2.2		1.2			12.4	1.8	14.2
		4036.4	63.0	2.0	4.2	5.0	1.2	9.2		2.2	0.2	1.0			11.4	0.6	12.0
		4036.8	62.8	2.4	2.0	3.0	0.2	8.4	2.0	3.6	0.2	2.6			12.6	0.2	12.8
		4038.7	66.6	2.8	1.0	1.6		9.6	0.6	2.0		0.2			15.4	0.2	15.6
		4041.0	60.5	2.6	2.2	5.0	1.2	11.1	1.6	1.6	0.2	1.2			12.2	0.6	12.8
		4043.1	20.6	2.4	2.2	19.6	1.0	7.6		1.0	0.2	39.0			6.4		6.4
		4043.6	67.0	2.0	0.4	2.2	0.2	7.8	1.0	2.6	0.2	1.2			14.8	0.6	15.4
		4045.7	69.2	2.8	0.6	2.0	1.0	7.4	1.0	2.2	0.2	0.6			13.0		13.0
		4048.0	68.2	1.8	3.2	1.2		8.2		2.0		1.2			12.4	1.8	14.2
		4049.5	65.8	2.0	4.2	4.2	0.6	9.4	0.2	1.2	0.2	0.2			11.0	1.0	12.0
		4051.6	71.4	1.0	1.6	1.2		8.4	0.2	1.6		0.0			13.8	0.8	14.6
		4052.7	63.1	2.0	2.6	3.0	1.2	10.5	1.2	2.0	0.2	0.2			14.0		14.0
		4054.9	68.0	1.0	2.4	1.0	0.6	9.6	0.6	2.2	0.2	0.6			13.2	0.6	13.8
		4057.2	65.0	2.2	2.2	1.6	0.2	8.0	0.2	3.0		0.6			16.0	1.0	17.0
		4059.5	70.6	2.0	2.6	0.8	0.2	7.4		2.0		0.6			11.8	2.0	13.8
		4061.9	70.7	2.4	0.6	3.2	0.2	6.3	1.0	2.2		0.0			13.4		13.4
		4063.7	69.8	1.4	1.6	3.6		7.2	0.6	0.2	0.6	0.6			13.4	1.0	14.4
		4064.0	69.0	1.6	1.6	3.0	0.2	10.0	0.2		0.6	0.0			13.2	0.6	13.8
		4065.1	68.6	1.6	0.6	2.2	1.6	7.2		0.2	0.2	10.2			7.6		7.6
		4065.8	39.2	2.6	0.6	17.0	2.6	5.0		0.6	1.2	25.6			5.6		5.6
		4066.5	48.3	2.0	4.6	15.2		7.7	1.0	1.8	0.6	2.6			15.4	0.8	16.2
		4067.0	56.0	2.4	7.6	9.2	4.0	7.0		0.6		5.2			8.0		8.0
		4068.2	60.1	2.4	1.0	8.2	1.0	8.9		1.2		0.0			16.6	0.6	17.2
		4068.9	51.8	2.4	8.0	8.6	1.2	7.2	1.0	0.2		6.0			13.0	0.6	13.6
		4070.0	65.8	1.6	2.8	1.4	0.8	7.4		2.2		2.0			15.0	1.0	16.0
	8b-3	3989.9	60.3	2.8	6.0	1.4	0.6	2.7		1.2		1.8			19.8	3.4	23.2
		3992.3	55.8	2.8	2.0	1.6	0.2	0.8	35.4		0.2	0.2	0.2	1.0			
		3993.8	62.0	2.6	3.4	2.0	0.2	5.0		0.8	0.2	2.2			18.4	3.2	21.6
		3996.9	60.4	2.0	3.0	2.2	1.0	3.2		0.6	0.2	4.2	0.2	0.4	19.2	3.4	22.6
		4039.6	71.5	0.4	3.0	1.2		7.1	0.4	0.4	0.6	2.0		0.2	11.6	1.6	13.2
		4116.0	66.4	2.2	3.4	1.2	0.2	10.6	0.2	0.8		1.6			11.8	1.6	13.4
	7b-24	4045.5	62.8	2.2	3.8	2.4	0.6	5.8	0.6	1.4	0.2	1.6			16.2	2.4	18.6
		4062.7	69.0	3.0	2.0	2.6	0.6	6.0		0.6	0.2	1.0			14.6	0.6	15.0
		4062.8	66.8	3.0	1.6	0.6	0.2	3.6	9.8			0.6			13.4	0.4	13.8
		4063.0	64.0	3.0	0.6	2.0	1.0	3.0	10.0		0.6	2.0			13.6	0.2	13.8
		4063.4	64.8	3.6	1.0	1.0	0.6	4.0	11.4			0.6	0.2		12.2	0.6	12.8
		4063.8	60.0	3.4	1.0	3.2	1.2	1.2	25.2		0.6	3.0		1.0	0.2		0.2
		4064.2	57.5	4.5	4.0	5.2	2.0		19.4		2.0	5.0	0.2	0.2			
		4064.3	69.0	4.0	1.5	2.0	0.5	1.0	19.2		0.6	2.0			5.6		
		4064.5	65.0	2.0	3.0	3.6	0.6	8.6	0.4	0.2	0.4	1.6			14.0	0.6	14.6
		4071.9	66.6	2.2	2.8	1.4	0.2	9.0		1.6		1.2		0.2	12.8	2.0	14.8
		4112.9	62.2	2.4	3.8	1.8	0.6	12.6		1.2	0.2	1.0			12.0	2.2	14.2
	8b-5	4086.5	65.0	0.6	3.4	4.8	0.8	10.0		0.4	0.2	0.2			12.6	2.0	14.6
		4145.0	66.0	1.4	4.4	1.8	0.6	10.4		0.8		1.0		0.2	12.2	1.2	13.4
		4300.8	60.3	1.2	4.0	0.6	1.4	14.9	0.6	2.4	0.4	1.4	0.2	0.2	11.0	1.4	12.4
	8b-AO6	4065.5	65.4	2.0	3.8	2.4	0.4	8.0		1.0		0.4			14.2	2.4	16.6
		4074.4	67.9	0.8	2.4	0.8	0.2	9.3		1.0		1.6			14.2	1.8	16.0
		4102.2	64.8	1.6	4.8	1.2		11.4		1.0	0.2	1.0			12.0	2.0	14.0
		4110.4	65.4	1.8	2.8	1.0	0.6	11.4	0.2	1.4	0.6	1.0			11.8	2.0	13.8
		4111.7	48.1	2.1	2	2	1	0.2	39.6		0.6	2.2	0.2	2			
	7b-26	4101.3	65.9	1.4	1.8	1.6	1.0	12.1		0.8	0.6	0.2			11.6	2.0	13.6
		4141.3	60.4	1.8	2.2	1.6	1.4	15.4		1.2	0.4	1.0			12.6	2.0	14.6
		4186.4	61.7	2.2	2.8	2.2	1.4	14.1		2.4	0.2	0.6			10.6	1.8	12.4
	7b-28	4080.9	69.4	2.4	1.0	1.0	0.4	9.0	1.0			0.4			14.4	1.0	15.4
		4081.1	50.3	3.7	2.0	2.2	0.2	0.2	34.4		0.6	4.6	0.2	1.8			
		4081.5	59.4	0.4	1.2	1.6	0.2	0.2	32.8			1.0		3.2			
		4082.6	51.7	1.3	0.2	2.0	0.6	1.0	39.0		0.6	1.0		2.6			
		4084.4	53.9	2.9	2.0	1.2	0.2	0.2	37.2		0.2	0.6		1.6			
		4084.8	69.7	1.1	1.6	1.0	0.6	0.2	24.2		0.6	0.6		0.4			
		4085.3	64.8	3.0	2.0	2.4	0.4	9.4	0.4	0.4		3.0			14.0	0.2	14.2
	8b-A10	4094.2	54.0	2.2	1.6	3.0	0.2	0.6	31.8		1.2	3.0	0.2	2.2			
		4103.1	51.0	1.8	1.6	2.0	0.2	0.2	38.4		0.6	1.8		2.6			
		4105.1	57.8	1.8	2.0	1.2	0.2	1.0	33.6		0.6	1.2		0.6			
		4105.4	64.3	1.9	1.0	1.6	0.6	12.0	1.0	0.4	0.2	13.0			4.0		4.0
Kingfisher-Brae 1	8a-8	3885.6	61.3	2.1	2.2	3.2	0.2	6.8		0.2		0.6	1.2	0.6	19.6	2.0	21.6
		3887.5	55.0	2.1	2.6	5.0	1.6	4.1	1.0	0.6		0.8	1.2	0.6	23.2	2.2	25.4
		3888.9	56.2	2.0	2.0	4.2	0.6	3.2	1.2	0.2	0.2	0.8	0.8	0.4	27.6	0.6	28.2
		3890.6	57.2	2.2	2.2	4.0	1.0	3.4	1.2	1.0	0.2	0.2	0.6	0.2	24.0	2.6	26.6
		3892.0	59.7	2.5	2.6	3.6	0.6	4.0	3.2	0.2		0.2	0.6	0.6	20.0	2.2	22.2
		3894.6	58.0	2.3	2.0	2.6	0.2	3.5	2.2	1.2		0.2	1.0	0.6	24.6	1.6	26.2
		3896.5	56.6	2.2	2.0	3.6	0.2	3.2	2.2		0.2	1.2	0.6	2.0	23.4	2.6	26.0
		3898.3	55.8	2.3	3.2	3.0	1.2	3.7	1.6	1.2	0.6	0.2	1.6	2.2	18.4	5.0	23.4
		3900.0	55.4	2.2	3.0	4.0	1.0	3.6	2.6	0.6	0.2	0.6	0.2	1.2	22.4	3.0	25.4
		3900.9	54.0	2.2	2.6	0.6	0.6	0.6	36.4		0.2	1.0	0.2	1.6			
		3901.4	52.6	2.7	1.6	0.6	0.6	1.0	37.9		0.6	1.2	0.2	1.0			
		3901.8	54.6	2.4	1.6	1.0		1.0	35.8			0.6	1.0	2.0			
		3902.5	50.4	1.8	3.0	0.6	0.6	0.6	38.0		0.2	1.0	1.6	2.2			
		3903.4	52.8	2.5	2.6	0.2	0.6	0.6	36.6		0.6	0.2	1.0	2.2			
		3904.0	51.6	2.4	3.0	1.0	0.2	1.0	34.6		1.0	0.6	2.4	2.0			
		3904.2	49.0	2.0	5.0	6.2	0.2	5.2	4.2	1.0	0.2	1.6	1.0	1.6	20.8	2.0	22.8
		3913.3	59.3	1.3	1.6	1.2	0.2	3.8	0.2	0.2	0.2	1.8	0.6	0.6	26.0	3.0	29.0
		3913.6	66.6	1.8	3.0	0.2	0.2	1.0	24.0			0.2	1.0	1.0	1.0		1.0
		3913.9	57.0	1.6	1.6	0.2	0.2	0.6	35.4		0.6	0.2	1.0	1.6			
		3914.1	50.4	2.7	2.2	0.2	0.6	1.6	37.7			1.2	2.0	1.4			
		3914.6	54.3	1.0	2.6	1.0	0.2	2.0	35.9			1.0	1.4	0.6			
		3914.9	54.7	2.3	1.6	0.2	0.6	2.0	36.0				1.6	1.0			
		3915.5	59.4	2.2	2.6	5.2	0.6	5.6	1.2	0.2	0.6	2.2	0.2	0.6	18.4	1.0	19.4
		3929.5	58.9	1.8	2.6	5.0		6.1	1.6		1.0	1.6	0.2	0.6	18.6	2.0	20.6
		3938.4	55.8	1.2	1.2	5.0	0.2	5.6	2.6	1.0		1.6	0.2	1.0	23.0	1.6	24.6
		3947.2	57.8	2.2	3.0	7.2	1.6	5.8	1.2	2.0	0.2	0.2	0.6	0.2	16.4	1.6	18.0
		3955.1	57.3	1.9	3.0	7.2	0.6	4.8	2.0	0.6		2.2	0.2	0.6	18.6	1.0	19.6
Kingfisher-Brae 2	8a-4	3989.7	58.8	0.8	2.6	3.2	0.8	10.4	0.4	0.8	0.2	4.0	0.4	0.6	15.3	1.7	17.0
		3995.2	59.6	1.2	3.4	3.6	0.8	9.8	2.2	0.8	0.4	3.6	0.4		13.7	0.5	14.2
		4004.7	61.2	0.8	3.0	4.4	0.6	10.4	0.2	0.6	0.4	4.8	0.2	0.2	11.7	1.5	13.2
		4010.4	65.5	0.6	1.6	4.0	0.6	8.7	0.8	1.2	0.2	3.4			12.6	0.8	13.4
		4015.1	64.4	1.6	2.6	4.6	0.8	8.4	0.2	0.8	0.2	2.2			13.0	1.2	14.2
		4019.0	58.7	0.7	1.2	5.4	0.6	12.2		0.6	0.6	7.0			12.0	1.0	13.0
		4022.1	57.4	2.4	3.2	1.0	0.6	0.2	32.4		1.6	0.2	0.2	0.8			
		4023.6	58.2	1.8	1.8	6.2	0.4	10.2	0.6	1.2	0.4	5.2			11.2	2.8	14.0

Table 5 Continued.

Field/ Reservoir	Well	Depth TVD ss (m)	Detrital Minerals Quartz	K-feldspar	Rock Fragments	Clay	Mica	Authigenic Minerals Quartz Cement	Calcite	Clay	Pyrite	Organic Material Organic Material	Sponge Spicules	Shell Fragments	Porosity Primary Porosity	Secondary Porosity	Total Porosity
Kingfisher-Brae 2	88-4	4028.8	59.8	1.1	1.8	6.2	0.8	10.5	0.2	0.8	0.2	2.6			15.0	1.2	16.2
		4030.3	61.6	1.7	3.0	4.0	1.0	11.1	0.4	1.0	0.8	2.2	0.2		12.0	1.0	13.0
		4033.7	62.1	1.3	1.6	7.8	0.4	9.4	1.4	0.2	0.6	1.6			12.2	1.4	13.6
		4053.9	61.4	1.0	2.4	4.8	0.6	12.0	0.4	0.2	0.4	3.4	0.2		13.0	0.2	13.2
		4081.0	58.6	1.6	3.2	6.2	1.4	12.0		0.4		2.6			13.2	0.8	14.0
		4094.5	57.7	2.3	1.6		1.0	1.4	34.6		0.4	1.0					
		4126.1	61.2	1.0	3.2	7.2	1.0	11.0	0.2	0.4	0.2	2.2			11.4	1.0	12.4
		4141.4	68.2	2.2	1.6	7.4	1.0	4.2	11.2	0.2	0.4	2.0			1.4		1.4

Rock fragments comprise a further 3.8±1.9 % of the Brae Formation sandstones in the Miller Field (Fig.15). In the Kingfisher Field, 3.7±1.3 % rock fragments are present in the Unit 1 reservoir and 3.3±1.0 % in the Unit 2 reservoir (Fig.15). Sedimentary rock fragments are commonly chert, siltstone and mudstone clasts. The siltstone fragments are mainly composed of quartz, micas and clay. Metamorphic rock fragments are also common and show micas of moderate to high birefringence and grains are typically oriented in one direction.

Feldspar abundance is similar in all Brae Formation reservoir sandstones : 2.8±0.8 % in the Miller Field, 2.9±0.5 % in the Unit 1 reservoir in the Kingfisher Field and 1.6±0.5 % in the Unit 2 reservoir in the Kingfisher Field. K-feldspar is the most common feldspar type present. Microcline and plagioclase are observed occasionally. K-feldspar is often partly dissolved.

Muscovite and organic material are minor constituents of the detrital framework in all reservoirs. Muscovite abundance is 0.7±0.6 % in the Miller Field, 0.9±0.7 % and 1.0±0.4 % in Unit 1 and 2 respectively in the Kingfisher Field. In the Miller Field reservoir, the abundance of organic material is 1.3±0.9 %. In a few thin sections organic matter abundances range from 10 to 25 %. Again, these thin sections are not representative of the bulk sandstone reservoir rock and were sampled in thinly interbedded coaly seams (Fig.16A). In the Brae Formation reservoir in the Kingfisher Field, organic matter abundance is 1.3±0.9 % in Unit 1 and 3.6±2.4 % in Unit 2. Organic material occurs usually as porefilling patches. Occasionally plant fragments can be clearly recognised (Fig.16B).

The sandstones in the Miller Field and the time equivalent Brae Unit 2 distal deposits in the Kingfisher Field contain very little bioclastic material (<1 %) (Fig.17A). Carbonate shells and sponge spicules composed of chert are observed occasionally in the sandstones, and also in places where the sandstones are completely calcite cemented (Fig.17B). The younger Brae Unit 1 deposits in the Kingfisher Field contain more sponge spicules and calcite shells (2.0±1.1 %) compared to the Brae Unit 2 deposits (Fig.17C & D). Also here, the spicules and shells are preserved both within and outside calcite concretions. The slightly higher abundance of bioclastic material seems to be characteristic of the sands sourced from the Northwest in the Brae area, and is also observed in the North Brae Field (McClure & Brown, 1990).

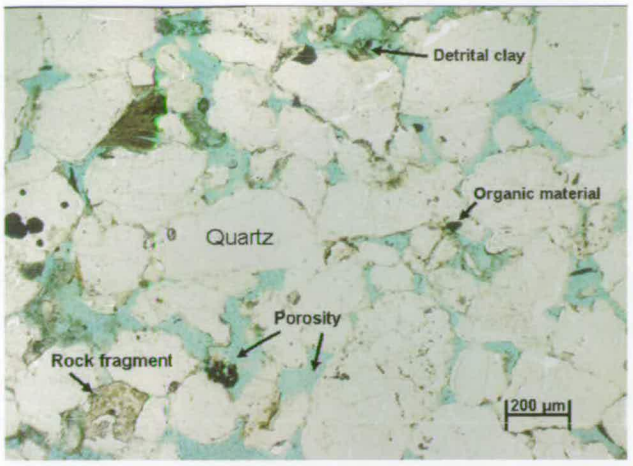

A Miller, Brae Unit 2
7b-26 / 4101.3 m

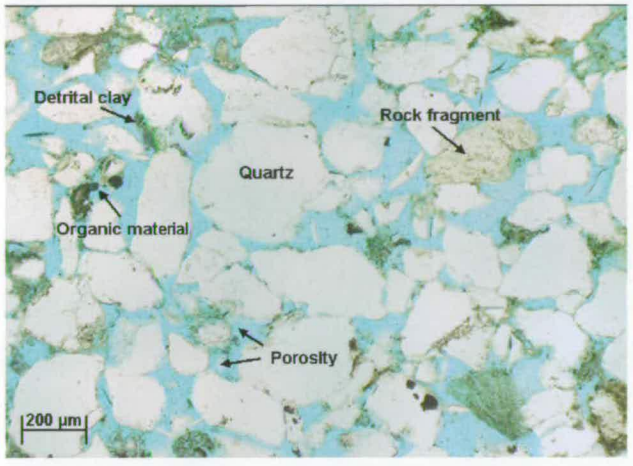

B Kingfisher, Brae Unit 1
8a-8 / 3887.5 m

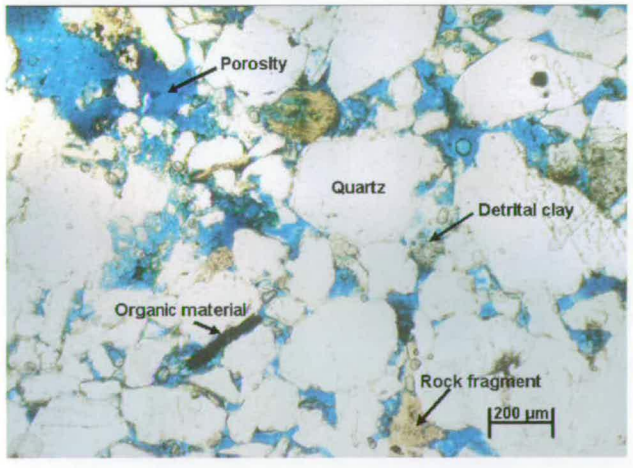

C Kingfisher, Brae Unit 2
8a-4 / 3989.7 m

Fig.15 Overview photomicrographs of the Brae Formation sandstones in the Brae Unit 2 reservoir in the Miller Field (**A**), the Brae Unit 1 reservoir in the Kingfisher Field (**B**) and the Brae Unit 2 reservoir in the Kingfisher Field (**C**). The sandstone in all three reservoirs is mainly composed of quartz and porespace (blue). Small amounts of detrital clay, rock fragments and organic matter can be recognised. The sands are all medium grained and moderately sorted.

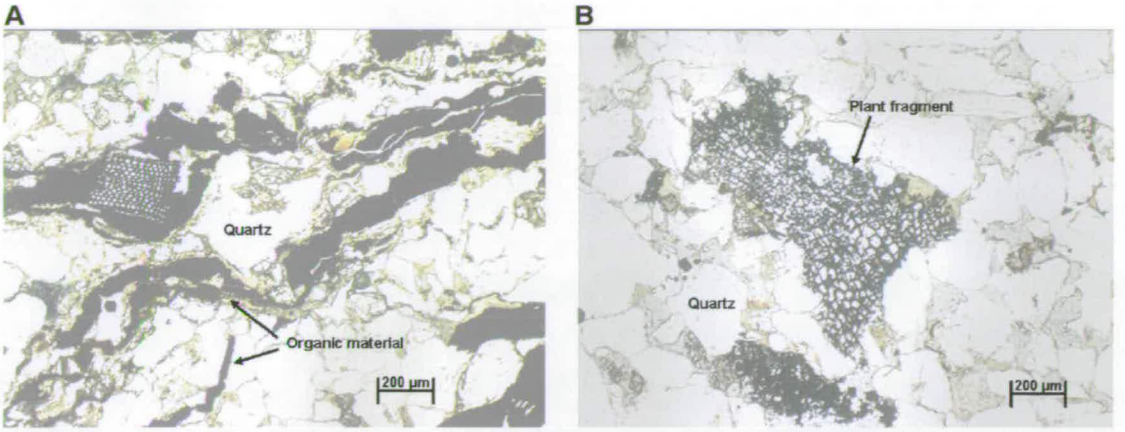

Fig.16 Photomicrographs of organic material in the Brae Formation sandstones. Abundant organic matter is occasionally observed in thinly interbedded coaly seams in the sandstones (**A**). Photomicrograph (**B**) shows a fragment of wood. Both samples are from well 7b-A03 in the Miller Field. Sample depths are 4043 m (**A**) and 4034 m (**B**).

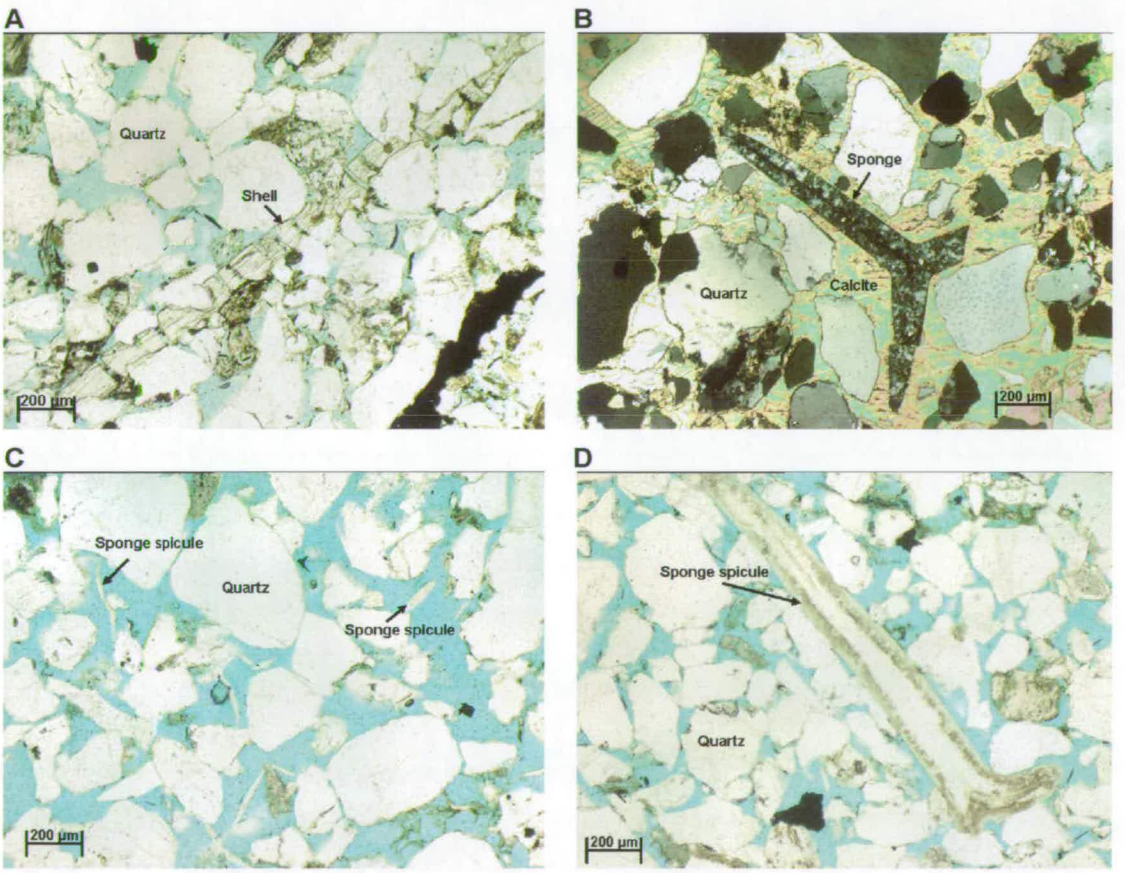

Fig.17 Photomicrographs of bioclastic material in the Brae Formation sandstones. In Unit 2 sands, carbonate shells are occasionally observed (**A**). Bioclasts in these sands are more commonly preserved in early calcite cemented parts, such as the sponge spicule shown in (**B**). Sponge spicules, and also shells, are more frequently encountered in the Brae Unit 1 sandstones. Spicules range in size from around 150 µm (**C**) to >1 mm (**D**). Samples A and B are from well 8b-3 in the Miller Field (sample depths 3993.8 and 3992.3 m). Samples C and D are from well 8a-8 in the Kingfisher Field (sample depths 3888.9 and 3890.6 m).

3.5 Texture

Beard and Weyl's (1973) experiments show the important role played by sorting in controlling porosity, and of grainsize in determining permeability, in sandstones. Well sorted sands yield better porosities than poorly sorted ones and permeability decreases as grainsize becomes finer. In order to evaluate textural control on the porosity and permeability differences between sandstones of normal and high reservoir quality groups, grainsize and sorting of the Brae Formation sandstones in thin sections was determined. The low reservoir quality group thin sections (carbonate cemented and mudrock) are excluded from the discussions below because they are not important in terms of reservoir rock volume. Results are presented in Table 6.

The Brae Formation sandstones in the Miller Field are medium-grained (328±78 μm) and moderately to well sorted. In the Kingfisher Field, the sands are also medium-grained and moderately sorted. Average grainsize in the Brae Formation Unit 1 and Unit 2 reservoirs in the Kingfisher Field is 310±36 μm and 324±31 μm respectively. Cross plots of permeability versus grainsize and porosity versus sorting are shown in Fig.18.

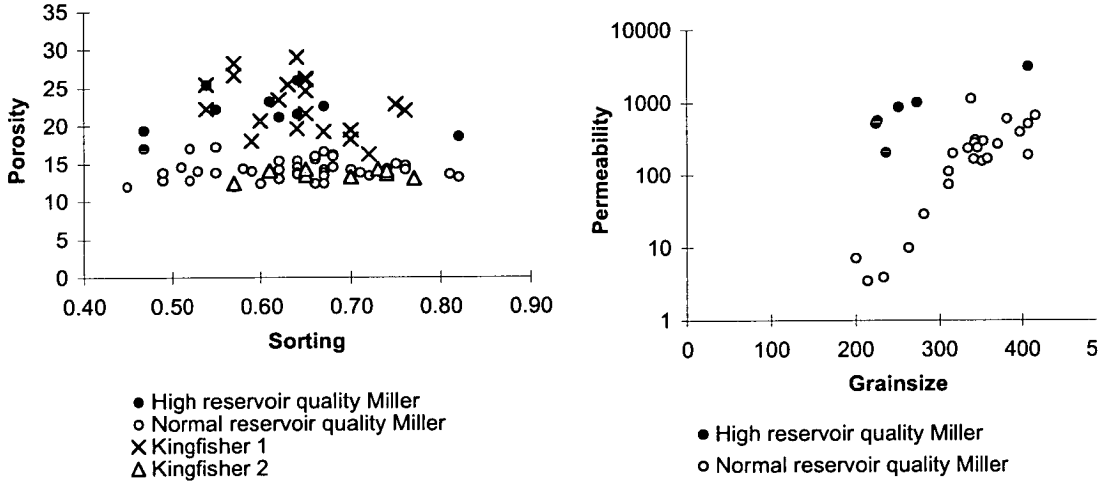

Fig.18 Cross-plot of porosity (%) versus sorting (phi standard deviation of grainsizes) (**A**) and permeability (mD) versus grainsize (μm) (**B**) for data from the Miller and Kingfisher Fields. All porosity data are thin section pointcount data. Permeability data are core measurements provided by BP-Amoco and their corresponding grainsizes were determined on thin sections made from the core plugs.
A There is no relation between porosity and sorting in the examined thin sections. Both high and normal porosity sandstones display a similar range in sorting values.
B There is a good correlation between permeability and grainsize in the normal and high reservoir quality group sandstones from the Miller Field. The coarse-grained sands display higher permeability than the finer-grained sands. Grainsize values for high and normal reservoir quality group samples straddle the same range.

If sandstone texture was the cause of the porosity difference between the high and normal reservoir quality sandstones in the Brae Formation reservoirs, then we should see that high reservoir quality group samples are coarser-grained and better sorted than the normal reservoir quality group samples. Fig.18A shows no obvious relationship between porosity and sorting in the thin sections examined. In the Miller Field, both high and normal porosity sandstones display a similar range in sorting values. Also in the Kingfisher Field there does not appear to be a relationship between porosity and sorting. The high porosity sands in Unit 1 display similar sorting values to the normal porosity sands in Unit 2. This illustrates that the porosity differences are not the result of sorting differences in these sediments.

From Fig.18B it can be seen that there is a good correlation between permeability and grainsize in the normal reservoir quality group sandstones in the Miller Field. The coarser-grained sandstone samples display higher permeabilities than the finer-grained samples. However, the high reservoir quality group sandstones display a similar range in grainsizes to the normal reservoir quality group sandstones, but their permeabilities are much higher. This illustrates that grainsize is not the controlling factor on the high permeabilities of high reservoir quality group sandstones. For the Brae Formation reservoir in the Kingfisher Field I was unable to plot grainsize versus permeability due to the lack of permeability data.

Textural analysis illustrates that the high porosity-permeability layers in the Brae Formation sandstones in the Miller Field are not of depositional origin. Also, the control on why the whole of the Unit 1 reservoir in the Kingfisher Field is of high reservoir quality, whilst the Unit 2 reservoir is of normal reservoir quality, appears not to be texturally related. The reservoir quality difference between the "high" and "normal" porosity sandstones must therefore be diagenetically controlled.

Table 6 (p.42) Textural characteristics of the Brae Formation sandstones in the Miller and Kingfisher Fields. The bulk of the sandstones are medium-grained and moderately sorted. Sorting is quantified as the standard deviation of grainsizes (phi-scale) measured in each sample (Folk, 1966). No relation between sorting and porosity was detected. All porosity values are pointcount values. In well 7b-A03 (Miller Field), permeability systematically varies with grainsize within normal as well as within high reservoir quality groups. Grainsizes from both groups straddle the same values. Textural data cannot explain the presence of different reservoir quality groups in the Brae Formation sandstones. Calcite cemented samples are shaded grey in the Table.

Field/ Reservoir	Well	Depth (TVD m)	Average Grainsize (μm)	Phi	Wentworth Size Class	Phi St. Dev.	Sorting	Porosity (%)	Permeability (mD)
Miller -	7b-AO3	4022.7	226	2.1	fine	0.55	moderately sorted	22.2	568
Brae Unit 2		4022.9	251	2.0	fine	0.54	moderately sorted	25.4	875
		4023.1	224	2.2	fine	0.47	well sorted	19.4	519
		4024.8	136	2.9	fine	0.50	well sorted	9.6	0.17
		4025.0	273	1.9	medium	0.62	moderately sorted	21.2	1010
		4025.3	407	1.3	medium	0.64	moderately sorted	26.0	3110
		4026.2	236	2.1	fine	0.47	well sorted	17.0	206
		4027.6	97	3.4	very fine	1.12	poorly sorted	3.0	5.4
		4029.4	370	1.4	medium	0.66	moderately sorted	12.4	266
		4031.8	341	1.6	medium	0.58	moderately sorted	14.4	185
		4034.0	311	1.7	medium	0.67	moderately sorted	14.2	74
		4036.4	200	2.3	fine	0.45	well sorted	12.0	7.2
		4036.8	214	2.2	fine	0.49	well sorted	12.8	3.5
		4038.7	416	1.3	medium	0.66	moderately sorted	15.6	658
		4041.0	263	1.9	medium	0.52	moderately sorted	12.8	10
		4043.1	256	2.0	fine	0.54	moderately sorted	6.4	4.3
		4043.6	352	1.5	medium	0.64	moderately sorted	15.4	295
		4045.7	351	1.5	medium	0.62	moderately sorted	13.0	155
		4048.0	357	1.5	medium	0.70	moderately sorted	14.2	170
		4049.5	233	2.1	fine	0.57	moderately sorted	12.0	3.9
		4051.6	407	1.3	medium	0.64	moderately sorted	14.6	503
		4052.7	311	1.7	medium	0.53	moderately sorted	14.0	113
		4054.9	397	1.3	medium	0.67	moderately sorted	13.8	388
		4057.2	316	1.7	medium	0.52	moderately sorted	17.0	198
		4059.5	343	1.5	medium	0.55	moderately sorted	13.8	305
		4061.9	342	1.5	medium	0.72	moderately sorted	13.4	276
		4063.7	407	1.3	medium	0.74	moderately sorted	14.4	189
		4064.0	381	1.4	medium	0.64	moderately sorted	13.8	593
		4065.1	393	1.3	medium	0.71	moderately sorted	7.6	46
		4065.8	201	2.3	fine	1.44	poorly sorted	5.6	3.5
		4066.5	345	1.5	medium	0.68	moderately sorted	16.2	240
		4067.0	213	2.2	fine	0.75	moderately sorted	8.0	1.5
		4068.2	338	1.6	medium	0.55	moderately sorted	17.2	1140
		4068.9	281	1.8	medium	0.81	moderately sorted	13.6	29
		4070.0	334	1.6	medium	0.66	moderately sorted	16.0	234
	8b-3	3988.9	228	2.1	fine	0.81	moderately sorted	23.2	
		3992.3	368	1.4	medium	0.64	moderately sorted	0	
		3993.8	309	1.7	medium	0.64	moderately sorted	21.6	
		3996.9	273	1.9	medium	0.67	moderately sorted	22.6	
		4039.6	416	1.3	medium	0.82	moderately sorted	13.2	
		4116.0	354	1.5	medium	0.67	moderately sorted	13.4	
	7b-24	4045.5	372	1.4	medium	0.82	moderately sorted	18.6	
		4062.7	331	1.6	medium	0.75	moderately sorted	15.0	
		4062.8	366	1.5	medium	0.71	moderately sorted	13.8	
		4063.0	316	1.7	medium	0.67	moderately sorted	13.8	
		4063.4	354	1.5	medium	0.69	moderately sorted	12.8	
		4063.8	340	1.6	medium	0.67	moderately sorted	0.2	
		4064.2	246	2.0	fine	0.74	moderately sorted	0	
		4064.3	301	1.7	medium	0.67	moderately sorted	0	
		4064.5	257	2.0	medium	0.51	moderately sorted	14.6	
		4071.9	358	1.5	medium	0.76	moderately sorted	14.8	
		4112.9	294	1.8	medium	0.62	moderately sorted	14.2	
	8b-5	4086.5	396	1.3	medium	0.68	moderately sorted	14.6	
		4145.0	399	1.3	medium	0.67	moderately sorted	13.4	
		4300.8	360	1.5	medium	0.60	moderately sorted	12.4	
	8b-AO6	4065.5	377	1.4	medium	0.67	moderately sorted	16.6	
		4074.4	406	1.3	medium	0.68	moderately sorted	16.0	
		4102.2	382	1.4	medium	0.59	moderately sorted	14.0	
		4110.4	252	2.0	medium	0.49	well sorted	13.8	
		4111.7	173	2.5	fine	0.50	moderately sorted	0	
	7b-26	4101.3	421	1.2	medium	0.64	moderately sorted	13.6	
		4141.3	356	1.5	medium	0.68	moderately sorted	14.6	
		4186.4	437	1.2	medium	0.67	moderately sorted	12.4	
	7b-28	4080.9	411	1.3	medium	0.62	moderately sorted	15.4	
		4081.1	268	1.9	medium	0.65	moderately sorted	0	
		4081.5	465	1.1	medium	0.73	moderately sorted	0	
		4082.6	462	1.1	medium	0.70	moderately sorted	0	
		4084.4	390	1.4	medium	0.64	moderately sorted	0	
		4084.8	450	1.3	medium	0.69	moderately sorted	0	
		4085.3	357	1.5	medium	0.76	moderately sorted	14.2	
	8b-A10	4094.2	395	1.3	medium	0.62	moderately sorted	0	
		4103.1	397	1.3	medium	0.83	moderately sorted	0	
		4105.1	343	1.5	medium	0.77	moderately sorted	0	
		4105.4	355	1.5	medium	0.68	moderately sorted	4.0	
Kingfisher -	8a-8	3885.6	272	1.9	medium	0.65	moderately sorted		
Brae Unit 1		3887.5	268	1.9	medium	0.54	moderately sorted		
		3888.9	379	1.4	medium	0.57	moderately sorted		
		3890.6	312	1.7	medium	0.57	moderately sorted		
		3892.0	328	1.6	medium	0.54	moderately sorted		
		3894.6	291	1.8	medium	0.65	moderately sorted		
		3896.5	288	1.8	medium	0.65	moderately sorted		
		3898.3	312	1.7	medium	0.62	moderately sorted		
		3900.0	326	1.6	medium	0.63	moderately sorted		
		3900.9	327	1.6	medium	0.63	moderately sorted		
		3901.4	357	1.5	medium	0.71	moderately sorted		
		3901.8	346	1.5	medium	0.72	moderately sorted		
		3902.5	301	1.7	medium	0.60	moderately sorted		
		3903.4	339	1.6	medium	0.72	moderately sorted		
		3904.0	320	1.6	medium	0.64	moderately sorted		
		3904.2	301	1.7	medium	0.75	moderately sorted		
		3913.3	337	1.6	medium	0.64	moderately sorted		
		3913.6	318	1.7	medium	0.60	moderately sorted		
		3913.9	355	1.5	medium	0.63	moderately sorted		
		3914.1	283	1.8	medium	0.60	moderately sorted		
		3914.8	310	1.7	medium	0.60	moderately sorted		
		3914.9	313	1.7	medium	0.67	moderately sorted		
		3915.5	314	1.7	medium	0.70	moderately sorted		
		3929.5	308	1.7	medium	0.60	moderately sorted		
		3938.4	265	1.9	medium	0.65	moderately sorted		
		3947.2	194	2.4	fine	0.59	moderately sorted		
		3955.1	304	1.7	medium	0.64	moderately sorted		
Kingfisher -	8a-4	3989.7	312	1.7	medium	0.76	moderately sorted		
Brae Unit 2		3995.2	310	1.7	medium	0.67	moderately sorted		
		4004.7	286	1.8	medium	0.70	moderately sorted		
		4010.4	395	1.3	medium	0.65	moderately sorted		
		4015.1	326	1.6	medium	0.65	moderately sorted		
		4019.0	325	1.6	medium	0.77	moderately sorted		
		4022.1	325	1.6	medium	0.72	moderately sorted		
		4023.6	333	1.6	medium	0.61	moderately sorted		
		4026.8	337	1.6	medium	0.72	moderately sorted		
		4030.3	251	2.0	medium	0.73	moderately sorted		
		4033.7	308	1.7	medium	0.74	moderately sorted		
		4053.9	344	1.5	medium	0.70	moderately sorted		
		4081.0	348	1.5	medium	0.74	moderately sorted		
		4094.5	312	1.7	medium	0.70	moderately sorted		
		4126.1	352	1.5	medium	0.57	moderately sorted		
		4141.4	321	1.7	medium	0.63	moderately sorted		

3.6 Diagenesis

The paragenetic sequence for the Brae Formation sandstones is identical in all the reservoirs examined and is shown in Fig.19. The timing of the events shown in Fig.19 is a combination of petrographic observations in thin section with burial and thermal history modelling of the sandstone reservoirs. Results of the reservoir modelling are discussed in following chapters of this thesis. The main diagenetic events that occurred in the sandstone reservoirs examined are described below.

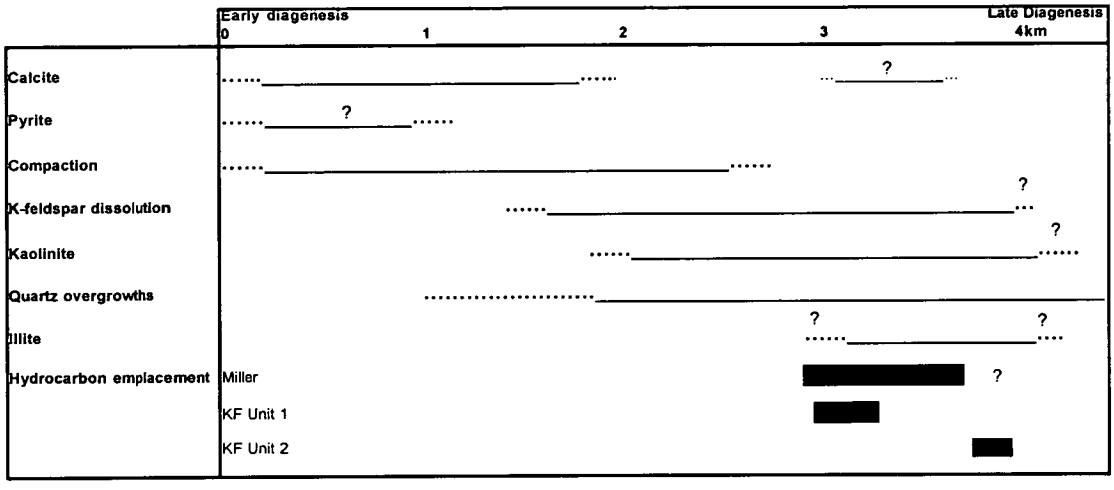

Fig.19 Paragenetic sequence, illustrating the chronological order of diagenetic events, for the Brae Formation sandstones. The timing of events is based on thin section petrography and burial and thermal history data from the reservoirs. The main diagenetic events are localised early calcite cementation, compaction and quartz cementation. All other chemical changes mentioned in the paragenesis were not of great influence in affecting reservoir quality.

Following deposition of the sediments, calcite cements were the first to precipitate. Stable isotope analyses of the calcite cement indicate that calcite precipitated from meteoric water during shallow burial (Appendix B). In most parts of the Brae Formation reservoirs there is no evidence of this early (pre-compaction) cementation. Locally however, the calcite has reduced porosity to almost zero (Fig.20A). Curved edges to calcite-cemented horizons in core suggest that the calcite cemented sandstone has a concretionary shape (Fig.20B). The concretions examined in the Miller and Kingfisher Fields have a thickness ranging from 2 to 11 m. Pointcount results (500 counts/thin section) are presented in Table 5. In the concretion centres, calcite abundances range from 25 to 40 %. The detrital grains are sometimes partly replaced by the cement and float in the calcite matrix or are in point contact. Towards the edges of concretions carbonate contents of 10 to 20 % were pointcounted. Calculated minus cement porosity (MCP) values range from 40 to 25 %

in the concretion centres to 25 to 20 % at the concretion edges. This indicates that calcite cementation began prior to, but also continued during, compaction. The decreasing MCP values towards the edges of the concretions reflect decreasing pore space volume during concretion growth. This reflects ongoing framework grain compaction during concretion growth. MCP values suggest that calcite cementation continued to burial depths of around 1.5 to 2 km maximum. Within the concretions, some authigenic pyrite occurs as framboids. From this it was concluded that also pyrite precipitation was an early diagenetic event. Pyrite abundance in, and also outside, the calcite cemented sandstones, is low (<1 %). Similar calcite concretions have been described and analysed by McLaughlin et al. (1994 and 1996) in the Brae Formation sandstone reservoir of the adjacent South Brae Field. Also here it was concluded from MCP values and stable isotope analyses that the carbonate cementation is an early diagenetic event.

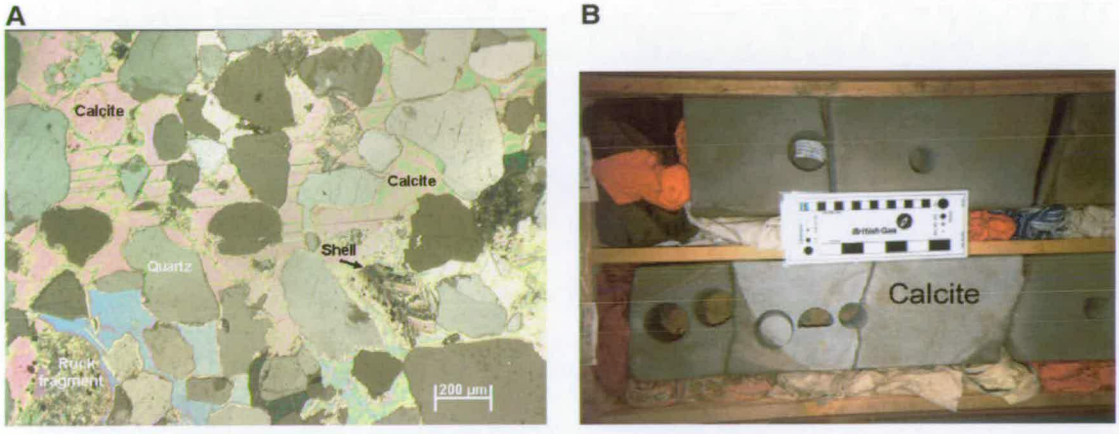

Fig.20 Photomicrograph of calcite cemented sandstone (**A**). This early cementation reduced porespace to zero. Curved edges in core (**B**) suggest a concretionary shape of the calcite cemented zones. Concretions are found in the Miller and in the Kingfisher Fields. Samples in (**A**) and (**B**) are from well 8b-3 (3992.3 m) in the Miller Field and well 8a-4 (4092 m) in the Kingfisher Field respectively. Note the preservation of a carbonate shell in the concretion.

Compaction due to overburden pressure is a major cause of porosity reduction in deeply buried sandstone reservoirs. Compaction can be subdivided into mechanical and chemical compaction. Mechanical compaction occurs at shallow depths while chemical compaction occurs with greater burial, especially in quartz-rich sandstones (Pittman& Larese, 1991). Early mechanical compaction reduces original porosity by (1) rearrangement and adjustment of grains as they move to more stable packing positions (Pittman& Larese, 1991), (2) plastic deformation of ductile sand grains (e.g. rock fragments, detrital clay), and (3) fracture or cleavage of brittle grains (e.g. quartz) (Hayes, 1979). Evidence of compaction in the thin sections of the Brae

Formation sandstones is provided by ductile rock fragments (eg. siltstone and clay fragments) and micas which are plastically deformed and squeezed in between adjacent rigid quartz grains (Fig.21A). Brittle deformation of quartz grains can be detected using CL microscopy. Quartz grains commonly display fractures which have been cemented at a later stage by quartz cement. Mechanical compaction stabilises when about 30 % (Houseknecht, 1987) to 26 % (Paxton et al., 1990) porosity is reached. This relates to burial depths between 1500-2500 m. Porosity loss below this depth is due to chemical compaction and, more importantly, to cementation. Chemical compaction at deeper burial depths is evidenced in the Brae Formation sandstones by quartz grains in irregular line contact with adjacent grains and by stylolites (Fig.21B). Stylolites are opaque because of the concentration of insoluble material (clays and organic matter) at the site where dissolution took place. Chemical compaction is a source recognised for silica for quartz cementation by many investigators (e.g. Houseknecht, 1988; Bjørlykke & Egeberg, 1993; Bjørkum, 1996).

Feldspars are commonly out of equilibrium with pressure, temperature and fluid chemistry in a diagenetic environment (Glassman, 1992). Therefore, they are subject to a variety of diagenetic alteration processes as they seek to reach a new equilibrium state. According to Glasmann (1992), early circulation of meteoric water in sandstones will result in feldspar dissolution during shallow burial (temperatures between 20-55 °C). The temperature range for complete dissolution, however, generally lies between 130 and 160 °C (Saigal et al., 1988; Milliken et al., 1989). K-feldspar in the Brae Formation sandstones is usually affected by dissolution (Fig.21). This dissolution created small amounts of secondary porosity (1.7±1.2 %). Secondary porosity is recognised when K-feldspar grains are partially dissolved, or when large pores are outlined by relict clay films (Fig.21). Dissolution of feldspars is typically accompanied by clay mineral precipitation. Which clay minerals will precipitate is controlled by the chemistry of the formation water and temperature (Worden & Morad, 2000). At moderate temperatures (<90-100 °C) kaolinite will form. At more elevated temperatures, remaining K-feldspars and kaolinite often react pervasively to form illite and quartz (Bjørlykke et al., 1992).

Authigenic clay is scarce in the Brae Formation sandstones (<3.5 %). It usually coats detrital grains or can be found in secondary pores where it was locally derived from feldspar dissolution. Pore filling clays are mainly detrital clay. According to Worden & Morad (2000), the formation of quartz and kaolinite or illite is

accompanied by the coprecipitation of carbonate cements such as calcite. The precipitation of calcite is initially encouraged because the feldspar dissolution reaction lowers pH. Subsequently, the precipitation of calcite releases protons that can in turn be used in further dissolution of feldspar. Silicate diagenesis appears to be intimately linked to the carbonate diagenetic system through their mutual, yet opposite, sensitivity to pH (Worden & Morad, 2000). Small amounts of late stage calcite cement (1.0±0.9 %), sometimes grown into secondary porespace (Fig.21D), have been observed in the thin sections examined.

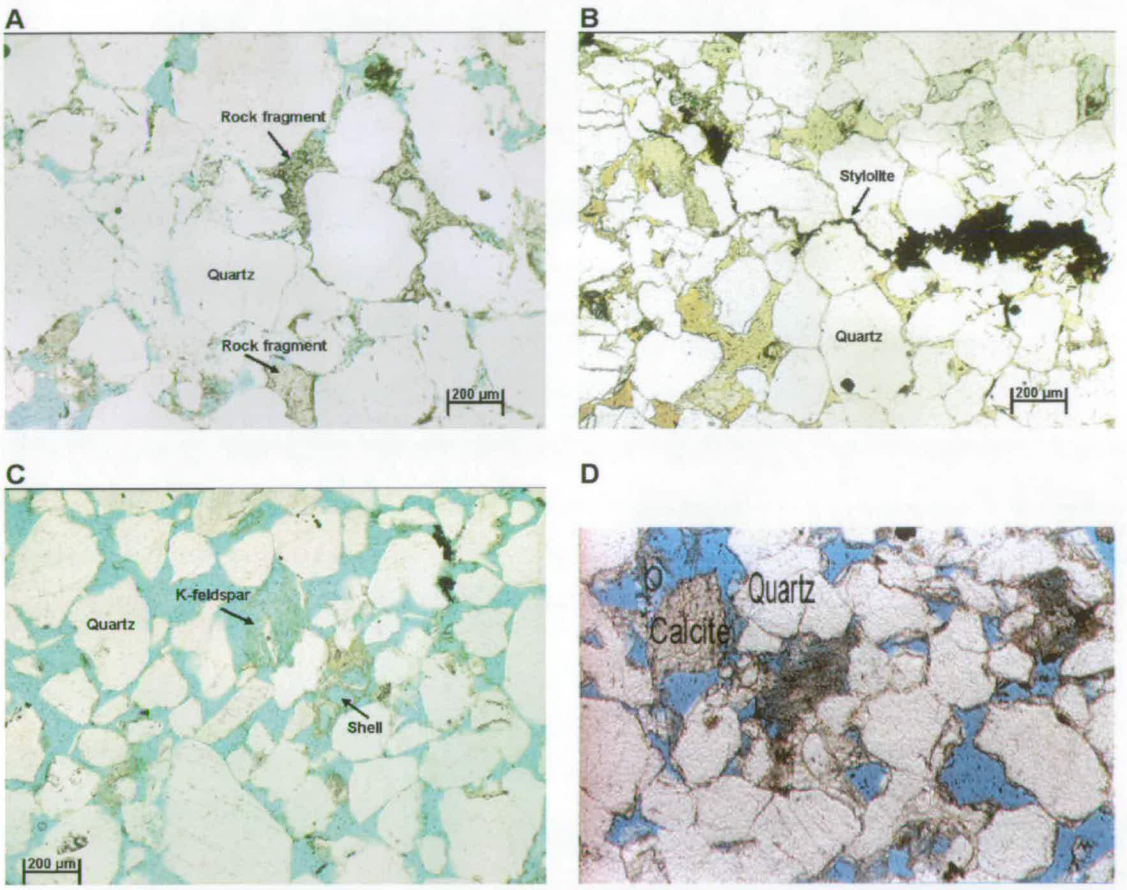

Fig.21 Compaction in the Brae Formation sandstones is witnessed by ductile deformation of rock fragments (mechanic compaction – photo **A**) and by stylolites (chemical compaction – photo **B**). The rock fragment in (**A**) is squeezed in between the adjacent quartz grains and occludes the porespace. The stylolite in (**B**) is composed of insoluble material (organics and clay). K-feldspar dissolution (**C**) in the sandstones creates small amounts of secondary porosity. Note the presence of a shell in this photomicrograph. Dissolution of the feldspars is typically accompanied by coprecipitation of calcite (**D**). The late stage calcite in (**D**) has precipitated in what appears as secondary porespace. Samples (**A**), (**B**) and (**D**) are from the Miller Field (well 7b-26 – 4186 m, well 7b-A03 – 4032 m and well 7b-A03 – 4026 m respectively). Sample (**C**) is from well 8a-8 in the Kingfisher Field (3889 m).

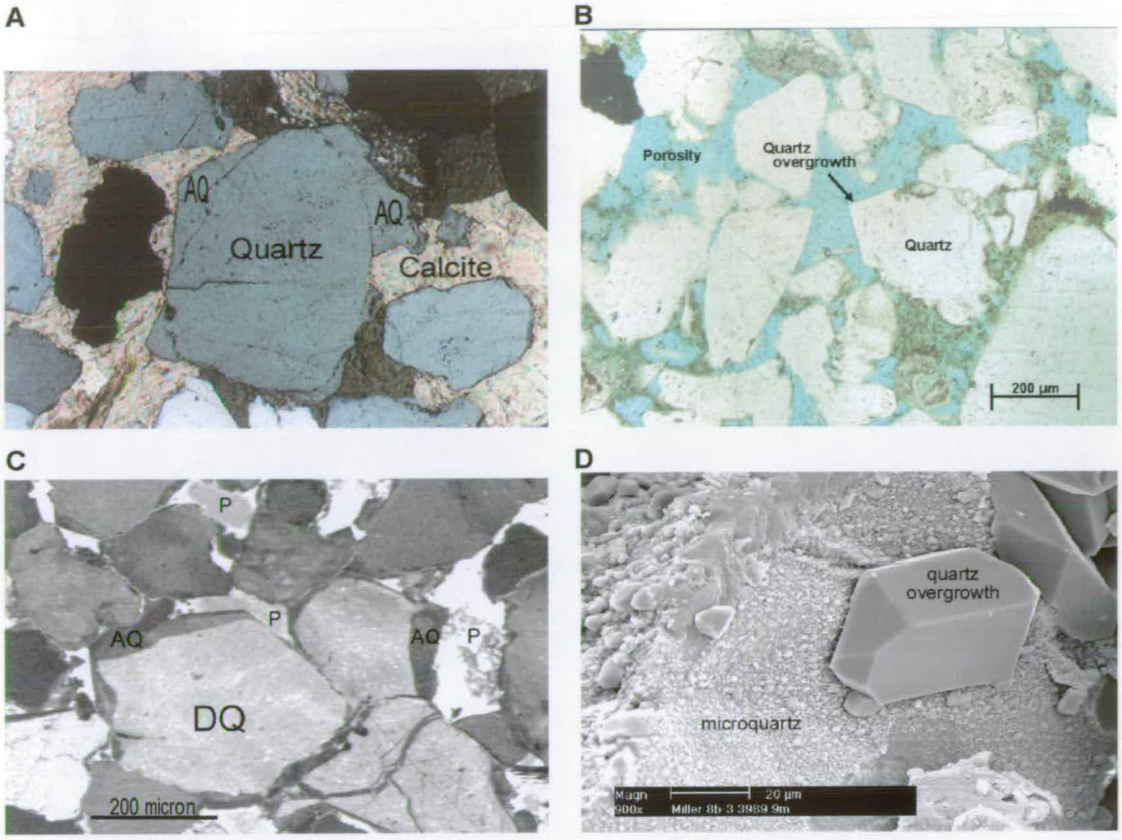

Fig.22 Quartz cement textures in the Brae Formation sandstones.
Early quartz cementation (**A**) is evidenced by overgrowths in calcite cemented sandstone parts (Miller Field, well 7b-28, 4082.6 m). Since the overgrowths are well developed and have straight crystal faces, it is unlikely that they are second cycle overgrowths. Under the optical microscope, straight crystal faces or euhedral outgrowths (**B**) are the only way of recognising quartz cement when dust rims are absent (Kingfisher Field, well 8a-8, 3900 m). Because nice crystal faces are not always developed, quartz cement is best studied under CL-light (**C**). Authigenic quartz (AQ) typically displays darker luminescence colours than detrital quartz grains (DQ). P stands for porosity (Kingfisher Field, well 8a-4, 4010 m). (**D**) is an SEM picture of a piece of rock. Euhedral quartz overgrowths and microquartz occur adjacent to each other (Miller Field, well 8b-3, 3990 m).

As in most clastic reservoirs, quartz cementation is a major cause of porosity loss at deeper burial. Quartz cementation is strongly affected by temperature (Blatt, 1979; Walderhaug, 1994; Bjørkumet al., 1998). Precipitationof quartz overgrowths in most sedimentary basins occurs during deep burial diagenesis (>2.5 km) at elevated temperatures, typically 70-130 °C (Giles et al., 1992; Gluyas et al., 1993). However, small amounts of quartz cement may develop slowly even at low temperature given enough time (Bjørkum et al., 1998). There is evidence of some early quartz cementation in the Brae Formation sandstones. Quartz overgrowths have been observed in the early calcite cemented concretions (Fig.22A). This suggests precipitation of silica at burial depths <1.5 km. The main phase of quartz cementation is interpreted to have occurred at deeper burial (>2.5 km). At those depths,

temperatures are more favourable for the kinetics of the geochemical processes that govern cementation (Worden & Morad, 2000). In the Brae Formation sandstones, quartz cement typically occurs as overgrowths. The overgrowths on detrital quartz grains can be recognised in thin section by straight crystal faces and/or euhedral termination in porespace (Fig.22B). The absence of dust rims, which indicate the boundary between detrital grain and overgrowth, made the quantification of quartz cement abundance in the Brae reservoirs difficult. Therefore, quartz cement volumes were quantified by means of SEM-CL (Appendix A). Under CL, overgrowths display different luminescence colours than the detrital quartz grains which therefore makes differentiation easier (Fig.22C). Quartz cement was also observed to have grown in fractures in mechanically broken detrital quartz grains (Fig.22C). On SEM images of rock pieces, euhedral quartz overgrowths and microcrystalline quartz are common (Fig.22D).

In the Miller Field, quartz cement abundances in the reservoir sandstones range from 2.7 to 15.4 % (Table 5). In the Brae Unit 1 and 2 reservoirs in the Kingfisher Field, quartz cement abundances range from 3.2 to 6.8 % and from 8.4 to 12.2 % respectively (Table 5). Plots of quartz cement abundance against porosity in the three Brae Formation reservoirs, show that high porosity sandstones have least quartz cement, and normal porosity sandstones have most quartz cement (Fig.23).

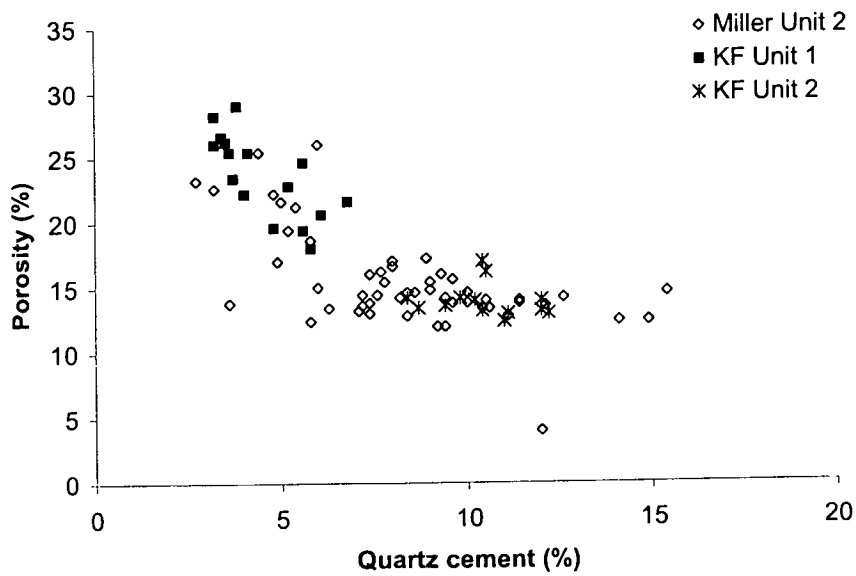

Fig.23 Quartz cement abundance (%) plotted versus porosity (pointcount %) for data from the Miller and Kingfisher Fields. The correlation coefficient between the datasets is 0.8 (81 samples; >99.9% significant). This illustrates that high porosity samples display lower quartz cement abundances than normal porosity ones.

Petrographic studies indicate that compaction and quartz cementation are the main causes for porosity loss in the Brae Formation sandstones. The reservoir quality differences in the sandstones appear to be controlled mainly by differential quartz cementation (Fig.23). The inverse relationship between quartz cement abundance and porosity is not perfect (Fig.23). This indicates that also other processes (e.g. detrital composition of the sands and texture causing differential compaction) influence porosity in the sandstones.

3.7 Quartz cement distribution

As mentioned above, quartz cement concentrations in the Miller Field reservoir sandstones range from 2.7 to 15.4 %. In Fig.24A, authigenic quartz abundance is plotted versus depth. On average, quartz cement abundance is lower in the oil leg of the reservoir (7.3±2.0 %) compared to in the water leg (12.5±1.8 %). In the crest of the field, there is <5 % of quartz cement. Across the oil leg there is a clear trend of increasing quartz cement abundance towards the OWC. When plotting the same data versus depth, but with data grouped by reservoir zone (Fig.12) then we see that in each zone quartz cement abundance increases with depth (Fig.24B). This trend is very pronounced in zones J and L. Quartz cement increase with depth in zone K is less pronounced. For zones M and N, only 2 and 1 datapoints were available respectively.

Quartz cement abundances in the Unit 1 and 2 reservoirs in the Kingfisher Field were also plotted versus depth (Fig.24C). No trends are noticeable. Quartz cement abundance in the Unit 1 reservoir is overall low (4.5±1.2 %). In contrast, the Unit 2 reservoir in the Kingfisher Field displays overall high quartz cement abundances. There is a small difference in cement abundance above and below the present day OWC. Average quartz cement abundance is 10.0±1.2 % in the oil leg, and 11.1±1.2 % in the water leg.

3.8 Discussion

Differential quartz cementation was identified from petrography as the cause for the reservoir quality variations within the Brae Formation sandstones. In the crest of the Miller Field, where porosities are highest, quartz cement abundance is particularly low (Fig.25A). Towards the OWC and in the water leg of the reservoir in the Miller Field, normal porosities and higher quartz cement abundances are found (Fig.25B).

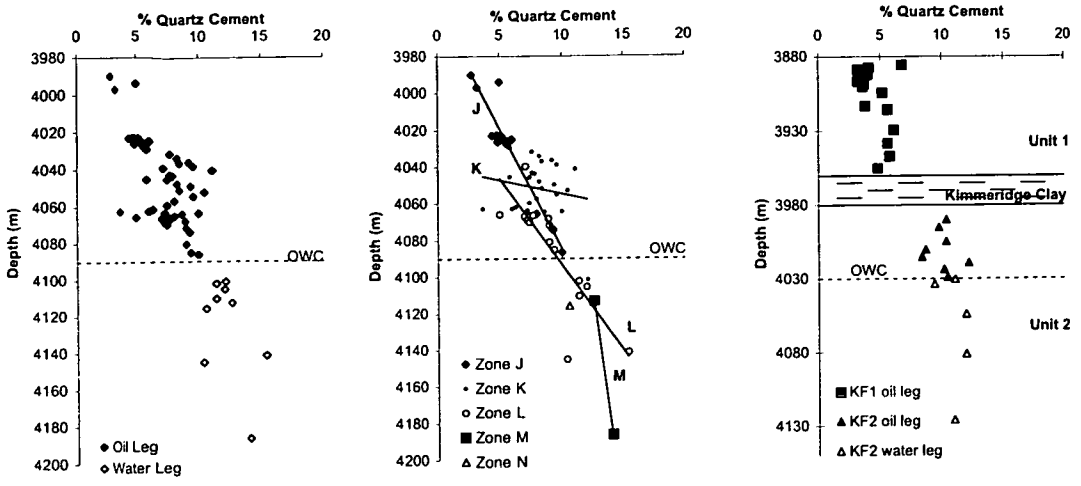

Fig.24 Quartz cement abundance (%) plotted versus depth (m TVD) for data from the Miller (**A** and **B**) and Kingfisher (**C**) Fields.
A In the Miller Field, quartz cement abundance increases systematically from the top of the reservoir (3980 m) across the oil leg towards the oil-water-contact (OWC) at 4090 m. In the water leg of the reservoir, quartz cement abundance is uniformly high.
B The same data as in graph (**A**) plotted versus depth, but with data grouped by reservoir zone. Quartz cement abundance increases with depth in each reservoir zone.
C In the Brae Unit 1 reservoir in the Kingfisher Field, quartz cement abundance is overall low. In the lower Unit 2 reservoir of the same field, separated from the upper reservoir by an interbedded layer of Kimmeridge Clay, quartz cement abundance is higher, as well in oil as in water leg (OWC at 4030 m).

Across the field, there is a subtle subtrend in quartz cement abundances which is related to reservoir zones. In each zone, quartz cement increases from top to bottom. The Brae Unit 1 reservoir in the Kingfisher Field is overall anomalously porous with low quartz cement abundance (Fig.25C). The Brae Unit 2 reservoir in the Kingfisher Field, on the other hand, displays normal porosity values with higher quartz cement abundances (Fig.25D).

Some authors have concluded that grain coatings of microquartz (Ramm et al., 1997) or chlorite clay (Heald & Larese, 1974; Ehrenberg, 1993; Aase et al., 1996) prevent quartz cementation. No evidence of chlorite precipitation on detrital quartz grains was observed in the Brae Formation sandstones. Microquartz, on the other hand, is very common. If microquartz would have inhibited the continuing growth of quartz cement, then high microquartz abundance would be expected in the crest of the reservoir in the Miller Field and also in the gas condensate reservoir in the Kingfisher Field. In the water zone of the reservoir in the Miller Field and in the Brae Unit 2 reservoir of the Kingfisher Field, where extensive quartz cementation occurred, no microquartz would be expected. Microquartz is abundant in the crest

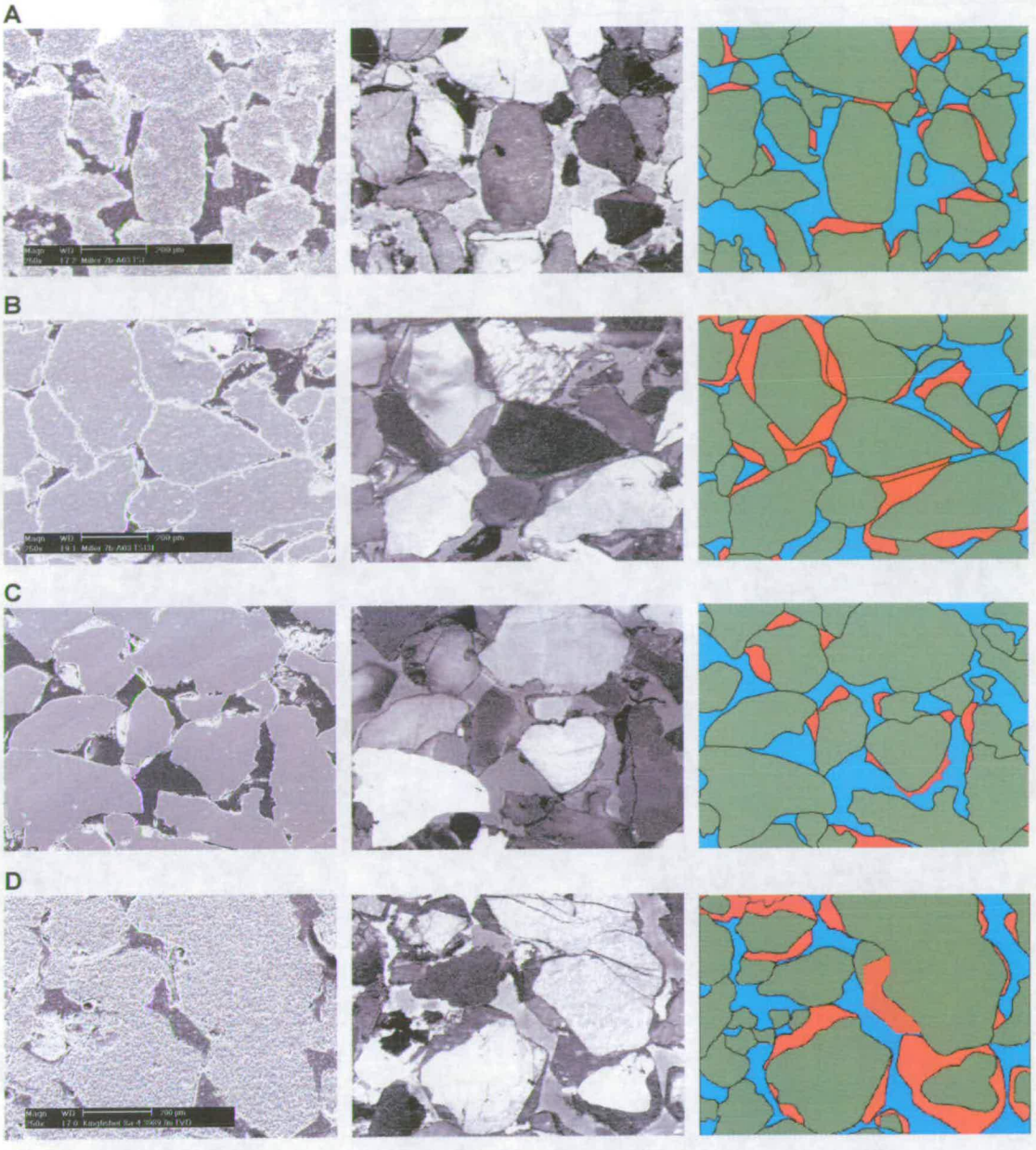

Fig.25 SEM secondary images (left column) and cathodoluminescence images (middle column) of thin sections of the Brae Formation reservoirs in the Miller and Kingfisher Fields. The pictures in the column on the right are false colour image interpretations of the cathodoluminescence images in the middle column (green=detrital grains, blue=porosity, red=quartz cement).
A Sample from well 7b-A03 in the Miller Field. This sample was taken from the high porosity zone (19 %)in the top of the reservoir at 4023 m and contains very little quartz cement (5 %).
B Sample from well 7b-A03 in the Miller Field. This sample was taken from normal porosity (14 %) sandstones deeper down in the oil zone (4053 m). Quartz overgrowths in this sample are well developed and count for 11 %.
C Sample from well 8a-8 in the Brae Unit 1 reservoir in the Kingfisher Field. This reservoir typically has high porosity (22 %) and low quartz cement abundances (4 %) (sample at 3892 m).
D Sample from well 8a-4 in the Brae Unit 2 reservoir in the Kingfisher Field. Normal porosity (17 %) and high quartz cement abundance (10 %) is typical for this reservoir (sample at 3990 m).

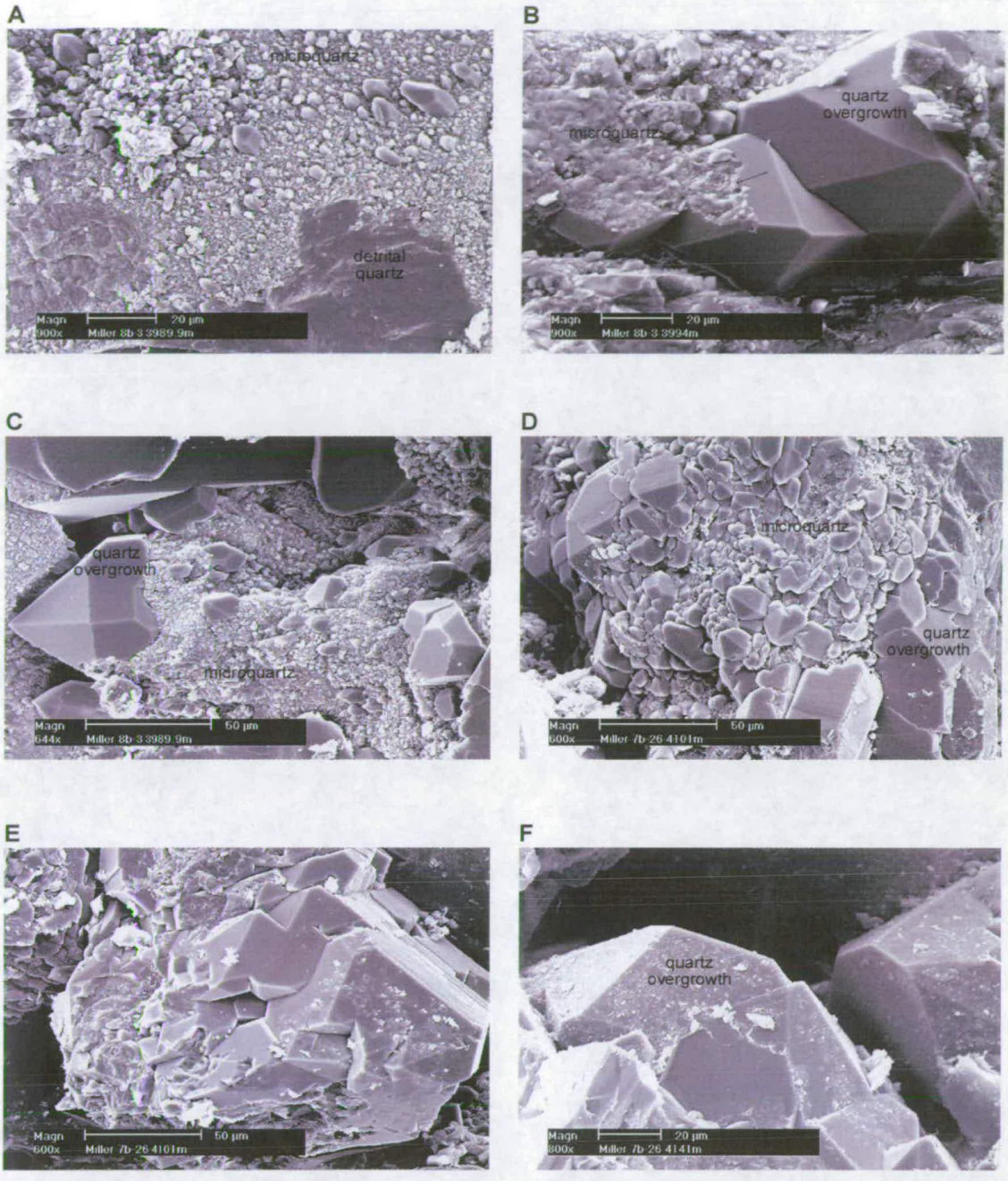

Fig.26 Stages in the growth process of quartz cement.
Picture (**A**) illustrates the onset of quartz cementation, microquartz growing on a detrital quartz grain surface. In a later stage, the microquartz crystals will form aggregate and grow out into larger overgrowths (**B**). The arrow on picture (**B**) points to an area on an euhedral quartz overgrowth which has not formed completely yet. The anhedral part of the overgrowth is still composed of microquartz. Eventually, also this overgrowth will grow to completeness and larger overgrowths will occur next to microquartz in the same sample, as can be seen in picture (**C**). Picture (**D**) illustrates that microquartz can also occur in the water zone of reservoirs. In picture (**E**), the shape of possibly one single detrital grain can be recognised. Several bigger overgrowths seem to lock into each other, and will eventually form single big overgrowths as in picture (**F**).

of the reservoir in the Miller Field (Fig.26A,B,C), and also in Brae Unit 1 reservoir in the Kingfisher Field. However, Fig.26 (D, E & F) illustrates that the microquartz can also occur directly adjacent to well-developed overgrowths, and is also present in water zone samples (Fig.26D & E). Therefore, microquartz appears to represent the earliest stage of nucleation of quartz crystals which intergrow subsequently with each other to form bigger overgrowths (Fig.26E).

Several researchers have explained quartz abundance heterogeneities within reservoirs as being the result of oil emplacement (Saigal et al., 1992; Emery et al., 1993; Gluyas et al., 1993). In those studies, quartz cement volumes have been found to be significantly higher in the water zones of oilfields than in the oil zones. There is general agreement that quartz cement in deeply buried clastic reservoirs is locally-derived from silica sources within, or close to, the sandstones. The rate of quartz cementation in sandstones during burial can therefore be viewed as three linked steps : A) dissolution of a silica source; B) silica transportation to the site of precipitation; C) quartz cement precipitation. Whichever of these steps is the slowest will be rate-limiting, dictating the overall rate of quartz cementation (Lasaga and Kirkpatrick, 1981). At depths <3 km, the slowest step is quartz precipitation because the water-film at grain-contacts is thick and diffusion is fast whereas kinetics of precipitation are slow because of low temperature (Renard et al., 2000). At greater depths, kinetics of quartz precipitation are activated by an increase of temperature and the limiting step becomes silica diffusion along the grain contacts (Renard et al., 2000). In mixed oil-water systems, quartz is considered to be preferentially water-wet (Barclay & Worden, 2000bis). Worden et al. (1998) hypothesized that in water-wet sandstones the rates of dissolution and precipitation are not affected by oil emplacement. However, the rate of quartz cementation will be slower in the oil leg than in the water leg because the rate of silica transport by diffusion is slowed due to the increased tortuosity of the diffusion path. This effect results in oil emplacement retarding quartz cementation and can lead to three possible scenarios (Fig.27). First is the case of an early oil charge (i.e. before the onset of quartz cementation). In this case, the oil leg of the reservoir will be saved from extensive cementation and anomalously high porosity can be preserved (Fig.27A). In the water leg of such reservoirs cementation will carry on unhindered, leading to a sharp contrast in quartz cement and porosity abundance below and above the OWC (Fig.27A). The second scenario is that cementation has started

already when hydrocarbons migrated into the reservoir. In this case, it is observed that quartz cement abundance gradually increases towards the OWC and at the same time porosity decreases (e.g. Emery et al., 1993) (Fig.27B). These gradients reflect a gradual oil-fill in the reservoir. Finally, if oil charge is very late (recent event) with respect to cementation, then most of the reservoir quality will be destroyed by cementation before oil-filling (Fig.27C). Poorer reservoir quality compared to early-charged reservoirs is the consequence in this case (Fig.27C).

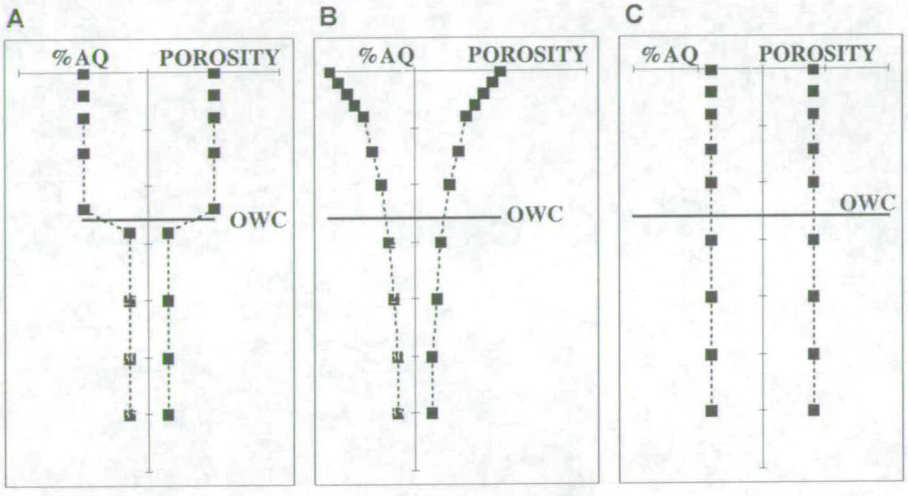

Fig.27 End member scenarios for the interaction between hydrocarbon emplacement and quartz cementation in clastic reservoirs. Imaginary quartz cement abundance and porosity percentages are plotted versus increasing depth in a reservoir.
A In the case of an early oil charge, the oil leg of the reservoir will be saved from extensive cementation and anomalously high porosity can be preserved. In the water leg of the same reservoir, cementation will continue leading to a sharp contrast in quartz cement abundance and porosity below and above the oil-water contact (OWC).
B In the case quartz cementation started before hydrocarbons filled the reservoir, it is often observed that quartz cement abundance increases, and porosity decreases at the same time, towards the OWC. These gradients reflect a gradual oil-fill of the reservoir.
C When oil charge is late with respect to cementation, most of the reservoir quality will be destroyed by cementation before the oil came in.

The quartz cement distribution and porosity pattern in the reservoir in the Miller Field can be explained by progressive hydrocarbon filling of the anticlinal field structure (Marchand et al., 2000). A model of hydrocarbon migration and accumulation in the reservoir in the Miller Field was designed by BP (Smalley et al., 1993) (Fig.28). High porosity zones (with low quartz cement) throughout the reservoir are believed to signify places where hydrocarbons started accumulating first (e.g. structural crests, crestal areas under bounding shale barriers) or are interpreted as hydrocarbon migration routes. In the model, oil enters the reservoir via the flanks of the anticlinal structure (Fig.28) and migrates along shale barriers. This explains the

higher abundance of high poroperm intervals in flank wells 7b-A11 and 8b-6 as the areas from where oil enters the reservoir. Oil subsequently migrates upward in the reservoir along the shales or breaks through the shale layers in places where shales are interrupted, e.g. NE of well A11 (Fig.28). Oil starts accumulating first in the crest of the field (e.g. 7b-A03, 8b-3, 8b-A02) or as ponds under laterally continuous shale barriers (e.g. 8b-3, 8b-A02). Consequently, quartz cementation slows down or halts first in these areas, leading to low quartz cement abundances and preservation of high porosities. Quartz cement abundances <3 % suggest a reasonably early oil charge with respect to the onset of quartz cementation. At greater depth in the reservoir, quartz cement continued to precipitate until inhibited by the developing oil column. This explains the observed increase of quartz cement abundance and the decrease of porosity with depth towards the present day OWC in the reservoir. The big difference in quartz cement abundance between top and bottom of the oil leg suggests a prolonged period of oil charge.

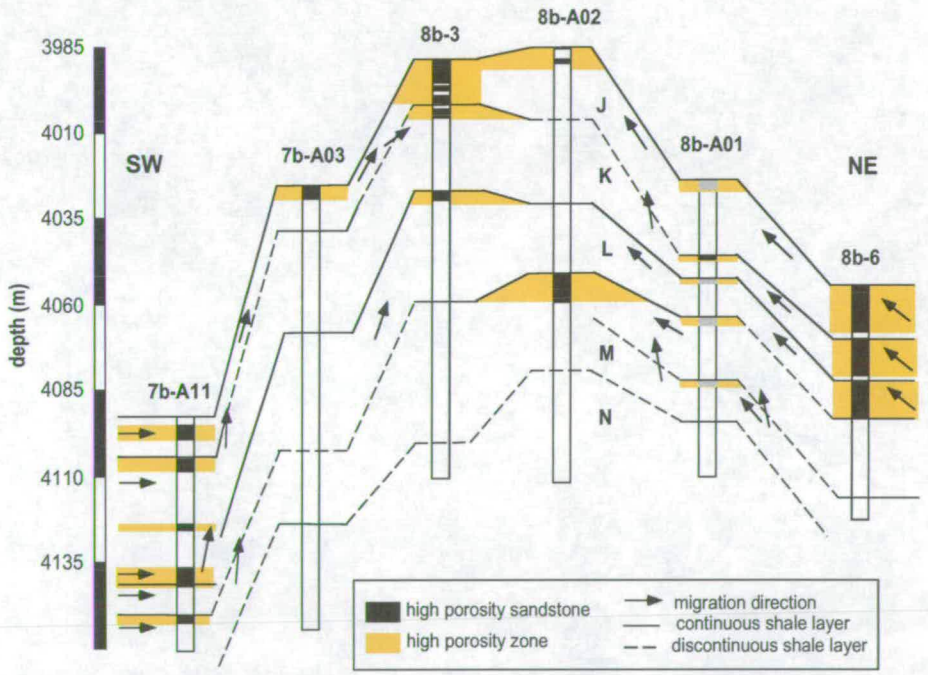

Fig.28 BP model of hydrocarbon migration and accumulation in the Brae Unit 2 reservoir in the Miller Field. Migration of hydrocarbons into the reservoir structure is indicated by arrows. High porosity (with low quartz cement) layers in the reservoir outline hydrocarbon migration routes or early accumulation areas. Oil enters the reservoir via the flanks of the structure (7b-A11, 8b-6) and migrates along shale barriers or breaks through these barriers in case they are not laterally continuous (e.g. NE of well A11). As a result, oil will start accumulation first in the crest of the field (e.g. 7b-A03, 8b-3, 8b-A02) or as ponds under laterally continuous shale barriers (e.g. 8b-3, 8b-A02). (After Smalley et al., 1993).

The patterns of quartz cement abundance and porosity in the Brae Unit 1 and Unit 2 reservoirs in the Kingfisher Field appear to conform with oil-quartz cement interaction scenarios A and B (Fig.27). High reservoir quality in most of the Brae Unit 1 reservoir can be explained by an early hydrocarbon charge. The lack of quartz cement abundance variation within the reservoir may indicate a rapid fill or may be due to the fact that the reservoir interval comprises only 75 m. Normal reservoir quality in Brae Unit 2 on the other hand can be explained by recent oil emplacement. A consequence of a recent oil charge is that quartz cement abundances will be similar in the oil and water legs of the reservoir. This is because water leg samples have not yet had enough time to grow significantly more quartz than in the oil leg.

3.9 Conclusions

1 In comparison to the regional North Sea porosity trend, parts of the oil leg in the reservoir of the Miller Field display exceptionally high porosities (av. 19.1±1.4 %) while other parts and water leg porosities are in agreement with values expected at around 4 kilometres burial (av. 14.3±0.5 %). High porosities are mainly concentrated along the top of reservoir zones under local or laterally extensive shale barriers. Porosity decreases to normal values towards the bottom of each reservoir zone and the OWC. The Unit 1 gas condensate reservoir in the Kingfisher Field, appears overall anomalously porous (av. 22.1±4.3 %). The Unit 2 oil reservoir in the Kingfisher Field shows little reservoir quality variation across the OWC. Oil and water leg average porosities are 14.4±1.4 % and 13.2±0.6 % respectively.

2 Petrographic analysis shows that reservoir quality differences between, and within, the reservoirs is not due to mineralogical or textural differences in the Brae sandstone Formation. The sandstones are medium-grained and moderately sorted, and subarkosic to sublithic (close to arenitic) in composition across the three reservoirs.

3 Differential quartz cementation was identified as the cause of the reservoir quality variations within the Brae Formation sandstones. In the crest of the Miller Field, where porosities are highest, quartz cement abundance is particularly low (3.6±1.2 %). Towards the OWC and in the water leg of this reservoir, normal porosities and higher quartz cement abundances (5 to 15 %) are found. Superimposed on this trend, are smaller subtrends of quartz cement

increase in each reservoir zone. The Brae Unit 1 reservoir in the Kingfisher Field is overall anomalously porous with low quartz cement abundance (4.5±1.2 %). The Brae Unit 2 reservoir in the Kingfisher Field, on the other hand, displays normal porosity values with higher quartz cement abundances (10.6±1.2 %).

4 The quartz cement distribution and porosity patterns in the Brae Formation reservoirs in the Miller and Kingfisher Fields are believed to be the result of the specific hydrocarbon emplacement history of each reservoir. When hydrocarbons enter a reservoir, the process of quartz cementation will slow down or halt completely. If a reservoir receives hydrocarbons early, quartz cement abundance will be low and high porosity can be preserved. If oil emplacement is a recent event, quartz cementation can continue over a prolonged period before oil charge, so destroying reservoir quality.

5 High porosity (with low quartz cement) layers throughout the reservoir in the Miller Field are believed to outline places where hydrocarbons started accumulating first (e.g. structural crests, crestal areas under bounding shale barriers) or are interpreted as hydrocarbon migration routes. Quartz cement abundances <3 % in the top of the reservoir in the Miller Field suggest a reasonably early oil charge with respect to onset of quartz cementation. The increase of quartz cement abundance and decrease of porosity in each reservoir zone and towards the OWC suggests a gradual fill over a long period of time. High quartz cement abundances in the water leg suggest continuation of quartz cementation through time.

6 High reservoir quality in the Brae Unit 1 reservoir in the Kingfisher Field can be explained by an early hydrocarbon charge. The lack of quartz cement abundance variation within the reservoir may indicate a rapid fill or may be due to the fact that the reservoir interval comprises only 75 m.

7 Normal reservoir quality in Brae Unit 2 in the Kingfisher Field can be explained by recent oil emplacement. A consequence of a recent oil charge is also that quartz cement abundances will be similar in the oil and water legs of the reservoir. This is because water leg samples have not yet had enough time to grow significantly more quartz than in the oil leg.

CHAPTER IV

FLUID INCLUSION MICROTHERMOMETRY

In this chapter :

- *At what temperatures did quartz cements grow in the Brae Formation reservoirs in Miller and Kingfisher Fields ?*
- *Are quartz growth temperatures different in oil zone and water zone samples ?*
- *Do quartz growth temperatures differ in the three reservoirs examined ?*
- *How did the salinity of fluids from which quartz precipitated evolve in the reservoirs and how does fluid inclusion salinity compare to present day formation water salinity ?*
- *What are the relative time relationships of the quartz cementation process in the three Brae Formation reservoirs studied ?*
- *Are hydrocarbon inclusions present in quartz overgrowths ?*
- *Are hydrocarbon inclusions proof of continued quartz cementation after oil emplacement ?*

4.1 Introduction

Quartz cementation exerts a major control on reservoir quality in the Brae Formation sandstone reservoirs in the Miller and Kingfisher Fields. The three reservoirs examined display distinctly different quartz cement abundances despite being buried to similar depths and temperatures. The variations in quartz cement distribution amongst (and also within) the Brae Formation reservoirs is thought to be

the result of the specific hydrocarbon emplacement and filling history in each reservoir.

In this chapter, I report and interpret the results of fluid inclusion microthermometry determination of the temperatures of quartz cementation and the salinity of fluids from which quartz precipitated. Minimum temperatures of quartz cementation were obtained by measurement of the homogenization temperatures of fluid inclusions in quartz cements (Roedder, 1979; Haszeldine et al., 1984; Walderhaug, 1990). The salinity of the fluids from which quartz cements precipitated was determined by measurement of ice melting temperatures during freezing and heating of the inclusions (Goldstein & Reynolds, 1992). The purpose of these microthermometric measurements is to determine the relative time relationships of the quartz cementation process amongst the three Brae Formation reservoirs studied. It would be expected that, if hydrocarbon emplacement prevented continuation of quartz cementation, oil zone samples should yield lower cementation temperatures than water zone samples. Also, if the time of hydrocarbon emplacement were different in the three reservoirs studied, this difference should be reflected in quartz growth temperatures. By comparing the range of growth temperatures of quartz cements in the different reservoirs, conclusions can be drawn regarding the relative time span over which quartz cementation occurred in each reservoir. By cross-plotting fluid salinity values with temperatures, the palaeofluid evolution in the reservoir can be reconstructed. Comparison of the fluid inclusion data with present day formation water salinity and reservoir temperature indicates whether quartz precipitated from recent, or from older, fluids in the reservoir.

Some authors assert that the occurrence of primary oil inclusions in quartz cement is evidence of continued quartz cementation in the presence of oil (e.g. Walderhaug, 1990 and 1994). Therefore, I also determined whether oil inclusions are present in samples from the Brae Formation reservoirs in the Miller and Kingfisher Fields. I will discuss the significance of such hydrocarbon inclusions and the consequences for the occurrence of quartz cementation in the presence of oil.

4.2 Methodology

Primary aqueous fluid inclusions represent small quantities of interstitial fluids trapped in a mineral crystal during precipitation. The determination of temperatures of phase changes within these fluid inclusions during heating or cooling of samples is termed microthermometry. Measurement of the homogenization temperature (T_h)

and temperature of last ice melting (T_m) in fluid inclusions provides information on the minimum temperature of quartz cementation, and the salinity of fluids from which quartz cement precipitated, respectively (Roedder, 1979; Haszeldine et al., 1984; Walderhaug, 1990).

T_h measurement A conspicuous feature of most aqueous fluid inclusions is a vapour or gas bubble (Fig.29A). The two phases (liquid and vapour) in the aqueous inclusions result from the fact that we are examining the fluid inclusions at a lower temperature than that at which they were trapped. Upon cooling to room temperature, the pressure in the inclusions drops below the saturation vapour pressure of the contained fluid and the fluid splits into two phases : liquid and vapour. By reversing the 'cooling down to room temperature process', i.e. heating the inclusion to the temperature of disappearance of the vapour bubble, a minimum temperature at which the inclusion was formed is obtained. The temperature at which the two phases in the inclusion homogenize is called the homogenization temperature (T_h). Measurement of the T_h of fluid inclusions in quartz overgrowths is perhaps the most direct way of determining the temperatures of quartz cementation in a sandstone. In order to know the true trapping temperatures of the inclusions in the mineral, a pressure correction needs to be applied. However, because the samples are from a hydrocarbon reservoir, waters within the fluid inclusions are likely to be methane-bearing. According to Hanor (1980), homogenization temperatures are in this case very similar to trapping temperatures and no pressure correction is required.

T_m measurement By freezing aqueous inclusions and subsequently warming them up to room temperature, information on the composition and salinity of the fluid from which the quartz precipitated can be obtained. The temperature at which the first melting of ice occurs, the eutectic temperature (T_e), is diagnostic of the major ions in solution in the fluid contained in the inclusion. If first melting occurs at a temperature of about –21 °C, the species in solution are dominated by NaCl (Goldstein & Reynolds, 1992). If first melting occurs at a temperature of about –50 °C, the dominant species in solution is $CaCl_2$ (Goldstein & Reynolds, 1992). Salt in solution in the fluid contained in the inclusion will cause a depression of the final ice melting temperature (Goldstein & Reynolds, 1992). The temperature at which the final melting of ice (T_m) occurs depends on the salinity of the fluid. The relationship

between freezing point depression and salinity varies slightly for the various species dominant in the fluid (Roedder, 1979). Most researchers report their interpretations of freezing point depression in weight % NaCl equivalent. This simply states the salinity of fluid inclusions assuming all dissolved species to be NaCl. According to Goldstein and Reynolds (1992), this yields a salinity that is fairly close to reality for many diagenetic systems.

The temperatures of phase changes in aqueous inclusions were measured with a modified USGS gas flow Fluid Inc stage mounted on a Leitz Metallux 3 microscope equipped with x3, x10, x20 and x60 objectives. The heating-cooling stage was calibrated with Flinc standards. During measurement of T_h, the sample was heated until homogenization was imminent. After homogenization was considered to have taken place, temperature was lowered slightly to observe if the gas bubble reformed. If a bubble did reform, this was considered to imply that homogenization had not taken place, since inclusions usually require at least 3-10 °C of cooling below their T_h before gas bubbles reform. By applying this cycling method, precise determinations of T_h for inclusions could be obtained. For determination of T_m, inclusions were frozen to at least –100 °C. First melting (T_e) in aqueous inclusions was difficult to observe because of the small size of the inclusions present (see below). Effort was concentrated into trying to determine T_m because of the quantitative information this temperature can provide about salinity. The last melting of ice can often be observed easily when the vapour bubble suddenly moves back in the inclusion. A common problem encountered, however, was the collapse of the vapour bubble on freezing. This resulted in metastable ice melting in the absence of a vapour phase (Goldstein & Reynolds, 1992). Because of this problem and also the small inclusion size, the number of T_m measurements is much smaller than the number of T_h determinations.

The UV fluorescence analyser on the Leitz Metallux 3 microscope was used to look for hydrocarbon-filled inclusions in the Brae Formation sandstone samples. Oil-filled inclusions in quartz cement can be detected by fluorescence emitted from the aromatic fraction of the oil under ultra-violet fluorescence illumination (McLimans, 1987). The fluorescence colours have been interpreted to reflect API values of the oil (Hagemann & Hollerbach, 1985; Lisk et al., 1998).

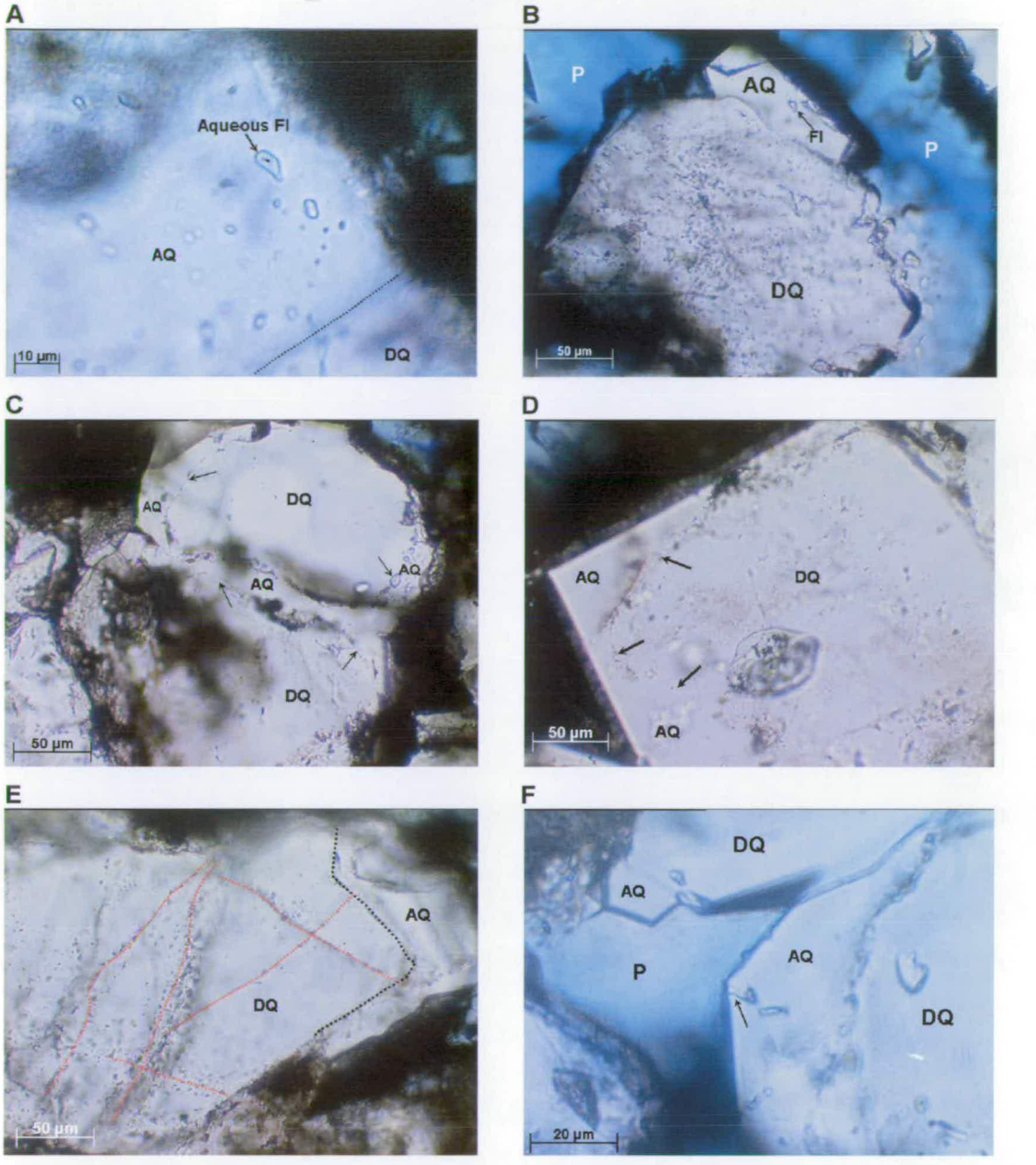

Fig.29 Photomicrographs of aqueous fluid inclusions in quartz cement in the Brae Formation sandstones.

(A) Primary aqueous fluid inclusion in authigenic quartz (AQ) – sample depth 3989.7 m, well 8a-8 (Kingfisher Field Brae Unit 2).

(B) Aqueous inclusions are frequently abundant in the detrital quartz grain (DQ) while the overgrowth (AQ) appears void of inclusions – sample depth 3887.3 m, well 8a-8 (Kingfisher Field Brae Unit 1).

(C) and (D) Primary inclusions are commonly present on the boundary or "dust rim" (arrows) between detrital grains (DQ) and overgrowths (AQ) and, less commonly, within the overgrowths themselves – sample depth 3955.1 m, well 8a-8 (Kingfisher Field Brae Unit 1) (C) and sample depth 3989.7 m, well 8a-4 (Kingfisher Field Brae Unit 2) (D).

(E) Trails of secondary inclusions, trapped in healed microfractures, cross-cut a detrital quartz grains (DQ) – sample depth 3989.7 m, well 8a-4 (Kingfisher Field Brae Unit 2).

(F) Reset aqueous fluid inclusion in authigenic quartz (AQ). This inclusion is connected by a microfracture (arrow) to the adjacent porespace (P) and will consequently provide unreliable information – sample depth 4081.0 m, well 8a-4 (Kingfisher Field Brae Unit 2).

4.3 Sample material

Polished wafers for fluid inclusion analysis were made from samples from 2 wells in the Miller Field (7b-26 and 7b-A03) and 2 wells in the Kingfisher Field (8a-4 and 8a-8). An overview of the depths sampled in each well is given in Table 7. Additional fluid inclusion data from Miller were reported by Hogg et al. (1993). Hogg et al.'s T_h measurements and salinity values from wells 8b-3, 7b-25, 8b-A10 and 8b-A11 have been incorporated with our own results (Appendix C).

Table 7 List of depths sampled (m TVD) for fluid inclusion wafers in the Brae Formation sandstone reservoirs in the Miller and Kingfisher Fields. For all samples, the number of T_h and T_m measurements performed is indicated. For the Miller Field, the reservoir zone from which the sample was taken is indicated.
(*) Measurements performed by Hogg et al. (1993)
(**) Measurements performed by Calum Macaulay
(***) Measurements performed by Ann Marchand

Field	Reservoir	Well	Sample Depths (m)	# T_h Measurements	# T_m Measurements	Reservoir Zone
Miller	Brae 2	7b-A03 (***)	4024.8	4	3	K
			4036.4	6	2	K
			4057.2	1	0	K
			4064.2	18	6	K
			4068.9	15	2	L
		8b-3 (*)	3993.0	8	6	J
			3998.2	4	5	K
			4009.1	16	10	K
			4012.7	10	10	K
			4021.3	15	17	K
		7b-25 (*)	4062.1	9	6	J
			4063.9	11	8	J
			4065.5	6	6	J
			4067.5	3	1	J
			4068.7	6	5	J
			4084.4	16	14	K
		8b-A10 (*)	4080.1	26	25	K
			4093.4	27	24	L
		8b-A11 (*)	4088.8	38	36	K
			4096.3	28	28	?
			4100.6	27	27	?
			4141.8	37	37	?
		7b-26 (**)	4101.3	21	9	K
			4186.4	19	4	N
Kingfisher	Brae 1	8a-8 (***)	3887.3	13	7	
			3904.2	7	1	
			3915.5	7	2	
			3955.1	11	2	
	Brae 2	8a-4 (***)	3989.7	6	0	
			4015.1	10	5	
			4028.8	24	3	
			4033.7	12	0	
			4081.0	6	0	
			4126.1	18	10	

4.4 Description of aqueous fluid inclusions

Fluid inclusions occur both in detrital quartz grains and in quartz overgrowths (Fig.29B and E). Primary inclusions, trapped during diagenetic quartz crystal

growth, are present on the boundary between detrital grains and overgrowths ("dust rim") (Fig.29C and D) and, less commonly, within the overgrowths themselves (Fig.29A and B). Secondary inclusions, trapped in healed microfractures, commonly cross-cut quartz grains (Fig.29E).

Primary aqueous inclusions in quartz overgrowths and in dust rims are sub-rounded to rectangular in shape and predominantly less than 5 μm in size. The small inclusion size severely complicated T_h and T_m measurements and usually only inclusions >5 μm in size permitted accurate measurement.

The quartz grains examined rarely show well developed dust rims, and aqueous fluid inclusions suitable for analysis in the dust rim were not observed in the samples. It was therefore necessary to find suitable inclusions for measurement within the overgrowths. Inclusions sufficiently large to allow reliable measurement proved difficult to find, especially in samples with low quartz cement abundances. Also, many overgrowths were devoid of inclusions (Fig.29C and D).

4.5 Homogenization temperatures of aqueous fluid inclusions

Miller (Brae Unit 2 reservoir) Data from the Miller Field show a wide range in T_h from aqueous inclusions of 69 to 142 °C (Appendix C and Fig.30A). The positively skewed frequency distribution (skewness +0.02) is according to Wilkinson et al. (1998) typical of most fluid inclusion data sets. The tail of data at the high T_h end of the distribution is probably mainly the result of measurement of inclusions which have stretched or leaked subsequently to trapping, or have necked down after nucleation of a vapour bubble (Wilkinson et al., 1998). The fact that measured T_h in the tail end of the histogram are higher than the present day reservoir temperature, which is 120 °C at 4 km (Rooksby, 1991), supports this hypothesis. From this present day reservoir temperature, a present day temperature gradient of 30 °C/km can be derived. Using this temperature gradient it can be calculated that the present day temperature in the deepest sample in which T_h was measured (4186.4 m) should be 125.6 °C. Therefore, the maximum reliable T_h in the population on the histogram in Fig.30A is considered to be 125 °C. In the discussions below, T_h measurements which are clearly higher than the relevant present day temperature are considered to be unreliable. Such measurements are believed to record reset inclusions and consequently yield unreliable results; they will be omitted from quartz cementation temperature discussions. Problems with fluid inclusion measurements are further discussed below.

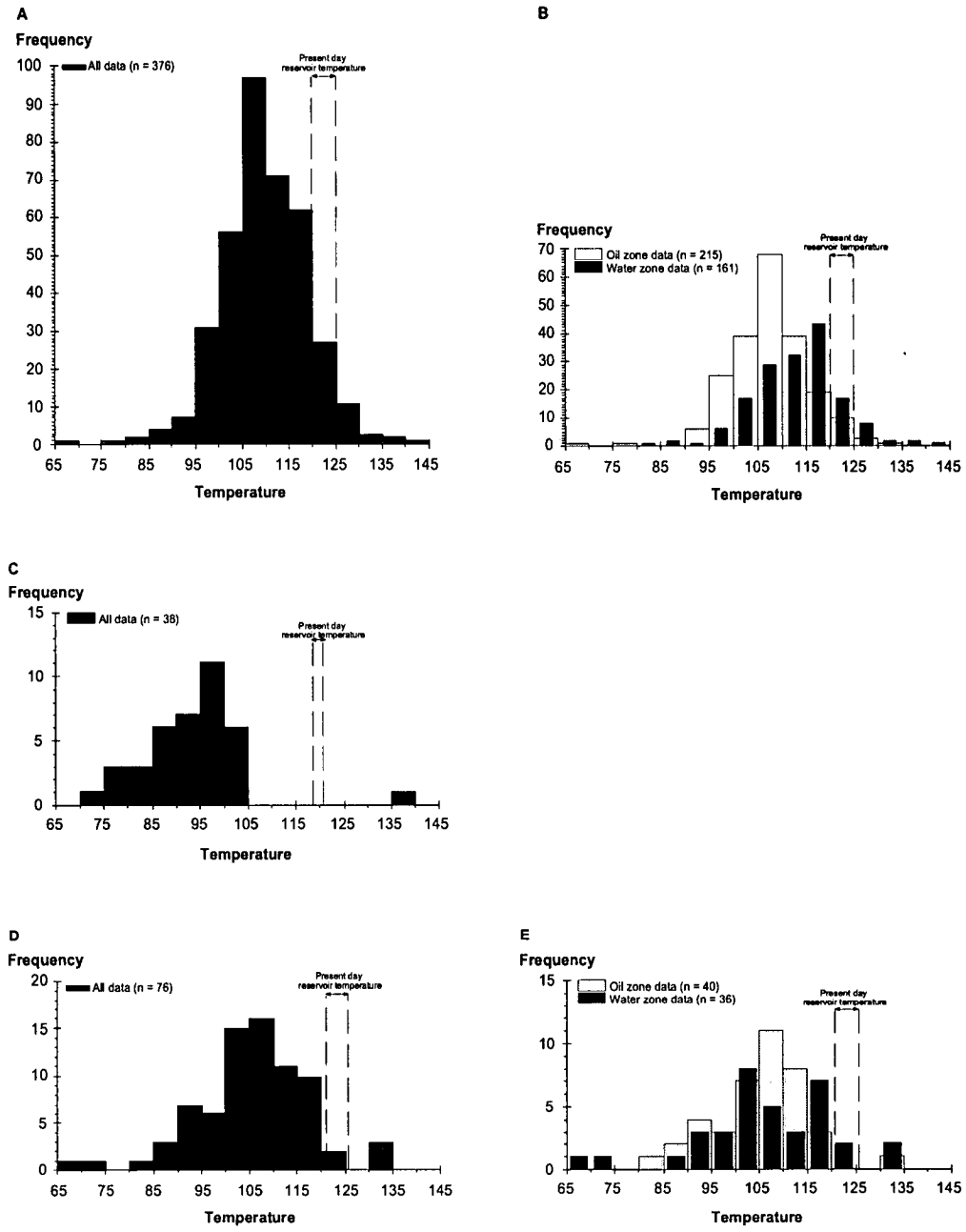

Fig.30 Histograms of homogenization temperatures (T_h) measured in aqueous fluid inclusions in quartz cement. On each histogram, the number of measurements (n) made and the present day reservoir temperature range is indicated.
(A) All T_h measurements from the Brae Unit 2 reservoir in the Miller Field. The bulk of the data range between 100 and 120 °C.
(B) T_h data from the Brae Unit 2 reservoir in the Miller Field split into an oil zone (grey bars) and water zone (black bars) group. The peak in the histogram of the oil zone data group (105-110 °C) is different than the peak in the histogram of the water zone data group (115-120 °C).
(C) All T_h measurements from the Brae Unit 1 reservoir in the Kingfisher Field. The bulk of the data range between 85 and 105 °C.
(D) All T_h measurements from the Brae Unit 2 reservoir in the Kingfisher Field. The bulk of the data range between 100 and 120 °C.
(E) T_h data from the Brae Unit 2 reservoir in the Kingfisher Field split into an oil zone (grey bars) and water zone (black bars) group. The peak in the histogram of the oil zone data group lies around 105-110 °C. No clear peak is present in the histogram of the water zone group, but the bulk of the data overlap with the oil zone T_h data (100-120 °C).

In Fig.30B, the data are split between an oil zone group (all T_h measurements in samples <4090 m) and a water zone group (all T_h measurements in samples >4090 m) group. From this Figure it is clear that the mean T_h of aqueous inclusions in quartz cements in the oil zone (107.0±7.8 °C) is lower than mean T_h of inclusions in the water zone (112.3±8.0 °C).

The lowest T_h recorded in oil zone samples is 69.0 °C (Appendix C). The present day reservoir temperature range for the measured oil zone samples can be calculated, assuming a temperature gradient of 30 °C/km, and ranges from 120 to 123 °C. Therefore, the highest reliable T_h measurements in the oil zone data population on Fig.30B are considered to be between 120 and 123 °C. The data presented on the histograms in Fig.31 are from samples located in the top of reservoir zones. The reservoir zone from which each sample comes is indicated in Table 7. Present day reservoir temperature for each sample (assuming a temperature gradient of 30 °C/km) is indicated on the histograms (Fig.31). In sample 3993 m (well 8b-3), which is located in the top of reservoir zone J, T_h ranges between 84 and 113 °C (Fig.31 and Appendix C). In sample 4024 m (well 7b-A03), also located in the top of zone J, T_h ranges between 97 and 108 °C (Fig.31 and Appendix C). Sample 3998 m, which is located in the top of zone K in well 8b-3, displays T_h values between 69 and 92 °C (Fig.31 and Appendix C). Sample 4069 m from well 7b-A03 is located in the top of reservoir zone L. Minimum and maximum reliable T_h measured in this sample are 97 and 110 °C respectively (Appendix C and Fig.31). All other oil zone samples in which T_h was measured, and which are not located near the top of a reservoir zone, display T_h values ranging between the lowest measured T_h (69.0 °C) and the present day temperature (Appendix C).

In water zone samples, the lowest measured T_h is 84.6 °C (Appendix C). The present day reservoir temperature ranges between 123 and 126 °C in the water zone samples (assuming a temperature gradient of 30 °C/km). Consequently, the highest reliable T_h measurements in the water zone data population on Fig.30B are considered to be between 120 and 125 °C.

Kingfisher (Brae Unit 1 reservoir) T_h for aqueous fluid inclusions in quartz cement from the gas condensate reservoir in the Kingfisher Field ranges from 74 to 135 °C (Appendix C and Fig.30C). Note that all samples are from the petroleum-bearing part of the reservoir. The present day temperature across the depth range of the samples in this reservoir is 118 (at 3887 m) to 121 °C (at 3955 m) (Shell Internal

Report). For this reason, T_h in excess of these present day temperatures are considered unreliable. The highest measured reliable T_h is therefore 104.1 °C (Appendix C). The mean T_h of aqueous inclusions in quartz cement in this reservoir is 92.8±8.2 °C. The bulk of the data set displays a T_h between 95 and 100 °C (Fig.30C).

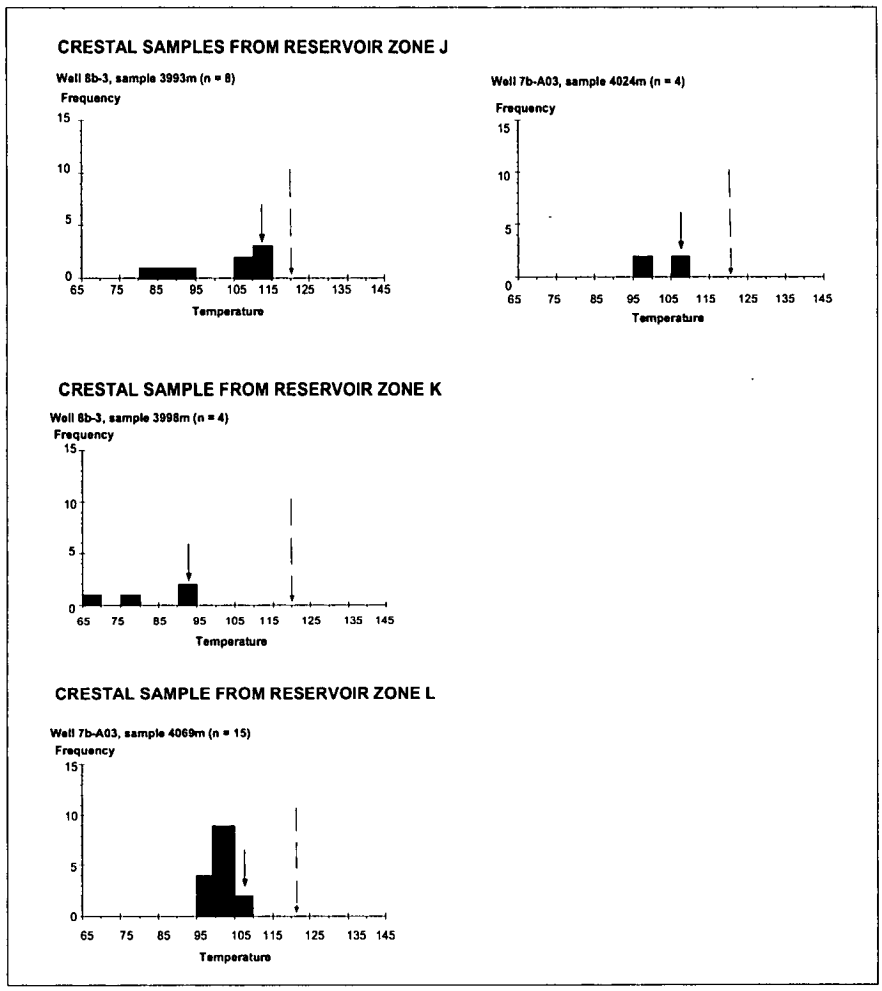

Fig.31 Histograms of homogenization temperatures (T_h) measured in aqueous fluid inclusions in quartz cement from oil zone samples located in the top of reservoir zones in the Miller Field. Sample depths and the number of measurements (n) made are indicated on each histogram individually. Dashed arrows represent the present day reservoir temperature of the samples in the histogram. Present day reservoir temperature was calculated assuming a temperature gradient of 30 °C/km. Solid arrows represent the maximum reliable measured T_h amongst the dataset. The maximum reliable T_h is the highest measured T_h amongst the dataset which is lower, or equal to, present day reservoir temperature. The data presented here illustrate that in the tops of reservoir zones, which display high porosity and low quartz cement abundances, the measured T_h are consistently lower than the present day reservoir temperature (105-110 °C in zone J; 90-95 °C in zone K; 105-110 °C in zone L).

Kingfisher (Brae Unit 2 reservoir) In samples from the Unit 2 reservoir in Kingfisher Field, T_h of aqueous fluid inclusions in quartz cement ranges from 67 to 132 °C (Appendix C and Fig.30D). Again, T_h data in the tail end of this histogram are higher than present day reservoir temperatures. According to Shell production test data (Shell Internal Report), the present day temperature range for the fluid inclusion samples studied is 122 (at 3989 m) to 126 °C (at 4126 m). For this reason, measured temperatures >126 °C are considered unreliable.

In Fig.30E, the data are split into an oil zone (all T_h measurements in samples <4030 m) and water zone (all T_h measurements in samples >4030 m) group. In oil and water zone samples, the lowest measured T_h are 81.2 and 67.4 °C respectively (Appendix C). The highest reliable T_h measurements in oil and water zone data are considered to be 120.0 and 123.7 °C respectively (Appendix C). The mean T_h of aqueous inclusions in quartz cement in the oil zone (104.5±8.7 °C) is only slightly lower than mean T_h in the water zone (104.8±12.6 °C). The peak of the histogram for the oil zone data lies between the 105-110 °C interval (Fig.30E). The water zone data are complexly distributed (Fig.30E). The bulk of the dataset however, lies between 100 and 120 °C and overlaps with the bulk of the oil zone data (Fig.30E).

4.6 Problems with measurements

Volume or pressure changes to fluid inclusions after entrapment affect the interpretation of measured data (Goldstein & Reynolds, 1992).

According to Roedder (1984), fluid inclusions may change their shape after they are entrapped. Some elongate or irregularly shaped inclusions may pinch off to form more than one inclusion. This process is known as *necking down*. When necking down pinches off a two phase vapor-liquid inclusion, it produces fluid inclusions with densities different from one another and different from the original inclusion entrapped (Goldstein & Reynolds, 1992).

Another mechanism of fluid inclusion alteration is caused by overheating (Goldstein & Reynolds, 1992). When aqueous fluid inclusions are heated beyond their temperature of homogenization or temperature of entrapment, thermal expansion of the liquid causes an internal increase in pressure relative to the external pressure (Goldstein & Reynolds, 1992). Such internal overpressure in the inclusion can result in *stretching* of the mineral host (volume expansion in the inclusion through plastic deformation) or *leakage* and *refilling* of the inclusion (Goldstein, 1986;

Prezbindowski & Larese, 1987; Burruss, 1987). Such re-equilibration caused by overheating results in density decrease in the fluid inclusion and an increase in its homogenization temperature (Goldstein & Reynolds, 1992). During overheating, the likelihood and extent of fluid inclusion re-equilibration is difficult to predict because of the many variables that control the re-equilibration of individual fluid inclusions (Roedder, 1984). It is thought that larger inclusions may re-equilibrate more easily than smaller ones (Bodnar & Bethke, 1984; McLimans, 1987). Fluid inclusions in soft cleavable minerals such as calcite may tend to re-equilibrate more easily than those in strong minerals such as quartz (Roedder, 1984). Also, the density and composition of the inclusion contents affect the inclusion's behaviour during overheating (Goldstein & Reynolds, 1992). With many variables controlling re-equilibration, it is probable that each fluid inclusion in a population of inclusions will respond differently to overheating. Some inclusions may not re-equilibrate at all and others may re-equilibrate to varying degrees and at various temperatures. Therefore, a population of fluid inclusions with originally homogeneous densities may be converted to a population with heterogeneous densities after overheating and re-equilibration has occurred (Goldstein, 1986; Prezbindowski & Larese, 1987).

In order to avoid measuring unreliable temperatures in aqueous fluid inclusions, care was taken to examine only regularly shaped inclusions. This was done to eliminate the problem of necking down. In studies of fluid inclusions in quartz cement, it has been claimed that homogenization temperatures in aqueous fluid inclusions are typically reset due to stretching of inclusions even at diagenetic temperatures (Osborne & Haszeldine, 1993). Such resetting would cause the measured T_h to reflect maximum burial temperatures rather than entrapment temperatures. Other authors, however, claim that aqueous fluid inclusions in quartz cement are not stretched and reset at diagenetic temperatures (Robinson et al., 1992). The main reason for Osborne and Haszeldine (1993) to claim that T_h is reset, is the apparent correlation between measured T_h in inclusions and present day temperature in many reservoirs. Because T_h values from aqueous inclusions in quartz cement in the Brae Formation sandstones are consistent among a large dataset composed of measurements in inclusions of different sizes and shapes, the bulk of the data is held to be reliable. Only inclusions which yielded measured T_h values clearly higher than present day sample temperature are thought to be reset. The correlation between T_h and present day temperature which Osborne and

Haszeldine (1993) observe can be explained by the fact that quartz precipitation rates increase dramatically as a function of temperature. Consequently, the higher abundance of inclusions with high T_h is the result of the bulk of the inclusion population being formed at higher entrapment temperatures and is not by itself evidence of stretching and resetting (Walderhaug, 1994).

4.7 Quartz cementation temperatures

Miller (Brae Unit 2 reservoir) Fig.31 shows that entrapment of inclusions in quartz overgrowths started at temperatures of approximately 85-95 °C in most of the samples examined from the Miller Field. In a few samples lower T_h values, between 69 and 80 °C, were measured. This temperature range for onset of quartz cementation is in agreement with quartz cementation temperatures reported by many other researchers who examined North Sea reservoir samples (Haszeldine et al., 1984; Burley et al., 1989; Walderhaug, 1994; Wilkinson et al., 1998; Worden & Morad, 2000) and is therefore considered to be reliable. According to Walderhaug (1990), quartz cementation actually starts at temperatures lower than the minimum measured T_h. This is because a certain amount of quartz cement needs to be precipitated first before inclusions can be surrounded and trapped by quartz. The amount of time required to form an inclusion will depend upon the quartz precipitation rate. Precipitation rates increase very rapidly with increasing temperature (Murphy et al., 1989; Oelkers et al., 1992). Walderhaug (1994) calculated that the time necessary for closing a typical small inclusion of 4 μm is approximately 40 My at 80 °C, 17 My at 100 °C, 6 My at 120 °C and 2 My at 140 °C. The scarcity of T_h measurements below 100 °C, and also the considerable variation in the temperature of onset of quartz cementation in various samples, is therefore probably the result of inclusions not having had time to form below 100 °C.

In water zone samples, the T_h distribution indicates that quartz cementation has continued to present day reservoir temperatures (Fig.30B). The fact that measured T_h in some samples is around the present day reservoir temperature also indicates that pressure corrections for T_h are negligible. Therefore, we can consider most measured T_h to be a good estimate of the actual entrapment temperature of the inclusion.

In oil zone samples located near the top of the reservoir zones, the maximum reliable T_h range is lower than the current reservoir temperature (Fig.31). This

implies that cementation in these areas of the reservoir was impeded at some time in the past. Samples from the top of the reservoir zones (i.e. 3993 m in well 8b-3 and 4024 m in well 7b-A03 for zone J; 3998 m in well 8b-3 for zone K and 4069 m in well 7b-A03 for zone L) systematically display the lowest maximum reliable T_h (Fig.31). In the top of zone J and zone L, quartz cementation was halted around 105-110 °C. In the top of zone K, the highest T_h recorded is 95 °C. Reservoir temperatures in these locations today are around 120-122 °C. This means that quartz cementation in the top areas of the different reservoir zones stopped when the temperature at those places was 10 to 15 °C, or even 25 °C in zone K, lower than the present day reservoir temperature. In samples from other areas in the reservoir zones (i.e. not the top), measured T_h values approach present day temperatures in the reservoir (Appendix C). This indicates continued quartz cementation up to recent times (to perhaps the last several My).

Kingfisher (Brae Unit 1 reservoir) In the gas condensate reservoir in the Kingfisher Field, quartz cementation was active at temperatures above 70 °C (Fig.30C). Because it takes a certain amount of time to entrap an inclusion in quartz, as explained above, the actual onset of quartz cementation in this reservoir must have occurred at an even lower temperature. The T_h distribution on the histogram in Fig.30C indicates that the main quartz cementation phase in this reservoir occurred from 90 to 105 °C. The highest measured reliable T_h is 104 °C (Appendix C). This maximum temperature at which quartz cement precipitated in the reservoir is 14 to 17 °C lower than the present day reservoir temperature (118-121 °C). These data therefore indicate that quartz cementation was impeded at the time the reservoir was buried to around 100-105 °C.

Kingfisher (Brae Unit 2 reservoir) The histograms in Fig.30D and E illustrate that entrapment of fluid inclusions in quartz overgrowths in the oil reservoir in the Kingfisher Field started mainly from 80 to 85 °C onwards. Two lower temperature measurements (67.4 and 74.1 °C) indicate that small amounts of quartz cement may also have precipitated before this main quartz precipitation phase (Appendix C). The scarcity of lower temperature inclusion measurements is again believed to be the consequence of low quartz precipitation rates below 100 °C (Walderhaug, 1994). The T_h distribution of measurements in water zone samples (Fig.30E) indicates that quartz cementation continues to present day reservoir temperatures. For oil zone

samples, the highest measured reliable T_h (120 °C), is only slightly lower than present day reservoir temperature (123 to 126 °C). The lack of T_h measurements above 120 °C in the oil zone samples, could indicate that quartz cementation was recently slowed down or halted.

4.8 Salinity of porefluids during quartz cementation

All salinity data discussed below are converted from T_m values measured in aqueous fluid inclusions. Salinity is expressed as weight % NaCl equivalent (wt% NaCl eq), and was converted from T_m by using the conversion table from Bodnar (1992) (Table 8). Converted salinities >23.18 wt% NaCl eq imply a system not only containing NaCl but additionally $CaCl_2$- and/or $MgCl_2$-components (Goldstein & Reynolds, 1992).

Table 8 Conversion table of measured T_m into salinity (expressed as wt% NaCl eq). T_m was converted into salinity by using the equation of Bodnar (1992).

T_m	,0	,1	,2	,3	,4	,5	,6	,7	,8	,9
0,	0.00	0.18	0.35	0.53	0.71	0.88	1.05	1.23	1.40	1.57
1,	1.74	1.91	2.07	2.24	2.41	2.57	2.74	2.90	3.06	3.23
2,	3.39	3.55	3.71	3.87	4.03	4.18	4.34	4.49	4.65	4.80
3,	4.96	5.11	5.26	5.41	5.56	5.71	5.86	6.01	6.16	6.30
4,	6.45	6.59	6.74	6.88	7.02	7.17	7.31	7.45	7.59	7.73
5,	7.86	8.00	8.14	8.28	8.41	8.55	8.68	8.81	8.95	9.08
6,	9.21	9.34	9.47	9.60	9.73	9.86	9.98	10.11	10.24	10.36
7,	10.49	10.61	10.73	10.86	10.98	11.10	11.22	11.34	11.46	11.58
8,	11.70	11.81	11.93	12.05	12.16	12.28	12.39	12.51	12.62	12.73
9,	12.85	12.96	13.07	13.18	13.29	13.40	13.51	13.62	13.72	13.83
10,	13.94	14.04	14.15	14.25	14.36	14.46	14.57	14.67	14.77	14.87
11,	14.97	15.07	15.17	15.27	15.37	15.47	15.57	15.67	15.76	15.86
12,	15.96	16.05	16.15	16.24	16.34	16.43	16.53	16.62	16.71	16.80
13,	16.89	16.99	17.08	17.17	17.26	17.34	17.43	17.52	17.61	17.70
14,	17.79	17.87	17.96	18.04	18.13	18.22	18.30	18.38	18.47	18.55
15,	18.63	18.72	18.80	18.88	18.96	19.05	19.13	19.21	19.29	19.37
16,	19.45	19.53	19.60	19.68	19.76	19.84	19.92	19.99	20.07	20.15
17,	20.22	20.30	20.37	20.45	20.52	20.60	20.67	20.75	20.82	20.89
18,	20.97	21.04	21.11	21.19	21.26	21.33	21.40	21.47	21.54	21.61
19,	21.68	21.75	21.82	21.89	21.96	22.03	22.10	22.17	22.24	22.31
20,	22.38	22.44	22.51	22.58	22.65	22.71	22.78	22.85	22.91	22.98
21,	23.05	23.11	23.18							

Miller (Brae Unit 2 reservoir) Data from the Miller Field show a range in salinity values of 0.5 to 26.6 wt% NaCl eq (Fig.32A and Appendix C). Reported present day formation water salinity values in the Brae Formation reservoir in the Miller Field range between 7.3 and 8.3 wt% NaCl eq (Smalley & Warren, 1994).

In Fig.33A, salinity is plotted versus T_h measurements. Here it can be seen that most aqueous fluid inclusions were trapped in quartz cement which precipitated from fluids with salinities of 5 to 15 wt% NaCl eq around 100 to 125 °C (Fig.33A).

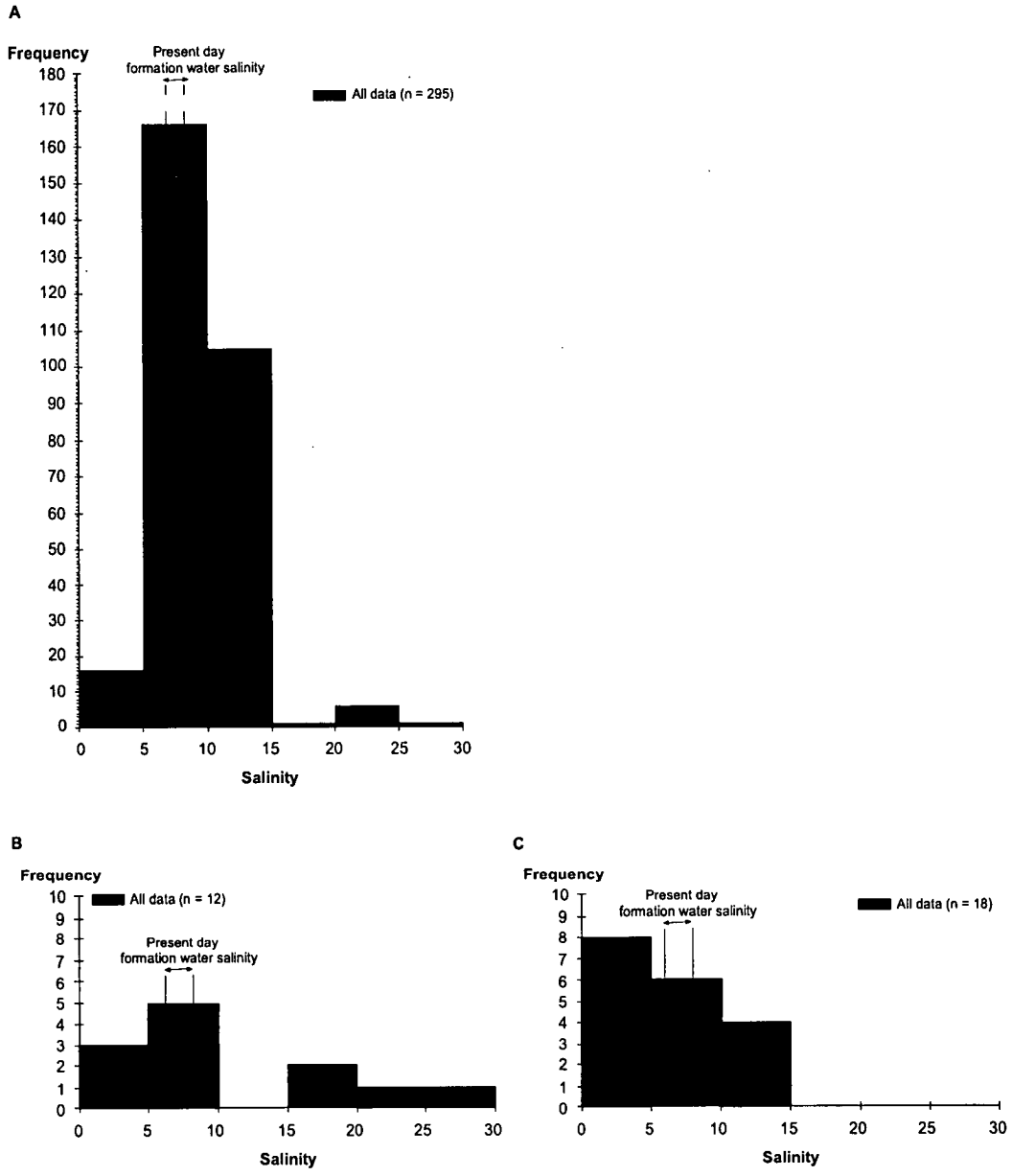

Fig.32 Histograms of the salinity (expressed as wt% NaCl eq) of aqueous fluid inclusions in quartz cement. Salinity was calculated from T_m measurements by using the equation of Bodnar (1992). On each histogram, the number of data n and the present day formation water salinity is indicated.
(A) All salinity data from the Brae Unit 2 reservoir in the Miller Field. Two salinity populations are noticeable. A large population (5-15 wt% NaCl eq) with salinity values ranging around present day formation water salinity (7-8 wt% NaCl eq) and a small population with high salinity (20-25 wt% NaCl eq) values.
(B) All salinity data from the Brae Unit 1 reservoir in the Kingfisher Field. Here also, two salinity populations are noticeable. The first population displays salinities similar to present day formation water salinity (5-10 wt% NaCl eq). The second population displays increased salinity values (15-30 wt% NaCl eq).
(C) All salinity data from the Brae Unit 2 reservoir in the Kingfisher Field. Only one salinity population is present. The data display a spread (5-15 wt% NaCl eq) around present day formation water salinity (6-8 wt% NaCl eq).

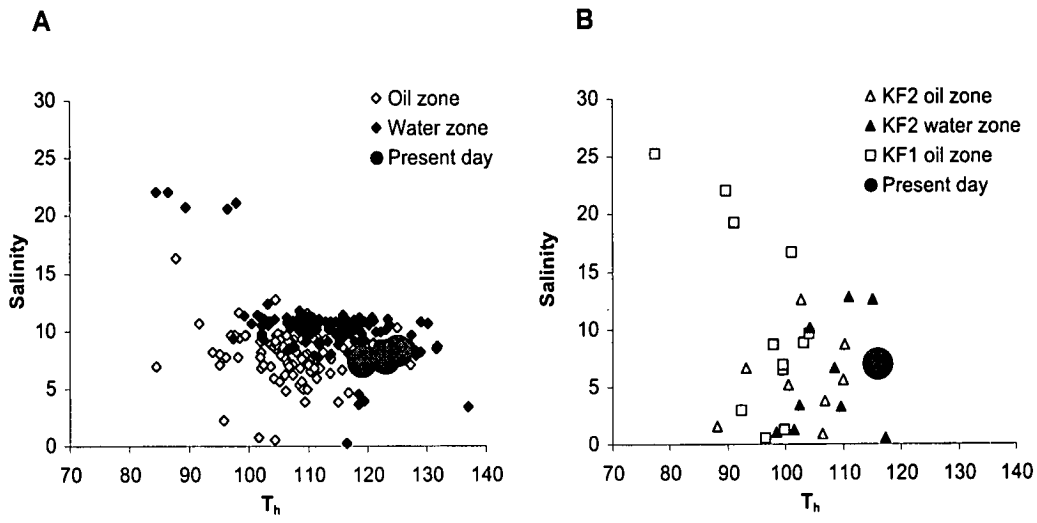

Fig.33 Homogenization temperatures (T_h) of aqueous fluid inclusions plotted versus salinity (expressed as wt% NaCl eq). Large circles represent present day formation water salinity and reservoir temperature conditions.
(A) Data from the Miller Field. This cross-plot illustrates that quartz cementation in the reservoir occurred initially from a high salinity fluid (20-25 wt% NaCl eq). With increasing temperature and burial, the fluid from which quartz precipitated became less saline and approaches present day salinity values. The same phenomenon is observed in the Brae Formation Unit 1 reservoir in the Kingfisher Field **(B)**. In the Brae Formation Unit 2 reservoir in the Kingfisher Field **(B)**, only the lower salinity-high temperature population is observed.

The smaller population of high salinity inclusions (20 to 25 wt% NaCl eq) noticeable on the histogram in Fig.32A, corresponds systematically with the lowest T_h measurements (80 to 95 °C).

If we make the reasonable assumption that fluid inclusions were trapped in increasingly younger quartz cement with increasing temperature, than it is possible to reconstruct palaeosalinity evolution in the reservoir by making temperature interval plots of salinity versus depth. In Fig.34, 5 cross-plots are presented of salinity versus depth with data in each plot from a different temperature interval i.e. <90 °C, 90-100 °C, 100-110 °C, 110-120 °C and >120 °C. The data in the plots are presented as averages of all salinity values measured in inclusions within one sample, with T_h of the inclusions in the relevant temperature interval. Fig.34A (T_h <90 °C) illustrates that quartz cementation started in high salinity fluids in both oil (11.6 to 26.6 wt% NaCl eq) and water zone samples (21.6 wt% NaCl eq). With time, and increasing temperature (T_h 90-100 °C), salinity values decrease but are still higher than present day formation water salinities (Fig.34B). In the oil zone, salinity ranges from 8.6 to 10.6 wt% NaCl eq. In the water zone there is a range

from 9.3 to 11.2 wt% NaCl eq. From 100 °C upwards (Fig.34C, D and E), salinity values in the oil zone group around present day formation water salinity values. In the water zone, it is not until 110-120 °C (Fig.34D) that water zone salinities evolve towards present day formation water salinities. Fig.34E illustrates that in the most recently precipitated quartz cements, salinities are similar to the present day formation water salinity.

Kingfisher (Brae Unit 1 reservoir) Data from the gas condensate reservoir in the Kingfisher Field show a range in fluid inclusion salinity values of 0.5 to 25.2 wt% NaCl eq (Fig.32B and Appendix C). Present day formation water salinity in the Kingfisher Field is 7±1 wt% NaCl eq (Shell, Internal Report). Salinity is cross-plotted with T_h on Fig.33B. Here again, the high salinity aqueous inclusions (15-30 wt% NaCl eq) correspond to the lowest measured T_h (75-90 °C). Inclusions trapped in quartz cement at higher temperatures (>90 °C), display salinities mainly around the value of present day formation water salinity (7 wt% NaCl eq) (Fig.32B and 33B).

Kingfisher (Brae Unit 2 reservoir) Salinities in the Brae Unit 2 reservoir in the Kingfisher Field range from 0.5 to 12.7 wt% NaCl eq (Fig.32C and Appendix C). This dataset lacks the small high salinity (>15 wt% NaCl eq) population measured in the other two Brae Formation reservoirs examined (Fig.33).

Fig.34 (p.77) Salinity data (expressed as wt% NaCl eq) from aqueous fluid inclusions in quartz cement from samples in the Miller Field plotted versus depth (in metres). Different plots represent data from different temperature intervals. Salinity values in the plots are averages of salinities calculated from all T_m measurements in fluid inclusions in one sample, with T_h taken from those same fluid inclusions in the particular temperature interval of the plot. Present day formation water salinity (from Smalley & Warren, 1994) is indicated on each plot. Yellow areas enclose oil zone data on the plots, whereas blue areas enclose water zone data.
The graph in **(A)** illustrates that quartz cementation started (T_h <90 °C) from high salinity fluids in both oil and water zones in the reservoir. With time, and increasing burial and temperature **(graphs B to E)**, formation water salinity values evolved towards present day formation water salinity. Since the reservoir was buried to 100-110 °C **(graph C)**, no change in formation water salinity has occurred in the oil zone. In the water zone, formation water salinity values kept evolving until the present day **(graphs C to E)**.

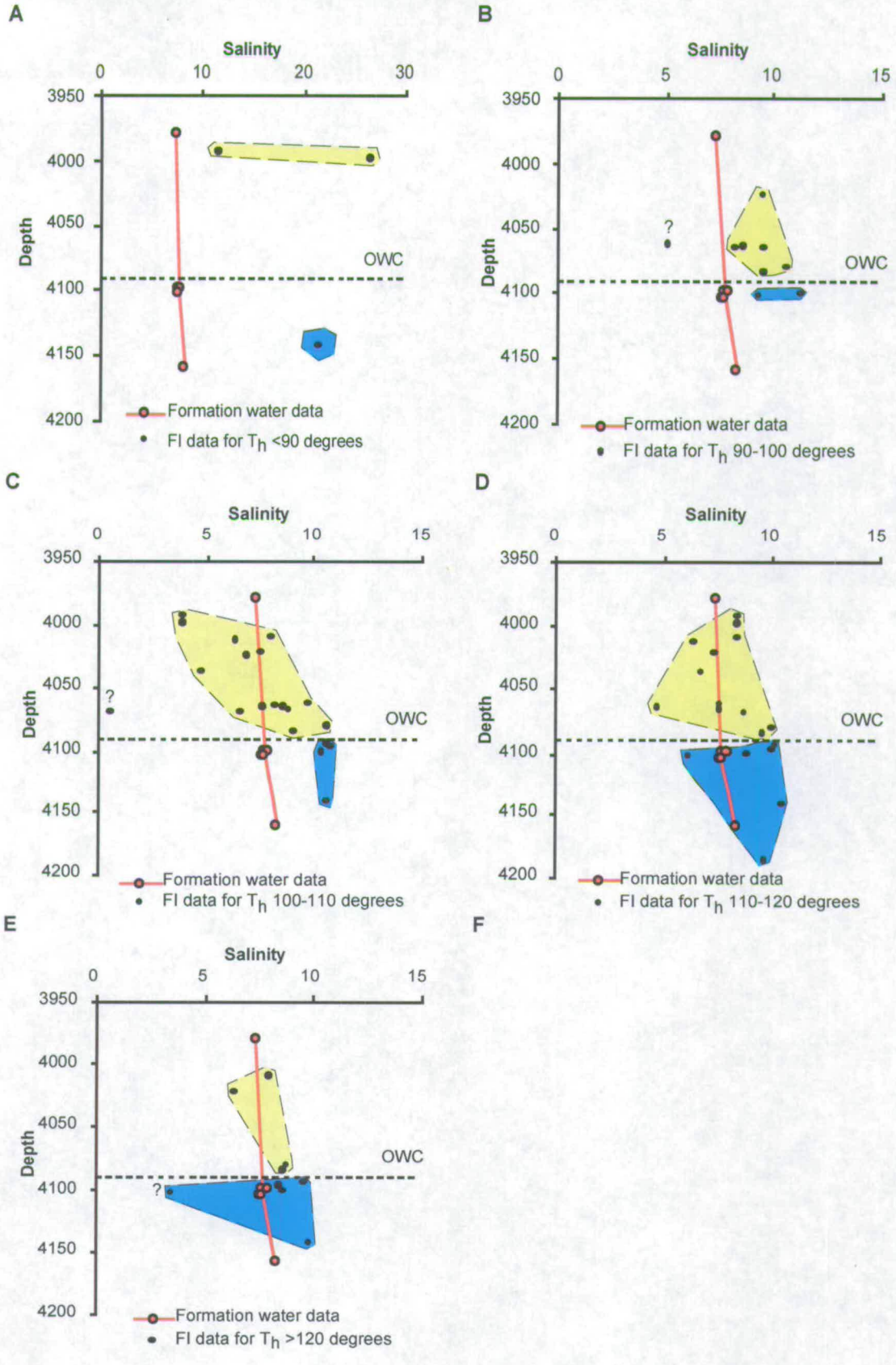
A
Salinity
0
10
20
30
3950
4000
4050
4100
4150
4200
Depth
OWC
Formation water data
FI data for Th <90 degrees
B
Salinity
0
5
10
15
?
OWC
Formation water data
FI data for Th 90-100 degrees
C
Salinity
0
5
10
15
?
OWC
Formation water data
FI data for Th 100-110 degrees
D
Salinity
0
5
10
15
OWC
Formation water data
FI data for Th 110-120 degrees
E
Salinity
0
5
10
15
OWC
?
Formation water data
FI data for Th >120 degrees
F

4.9 Petroleum inclusions

Petroleum inclusions are rare in samples from both the Miller and Kingfisher Fields. Where present, they occur in secondary trails in detrital quartz (Fig.35E and F) or as irregularly shaped single inclusions within detrital quartz (Fig.35A and B). The petroleum inclusions are typically irregularly shaped and are often much larger (up to 25 μm) than aqueous inclusions (Fig.35C and D). They occur in oil and water zone samples in similar shapes and numbers.

Some researchers use the presence of primary oil inclusions enclosed within quartz overgrowths as an argument for continued quartz cementation in the presence of petroleum (eg. Oelkers et al., 1992; Saigal et al., 1992; Walderhaug, 1994 and 1996; Bjørkum et al., 1998). The lack of primary oil inclusions in quartz overgrowths in the Brae Formation sandstones indicates that the entrapment of petroleum inclusions was not contemporaneous with extensive quartz cementation. The shape and location of oil inclusions in the detrital quartz grains suggests that oil migrated into the inclusions via microcracks linking the inclusions with the porespace (Fig.35B and D), or via secondary microfractures (Fig.35F). Note that the grains with petroleum-filled inclusions lack authigenic overgrowths (Fig.35), and no petroleum inclusions have been observed within quartz overgrowths. These observations indicate that no cementation occurred after oil-fill and the petroleum inclusions in the examined samples are the result of a post oil-fill physical process.

Other researchers who have observed primary oil inclusions in quartz cement (e.g. Munz et al., 1999) find that they tend to be trapped at the interface between detrital grain and overgrowth. According to R. Larese (personal communication), inclusions located on this boundary are especially prone to leaking (i.e. oil replacing aqueous fluid) and can consequently not be used as evidence for continued cementation in the presence of oil. R. Larese's (personal communication) finding is based on the observation of inclusion populations located on dust rims which contain aqueous as well as oil-filled inclusions.

4.10 Discussion

From the petrographic study it was clear that the three studied Brae Formation reservoirs display distinctly different quartz cement abundances despite being buried to similar depths and temperatures (Chapter 3). The most plausible

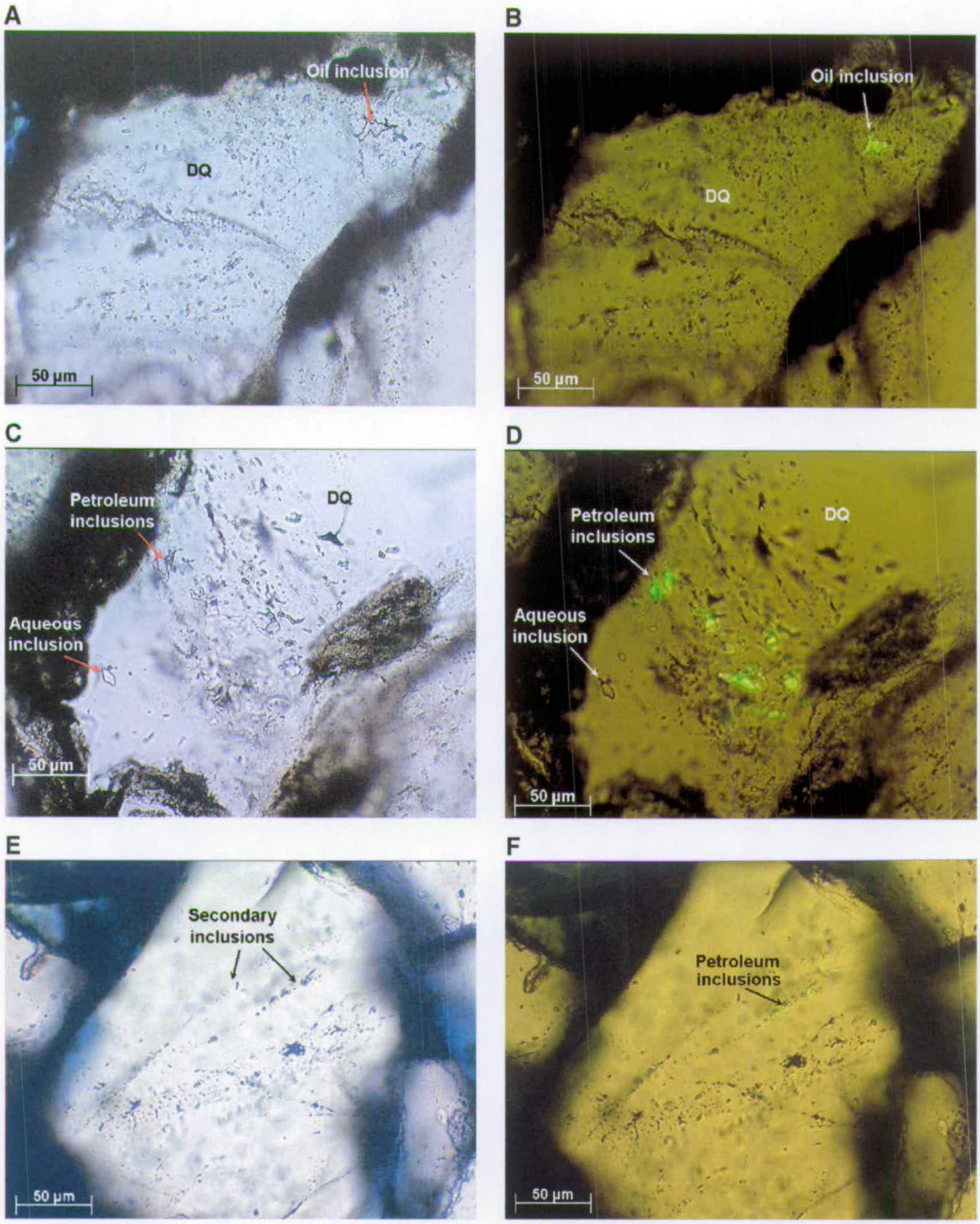

Fig.35 Photomicrographs of petroleum fluid inclusions in quartz cement in the Brae Formation sandstones. Photomicrographs in the left column are taken under plane polarized light. Photomicrographs in the right column show the same field of view as the ones in the left column, but are taken under a combination of plane polarized and UV light.
(A and B) Petroleum inclusions are rare in the studied samples and occur as irregularly shaped inclusions in detrital quartz (DQ) grains – sample depth 4028.8 m, well 8a-4 (Kingfisher Field Brae Unit 2).
(C and D) The irregular shape of petroleum inclusions in detrital quartz (DQ) suggests that they are reset. Petroleum inclusions are also typically larger than aqueous inclusions – sample depth 4028.8 m, well 8a-4 (Kingfisher Field Brae Unit 2).
(E and F) Trail of petroleum inclusions, occurring together with aqueous inclusions, in a microfracture cross-cutting a detrital quartz grain – sample depth 3887.3 m, well 8a-8 (Kingfisher Field Brae Unit 1).

explanation for these quartz cement patterns in the Miller and Kingfisher Fields is that cementation was hindered as a result of oil emplacement in the reservoirs. Fluid inclusion data confirm this hypothesis.

Oil filling In the Brae Unit 2 reservoir in the Miller Field, quartz cement was precipitated from at least 70 °C onwards (Fig.30A). The high porosity layers throughout the reservoir, which are generally the crestal areas under bounding shale barriers, display systematically the lowest measured maximum T_h (105-110 °C in zones J and L and 95 °C in zone K; Fig.31) and the lowest quartz cement volumes (3-5 %; Fig.24). This is a strong indication that oil emplacement impeded quartz cementation in the crestal areas of the reservoir zones first. The data suggest that quartz cementation in the top areas of the reservoir zones stopped when the temperature in those areas of the reservoir was 10 to 15 °C (zone J and L), or even 25 °C (zone K) lower than the present day reservoir temperature. The data equally indicate that the earliest oil entered zone K of the Miller Field when the reservoir was buried to 95 °C. When the reservoir was buried to 105-110 °C, oil had started to fill also zones J and L. In all other samples across the reservoir, temperatures close to present day reservoir temperatures can be measured. This indicates that the reservoir only recently filled to its present day level (OWC 4090 m). This implies that the filling of the Brae Formation Unit 2 sandstone reservoir in the Miller Field was not a rapid process, but took place over a prolonged period of time. This long period of progressive oil-fill allowed the differential quartz cementation pattern to develop as the OWC moved down gradually. In the water zone of the reservoir, T_h measurements similar to present day reservoir temperatures (Fig.31) and higher quartz cement abundances (10-15 %; Fig.24) indicate continuing quartz precipitation.

In the Brae Formation Unit 1 and Unit 2 reservoirs in the Kingfisher Field, quartz cement was also precipitating from at least 70 °C onwards (Fig.30C and D). The maximum measured T_hs do not vary between samples from different depths across the respective reservoirs. In the Unit 1 gas condensate reservoir, maximum measured T_h does not exceed 105 °C (Fig.30B). This indicates that cementation in this reservoir was impeded when buried to approximately 15 °C lower than the present day reservoir temperature (118-121 °C). Consequently, the reservoir sandstones were saved from extensive cementation and low quartz cement

abundances (generally <5 %) prevail (Fig.24). The lack of quartz cement abundance variation in the reservoir (Fig.24) suggests that petroleum filling of the structure probably occurred rapidly at burial temperatures of around 105 °C. In the Unit 2 oil reservoir, maximum measured T_h (120 °C) in oil zone samples is close to the present day reservoir temperature (123-126 °C; Fig.30C). Here also, quartz cement abundance does not vary significantly across the oil zone (Fig.24). This indicates a recent, possibly still ongoing, relatively rapid oil-fill. Because this reservoir spent a long period of time oil-free, quartz cement abundances are higher (8-12 %) than in the gas condensate reservoir (Fig.24). Fluid inclusion temperatures from water zone samples in the Brae Unit 2 oil reservoir indicate continuing precipitation of new quartz cement (Fig.30C).

Salinity Two populations of salinity values can be differentiated in the Brae Unit 2 reservoir in the Miller Field and the Brae Unit 1 reservoir in the Kingfisher Field (Fig.32). Initially, quartz cement in these reservoirs precipitated from high salinity (15-30 wt% NaCl eq) fluids at temperatures around 70-95 °C (Fig.33). Later, at deeper burial, quartz cementation occurred at higher temperatures (>95 °C) from fluids with salinity (mainly between 5 and 10 wt% NaCl eq) comparable to present day formation water salinity (6-8 wt% NaCl eq; Fig.33). In the Brae Unit 2 reservoir in the Kingfisher Field, evidence was found only for quartz cementation in the less saline and higher temperature type fluid (Fig.33).

Worden (1996) identified three mechanisms to explain increased salinity in formation waters : sea water evaporation, diagenetic reactions and salt dissolution. Sea water evaporation, a near surface process, cannot have caused elevated salinity in the Brae reservoir formation waters because of the deep-marine deposition environment of the sandstones. A plausible explanation for the high salinity fluid inclusions in quartz cement of the Brae Formation sandstones could be clastic diagenesis. According to Worden (1996), hydration reactions such as K-feldspar dissolution can increase salinity. K-feldspar reacts with formation water to form kaolinite. This reaction also releases silica into the porewater, which then can reprecipitate as quartz cement. The K-feldspar dissolution reaction reduces water volume and increases salinity in the remaining pore water. K-feldspars in the Brae Formation sandstones are typically affected by dissolution (Chapter 3). However, they are present only in limited amounts (<4.5 %) and also the amount of authigenic kaolinite is small (<3.5 %). Therefore, it seems unlikely that K-feldspar reactions

can be held solely responsible for the high porewater salinities recorded in fluid inclusions in early quartz cement. A final possible explanation for the high salinity palaeofluids is migration of salt-rich waters, which mixed with local formation waters, through the Brae Formation sandstones. The temperature range of 70-95 °C corresponds with the period of time when mechanical compaction in the sandstones was coming to an end (~1500-2500 m; see Chapter 3) and no significant amounts of quartz cement were yet precipitated (Chapter 3). This means that during the temperature interval of 70-95 °C, post-compaction - pre-cementation porosities of 26 (Paxton et al., 1990) to 30 % (Houseknecht, 1987) were most likely present in the sandstones. Such porosities could easily have permitted through-flow of fluids from outside the Brae Formation. A possible origin for the salt rich fluids could be the underlying Permian marginal marine Zechstein facies (Hodgson et al., 1992; Kerlogue et al., 1994; Thomas & Coward, 1996). According to Burley et al. (1989), the Zechstein brine is distinctly enriched in sulphate and bicarbonate. Geochemical analyses of present day formation water from the Brae Unit 2 reservoir in the Miller Field indicate a high bicarbonate content (1040-2520 mg/l; Smalley & Warren, 1994). This could be interpreted as a remnant of the ancient palaeofluid.

Around 90-95 °C, a change in reservoir hydrology occurred in the Brae Unit 2 and Brae Unit 1 reservoirs in the Miller and Kingfisher Fields respectively (Fig.33). From aqueous fluid inclusion T_h data and quartz cement abundance patterns, it was concluded that this temperature range represents the initial stage of petroleum emplacement into these reservoirs. During the initial stages of petroleum charge, when oil saturations are low, quartz cementation probably continues but at a reduced precipitation rate (Walderhaug, 1996; Worden et al., 1998). In the aquifer of the reservoirs, quartz continues to precipitate at increasing rates with increasing temperature (Walderhaug, 1994). Increasing quartz cement abundance in the water zones and petroleum emplacement in the oil zones of the reservoirs will have decreased porosities and permeabilities in the Brae Formation. This will have limited continued influx of salt-rich external fluids. Also, clay mineral reactions (particularly the transformation of illite to smectite) in source rock shales interbedded with the Brae Formation sandstones generate H_2O-rich porewaters (Scotchman et al., 1989). These shale dehydration waters may have diluted the high salinity fluids in the reservoirs and may have caused the salinity of fluid inclusions incorporated in quartz cement to drop to values comparable to present day formation water (5-10 wt% NaCl eq). In the Brae Unit 2 reservoir in the Miller Field, and also in the Brae

Unit 1 reservoir in the Kingfisher Field, no evolution in oil zone salinity has occurred since the reservoir reached 100-110 °C (Fig.34). This indicates that, after oil emplacement, porewaters in the reservoirs remained static and no mixing with the underlying aquifer waters occurred. In the water zone of the Brae Unit 2 reservoir in the Miller Field, salinity continued to evolve towards present day formation water salinity values (Fig.34).

The lack of high salinity fluid inclusions in quartz cements in the Brae Unit 2 sandstone reservoir in the Kingfisher Field (Fig.32C) can be explained by the fact that only a limited amount of measurements were performed in samples from this reservoir. Quartz cements precipitated in this reservoir at temperatures below 90 to 100 °C are volumetrically almost insignificant in comparison to total quartz cement volumes. The bulk of the quartz cement precipitated at temperatures >100 °C. Therefore, the probability of finding fluid inclusions in early quartz cements (low temperature – high salinity) is low.

Petroleum inclusions Petroleum-filled inclusions in samples from the Brae Formation reservoir sandstones in the Miller and Kingfisher Fields cannot be used as evidence for continued quartz cementation in the presence of oil. It can be argued, however, that the petroleum-filled inclusions in detrital quartz grains and microfractures imply some continuation of cementation after entrapment in order to seal the inclusions from the external environment. According to Worden & Morad (2000), the key question is what oil saturation level is necessary during quartz cementation in order to give rise to oil inclusions. It seems unlikely that petroleum inclusions can be trapped at high oil saturation when most of the water has been displaced from the reservoir rocks. Therefore, most authors have concluded that petroleum inclusions are trapped on oil migration routes (e.g. Bodnar, 1990; Munz et al., 1999) or in the transition zone between oil and water (Oxtoby et al., 1995). This implies that primary oil inclusions in quartz cement in oil zone samples were trapped during the earlier stages of oil emplacement. Water saturation in the reservoir is still high at this stage and neither flow rates nor diffusion rates are significantly reduced, permitting quartz to continue to grow unhindered (Worden & Morad, 2000). With rising oil saturation, it seems most probable that quartz cementation in the oil zone sandstones is strongly inhibited by oil emplacement compared to the underlying aquifer sandstones.

4.11 Conclusions

1 Quartz cement was being precipitated in all three Brae Formation reservoirs studied from at least 70 °C onwards.

2 In the Miller Field, quartz growth temperatures are different between oil and water zone samples. In the oil zone, T_h is lowest in the crestal areas of the reservoir zones (95-105 °C). Deeper down in the reservoir zones, T_h approaches present day reservoir temperatures. This pattern corresponds with low quartz cement abundances in the crestal areas of the reservoir (3-5 % quartz cement), and higher quartz cement abundances with increasing depth (5-12 % quartz cement). In the water zone of the reservoir, T_h close to present day reservoir temperature (120-125 °C) indicates continuing quartz cementation up to the present day.

3 In the gas condensate reservoir in the Kingfisher Field (Brae Unit 1), quartz cementation continued until the reservoir was buried to 105 °C. From this time onwards until the present day (reservoir temperature 118-121 °C), no evidence of new quartz cement precipitation is found. This is reflected in an overall low quartz cement abundance (<6 %).

4 In the oil reservoir in the Kingfisher Field (Brae Unit 2), quartz growth temperatures in oil zone samples (up to 120 °C) are only slightly lower than in water zone samples (up to 125 °C). These temperatures, which are close to present day reservoir temperature (123-126 °C), indicate presently ongoing quartz cementation. This resulted in overall high quartz cement abundances (8-12 %) throughout the reservoir.

5 In the Miller Field, the correlation between fluid inclusion homogenisation temperatures and quartz cement abundances indicates that the systematic decline in porosity and the increase of quartz cement volume with depth resulted from gradual petroleum fill from the crest of the reservoir down. In this reservoir, oil charge began when the Brae Formation sandstones were buried to temperatures of 95-105 °C. The higher quartz growth temperatures deeper down in the reservoir oil zone, and corresponding higher quartz cement volumes, suggest a slow oil fill over a prolonged period of time. In the Brae Unit 1 reservoir in the Kingfisher Field, petroleum emplacement was completed when the reservoir was buried to 105 °C. Lack of quartz cement variation across the oil zone may indicate a rapid fill. In the Brae Unit 2 reservoir in the Kingfisher Field, oil charge was a recent event. This is indicated by quartz growth

temperatures similar to the present day reservoir temperature, and similar quartz cement volumes in the oil and water zone samples.

6 Quartz cements in the Brae Formation reservoirs of the Miller and Kingfisher Fields precipitated initially from high salinity (15-30 wt% NaCl eq) – low temperature (70-95 °C) fluids. High salinity in these reservoirs was possibly the result of through-flow of salt-rich fluids derived from underlying formations (Zechstein?). High porosities and permeabilities, and low cement volumes in the sandstones around that temperature range support the hypothesis of an open system allowing influx of fluids. From 95 °C onwards, the salinity of the fluid from which quartz cement precipitated (0.5-15 wt% NaCl eq) was more similar to the present day formation water salinity (6-8 wt% NaCl eq). Around this temperature, petroleum had started to fill the Brae Unit 2 reservoir in the Miller Field and the Brae Unit 1 reservoir in the Kingfisher Field and closed down quartz cementation. Cementation continued in the aquifers and across the whole Brae Unit 2 reservoir in the Kingfisher Field which experienced a recent oil fill.

7 Petroleum inclusions in the Brae Formation sandstones are rare. They occur either as single inclusions in detrital quartz grains or as lines of inclusions in microfractures. The lack of primary oil inclusions in quartz overgrowths in the Brae Formation sandstones indicates that the entrapment of petroleum inclusions was not contemporaneous with extensive quartz cementation.

CHAPTER V

BASIN MODELLING

In this chapter :

- *What are the burial and temperature histories of the Brae Formation sandstones and of the Kimmeridge Clay source rocks ?*
- *When did quartz cementation begin in the reservoirs of the Miller and Kingfisher Fields ?*
- *When were hydrocarbons emplaced in the reservoirs of the Miller and Kingfisher Fields ?*
- *Is there a relationship between the timing of hydrocarbon emplacement and the abundance and distribution of quartz cement in the reservoirs ?*

5.1 Introduction

In the Brae Formation Unit 2 oil reservoirs in the Miller and Kingfisher Fields, and also in the Brae Unit 1 gas condensate reservoir in the Kingfisher Field, the timing of hydrocarbon (HC) emplacement is considered to have had a strong impact on reservoir quality. This hypothesis is based upon quartz cement growth temperatures, derived from the fluid inclusion study in Chapter 4, and petrographic quartz cement abundance data (Chapter 3). Reservoirs, or parts of reservoirs, which are thought to have had an early hydrocarbon fill display systematically low quartz cement abundances and the lowest quartz cementation temperatures (e.g. crestal areas of Brae Unit 2 reservoir in the Miller Field and Brae Unit 1 reservoir in the Kingfisher Field). Reservoirs, or parts of reservoirs, which are thought to have had only a recent hydrocarbon fill display systematically high quartz cement abundances and the highest quartz cementation temperatures (e.g. lower areas of Unit 2 reservoir in the Miller Field and Unit 2 reservoir in the Kingfisher Field).

In this chapter, I detail the reconstruction of the burial and thermal history of the reservoirs and source rocks with a 1D-modelling package BasinMod®. Subsequently, by integrating quartz cement growth temperatures with the reservoir rocks' thermal histories, I determined the duration of quartz cementation in each Brae Formation reservoir studied. The absolute time at which hydrocarbons enter a reservoir is difficult to constrain. I gained an approximate insight into oil emplacement timing by calculating the maturity of the source rocks according to Lopatin's method. Finally, I examined whether there is a relationship between the timing of oil charge and quartz cement abundance in each reservoir. If such a relationship can be shown, then the hypothesis that oil emplacement slows quartz cementation holds true.

5.2 Methodology

BasinMod® 1D modelling software was used to calculate the burial and thermal histories of reservoir rocks and source rocks. The BasinMod® software is licensed and produced by Platte River Associates, Inc.; a petroleum systems analysis company based in Boulder (Colorado - USA). The maturity of the source rocks was calculated according to the method of Lopatin (1971).

Burial history The main input parameter for generating the burial history of the Brae Formation sandstones was stratigraphic well log data. For this purpose, composite logs (1:500) of well 16/8b-3 in the Miller Field and well 16/8a-1 in the Kingfisher Field were used. Stratigraphic data such as formation names, initial ages, depths of formation tops and formation thicknesses were entered into a master spreadsheet in the computer program. The data entered for wells 16/8b-3 and 16/8a-1 are given in Table 9. Depths for all measured input data were entered relative to sealevel. The burial depth history of rocks in each well was subsequently determined by backstripping and decompacting the sediments. Backstripping involves the sequential removal of sediment packages, in this case formations, back in time and restoring the historical sediment package thicknesses and depths (Iliffe & Dawson, 1996). Historical sediment thicknesses were determined by utilising an empirical compaction model. Compaction is an essential consideration in basin modelling since compaction corrections will have an impact on thermal history which, in turn, affects the timing of source rock maturity, petroleum generation and expulsion

Table 9 Stratigraphic input data, derived from composite well logs, for reconstruction of burial histories with BasinMod®. The data are tabled as they feature in the master input spreadsheet of the program.

Location	Well	Formation or Event Name	Begin Age (My)	Well Top (m)	Present Thickness (m)
Miller	8b-3	Recent-Pliocene	5.3	108.2	422.5
		Miocene	23.7	530.7	377.6
		Oligocene	36.6	908.3	302.4
		Eocene	57.8	1210.7	836.7
		Palaeocene	66.4	2047.4	696.7
		Danian	70.0	2744.1	89.7
		Cretaceous	143.0	2833.8	1085.4
		KC1	144.3	3919.2	70.7
		Brae2	148.6	3989.9	283.1
		KC2	148.9	4273.0	10.1
		Brae3	150.2	4283.1	72.2
		KC3	157.0	4355.3	482.5
Kingfisher	8a-1	Recent-Pliocene	5.3	106.1	409.9
		Miocene	23.7	516.0	365.8
		Oligocene	36.6	881.8	646.2
		Eocene	57.8	1528.0	551.7
		Palaeocene	66.4	2079.7	530.3
		Danian	70.0	2610.0	79.3
		Cretaceous	143.0	2689.3	1142.1
		KC1	145.0	3831.4	53.9
		Brae1	146.5	3885.3	73.2
		KC2	149.0	3958.5	27.7
		Brae2	151.0	3986.2	62.2
		KC3	152.0	4048.4	10.7
		Brae3	153.0	4059.1	107.0
		KC4	157.0	4166.1	505.3

(BasinMod 1D Manual, 1996). The method of Sclater and Christie (1980) was used for the compaction correction calculations. This method considers the effect of mechanical compaction which occurs in the sediment as a result of loading. Sclater and Christie (1980) empirically derived a relationship between porosity and depth based on a study of eight wells on the flanks of, and in the middle of, the Central Graben (North Sea). The equation relating porosity to depth is :

$$\phi = \phi_0 . e^{(-Kz)} \qquad (eq\ 1)$$

where ϕ is porosity, ϕ_0 is depositional porosity, K is a compaction factor [cm^{-1}] adjusted for varying compressibilities of different lithologies and z is depth [cm]. Parameters for the Sclater and Christie exponential relationship for various normally pressured North Sea lithologies are presented in Table 10. Backstripping and sediment decompaction calculations in BasinMod® are performed for each formation individually. Apart from formation age and depth, lithological composition also has to be entered as an input parameter for each formation. The program contains a lithology library for easy entry and retrieval of lithological data. The library contains

Table 10 Input parameters for the Sclater & Christie exponential relationship between porosity (ϕ) and depth for various normal pressured North Sea lithologies. (source : Sclater & Christie, 1980)
ϕ_0 = depositional porosity
K = compaction factor [cm^{-1}]

Lithology	ϕ_0	Compaction factor (K)
Shale	0.63	0.51×10^{-5} /cm
Sand	0.49	0.27×10^{-5} /cm
Chalk	0.70	0.71×10^{-5} /cm
Shaley sand	0.56	0.39×10^{-5} /cm

Table 11 BasinMod® lithology library as presented in the program. This table contains rock property data for eight default lithologies. (source : BasinMod® Manual, 1996)

Lithology	Initial Porosity	Reciprocal Compaction Factor (km^{-1})	Exponential Compaction Factor (km^{-1})	Matrix Density (g/cm^3)	Grainsize (mm)	Quartz Fraction	Clay Coating Fraction on Quartz	Matrix Thermal Conductivity (W/m.C)	Matrix Heat Capacity ($kJ/m^3.C$)	Initial Vertical Permeability (mD)
Sandstone	0.45	1.75	0.27	2.64	0.5	0.9	0	4.4	2800	30000
Siltstone	0.55	2.2	0.41	2.64	0.0156	0.5	0	2	2650	100
Shale	0.6	2.4	0.51	2.6	0.0004	0.25	0	1.5	2100	10
Limestone	0.6	1.5	0.22	2.72	0.5	0	0	2.9	2600	5000
Dolomite	0.6	1.5	0.22	2.85	0.5	0	0	4.8	2600	5000
Evaporite	0	0	0	2.15	0.0004	0	0	5.4	1750	1.00E-09
Kerogen	0.9	3.5	0.7	1.8	0.0004	0	0	0.3	950	10
Igneous	0	0	0	2.65	0.0001	0	0	2.9	2500	1.00E-09

a default set of eight pure lithologies along with the rock property values required for calculations (Table 11). The rock properties include initial porosity and permeability, compaction factor, density, grain size, quartz fraction and quartz grain clay coating fraction, conductivity and heat capacity. From well log examination, it was clear that the formations defined for wells 16/8b-3 and 16/8a-1 (Table 9) were a mixture of the pure default lithologies available in the program. Therefore, the "Lithology Mix" option was used to create mixed lithologies by specifying percentages of the pure lithology components. The rock properties for the lithology mixes were interpolated from the values of the pure lithologies. An overview of the mixed lithologies used for constructing the burial graphs of the Brae Formation sandstones is given in Table 12. Default porosity and grainsize values for the Brae Formation sandstones in the Miller and Kingfisher Field were modified and replaced by average measured values (Table 13).

Thermal history BasinMod® provides a range of options to assist in the reconstruction of thermal histories. In the various options, the present day geothermal gradient or heat-flow condition of the examined well is typically used as the known pivotal point from which some reasoned estimate of the thermal history is

Table 12 Percentage of pure lithology components present in each formation defined for wells 8b-3 and 8a-1. The composition of each formation was derived from well log information.

Location	Well	Formation or Event Name	Lithological Composition				
			sandstone	siltstone	shale	limestone	igneous
Miller	8b-3	Recent-Pliocene	39	3	58	0	0
		Miocene	44	4	45	7	0
		Oligocene	7	91	0	2	0
		Eocene	11	12	70	7	0
		Palaeocene	65	9	20	2	4
		Danian	0	0	0	100	0
		Cretaceous	0	0	45	55	0
		KC1	5	9	86	0	0
		Brae2	84	0	16	0	0
		KC2	0	0	100	0	0
		Brae3	55	0	45	0	0
		KC3	21	0	78	1	0
Kingfisher	8a-1	Recent-Pliocene	0	0	100	0	0
		Miocene	10	0	90	0	0
		Oligocene	24	7	69	0	0
		Eocene	16	12	72	0	0
		Palaeocene	66	5	28	1	0
		Danian	0	0	0	100	0
		Cretaceous	0	0	41	59	0
		KC1	5	10	85	0	0
		Brae1	70	0	30	0	0
		KC2	11	0	89	0	0
		Brae2	60	0	40	0	0
		KC3	17	0	83	0	0
		Brae3	40	0	60	0	0
		KC4	15	0	85	0	0

constructed (Iliffe & Dawson, 1996). It is believed that more realistic thermal models can be produced by estimating heat flow rather than by estimating geothermal gradients (BasinMod® 1D Manual, 1996). This is because present day heat flow values can be derived from measured bottom-hole temperatures in wells and can be applied by analogy to the past. Attempts to reconstruct geothermal gradients back through time will always contain a certain degree of uncertainty. Additionally, using geothermal gradients for calculating temperature history does not take the thermal conductivity of the rocks into account. For these reasons, the steady-state-heat flow module was used for calculating the temperature histories in the Miller and Kingfisher areas. Present day heat flow values for wells 16/8b-3 and 16/8a-1 were derived from measured bottom-hole temperatures and are presented in Table 13. These present day heat flow values were used to reconstruct the thermal histories of the models. The assumption that heat flow did not change through the geological history of the rocks is not necessarily a true reflection of reality. However, no palaeogeothermal data for the studied areas were available. Therefore, the simplest option was followed and thermal histories were reconstructed based on the derived present day heat flow values instead of making unquantified assumptions

about palaeo-heat flow values. The temperature history curves were generated by calculating the temperature for each formation at every time interval by using the following equation:

$$HF = k.\ dT/dz \quad (eq\ 2)$$

where HF is heatflow [$W.m^{-2}$], k is thermal conductivity [$W.m^{-1}K^{-1}$], T is temperature [K] and z is depth [m]. BasinMod® default thermal conductivity values (Table 14) were used in the calculations. Again, values for mixed lithologies were interpolated from the values of the pure lithologies. The default conductivities used in BasinMod® are the result of experimental work performed by Brigaud and Vasseur (1989).

Table 13 Input parameters derived from real geophysical measurements (except * and **) used in calculations of burial and temperature histories by BasinMod®. (source data : Rooksby, 1991; Shell Internal Report)
* as determined by optical microscopy
** calculated from measured present day reservoir temperature

Well	Formation	Depth (m)	BHT (°C)	Fluid pressure (MPa)	Grainsize(*) (μm)	Porosity (%)	HF(**) (mW/m^2)
8b-3	Brae 2	3990	120	50	328	13	44.6
8a-1	Brae 1	3880	115	49.3	310	30	41.3
8a-1	Brae 2	3990	120	49.6	324	15	41.3

Table 14 BasinMod® default thermal conductivity values. These values are used by the program for calculation of heatflow in the different formations. (source : BasinMod® Manual, 1996)

Lithology	Thermal Conductivity Value (mcal/cm.s.C)	(W/m.C)
Sandstone	10.51	4.4
Siltstone	4.78	2
Shale	3.58	1.5
Limestone	6.93	2.9
Dolomite	11.46	4.8
Evaporite	12.9	5.4
Igneous	6.93	2.9

Maturity Maturity refers to a prediction of the relative transformation state of any organic material with respect to the formation to oil and gas (Iliffe & Dawson, 1996). Since organic transformation reactions are temperature dependent, the temperature histories constructed for the formations were used for maturity prediction calculations. The maturity of the Kimmeridge Clay Formation was

calculated by means of the Time Temperature Index (TTI) (Lopatin, 1971). This method considers time and temperature as the two factors important to oil generation and destruction. Lopatin (1971) assumed that the dependence of maturity on time is linear; that is, doubling the kerogen cooking time at a constant temperature doubles the maturity. Lopatin divided the temperature profile into 10 °C intervals. He chose the 100-110 °C interval as the base interval and assigned it an index of n=0. The other intervals were assigned the index values shown in Table 15. Lopatin then defined a γ factor, which reflects the exponential dependence of maturity on temperature. He assumed that the rate of maturation increased by a factor of 2 for every 10 °C increase in reaction temperature. Thus within any 10 °C temperature interval T_i-T_{i+1}, the temperature factor γ is equal to 2^n, where $n=(T_i-100)/10$ (Table 15). For his time factor, Lopatin used the length of time (in My) that the sediment spent in each temperature interval. The maturity added in any temperature interval i is given by :

$$Maturity_i = 2^n{}_i.\Delta t_i \qquad (eq\ 3)$$

where Δt_i is the length of time spent by the sediment in the ith temperature interval. Because maturation effects on the organic material are additive, the total maturity (or TTI) of a given sediment is equal to the sum of the maturities acquired in each temperature interval :

$$TTI = \sum_{n_{min}}^{n_{max}} 2^n.\Delta t_n \qquad (eq\ 4)$$

where n_{max} and n_{min} are the n-values of the highest and lowest temperature intervals encountered. According to Lopatin (1971), the oil generative window of source rocks lies between TTI values of 15 to 160. Shales with TTI <15 are immature, whereas shales with TTI >160 are overmature.

If Lopatin's method is correct, the TTI values should correlate with data obtained from other methods of evaluating the thermal maturity of organic material. For this reason, the calculated TTI values were converted into vitrinite reflectance (Ro) values according to the method of Waples (1980) :

$$\log TTI = 4.1152 \log Ro + 1.8189 \qquad (eq\ 5)$$

The calculated Ro values were subsequently compared (section 5.3) to measured Ro values obtained from BP-Amoco for North Sea block 16/7b (Table 16).

Table 15 Temperature indices (n) as assigned by Lopatin (1971) to different temperature intervals. The temperature factor γ, which reflects the exponential dependence of the maturity of rocks on temperature, is calculated for each temperature interval as $\gamma = 2^n$ (Lopatin, 1971). Temperature indices are essential input parameters for source rock maturity prediction calculations according to Lopatin's method.

Temperature Interval (°C)	n	Temperature Factor γ
20-30	-8	0.00390625
30-40	-7	0.0078125
40-50	-6	0.015625
50-60	-5	0.03125
60-70	-4	0.0625
70-80	-3	0.125
80-90	-2	0.25
90-100	-1	0.5
100-110	0	1
110-120	1	2
120-130	2	4
130-140	3	8
...	...	...

Table 16 Vitrinite reflectance data (% Ro) measured in Kimmeridge Clay source rocks in well 16/7b-20 in the Miller Field. (source data : BP-Amoco)

Location	Well	Depth (m)	Vitrinite reflectance %Ro
UK block 16	16/7b-20 (Miller)	1020	0.30
		1110	0.29
		1200	0.33
		1290	0.32
		1380	0.32
		1590	0.35
		1650	0.32
		1740	0.40
		1830	0.36
		1920	0.35
		2010	0.42
		2100	0.38
		2190	0.38
		2670	0.36
		2760	0.47
		2850	0.53
		3000	0.54
		3648	0.68
		3817	0.73
		3827	0.89
		3904	1.02
		3990	1.17

5.3 Results of modelling and maturity calculations

Burial and temperature history Burial and temperature history diagrams of the Brae Formation sandstones in the Miller and Kingfisher Fields appear very similar (Fig.36). Reconstruction of the burial histories was straightforward because burial has been essentially continuous since time of deposition until the present. Present day heatflow was calculated based upon corrected bottom-hole temperatures, which are around 120 and 115 °C in the Miller (Rooksby, 1991) and Kingfisher Fields (Shell, internal unpublished report) respectively. Calculated heat flow values are

44.6 mW/m^2 in the Miller Field and 41.3 mW/m^2 in the Kingfisher Field. These data are presented in Table 13 and suggest that the present day geothermal gradient is 30 °C/km in both fields.

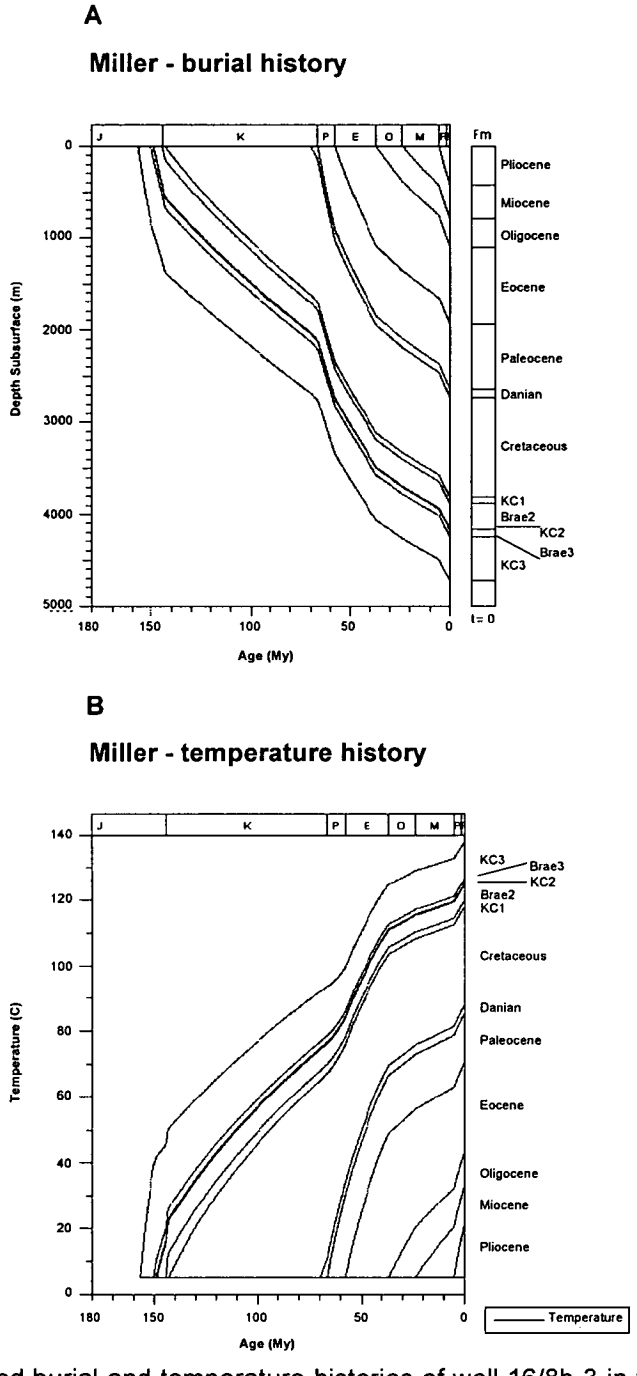

Fig.36 Reconstructed burial and temperature histories of well 16/8b-3 in the Miller Field and well 16/8a-1 in the Kingfisher Field from BasinMod®.
(A) Burial depth plotted versus time for all formations defined in well 8b-3 in the Miller Field.
(B) Temperature evolution through time for all formations defined in well 8b-3 in the Miller Field.

C

Kingfisher - burial history

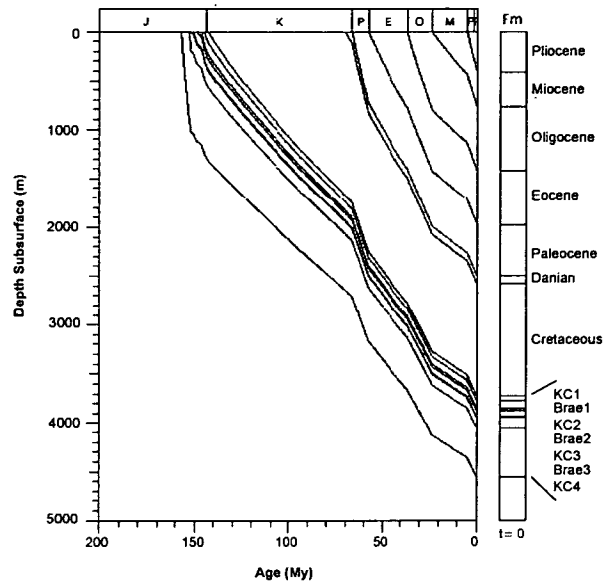

D

Kingfisher - temperature history

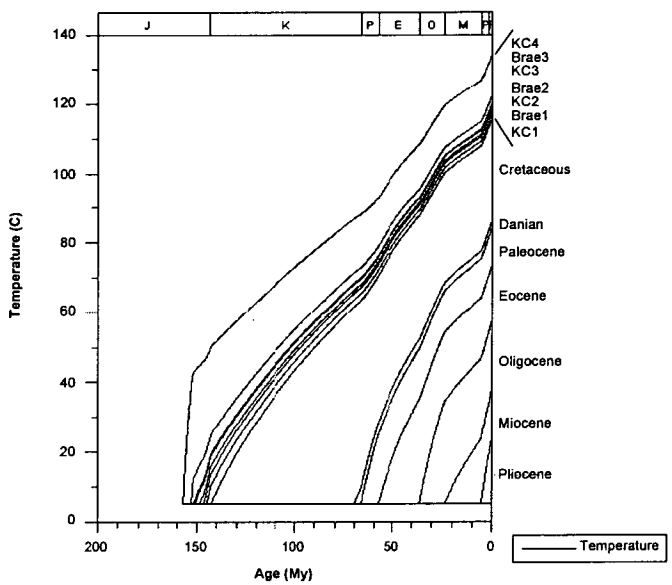

Fig.36 (Continued) Reconstructed burial and temperature histories of well 16/8b-3 in the Miller Field and well 16/8a-1 in the Kingfisher Field from BasinMod®.
(C) Burial depth plotted versus time for all formations defined in well 8a-1 in the Kingfisher Field.
(D) Temperature evolution through time for all formations defined in well 8a-1 in the Kingfisher Field.

Maturity The hydrocarbons in the Brae Formation Unit 2 sandstones are sourced from Kimmeridge Clay interbedded with the reservoir rocks and in the vicinity of the reservoirs (Mackenzie et al., 1987). For this reason, the time-temperature index (TTI) was calculated for the Kimmeridge Clay (KC) layers which immediately over- and underlie the Brae Unit 2 reservoirs in the Miller and Kingfisher Fields.

The calculated TTI values for KC 1 and 2 in the Miller Field, which respectively overlie and underlie the Brae 2 reservoir (Table 9), are 75 and 85 respectively (Table 17). These values correspond to vitrinite reflectance values (Ro) of 1.03 and 1.06 (eq 5). In the Kingfisher Field, KC 2 and 3 over- and underlie the Brae 2 reservoir (Table 9). Calculated TTI values for these formations are 32 and 54 respectively (Table 17), corresponding to Ro values of 0.84 and 0.95 (eq 5). In all cases, there is reasonable agreement between calculated Ro and measured Ro values (Fig.37), which supports the validity of the method.

By plotting the cumulative maturity of the KC in the Miller and Kingfisher Fields versus time, the oil generation windows of the source rocks can be determined (Fig.38). In the Miller Field, the cumulative maturity value of the KC reaches the oil production window around 40 Ma. In the Kingfisher Field, oil generation from interbedded KC does not occur until 15 to 10 Ma.

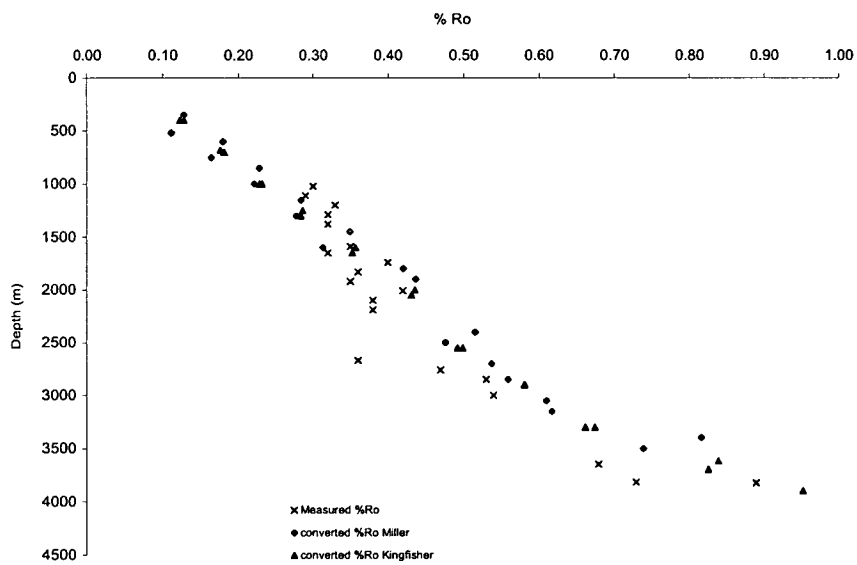

Fig.37 Measured and calculated vitrinite reflectance (%Ro) data for Kimmeridge Clay source rocks in the Miller and Kingfisher Fields plotted versus depth. Measured data were obtained from BP-Amoco. The other data were obtained from Kimmeridge Clay maturity values, calculated according to the method of Lopatin (1971), which were subsequently converted into %Ro with the equation of Waples (1980). The good correlation between measured and calculated %Ro values supports the validity of Lopatin's method.

The hydrocarbons in the Brae Formation Unit 1 reservoir in the Kingfisher Field are thought to have migrated from KC source rock deeper in the graben (east from the Kingfisher Field) (MacKenzie et al., 1987; Reitsema, 1983). In order to calculate the maturity of these source rocks, a burial and temperature history diagram of a pseudowell through the HC kitchen area east of the Kingfisher Field had to be reconstructed. Input data for such a reconstruction should be based on seismic lines across the area east of the Kingfisher Field, in order to have realistic estimates of the present day depth of the KC Formation and other formations. Unfortunately, Shell and BP-Amoco have not been able to provide any such information which made reconstruction of a burial and temperature history, and subsequent maturity calculation, impossible.

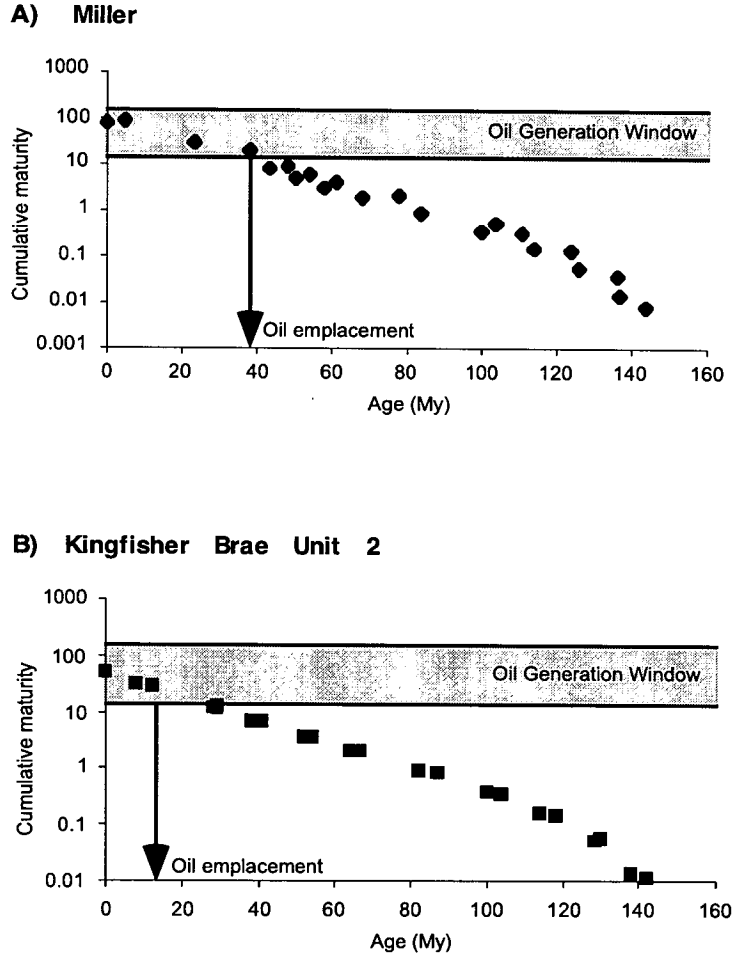

Fig.38 Cumulative maturity values of Kimmeridge Clay interbedded with the Brae Unit 2 reservoirs in the Miller **(A)** and Kingfisher Fields **(B)** plotted versus time. The oil generative window of source rocks lies between a cumulative maturity value of 15 and 160 (Lopatin, 1971). The Kimmeridge Clay source rocks in the Miller and Kingfisher Fields enter the oil generation window around 40 and 15-10 Ma respectively.

Table 17 Maturity calculated according to Lopatin's method (1971) for Kimmeridge Clay layers directly over- and underlying the Brae Formation Unit 2 sandstones in the Miller and Kingfisher Fields.
Maturity is calculated initially for each temperature interval individually according to eq 3 (see text). Δt_i (in My) is the length of time spent by the sediment in the ith temperature interval. Δt_i is calculated as the difference between the time when the sediment entered (t_n) and left (t_{n+1}) the temperature interval respectively. t_n and t_{n+1} are derived from constructed burial and temperature histories. The total maturity (TTI) of each source rock formation is given by the cumulative maturity. This value can be converted into vitrinite reflectance (% Ro) by using eq 5 (see text) from Waples (1980).

Field	Formation	Temperature Interval (°C)	n	2^n	t_n (My)	t_{n+1} (My)	Δt (My)	Maturity	Cumulative Maturity	Calculated % Ro
Miller	KC1	10 to 20	-9	0.00195313	144	137	7	0.01367188	0	0.13
		20 to 30	-8	0.00390625	137	126	11	0.04296875	0	0.18
		30 to 40	-7	0.0078125	126	114	12	0.09375	0	0.23
		40 to 50	-6	0.015625	114	100	14	0.21875	0	0.28
		50 to 60	-5	0.03125	100	84	16	0.5	1	0.35
		60 to 70	-4	0.0625	84	68	16	1	2	0.42
		70 to 80	-3	0.125	68	58	10	1.25	3	0.48
		80 to 90	-2	0.25	58	50	8	2	5	0.54
		90 to 100	-1	0.5	50	43	7	3.5	9	0.61
		100 to 110	0	1	43	23	20	20	29	0.82
		110 to 120	1	2	23	0	23	46	75	1.03
	KC2	10 to 20	-9	0.00195313	148	144	4	0.0078125	0	0.11
		20 to 30	-8	0.00390625	144	136	8	0.03125	0	0.16
		30 to 40	-7	0.0078125	136	124	12	0.09375	0	0.22
		40 to 50	-6	0.015625	124	111	13	0.203125	0	0.28
		50 to 60	-5	0.03125	111	104	7	0.21875	1	0.31
		60 to 70	-4	0.0625	104	78	26	1.625	2	0.44
		70 to 80	-3	0.125	78	61	17	2.125	4	0.52
		80 to 90	-2	0.25	61	54	7	1.75	6	0.56
		90 to 100	-1	0.5	54	48	6	3	9	0.62
		100 to 110	0	1	48	38	10	10	19	0.74
		110 to 120	1	2	38	5	33	66	85	1.06
Kingfisher	KC2	10 to 20	-9	0.00195313	145	138	7	0.01367188	0	0.13
		20 to 30	-8	0.00390625	138	128	10	0.0390625	0	0.18
		30 to 40	-7	0.0078125	128	114	14	0.109375	0	0.23
		40 to 50	-6	0.015625	114	100	14	0.21875	0	0.29
		50 to 60	-5	0.03125	100	82	18	0.5625	1	0.36
		60 to 70	-4	0.0625	82	64	18	1.125	2	0.43
		70 to 80	-3	0.125	64	52	12	1.5	4	0.49
		80 to 90	-2	0.25	52	38	14	3.5	7	0.58
		90 to 100	-1	0.5	38	28	10	5	12	0.66
		100 to 110	0	1	28	8	20	20	32	0.84
	KC3	10 to 20	-9	0.00195313	148	142	6	0.01171875	0	0.12
		20 to 30	-8	0.00390625	142	130	12	0.046875	0	0.18
		30 to 40	-7	0.0078125	130	118	12	0.09375	0	0.23
		40 to 50	-6	0.015625	118	104	14	0.21875	0	0.28
		50 to 60	-5	0.03125	104	87	17	0.53125	1	0.35
		60 to 70	-4	0.0625	87	67	20	1.25	2	0.44
		70 to 80	-3	0.125	67	54	13	1.625	4	0.50
		80 to 90	-2	0.25	54	41	13	3.25	7	0.58
		90 to 100	-1	0.5	41	29	12	6	13	0.67
		100 to 110	0	1	29	12	17	17	30	0.83
		110 to 120	1	2	12	0	12	24	54	0.95

5.4 Timing of quartz cementation

The time period over which quartz cementation took place in the Brae Formation reservoirs studied can be determined by combining quartz cementation temperatures with the modelled burial and thermal histories of the rocks. Quartz cementation temperatures were determined by microthermometric measurements of fluid inclusions in quartz cements (Chapter 4). To allow, in addition, the determination of the burial depths at which quartz cementation occurred, isotherms were plotted directly onto the previously constructed burial history graphs of wells 8b-3 (Miller Field) and 8a-1 (Kingfisher Field) (Fig.39).

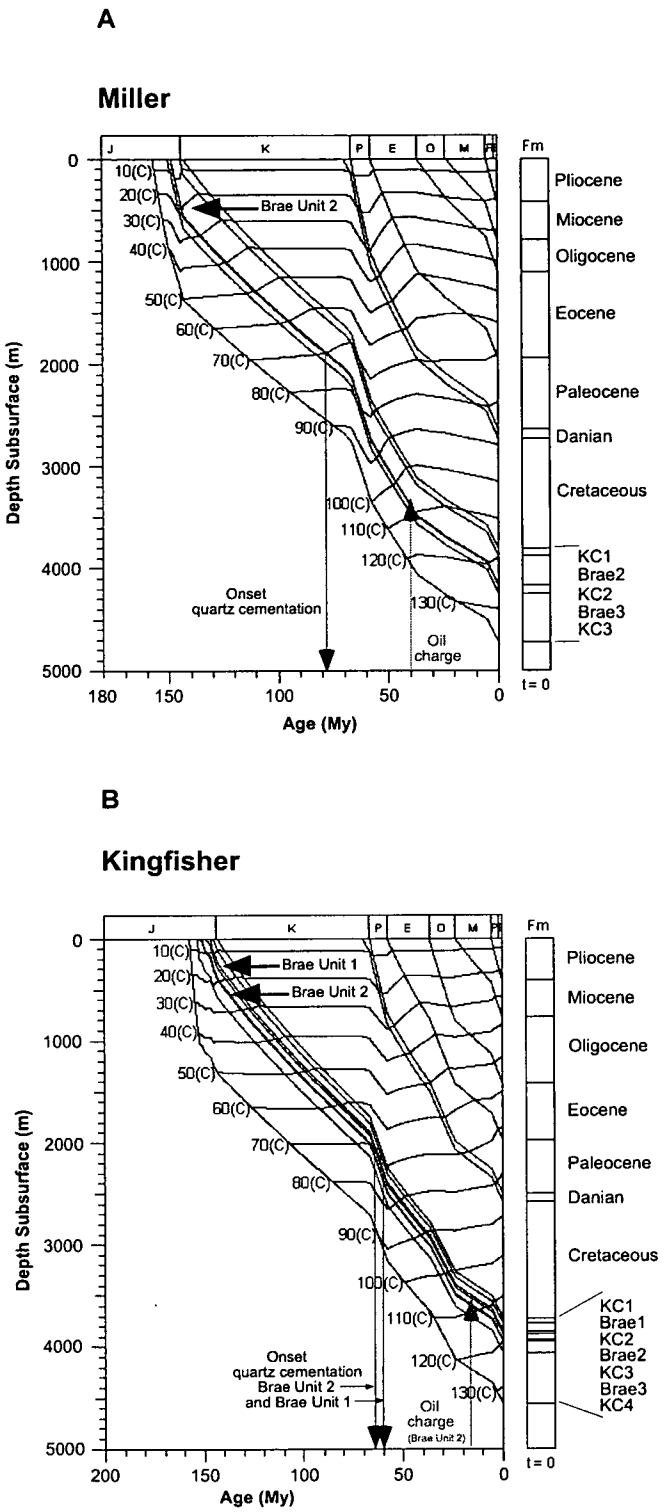

Fig.39 Burial histories combined with isotherms for well 8b-3 in the Miller Field **(A)** and well 8a-1 in the Kingfisher Field **(B)**.
Quartz precipitated in all three reservoirs studied from 70 °C onwards. The Brae Unit 2 reservoirs in the Miller and Kingfisher Fields passed the 70 °C isotherm around 78 Ma **(A)** and 65 Ma **(B)** respectively. Oil emplacement in both reservoirs was later than the onset of quartz cementation. The Brae Unit 1 reservoir in the Kingfisher Field did not reach 70 °C until 60 Ma **(B)**.

Miller (Brae Unit 2 reservoir) Fluid inclusion homogenization temperatures indicate that quartz cement was being precipitated in this reservoir from at least 70 °C onwards (Chapter 4). From Fig.39A, it can be seen that the Brae Unit 2 sandstone Formation in well 8b-3 passed through the 70 °C isotherm around 78 Ma at a burial depth of approximately 1900 m. It was concluded from homogenization temperatures in oil zone samples that quartz cementation was impeded at different times in the reservoir. In the crestal areas of reservoir zones, cementation occurred in the sandstones until the temperature reached 95-105 °C (Chapter 4). This temperature was reached in well 8b-3 around 45-40 Ma when the reservoir was buried to approximately 3000-3300 m (Fig.39A). Quartz cementation temperatures are higher in deeper parts of the reservoirs (110-115 °C) (Chapter 4). This indicates that quartz cementation occurred over longer periods of time deeper down in the reservoir zones. The highest recorded quartz growth oil zone temperatures near the OWC are around 120 °C (Appendix D). The Brae Unit 2 reservoir reached this temperature in well 8b-3 only in recent times (3-0 Ma) (Fig.39A). From quartz growth temperatures in water zone samples it was concluded that cementation in the aquifer of the reservoir is still ongoing at the present time (Chapter 4).

Kingfisher (Brae Unit 1 reservoir) The lowest quartz growth temperature recorded in this reservoir is 74 °C (Appendix C). The Brae Unit 1 sandstone reservoir in well 8a-1 was buried to approximately 2300 m around 60 Ma when this temperature was reached (Fig.39B). Most quartz cement was precipitated in this reservoir when the temperature was around 90 to 100 °C (Chapter 4). This temperature range was reached in well 8a-1 at 2900 to 3300 m burial depth around 40 to 30 Ma (Fig.39B). There is no evidence for substantial quartz cement growth at deeper burial and higher temperatures (Chapter 4).

Kingfisher (Brae Unit 2 reservoir) In this reservoir also, the earliest evidence for quartz cementation is at temperatures around 70 °C (Chapter 4). The Brae Unit 2 Formation in well 8a-1 passed through the 70 °C isotherm around 65 Ma (Fig.39B). The reservoir was at that time buried to approximately 2100 m (Fig.39B). Quartz growth temperatures of up to 120 °C were measured in oil zone samples of this reservoir (Chapter 4). This temperature was reached in recent times only in the Brae Unit 2 Formation in well 8a-1 (Fig.39B). Quartz cementation in the aquifer is still ongoing at the present day.

5.5 Timing of hydrocarbon emplacement

Maturity calculations indicate that KC source rocks interbedded with the Brae Formation Unit 2 sandstones in the Miller Field started generating oil at around 40 Ma. Around this time, the reservoir sandstones were buried to 3100-3400 m and then temperatures ranged between 100-110 °C (Fig.39A). This temperature and depth interval at which the source rocks were generating oil overlaps with the temperature and depth interval when quartz cementation was halted (90-95 °C, 3000-3300 m) in the crestal areas of the Miller Field.

Maturity calculations for KC source rocks in the Kingfisher Field indicate oil generation from around 15 Ma onwards. This oil charged the Brae Unit 2 oil reservoir in the field (Mackenzie et al., 1987). Around 15 Ma, the reservoir was buried to 3500 m and had reached a temperature of almost 110 °C (Fig.39B). Quartz cement abundance and growth temperatures in the reservoir sandstones indicate a recent inhibition of quartz precipitation (115-120 °C).

Placing a time constraint on hydrocarbon emplacement in the Brae Unit 1 reservoir in the Kingfisher Field is difficult. The maturity of the deep source rocks from which hydrocarbons were expelled could not be calculated because of the different and distal location of the kitchen area. The observation that no precipitation of quartz cement occurred at temperatures higher than 100-105 °C in this reservoir, indicates that hydrocarbons were present at least from 30 Ma onwards.

5.6 Discussion

The similarity between the time of source rock oil generation and the time at which quartz cementation ended in the Brae Unit 2 reservoir rocks of the Miller and Kingfisher Fields is direct evidence of the inhibiting effect of oil charge on quartz cementation. In the Miller Field, hydrocarbon emplacement from 40 Ma onwards overlaps in time with the end of quartz cementation in crestal areas of the field. In the Kingfisher Field, oil is thought to have entered the Brae Unit 2 reservoir from 15 Ma onwards. Quartz growth temperatures in this reservoir indicate that quartz cementation was halted in recent times. The small time lapse between oil charge and cementation inhibition may, however, indicate a continuation of quartz cementation after initial oil charge when oil saturation was still low.

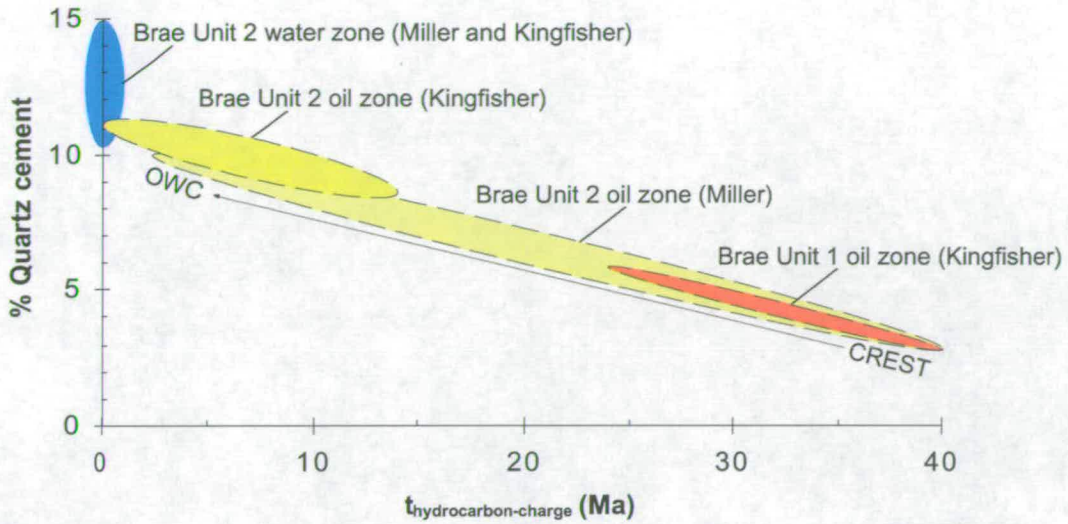

Fig.40 Cross plot of time of oil charge (Ma) versus quartz cement abundance (%) in the different reservoirs studied. There is an inverse correlation between these two parameters in the reservoirs. The earlier oil charged the reservoir, the less quartz cement precipitated in the sandstones (e.g. Brae Unit 1 reservoir in the Kingfisher Field and crestal areas in the Brae Unit 2 reservoir in the Miller Field). The more recently oil charge took place, the higher the quartz cement abundance in the sandstones (e.g. lower parts of the Brae Unit 2 reservoir in the Miller Field and the Brae Unit 2 reservoir in the Kingfisher Field). Water zone samples which remained continuously hydrocarbon-free display the highest quartz cement abundances in all reservoirs.

The effect of oil on quartz cementation can be illustrated quantitatively when combining modelling results with petrographically determined quartz cement abundances. In Fig.40, quartz cement abundance is plotted against the time of hydrocarbon charge for the different reservoirs. Water zone samples of the Brae Unit 2 reservoirs in the Miller and Kingfisher Fields, which remained hydrocarbon-free since the onset of quartz cementation (78 and 65 Ma respectively) until the present day, consistently have the highest quartz cement abundances (>10 %) (Fig.40). Depending on the time of hydrocarbon charge in the different reservoirs, oil zone samples display more, or less, quartz cement (Fig.40). Oil charge in the Brae Unit 2 reservoir in the Miller Field started around 40 Ma in the crestal parts of the reservoir. In those crestal areas, quartz cement abundances are lowest (<5 %) (Fig.40). Quartz growth temperatures indicate that oil-fill in this reservoir was not completed until recent times (Chapter 4). This means that with increasing depth in the oil zone, the sandstones had a progressively longer time available for quartz cementation. This is reflected in increasing amounts of quartz cement with depth in the reservoir (3 to 10 %). Quartz cement abundances in oil zone samples from the

Brae Unit 2 reservoir in the Kingfisher Field are only slightly lower than those in water zone samples (Fig.40). This is due to the reservoir's recent oil charge (Fig.40). Quartz cementation temperatures in the Brae Unit 1 reservoir in the Kingfisher Field suggest that hydrocarbons were present at least from 30 Ma onwards. Quartz cement abundance in this reservoir ranges between 3 and 6 %. This is similar to the abundance of quartz cement in the crestal parts of the Brae Unit 2 reservoir in the Miller Field where oil-charge took place around 40 Ma. Therefore, it seems reasonable to suggest that in the Kingfisher Field hydrocarbons also started entering the Brae Unit 1 reservoir around this time (Fig.40).

5.7 Conclusions

1 The burial and temperature history of the Brae Formation sandstones is similar in the Miller and Kingfisher Fields. Burial of the reservoir rocks was essentially continuous from the time of deposition of the sands until the present. The reservoirs are currently buried to ~4 km at temperatures around 120 °C.

2 Quartz cementation in all the reservoirs studied started around 70 °C. The Brae Unit 2 oil reservoirs in the Miller and Kingfisher Fields passed the 70 °C isotherm at around 78 and 65 Ma respectively. The shallower Brae Unit 1 gas condensate reservoir in the Kingfisher Field did not reach 70 °C until around 60 Ma.

3 Quartz cementation in the crestal parts of the Miller Field ended at around 95-105 °C. This temperature was reached in the reservoir at around 45-40 Ma. Deeper in the reservoir, quartz cementation continued over a longer period of time. Near the OWC, cementation stopped only in recent times (3-0 Ma) when the temperature was around 120 °C. In the Brae Unit 2 reservoir in the Kingfisher Field, quartz cementation temperatures in the oil zone indicate that quartz precipitation continued until recent times. In the Brae Unit 1 reservoir in the Kingfisher Field, no significant amounts of quartz cement were precipitated above 100 °C. This temperature was reached in the reservoir at around 40 to 30 Ma.

4 The hydrocarbons in the Brae Formation Unit 2 sandstones are sourced from Kimmeridge Clay interbedded with the reservoir rocks and in the vicinity of the reservoirs. Maturity calculations of Kimmeridge Clay source rocks in the Miller Field indicate oil generation from around 40 Ma. In the Kingfisher Field, source rocks enter the oil-generation windows around 15 Ma. The hydrocarbons in the

Brae Formation Unit 1 reservoir in Kingfisher are thought to have migrated from source rocks deeper in the graben. Due to a lack of information about this kitchen area, it was not possible to calculate source rock maturity and subsequently to estimate the time of hydrocarbon emplacement in this Brae Unit 1 reservoir.

5 The similarity between the time of source rock oil generation and the time at which quartz cementation ended in the Brae Unit 2 reservoir rocks of the Miller and Kingfisher Fields, is direct evidence of the inhibiting effect of oil saturation on quartz cementation.

6 There is an inverse correlation in the reservoirs studied between the abundance of quartz cement in the sandstones and the time of oil charge. Reservoirs, or parts of reservoirs, which received an early oil charge (e.g. structural crest in Miller Field, Brae Unit 1 reservoir in Kingfisher Field) have least quartz cement (<6 %). Reservoirs, or parts of reservoirs, with recent oil charge (e.g. near the OWC in Miller Field, the Brae Unit 2 reservoir in Kingfisher Field) display higher quartz cement abundances (up to 10-12 %). Water zone samples from the Brae Unit 2 reservoirs in the Miller and Kingfisher Fields, which remained hydrocarbon-free since the onset of quartz cementation until the present day, consistently have the highest quartz cement abundances (>10 %).

CHAPTER VI

QUARTZ CEMENTATION MODELLING

In this chapter :

- *How accurate are existing numerical models at predicting quartz cement abundances and porosities in reservoirs with anomalous quartz cement and porosity distributions such as the Brae Formation reservoirs studied ?*
- *If reservoir quality predictions made by such models prove incorrect, how can predictions be improved ?*
- *Are quartz precipitation rates lower in the oil zones of reservoirs compared to in the water zones ?*
- *How much does oil slow down quartz cementation ?*

6.1 Introduction

Models published recently enable the prediction of quartz cementation and concomitant porosity loss in quartzose sandstones (Walderhaug, 1994 & 1996; Oelkers et al., 1996 & 2000; Bjørkum et al, 1998; Lander & Walderhaug, 1999; Walderhaug et al., 2000). In such models, quartz cementation is regarded as a three-step process; silica is internally sourced from quartz dissolution at stylolites, diffuses over short distances and precipitates onto clean quartz surfaces (Walderhaug, 1996; Bjørkum et al, 1998; Oelkers et al., 2000). Precipitation is hereby regarded as the rate-limiting step controlling the quartz cementation process. The effect of hydrocarbon emplacement on quartz cementation is not incorporated in such reservoir quality prediction models. Walderhaug (1994) reasoned that as long as sandstones remain water-wet, quartz precipitation rates would not be affected by hydrocarbon emplacement. Lack of clearly observed evidence for

different quartz cement volumes and precipitation rates between water and oil zones has been used to support this statement (Ramm, 1992; Walderhaug, 1994). A numerical model for quartz cementation and porosity prediction called Exemplar™ was developed by Lander and Walderhaug (1999). In this software package, quartz cement volumes in sandstones are calculated by using quartz precipitation rates which were empirically derived using data from the Norwegian Continental Shelf. Since this data set displays no significant difference in quartz precipitation rates between oil and water zone samples (Walderhaug, 1994), an inevitable consequence will be that, when applying the model, similar cement volumes will be predicted in oil and water zones of reservoirs. The Brae Formation sandstone reservoirs in the Miller and Kingfisher Fields, however, display heterogeneous quartz cement abundances at similar burial depths. A consequence of applying current reservoir quality prediction tools, such as Exemplar™, to the Brae Formation reservoirs would be that quartz cement abundances in the oil zones could be seriously overestimated.

In this Chapter, I test the adequacy of Exemplar™ for predicting porosity and quartz cement abundances in the Brae Formation reservoirs in the Miller and Kingfisher Fields. Petrographic (Chapter 3), fluid inclusion (Chapter 4) and basin modelling (Chapter 5) studies all indicate that hydrocarbon charge in these reservoirs had an inhibiting effect on quartz cementation. As a result, lower quartz cement abundances, and high porosities, are observed in the structural crests of reservoirs (e.g. Brae Formation Unit 2 reservoir in the Miller Field) and in reservoirs which were charged early with respect to the onset of quartz cementation (e.g. Brae Formation Unit 1 reservoir in the Kingfisher Field). To date, no attempt has been made to quantify this retardation effect of oil on quartz cementation. Software packages such as Exemplar™ are quick and easy to use tools for assessing quartz precipitation rates quantitatively. I used this programme for constraining quartz precipitation rates for oil and water zone samples in the Brae Formation sandstone reservoirs. Any difference in quartz precipitation rates between oil and water zone samples, from the time of oil emplacement in the reservoirs onwards, can be regarded as quantitative proof of the effect of oil on quartz cementation (if other factors can be shown to be equal). After establishing the rate of quartz precipitation in oil filled reservoirs, I will also discuss the consequences of my results for the predictive capacity of modelling software such as Exemplar™, and how oil reservoir predictions can be improved. Accurate prediction of oil zone porosity in reservoirs is

of economic significance for oil companies because such predictions can be taken into account for assessing reservoir performance and for decisions on positioning of wells during the appraisal and production stages of oilfields.

6.2 Methodology

I used Exemplar™ software at BP Amoco (Sunbury) during two periods of work; the first from February 29th until March 3rd 2000 and the second resident from May 16th until May 17th 2000. The Exemplar™ software is licensed and produced by Geologica; a reservoir quality consultancy company based in Stavanger (Norway). All algorithms used in the software for predicting porosity and quartz cement abundances in sandstone reservoirs are published in Walderhaug (1994 and 1996) and in Lander & Walderhaug (1999). A full account of all algorithms present in the Exemplar™ software, and how they were derived, is given in Appendix D. In this methodology paragraph, I provide a basic overview of the main algorithm in the software programme which is used to calculate, and predict, quartz cement abundances.

In Exemplar™ software, quartz cement volumes are calculated as the sum of a series of integrals with small time steps (Walderhaug, 1994; Lander and Walderhaug, 1999) :

$$m = \int_{t_o}^{t_1} A_1 r(t)\, dt + \int_{t_1}^{t_2} A_2 r(t)\, dt + \ldots + \int_{t_{n-1}}^{t_n} A_n r(t)\, dt \quad (eq\ 6)$$

where m is moles of quartz cement precipitated per cm^3 sandstone, A is the surface area in cm^2 per cm^3 sandstone, t is the time in seconds (t_0 and t_n the time when quartz cementation starts and terminates), and r is the rate of quartz cementation in $moles.cm^{-2}.s^{-1}$. Quartz cementation time t and surface area A can be derived from burial history modeling and petrographic data respectively. Quartz cementation rates in the software are expressed by a logarithmic function of temperature which was empirically derived using data from the Norwegian continental shelf (Walderhaug, 1994). This temperature dependence of quartz cementation rates can be expressed by Arrhenius law :

$$\ln r = \ln B - E_a/R.T \quad (eq\ 7)$$

where r is the quartz cementation rate [$moles/cm^2.s$], parameter B is the pre-exponential or frequency factor, E_a is the activation energy [J/mole], R is the gas constant [J/K.mole] and T is temperature [K]. Default reaction kinetics, derived

using data from the Norwegian continental shelf (Walderhaug, 1994), are E_a=58 J/mole and B=5x10^{-12}.

6.3 Modelling input data

Input data needed to conduct a simulation include texture and composition of the sandstone samples, burial history information and parameter values for the compaction and quartz cementation algorithms (Appendix D). Data for 20 samples from the Miller Field (13 oil zone and 7 water zone samples), 10 samples from the Brae Formation Unit 1 reservoir in the Kingfisher Field and 10 samples from the Brae Formation Unit 2 reservoir in the Kingfisher Field (5 oil zone and 5 water zone samples) were selected for the modelling (Table 18). An account of all input parameters in the programme for these samples is given in Appendix D.

Table 18 Overview of samples selected from the Miller and Kingfisher Fields for the Exemplar™ modelling. Measured quartz cement abundances (SEM-CL) and pointcount porosities are listed. Percentages of grain coating applied to each oil zone sample in order to obtain correct quartz cement abundance predictions are tabled, as well as the derived average quartz precipitation rates (calculated over the time span since oil charge until the present) for oil and water zone samples. The estimated time of oil charge is also indicated for each sample together with the sample's temperature at this time. The present day temperature for each sample is listed for comparison.

Field	Reservoir	OWC (m)	Sample	Oil/Water zone	Measured Quartz cement (%)	Measured Porosity (%)	$t_{oil\ charge}$ (Ma)	$T_{present}$ (°C)	$T_{HC\ charge}$ (°C)	% coating	Av. $r_{HC\ charge}$ (moles/cm².s)
Miller	Unit 2	4090	3989.9	oil	2.7	23.2	49	120.0	90.0	100	0
Miller	Unit 2		3993.8	oil	5.0	21.6	32	120.4	106.2	83	2.84E-22
Miller	Unit 2		3996.9	oil	3.2	22.6	41	120.7	101.3	100	0
Miller	Unit 2		4022.7	oil	4.8	22.2	42	123.2	102.4	100	0
Miller	Unit 2		4029.4	oil	5.8	12.4	17	123.9	114.1	50	1.49E-21
Miller	Unit 2		4039.6	oil	7.1	13.2	8	124.9	117.9	27	4.15E-21
Miller	Unit 2		4043.6	oil	7.8	15.4	17	125.3	115.5	52	1.50E-21
Miller	Unit 2		4045.5	oil	5.8	18.6	22	125.5	114.2	63	9.90E-22
Miller	Unit 2		4057.2	oil	8.0	17.0	22	126.6	115.3	62	1.08E-21
Miller	Unit 2		4062.7	oil	6.0	15.0	24	127.2	115.2	67	8.86E-22
Miller	Unit 2		4064.5	oil	8.6	14.6	25	127.3	115.1	69	8.15E-22
Miller	Unit 2		4068.2	oil	8.9	17.2	11	127.7	119.7	39	2.88E-21
Miller	Unit 2		4071.9	oil	9.0	14.8	10	128.1	120.4	33	6.00E-21
Miller	Unit 2		4101.3	water	12.1	13.6		131.0			5.68E-20
Miller	Unit 2		4102.2	water	11.4	14.0		131.1			5.70E-20
Miller	Unit 2		4110.4	water	11.4	13.8		131.9			5.90E-20
Miller	Unit 2		4112.9	water	12.6	14.2		132.1			5.97E-20
Miller	Unit 2		4116.0	water	10.6	13.4		132.4			6.05E-20
Miller	Unit 2		4141.3	water	15.4	14.6		134.9			6.73E-20
Miller	Unit 2		4186.4	water	14.1	12.4		139.3			8.13E-20
Kingfisher	Unit 1	3993	3887.5	oil	4.1	25.4	31	115.8	95.6	80.5	3.36E-22
Kingfisher	Unit 1		3890.6	oil	3.4	26.6	32	116.1	95.1	81	3.19E-22
Kingfisher	Unit 1		3894.6	oil	3.5	26.2	34	116.5	93.7	84	2.62E-22
Kingfisher	Unit 1		3900.0	oil	3.6	25.4	30	117.0	97.7	76	4.36E-22
Kingfisher	Unit 1		3904.2	oil	5.2	22.8	22	117.4	104.1	60	8.89E-22
Kingfisher	Unit 1		3913.3	oil	3.8	29.0	30	118.3	98.9	77.5	4.52E-22
Kingfisher	Unit 1		3929.5	oil	6.1	20.6	20	120.0	107.4	56	1.23E-21
Kingfisher	Unit 1		3938.4	oil	5.6	24.6	29	120.8	102.2	75	5.58E-22
Kingfisher	Unit 1		3947.2	oil	5.8	18.0	34	121.7	98.7	84.5	3.42E-22
Kingfisher	Unit 1		3955.1	oil	4.8	19.6	24	122.5	108.1	66	9.35E-22
Kingfisher	Unit 2	4030	3989.7	oil	10.4	17.0	2	114.4	112.4	30	3.58E-21
Kingfisher	Unit 2		4004.7	oil	10.4	13.2	3	115.8	112.8	30	3.69E-21
Kingfisher	Unit 2		4019.0	oil	12.2	13.0	0	117.2	117.2	0	5.34E-20
Kingfisher	Unit 2		4023.6	oil	10.2	14.0	0	117.7	117.7	0	5.46E-20
Kingfisher	Unit 2		4028.8	oil	10.5	16.2	0	118.2	118.2	3	5.82E-20
Kingfisher	Unit 2		4030.3	water	11.1	13.0		118.3			5.62E-20
Kingfisher	Unit 2		4033.7	water	9.4	13.6		118.6			5.71E-20
Kingfisher	Unit 2		4053.9	water	12.0	13.2		120.6			6.24E-20
Kingfisher	Unit 2		4081.0	water	12.0	14.0		123.2			7.03E-20
Kingfisher	Unit 2		4126.1	water	11.0	12.4		127.6			8.54E-20

6.4 Results of quartz cementation modelling

Exemplar™ was used to predict quartz cement abundance in the samples studied. In the first simulation, quartz precipitation rates were derived from the default reaction kinetics (E_a = 58 J/mole and B = 5.10^{-12}) in the programme (Fig.44A). A cross plot of measured versus predicted % quartz cement (Fig.41A) shows that large discrepancies occur between measured and predicted amounts of quartz cement. For oil zone samples, errors are greater than water zone samples (Fig.41A). In the Miller Field, the average difference between predicted and measured values ($\Delta_{pred.-meas.}$) for oil zone and water zone samples is 11.9±4.8 % and 5.7±2.4 % respectively. In the Brae Unit 1 reservoir in the Kingfisher Field, average $\Delta_{pred.-meas}$ for oil zone samples is 11.0±2.3 %. For samples from the Brae Unit 2 reservoir in the Kingfisher Field, average $\Delta_{pred.-meas.}$ is 2.1±1.3 % and 2.3±2.7 % for oil and water zone samples respectively. Thus, the initial simulation is unsatisfactory.

In order to derive correct quartz precipitation rates in oil and water zone samples, it is important to match the amount of quartz cements predicted by Exemplar™ to the measured quartz cement volumes (eq 6) in the samples. Therefore, the reaction kinetics E_a and B (eq 7) were fine-tuned so as to match the observed amounts of quartz cement in the water zone samples (Fig.44B). The results of this simulation are presented in Fig.42. A cross-plot of the water zone calibration data shows a clustering around the 1:1 predicted versus measured line (Fig.41B) and is judged successful. Average $\Delta_{pred.-meas.}$ is -0.1±2.2 % and -0.1±2.5 % for water zone samples from the Brae Unit 2 reservoirs in the Miller and Kingfisher Fields respectively. When applying the same reaction kinetics to oil zone samples, predictions yield a gross over-estimation of the amount of quartz cement (Fig.41B). Discrepancies between predicted and measured quartz cement values for oil zone data from the Unit 2 and Unit 1 reservoir in the Miller and Kingfisher Fields are on average 6.5±4.4 % 8.2±2.2 % respectively. Note that these reservoirs experienced an early hydrocarbon charge (at least 40 Ma). Quartz cement abundance predictions for oil zone samples from the Unit 2 reservoir in the Kingfisher Field, which had a recent oil emplacement (15 Ma), are much better : $\Delta_{pred.-meas}$ is -0.3±1.2 %. A consequence of the over-estimation of the amounts of quartz cement in oil zone samples, especially in the Brae Unit 2 reservoir of the Miller Field and the Brae Unit 1 reservoir of the Kingfisher Field, is that porosities in the oil zones of the reservoirs will be under-

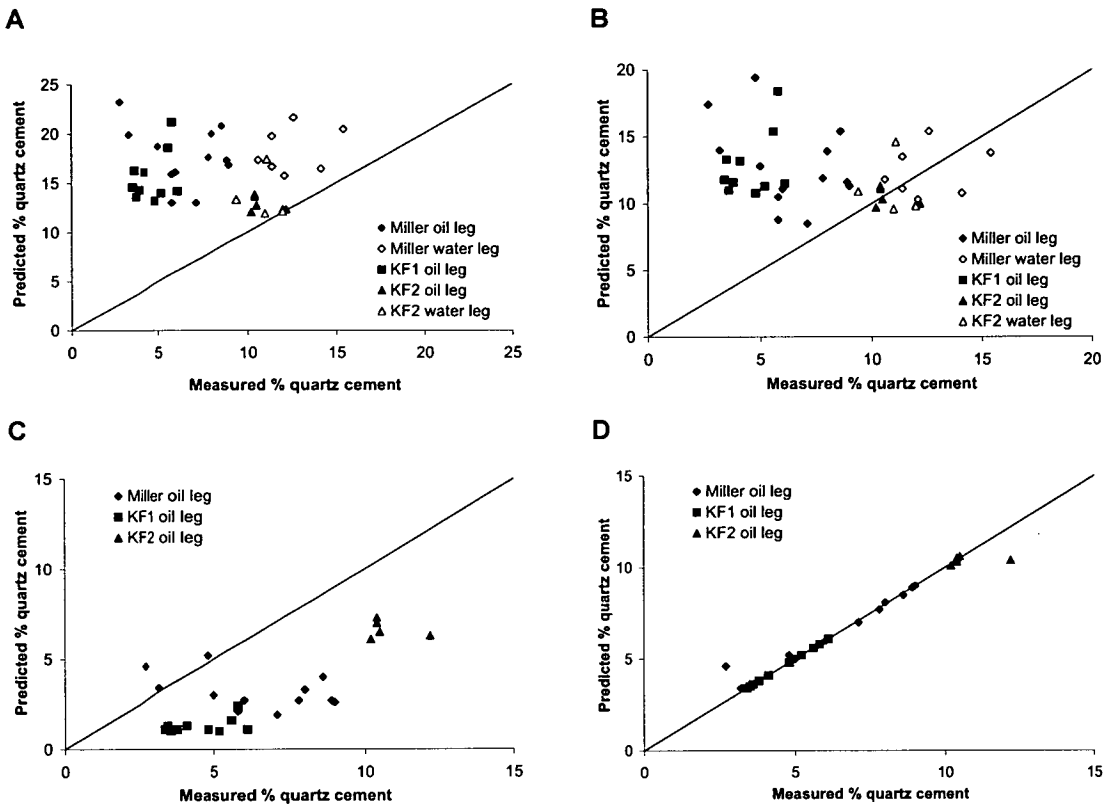

Fig.41 Measured versus predicted quartz cement abundances (volume %) for water and oil zone samples in the reservoirs of the Miller and Kingfisher Fields.
A Quartz cement abundances predicted by applying default Exemplar™ reaction kinetics in the programme's quartz cementation algorithm.
B Quartz cement abundances predicted after calibrating reaction kinetics in the programme's quartz cementation algorithm onto water zone samples from the reservoirs studied.
C Quartz cement abundances predicted in the oil zones, by taking the effect of hydrocarbon emplacement into account by using the grain coating module in Exemplar™ as a proxy for reduction of grain surface area. 100% coating was assumed.
D Quartz cement abundances predicted in oil zones by applying different amounts of coating on samples in order to match the predicted quartz cement abundance to the measured quartz cement content. No match was obtained for one sample from the Miller Field and one sample from the Kingfisher Field. Despite applying 100% coating to the Miller Field sample, quartz cement abundance was still overestimated. Despite not applying any coating (0%) to the Kingfisher Field sample, quartz cement abundance was still underestimated. Both can be explained by errors on the measured quartz cement abundances made by petrographic techniques.

predicted by the software programme. This is illustrated in Fig.43. In the reservoir oil zone of the Miller Field, porosity is under-predicted ranging from 1 to as much as 14 % (Fig.43). In the Brae Unit 1 reservoir in the Kingfisher Field, porosity is under-predicted by 5 to 12 % (Fig.43). The porosity predictions in the Brae Unit 2 reservoir in the Kingfisher Field are more accurate (Fig.43). This is not surprising since quartz cement abundance predictions are also much better for this reservoir (Fig.41B).

A Brae Unit 2 – Miller Field

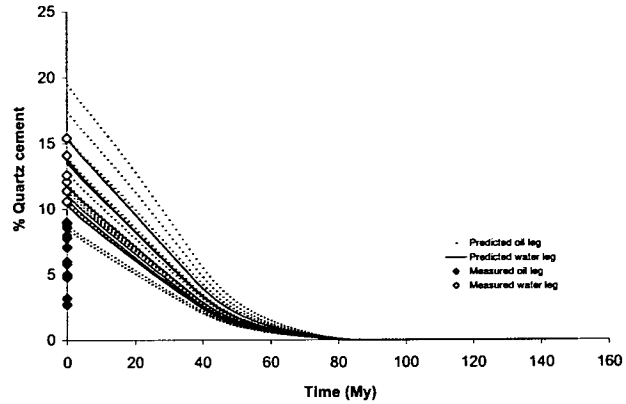

B Brae Unit 1 – Kingfisher Field

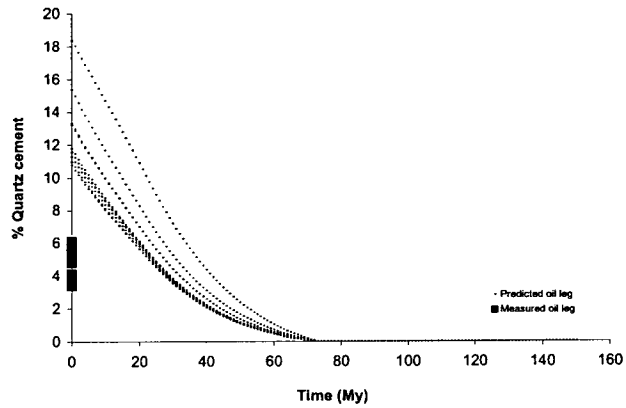

C Brae Unit 2 – Kingfisher Field

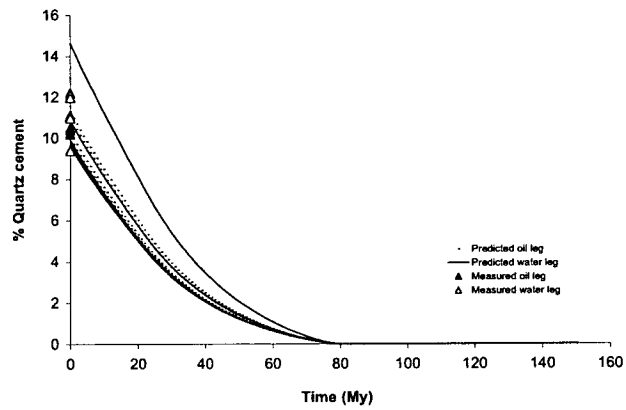

Fig.42 Percentage of quartz cement predicted by Exemplar™ for samples from the Brae Formation reservoirs in the Miller and Kingfisher Fields. Modelling starts at the time of sandstone deposition (~150 Ma) and progresses in time steps of 1 My until the present. Present day measured quartz cement abundances are plotted on the y-axis of the diagrams (time 0) for comparison.
A Simulation of quartz cementation in the Brae Formation Unit 2 reservoir in the Miller Field. Predicted water leg quartz cement abundances are reasonably accurate, but oil leg quartz cement abundances are overestimated.
B Simulation of quartz cementation in the Brae Formation Unit 1 reservoir in the Kingfisher Field. Predicted oil leg quartz cement abundances are overestimated.
C Simulation of quartz cementation in the Brae Formation Unit 2 reservoir in the Kingfisher Field. Predicted oil and water leg quartz cement abundances are reasonably accurate.

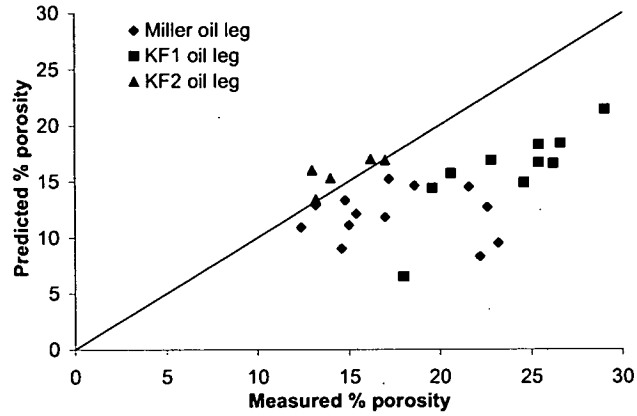

Fig.43 Measured versus predicted porosities (volume %) for oil zone samples in the reservoirs of the Miller and Kingfisher Fields. Porosities were predicted after calibrating reaction kinetics in the programme's quartz cementation algorithm on the water zone samples studied. Despite the close proximity of the water to the oil zones in the reservoirs (max. 110 m) and the similar petrographic and textural characteristics of water and oil zone samples, the program underestimates porosity in practically all oil zone samples.

The only parameter which can explain why predictions of quartz cement abundances and porosities in oil zone samples are inaccurate is quartz precipitation rate (eq 6). Oil zone samples are texturally similar to water zone samples (Chapter 3 and Appendix D), therefore surface area A does not differ significantly between the datasets (eq 6). Also, all samples experienced an identical burial and temperature history (Chapter 5 and Appendix D). Therefore, the time of the onset of quartz cementation is approximately the same in oil and water zones within the reservoirs, and possible temperature differences due to depth differences between oil and water zone samples are negligible (maximum 3 °C).

6.5 Quartz precipitation rates

To accurately compare quartz precipitation rates in the water zone with quartz precipitation rates in the oil zone, it is necessary to calculate average quartz precipitation rates which occurred in the water and oil zones subsequent to hydrocarbon emplacement in the reservoir. All quartz precipitation rates mentioned below are average values calculated in this way.

As there is a good match between predicted and measured quartz cement abundances for water zone samples (Fig.41B), the average quartz precipitation rates derived over the time interval from hydrocarbon emplacement until the present day reflect correct water zone precipitation rates. These calculated average water zone precipitation rates are plotted on an Arrhenius plot in Fig.44B and are also

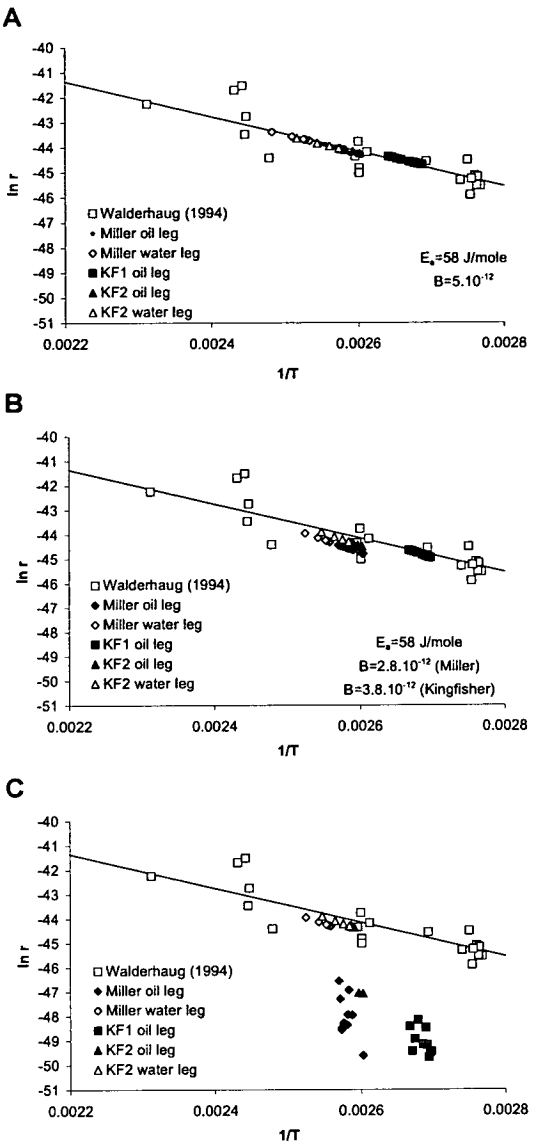

Fig.44 Quartz precipitation rates in the Exemplar™ software are expressed by the Arrhenius equation. In this equation, the temperature dependence of reactions rates is described by two parameters; E_a (activation energy in J/mole) and B (frequency factor). These two parameters are referred to as the reaction kinetics.

A Default reaction kinetics in the software are derived from Jurassic sandstones of the Norwegian continental shelf (Walderhaug, 1994). In the Arrhenius plot, E_a=58 J/mole and $B=5.10^{-12}$ are the parameters of the best fit line (solid line) through Walderhaug's dataset. When using these values for calculating quartz precipitation rates in the reservoirs from the Miller and Kingfisher Fields, naturally they will plot on the best fit line.

B In this plot, the quartz precipitation rates in the reservoirs from the Miller and Kingfisher Fields were calculated by using reaction kinetics which provide a good match between measured and predicted quartz cement abundances in the water zones of the reservoirs; E_a=58 J/mole, $B=2.8.10^{-12}$ (Miller Field) and $B=2.8.10^{-12}$ (Kingfisher Field).

C Water zone precipitation rates on this plot are identical to those in B, but the oil zone precipitation rates presented were obtained by matching measured and predicted quartz cement abundances in the oil zones of the reservoirs. Whereas water zone precipitation rates are similar in the Brae Formation reservoirs and the Norwegian continental shelf, oil zone precipitation rates are clearly smaller.

listed in Table 18. The water zone quartz precipitation rates from Brae Formation Unit 2 reservoirs in the Miller and Kingfisher Fields, appear quite similar to precipitation rates empirically derived on data from the Norwegian continental shelf (Fig.44B).

The average precipitation rates for oil zone samples presented on Fig.44B are, however, apparent rates since predicted amounts of quartz cement do not match measured quartz cement abundances (Fig.41B). Exemplar™ systematically overestimates quartz cement abundances in oil zone samples (Fig.41B), which implies that precipitation rates in oil zones must be lower than in water zones. This reflects the retard effect of hydrocarbons on the quartz cementation process. The modelling software cannot directly take the effect of hydrocarbons on quartz precipitation rates into account. Therefore, an indirect route for the determination of quartz precipitation rates in the presence of hydrocarbons was followed.

As mentioned earlier, quartz cementation is regarded as a three-step process in the Exemplar™ software; silica is internally sourced from quartz dissolution at stylolites, diffuses over short distances and precipitates onto clean quartz surfaces (Walderhaug, 1996). Of the three steps that control this quartz cementation process, silica precipitation is considered to be the rate-limiting or controlling step. However, according to Worden et al. (1998), the rate of diffusion of silica through remaining pore-waters will become the rate-determining-step after hydrocarbons have entered a reservoir. This means that, when oil displaces water from pore-space in a sandstone, the rate of diffusion of silica will control the overall rate of quartz cement growth.

There is no known method of measuring this diffusion rate in the subsurface. In practical applications of predicting quartz cement volumes, this reduced diffusion rate can be considered as equivalent to a water-saturated pore-space with a reduced area on each quartz grain being available for quartz precipitation. Therefore, a reduced diffusion rate was simulated by means of a proxy reduction of grain surface area. The presence of authigenic clay coatings (Heald & Larese, 1974; Ehrenberg, 1993; Olsen et al., 1996) or microquartz (Aase et al., 1996; Ramm et al., 1997) on detrital quartz grains is considered to prevent quartz cementation. Therefore, a grain-coating module is included in the Exemplar™ software. It is important to emphasize that no natural clay coatings are observed in the Brae Formation sandstones (Chapter 3). In Chapter 3 it was also concluded that

microquartz crystals in the Brae Formation sandstones represent the earliest stage of quartz cementation, and do not act as a coating which prevents further quartz growth. This conclusion was derived from the observation of microquartz crystals directly adjacent to large quartz overgrowths, and from the presence of microquartz crystals in water zone samples which have experienced extensive quartz cementation (Chapter 3). Hence, the simulation of reduced diffusion rates by means of a proxy reduction of grain surface area will not be affected by natural variability within the sandstones.

In the Exemplar™ simulations discussed below, the simplifying assumption was made that hydrocarbons charged the entire oil zone simultaneously. A more precise representation would probably be a progressive filling of the reservoirs, but the time taken to fill the reservoirs in the Miller and Kingfisher Fields is not known.
First, a 100% grain coating was applied on all oil zone samples subsequent to hydrocarbon charge. A cross plot of measured versus predicted quartz cement abundances is given in Fig.41C. In practically all samples from all reservoirs, the simulation has under-predicted measured quartz cement abundances. This could mean that displacement of water by hydrocarbons in the sandstone pore-spaces does not stop quartz cementation, but merely slows it down. In order to determine the rates of quartz precipitation for oil zone samples, different amounts of clay coating were applied to individual samples to match the predicted quartz cement abundance in each sample to its measured quartz cement content. The amount of clay coating needed on each oil zone sample to match quartz cement prediction with measurement (Fig.41D), is shown in Table 18. From these correctly predicted quartz cement abundances in oil zones, it was possible to calculate average quartz precipitation rates over the time interval since hydrocarbon emplacement until the present day. Quartz precipitation rates are listed in Table 18 and plotted on an Arrhenius plot in Fig.44C. Quartz precipitation rates in the oil zone of the reservoir in the Miller Field and of the Brae Formation Unit 1 reservoir in the Kingfisher Field are considerably less than calculated water zone precipitation rates (Fig.44C). Below, results are discussed individually for each of the three reservoirs examined.

Brae Unit 2 in Miller The quartz precipitation rates in the oil and water zone of the Brae Formation 2 reservoir in the Miller Field (Table 18) are on average $1.5.10^{-21}\pm1.8.10^{-21}$ moles/cm^2.s and $6.3.10^{-20}\pm0.9.10^{-20}$ moles/cm^2.s respectively.

The amount of coating needed on oil zone samples, in order to match quartz cement predictions to measurements, varies between 100 and 27 % and differs according to the position of the sample in the reservoir (Table 18). Samples in the oilfield crest require up to 100% coating and the amount of coating decreases progressively towards the oil-water contact (Table 18). Consequently, the calculated quartz precipitation rates for oil zone samples are lowest in the crest of the field and increase towards the oil-water contact (Fig.45A). In the water zone, quartz precipitation rates appear to be fairly constant (Fig.45A).

Brae Unit 1 in Kingfisher Quartz precipitation rates in this reservoir are overall very low : $5.8.10^{-22}\pm3.3.10^{-22}$ moles/cm^2.s on average (Fig.45B). The amount of coating needed on oil zone samples was overall high : 56 to 85 % (Table 18).

Brae Unit 2 in Kingfisher The quartz precipitation rates in the oil and water zone of the Brae Formation 2 reservoir in the Kingfisher Field are very similar : average $3.5.10^{-20}\pm2.8.10^{-20}$ moles/cm^2.s and $6.6.10^{-20}\pm1.2.10^{-20}$ moles/cm^2.s respectively (Table 18). Again, the amount of coating needed on oil zone samples, in order to match quartz cement predictions to measurements, is highest (30 %) in the samples located in the crest of the reservoir (Table 18). Towards the oil-water contact, only 3 % or no coating at all was required. Quartz precipitation rates in the top of the reservoir are lower than near the oil-water contact (Fig.45C). Around the oil-water contact, precipitation rates become identical to water leg rates.

When all quartz precipitation rates which result in correct prediction of quartz cement abundances for oil and water zone samples are plotted onto an Arrhenius plot (Fig.44C), it becomes clear that cementation rates in the oil zones are lower than in the water zones. The retard effect of oil on cementation becomes more pronounced the earlier the reservoir received the oil-fill. In the reservoir in the Miller Field, where oil entered around 40 Ma, quartz precipitation rates in the water zone are up to 2 orders of magnitude higher than in the oil leg (Table 18). In the oil zone, precipitation rates are in the order of 10^{-21} to 10^{-22} moles/cm^2.s, or are zero. In the Brae Formation Unit 1 reservoir in the Kingfisher Field, which also experienced early hydrocarbon emplacement, quartz precipitation rates in the oil zone are overall low : generally in the order of magnitude of 10^{-22} moles/cm^2.s (Table 18). In the Brae Formation Unit 2 reservoir in the Kingfisher Field, which had a recent oil-fill around

15 Ma, hardly any difference exists between oil and water zone quartz precipitation rates. Oil zone quartz precipitation rates are all in the order of magnitude of 10^{-20} moles/cm^2.s, which is similar to water leg precipitation rates in the Kingfisher and Miller Fields (Table 18).

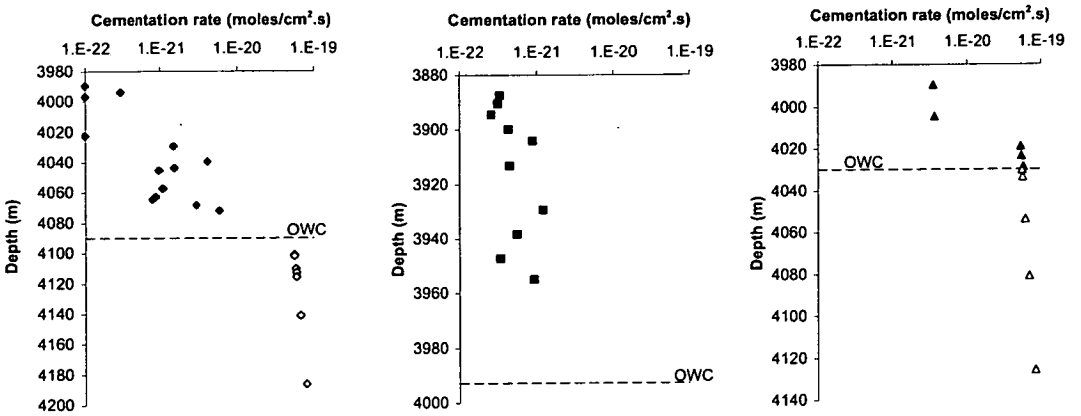

Fig.45 Average quartz precipitation rates, since time of oil charge until the present, plotted versus depth in the reservoirs examined. Quartz precipitation rates are plotted on a logarithmic scale. Samples yielding zero as their quartz precipitation rate have been plotted as 1.10^{-22} because log zero can not be plotted.
A In the Brae Formation Unit 2 reservoir in the Miller Field, calculated precipitation rates appear lowest in the structural crest and increase towards the oil-water contact (OWC). There is a gentle increase in precipitation rate noticeable in the water zone of the reservoir.
B In the Brae Formation Unit 1 reservoir in the Kingfisher Field, calculated precipitation rates appear overall small.
C In the Brae Formation Unit 2 reservoir in the Kingfisher Field, calculated precipitation rates are generally similar in oil and water zones of the reservoir. Only in the top two samples of the reservoir are precipitation rates slightly lower.

6.6 Discussion

The data presented above demonstrate quantitatively that quartz precipitation rates in the oil zones of reservoirs are lower than in water zones (Fig.45). The fact that quartz precipitation rates from water zone samples from different reservoirs display similar values (Table 18), supports the validity of the data presented.

Quartz precipitation rates in the oil zones appear to vary vertically through the reservoirs (Fig.45). When plotting these precipitation rates versus height above oil-water contact (OWC), a trend of decreasing quartz precipitation rates with increasing height above OWC is observed (Fig.46). This can be explained in two ways. The first explanation is that transport of quartz, by diffusion in residual pore water, is hindered more in the crest of the field, because of lower residual water

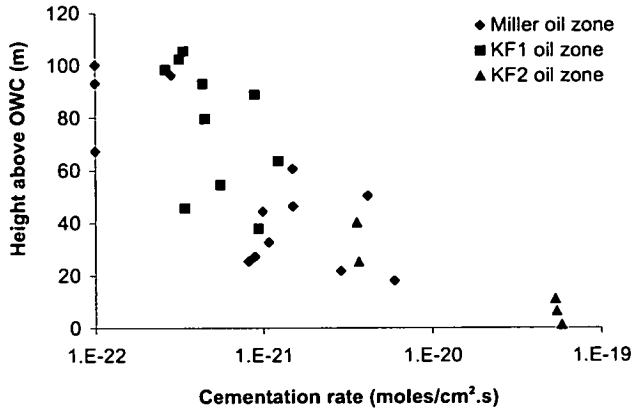

Fig.46 Average quartz precipitation rates plotted versus height above oil-water contact (OWC). There is a noticeable trend of decreasing quartz precipitation rate with increasing distance from the OWC. This trend is the direct consequence of assuming an instantaneous, as opposed to progressive, oil-fill in the reservoirs. As a consequence, samples progressively closer to the OWC have spent less time in oil and their average rates of quartz precipitation appear lower.

saturations in this part of the reservoir. Near the OWC, where residual water saturations become higher, transport is hindered less which results in higher precipitation rates. If this explanation is true, variable saturations of residual water would be expected to exist vertically through the oilfield. Water saturations (S_w) in well 8b-3 (Miller Field) were calculated by Dr. Rider (Rider-French Consulting Ltd) by using electrical resistivity on wireline logs. In Fig.47, S_w in well 8b-3 (Miller Field) is plotted versus depth in the reservoir. Although S_w varies across the reservoir oil zone, there is no noticeable trend of decreasing S_w with increasing height above OWC (Fig.47). For this reason, the hypothesis that quartz cementation is retarded more in crestal areas of reservoirs than near the OWC, because of higher oil saturation in the crests, can be rejected.

A second explanation is that quartz precipitation rates appear different vertically through the oil zones because of the assumption that oil charged the reservoirs instantaneously. In reality, oil charge may have taken place over several millions of years, so that samples progressively deeper below the oilfield crest have spent progressively less time in oil. Thus, quartz precipitation rates in oil zone samples are systematically overestimated, and the true precipitation rate in oil is constant, and represented by the slow rate characteristic of the reservoir crest. This slow rate should be applied for progressively smaller timespans as depth increases below the oilfield crest. This is considered to be a better explanation. Since the calculated lowest quartz precipitation rates in the oil legs equal zero, or approximate zero, it

can be concluded that hydrocarbon emplacement in reservoirs does virtually stop quartz cementation.

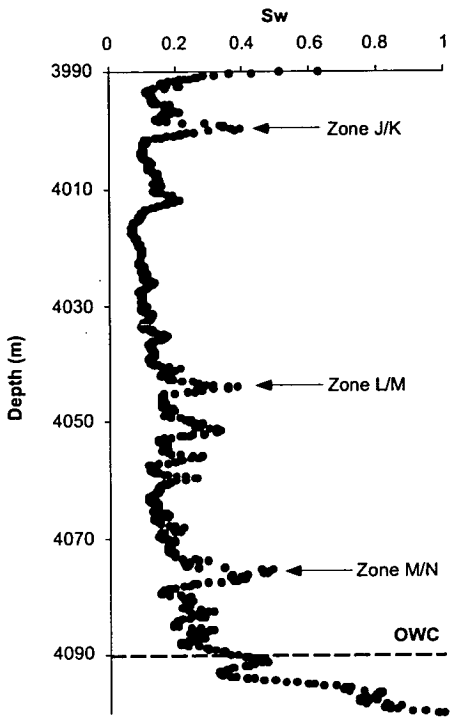

Fig.47 Water saturations (S_w) in well 8b-3 (Miller Field) plotted versus depth. S_w, calculated from the well resistivity log, is generally <0.2 across the reservoir oil zone. A few higher values correspond to shale breaks between different reservoir zones. Below the OWC, there is a transition zone of about 10 m thickness across which S_w evolves towards 1.

Following the conclusion that hydrocarbon emplacement virtually stops quartz precipitation, it becomes possible from the simulation results to determine the exact time and duration of oil-fill in the reservoirs examined. It is clear that the amounts of quartz cement that can be precipitated after oil charge, when precipitation rates are virtually zero, will be negligible. Therefore, the quartz cement volumes present in each sample must be precipitated before hydrocarbon emplacement. The time at which the amount of quartz cement present in a sample equals the amount of quartz cement predicted by the software programme can consequently be taken to represent the time of hydrocarbon charge. In the time period before oil-fill, quartz precipitation rates in the oil zones are similar to those in the water zones of reservoirs. Therefore, the simulation where quartz cement abundances in the reservoirs were predicted by using precipitation rates derived from calibrated reaction kinetics on the water zones of the reservoirs must be used (Appendix D – Table D.4). The time of oil emplacement (time when predicted amount of quartz

cement in sample = measured amount of quartz cement of sample) for each sample is listed in Table 18 and is plotted versus present day reservoir depth in Fig.48. Oil charge in the reservoir in the Miller Field started in the crestal areas around 49-40 Ma (Table 18 & Fig.48). From the temperature history input data in Exemplar™ (Appendix D) it can be calculated that at that time, the reservoir temperature was around 90 to 102 °C (Table 18 & Fig.48). This temperature range is in close agreement with fluid inclusion homogenization temperatures measured in quartz cements (95 to 110 °C) in those areas of the Miller Field (Chapter 4). Oil charged the reservoir slowly, and approached the present day OWC only around 8 Ma when the reservoir temperature had increased to 118 °C (Table 18 & Fig.48). Maximum fluid inclusion homogenization temperatures measured in quartz cements near the OWC are around 115 °C (Chapter 4). Hydrocarbons charged the entire Brae Formation Unit 1 reservoir in the Kingfisher Field rapidly; over the course of 34 to 22 Ma (Table 18 & Fig.48). During this time period, calculated reservoir temperatures increased from 94 to 104 °C (Table 18 & Fig.48). Again, this temperature range is in close agreement with fluid inclusion homogenization temperatures measured in quartz cements (90 to 105 °C) (Chapter 4). Oil charge in the Brae Formation Unit 2 reservoir in the Kingfisher Field appears to be an even more recent event than previously assumed. According to the simulation results, oil entered only 3 Ma (115 °C) and oil-fill continues up to the present day (118 °C) (Table 18 & Fig.48). The highest fluid inclusion homogenization temperatures measured in quartz cements in this reservoir are around 120 °C (Chapter 4).

6.7 Exemplar™ : how predictive is the model ?

Exemplar™ is marketed as a numerical model of compaction and quartz cementation to provide a general method suited for porosity prediction, prior to drilling, of sandstone reservoirs (Lander & Walderhaug, 1999). It is claimed that the model provides reasonably accurate reservoir quality predictions for quartz-arenites, sublith-arenites and subarkoses, but more geologic data sets are needed for calibration before the model can be applied confidently in ductile grain-rich rocks (Lander & Walderhaug, 1999). In this paragraph, I discuss a few observations about the predictive capacity of Exemplar™ and how predictions can be improved.

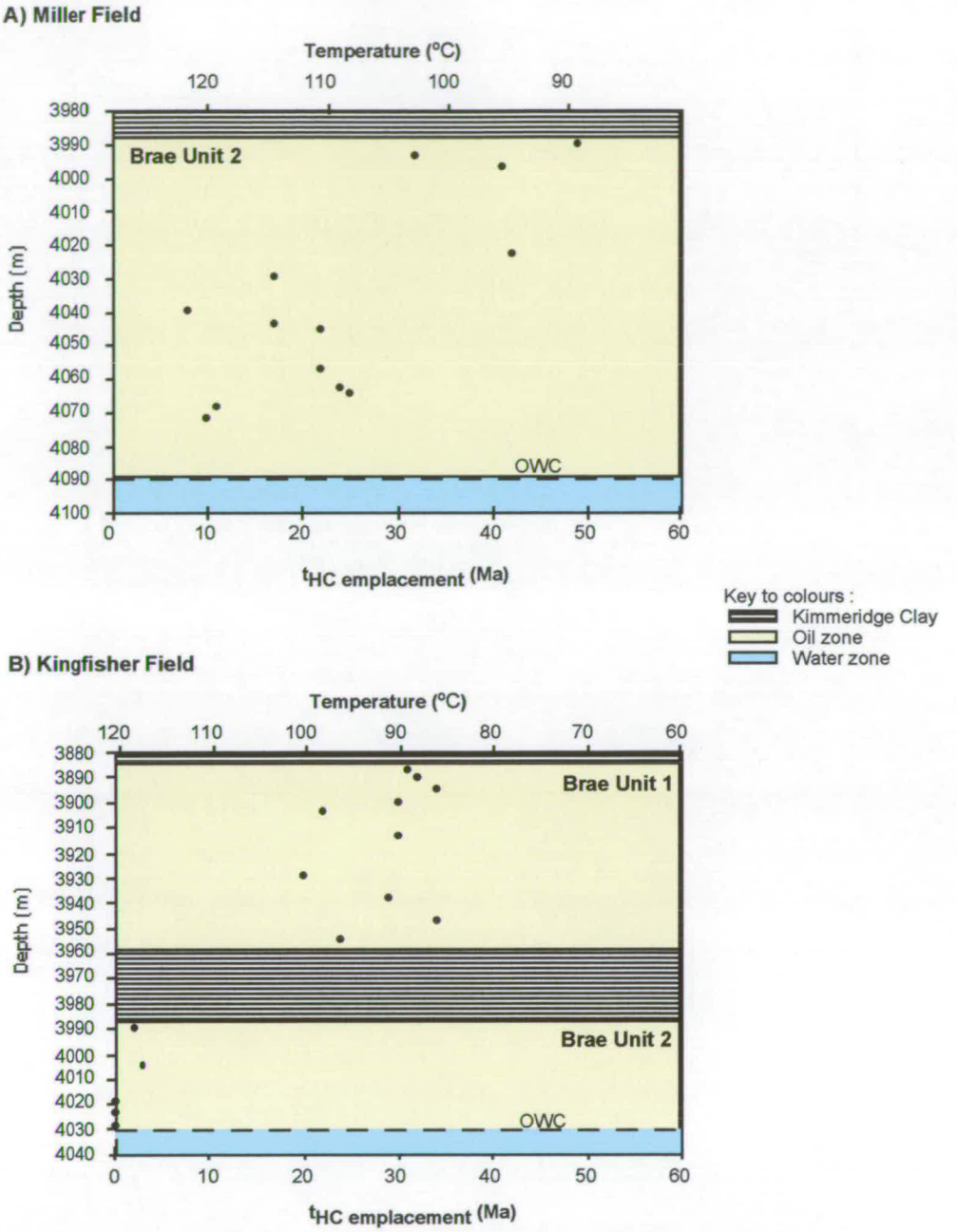

Fig.48 Time (Ma) of hydrocarbon emplacement (HC), and reservoir temperature (°C), versus present day depth (m) in the reservoirs in the Miller and Kingfisher Fields.
A Oil charge in the crestal areas of the Brae Unit 2 reservoir in the Miller Field started around ~49-40 Ma (temperature range ~90 to ~102 °C). Oil charged the reservoir slowly, and approached the present day oil-water contact (OWC) around 8 Ma (temperature ~118 °C).
B Hydrocarbon emplacement in the Brae Unit 1 reservoir in the Kingfisher Field occurred from ~34 to 22 Ma (temperature range ~94 to ~104 °C). Oil charge in the Brae Unit 2 reservoir in the Kingfisher Field occurred in recent times (~3 Ma) when reservoir temperatures were ~118 °C.

The input data needed for the model require petrographic knowledge of the targeted reservoir rocks. Parameters such as mineralogical composition and texture exert important influences on the predictions of quartz cement abundances and porosities. Such detailed lithological knowledge can not be obtained in the pre-drilling stage, but needs examination of actual core samples.

When using default reaction kinetics in the programme, obtained from calibration of data from the Norwegian continental shelf, discrepancies occur between measured and predicted quartz cement volumes (Fig.41A). Therefore, it is important to calibrate the reaction kinetics to the data set being examined in order to optimize predictions. This requires, again, pre-drilling lithological knowledge. According to Walderhaug (2000), the variation in optimal reaction kinetics between data sets is probably due to inaccurate temperature histories. Also, improving the quartz surface area function (Appendix D) may reduce the range of optimal values for the kinetic parameters (Walderhaug, 2000).

Exemplar™ does not incorporate the effect of oil emplacement on quartz cementation. When predicting quartz cement abundances by assuming that quartz precipitation rates in oil zones are similar to water zone precipitation rates, large errors on predicted results occur (Figs.41B and 43). This will be the case anywhere that oil zone samples are similar to water zone samples in terms of petrography and burial history, and where the reservoir has been hydrocarbon filled for a prolonged period of time. This is demonstrated by the attempt at predicting quartz cement abundances in the oil zones of the reservoirs in the Miller and Kingfisher Fields with Exemplar™, which used precipitation rates derived from reaction kinetics that represent water zone samples (Fig.42). Oil zone predictions for the reservoirs in the Miller Field and Brae Unit 1 in the Kingfisher Field are particularly unsuccessful since these reservoirs were hydrocarbon wet for longest (Fig.42). Predictions for the Brae Unit 2 reservoir in the Kingfisher Field are good since the reservoir experienced a recent oil fill (<10 Ma) (Fig.42). A direct consequence of not taking lower oil zone precipitation rates into account is that oil zone porosity predictions can be much underestimated. This will result in errors on field volume calculations in the appraisal stage and in erratic assessments of reservoir performance during production. A prerequisite for improving predictions of quartz cement abundances, and consequently also porosities, in oil-filled reservoirs is to know the approximate time of hydrocarbon emplacement. This can be easily and quickly obtained from source rock modelling. From the time of hydrocarbon emplacement to the present

day, quartz cement abundance must be calculated by employing different rates of quartz precipitation for oil and water zone samples. It has been demonstrated above that, once the rocks fill with oil, quartz precipitation rates will approximate zero. However, since there is usually no information on the time span of the filling of a reservoir, the danger exists that quartz cement abundances could be under-predicted if precipitation rates were modelled to become zero across the whole reservoir at the estimated time of hydrocarbon emplacement. This would be the case for reservoirs which experienced an oil charge over a prolonged period of time (e.g. in the Miller Field). Because there is no known pre-drill method of determining the duration of hydrocarbon charge in reservoirs, oil zone reservoir quality predictions are best made for two end-member scenarios (apply zero precipitation rates for the possibility of instantaneous oil-fill and apply precipitation rates similar to those in the water zone for the possibility of a prolonged period of oil-fill).

6.8 Conclusions

1 Exemplar™ is marketed as a numerical model which provides a general method for porosity prediction, prior to drilling, of sandstone reservoirs. Input data needed for the model, however, require post-drilling petrographic knowledge of the targeted reservoir rocks. It also proves to be essential to calibrate reaction kinetics in the programme onto the specific data sets being examined in order to optimize predictions.

2 After calibration of the reaction kinetics in the programme on water zone samples from the reservoirs in the Miller and Kingfisher Fields, the model accurately predicts the water zone reservoir quality but underestimates oil zone reservoir quality in those fields. This is because the retarding effect of hydrocarbon emplacement on quartz cementation is not incorporated in the software.

3 Average quartz precipitation rates in the water zones of the Miller and Kingfisher Fields are in the order of 10^{-20} moles/cm^2.s. Depending on the time of hydrocarbon charge in the reservoirs, calculated average quartz precipitation rates for oil zone samples range from zero to values similar to those in water zone samples. Quartz precipitation rates in reservoirs with recent oil-fill (Brae Unit 2 in the Kingfisher Field) are similar in both water and oil zones. Quartz precipitation rates in reservoirs which have been hydrocarbon-filled over a prolonged period of time (Brae Unit 2 in the Miller

Field and Brae Unit 1 in the Kingfisher Field) are at least two orders of magnitude lower (and may be zero) in the oil zones than in the water zones.

4 Reservoirs which gradually filled with oil, such as the Brae Formation reservoir in the Miller Field, display a trend of decreasing quartz precipitation rates with increasing height above the oil-water contact. This is interpreted to be a consequence of the assumption made for the modelling that oil charged the reservoir instantaneously. As a result, quartz precipitation rates are systematically overestimated and the true precipitation rate in oil is represented by the lowest rate (near zero) at the reservoir crest.

5 A consequence of the inhibiting effect of hydrocarbons on quartz cementation is that, if it is assumed that quartz precipitation rates in oil and water zones of reservoirs are similar, this could result in underestimation of oil zone porosities. This will result in errors in field volume calculations in the appraisal stage and in erratic assessments of reservoir performance during production.

6 It is possible from the simulation results to derive the exact time of hydrocarbon emplacement and the duration of oil-fill in the reservoirs examined. Oil charge in the Brae Unit 2 reservoir in the Miller Field started in the crestal areas around 49-40 Ma. Oil filled this reservoir slowly, and approached the present-day oil-water contact only around 8 Ma. Hydrocarbons charged the entire Brae Unit 1 reservoir in the Kingfisher Field rapidly (from 34 Ma to 22 Ma). Oil charge in the Brae Unit 2 reservoir in the Kingfisher Field was a recent event (3 Ma) and probably still continues at the present. When these time spans are translated into temperature ranges, by using thermal history models, then there is close agreement between the modelled quartz precipitation temperature results and the maximum measured homogenization temperatures in fluid inclusions in the quartz cements in each reservoir.

CHAPTER VII

POREFLUID EVOLUTION

In this chapter :

- *What is the oxygen isotopic composition of quartz cements in the Brae Formation sandstones ?*
- *How do the results of conventional oxygen isotope analysis compare with in-situ oxygen isotopic compositions obtained by ion microprobe analysis ?*
- *Is there any variation in oxygen isotopic composition of quartz cements within, and possibly also between, the different reservoirs examined ?*
- *From which type of porefluid did quartz cements precipitate and what are the implications for fluid flow mechanisms into and/or within the reservoirs in the Brae Formation ?*
- *What is the palaeo-fluid evolution in the Miller and Kingfisher Fields ?*

7.1 Introduction

In order to understand and predict the diagenetic history of a sandstone reservoir, it is critical to examine the hydrogeologic regime that operated in the sedimentary basin throughout geological history (Galloway, 1984), because fluids both dissolve grains in sandstones and carry the dissolved species which precipitate as cements. The volumes of quartz cements contained in the Brae Formation sandstones imply transport of significant quantities of silica. Potential sources of silica might be found within the Brae Formation sandstones, or silica could be transported from an external source into the sandstones. In either case, silica supply will be governed by fluid flow (advective or diffusive). Constraining the hydrogeological regime which operated during the geological history of the sandstones studied can therefore

enhance understanding of the quartz cementation processes operative within the Brae Formation reservoirs. Because the hydrogeology of a basin evolves, the composition of present day porewaters deduced from field measurements will not necessarily represent those waters formerly present in the pore system (Harrison & Tempel, 1993). The oxygen isotopic composition of diagenetic minerals can offer clues to the origin of palaeo-fluids, provided precipitation temperatures are known (Longstaffe, 1989). Not surprisingly, studies of isotopic composition of diagenetic minerals have been widely used to help constrain palaeo-fluid flow models (e.g. Milliken et al., 1981; Sullivan et al., 1990; Haszeldine et al., 1992; McAulay et al., 1994; Macaulay et al., 1997).

In this chapter, I report and interpret the results of oxygen isotope analysis of quartz cements from the Brae Formation reservoirs in the Miller and Kingfisher Fields. I carried out both conventional oxygen isotope analysis (based on physical separation of quartz from core material) and in-situ oxygen isotope analysis using the ion microprobe. The conventional analysis technique generates an average oxygen isotopic ratio for the quartz cements present in a sample. With the ion microprobe, individual quartz overgrowths, and potentially also different growth zones in the overgrowths, can be analysed in situ. I compare the results from both analytical techniques and look for variations in the oxygen isotopic composition of quartz cements in the Brae Formation reservoirs and the implications of such variations. In previous chapters, I have constrained temperatures of quartz cement precipitation in the Brae Formation sandstones by means of fluid inclusion analysis (Chapter 4) and reconstruction of thermal histories (Chapter 5). I use this information, in combination with the oxygen isotopic composition of quartz cements, to gain insight into palaeo-fluid composition, and fluid composition evolution, during the geological histories of the reservoirs studied.

7.2 Conventional oxygen isotope analysis

Methodology All samples analysed for oxygen isotope ratios in the conventional way were performed at the Scottish Universities Environmental Research Centre (S.U.E.R.C.) in East-Kilbride. The method of conventional oxygen isotope analysis on authigenic quartz has recently been described by Macaulay et al (2000) and the following is extracted from that paper. Oxygen isotope analyses of quartz overgrowths are made by extracting O from samples of ~1 mg weight using a laser fluorination system based on that of Sharp (1990). Oxygen is released from the

samples by heating them with a CO_2 laser whilst inside a ClF_3-charged chamber. The O is then converted to CO_2 and analysed on a VG PRISM III mass spectrometer. In this technique each sample is reacted to completion so that all O is collected, and as a result no laser correction factor is required. The analytical precision of the laser fluorination technique is ±0.2 ‰.

Standards The standard used in this study was an S.U.E.R.C. internal laboratory standard which consists of vein quartz and is known as SES quartz ($\delta^{18}O_{SMOW}$ = +10.3 ‰). Each sample holder for the laser fluorination line holds 10 samples and at least 2 quartz standards were included in each batch of samples. The analytical precision of oxygen isotope analyses using the laser fluorination line, based on repeat analyses of standards, is ± 0.2 ‰.

Samples Five samples from the Brae Formation Unit 1 and six samples from the Brae Formation Unit 2 reservoirs in the Kingfisher Field, and two samples from the Brae Formation Unit 2 reservoir in the Miller Field, were selected for analysis. The number of Miller Field samples is restricted because eleven samples from this field were already analysed by myself as part of a research project funded by the Flemish government (VIS 95-4) and conducted at the Katholieke Universiteit Leuven (Belgium) during the period of April-May 1997. The results of these analyses (Batch 1 results) will be incorporated with the present results (Batch 2 results).

Sample preparation Conventional oxygen isotope analysis of authigenic quartz requires separation of the quartz overgrowths from the detrital quartz grains. This was achieved by applying the method of Lee & Savin (1985) to the selected samples. The quartz overgrowths were physically removed from the detrital grains by a combination of etching in hydrofluoric acid (HF) followed by agitation in an ultrasonic bath. Subsequently, each sample was sieved into four size fractions for analysis; <30 μm, 30-52 μm, 52-80 μm and >80 μm. This concentrates the overgrowths in the smaller grain size fractions.

7.3 Ion microprobe oxygen isotope analysis

Methodology All samples were analysed for oxygen isotope ratios with a Cameca ims-4f ion microprobe equipped with a Charles Evans & Associates control system at the University of Edinburgh. The samples were bombarded in the ion microprobe

with a focused (20-30 μm) primary beam of $^{133}Cs^{+}$. An initial burn-in time of 3 minutes was used to sputter through the gold coat and to stabilize the secondary ion current prior to each analysis. The surface charge of the sample was neutralized with a normal-incidence electron flood gun. Negative high energy (offset 350 V) secondary ions ($^{18}O^{-}$ and $^{16}O^{-}$) were accelerated and focussed into a mass spectrometer where the isotopes are separated and subsequently counted with an electron multiplier. For each analysis of $^{18}O/^{16}O$ in quartz, secondary $^{18}O^{-}$ and $^{16}O^{-}$ ions were collected with total counting times of 640 and 80 s respectively. The total counting times were made up of 80 cycles of counting for 8 s on ^{18}O and 1 s on ^{16}O yielding a theoretical precision of ±1 ‰.

Standards Quartz analyses were standardised against Bogala Quartz (BOG) ($\delta^{18}O_{SMOW}$ = 12.3±0.3 ‰; Elsenheimer & Valley, 1993). The homogeneity of this standard at the scale of ion microprobe analysis was demonstrated by Graham et al. (1996). At the start and end of the day, at least 3 standard analyses were made. Also, 2 to 3 standard analyses were made after every 6 to 8 unknown analyses. Fig.49 shows the measured $\delta^{18}O$ compositions in Bogala quartz throughout the analytical session. The standard analyses were used for correcting the data for the effect of instrumental mass fractionation. The drift in instrumental mass fractionation has been attributed to progressive ageing of the electron multiplier (Eiler et al., 1995). The result of this effect is a depletion of the measured isotope ratio in the heavier isotope relative to the true composition (Lewis, 1999). The drift is generally linear with time, and can be corrected by least-squares regression (e.g. Valley & Graham, 1991).

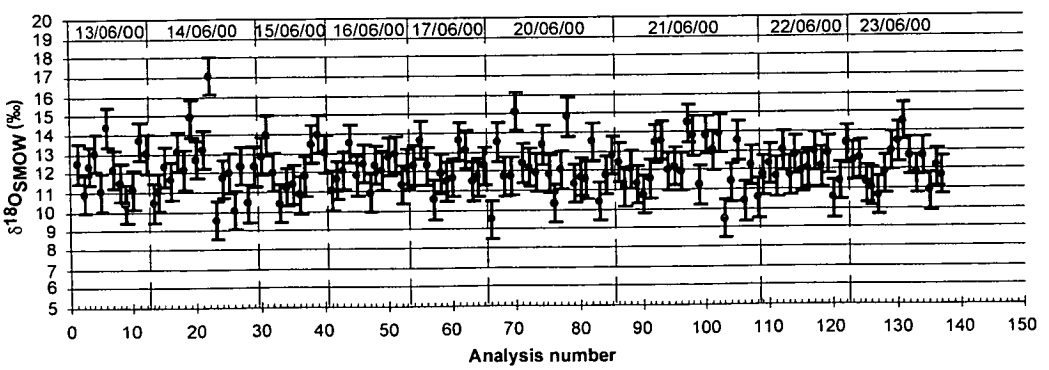

Fig.49 Ion microprobe results of the $\delta^{18}O$ analyses of the Bogala quartz standard throughout the analytical session (June 13th to 23rd 2000). The error bars are the internal reproducibility of individual ion microprobe analyses (±1 ‰).

Samples Nine samples were selected for analysis : 2 oil zone and 1 water zone sample from the Brae Formation Unit 2 reservoir in the Miller Field; 3 oil zone samples from the Brae Formation Unit 1 reservoir in the Kingfisher Field; 1 oil zone and 2 water zone samples from the Brae Formation Unit 2 reservoir in the Kingfisher Field. All samples were analysed during a two week period from June 12th to June 23rd 2000.

Sample preparation Samples for analysis were made into polished thin sections (30 μm thick) and cut to circles of 1 inch diameter in order to fit into the ion probe sample holders. As quartz is an electrical insulator, the sections are gold coated to effectively prevent charge build up on the sample surface.

For each thin section sample, the area chosen for oxygen isotope analysis with the ionprobe has to be imaged at both low and high magnifications to allow easy re-location of the area chosen for analysis. Sample maps were made for each thin section with the SEM in secondary electron (SE) mode (magnification x65). Because in this imaging mode it is impossible to differentiate between authigenic and detrital quartz, a few areas in each sample were selected for construction of a more detailed sample map (magnification x250) in cathodoluminescence (CL) mode. The SEM SE and CL photomicrograph maps are then used during the SIMS analysis session to facilitate identification of the area of interest in the reflected light optical viewing system of the Cameca ims-4f.

7.4 Data quality control

Conventional analysis The oxygen isotope data obtained for each size fraction in every sample are listed in Table 19. A problem inherent in the method of physical removal of overgrowths, by employing the HF etching technique, is that overgrowths may be only partly separated from detrital quartz grains. Also, weaknesses in quartz grains (such as fractures) are attacked by the HF acid causing disintegration of the quartz grains into small fragments (Brint et al., 1991). For these reasons, the various size fractions (<30 μm, 30-52 μm, 52-80 μm and >80 μm) analysed for each sample are inevitably composed of mixtures of detrital and authigenic quartz. The quality of quartz separation was checked in each size fraction of every sample by SEM-CL. The oxygen isotope composition of pure detrital and authigenic quartz in every sample was determined by means of the mass balance technique of Milliken et al. (1981). In this technique, the percentages

of authigenic quartz determined in each size fraction are cross-plotted versus the $\delta^{18}O_{SMOW}$ values in those size fractions. The $\delta^{18}O_{SMOW}$ values for pure authigenic and detrital quartz are than obtained by extrapolation towards 100 and 0 % authigenic quartz respectively.

Table 19 Results of conventional oxygen isotope analysis. Four size fractions were separated and analysed for each sample.
Batch 1 results : analytical session April-May 1997.
Batch 2 results : analytical session July 1999.

Oilfield/ Reservoir	Well	Sample/ Batch	Depth (m TVD)	$\delta^{18}O$ measured in the size fractions >80µm (‰)	80-52µm (‰)	52-30µm (‰)	<30µm (‰)
Miller	7b-20	4037.25/1	4011.7	14.4	15.2	14.9	15.3
Brae Unit II	7b-20	4045.35/1	4019.8	14.4	14.9	15.5	15.7
	7b-20	4124.5/1	4100.1	14.0	15.4	16.2	16.2
	7b-24	4066.55/1	4045.5	15.4	15.9	16.1	16.4
	7b-24	4093.25/1	4071.9	15.1	15.0	15.9	16.3
	8b-3	13163/1	3993.8	15.2	15.5	15.9	16.5
	8b-3	13173/2	3996.9	12.4	16.8	18.0	18.2
	8b-3	13569/1	4116.0	14.3	15.6	15.7	15.8
	8b-3	15312/1	4039.6	9.4	13.4	13.7	16.5
	8b-A06	5873.35/1	4065.5	14.9	15.4	15.8	16.0
	8b-A06	5887.1/1	4074.4	15.2	15.8	16.2	16.1
	8b-A06	5927.8/2	4102.2	13.2	14.8	15.6	16.8
	8b-A06	5939.85/1	4110.4	14.7	15.8	15.8	16.2
Kingfisher	8a-8	13337/2	3887.5	11.6	15.6	16.3	16.7
Brae Unit I	8a-8	13353/2	3892.0	12.3	15.8	17.2	17.4
	8a-8	13395.8/2	3904.2	12.0	15.6	17.6	18.2
	8a-8	13450/2	3920.1	12.1	17.4	18.2	18.3
	8a-8	13512.4/2	3938.4	12.1	15.8	18.0	18.4
Kingfisher	8a-4	13143/2	3989.7	12.8	13.5	17.3	16.4
Brae Unit II	8a-4	13225/2	4015.1	14.0	15.9	17.2	17.4
	8a-4	13274/2	4030.3	14.4	15.8	18.2	18.5
	8a-4	13320.3/2	4044.7	13.5	16.0	17.3	17.5
	8a-4	13437.5/2	4081.0	13.4	15.9	16.1	18.0
	8a-4	13582.7/2	4126.1	12.7	17.1	18.2	18.6

Table 20 Percentages of authigenic quartz determined in each size fraction of every sample used for conventional oxygen isotope analysis. Authigenic quartz percentages were determined by SEM-CL combined with image analysis (Appendix A).

Oilfield/ Reservoir	Well	Sample/ Batch	Depth (m TVD)	% quartz cement in the size fractions >80µm (%)	80-52µm (%)	52-30µm (%)	<30µm (%)
Miller	7b-20	4037.25/1	4011.7	7.0	13.4	30.6	33.3
Brae Unit II	7b-20	4045.35/1	4019.8	11.6	12.9	14.2	62.8
	7b-20	4124.5/1	4100.1	8.8	18.6	37.4	44.3
	7b-24	4066.55/1	4045.5	11.7	25.0	24.8	49.2
	7b-24	4093.25/1	4071.9	18.7	16.8	65.1	81.2
	8b-3	13163/1	3993.8	8.4	17.1	37.1	52.3
	8b-3	13173/2	3996.9	8.4	48.0	78.8	80.2
	8b-3	13569/1	4116.0	12.3	23.7	35.7	54.9
	8b-3	15312/1	4039.6	7.0	7.5	32.3	58.2
	8b-A06	5873.35/1	4065.5	14.6	21.3	47.3	72.8
	8b-A06	5887.1/1	4074.4	10.7	23.0	49.7	62.5
	8b-A06	5927.8/2	4102.2	15.4	42.9	49.4	59.1
	8b-A06	5939.85/1	4110.4	14.1	23.7	33.0	52.8
Kingfisher	8a-8	13337/2	3887.5	7.7	27.2	34.9	65.9
Brae Unit I	8a-8	13353/2	3892.0	4.9	35.5	34.7	53.4
	8a-8	13395.8/2	3904.2	4.3	30.8	38.6	76.1
	8a-8	13450/2	3920.1	6.1	43.1	34.5	70.1
	8a-8	13512.4/2	3938.4	6.0	30.2	55.2	48.8
Kingfisher	8a-4	13143/2	3989.7	13.0	21.1	47.1	37.1
Brae Unit II	8a-4	13225/2	4015.1	12.4	28.9	50.2	70.2
	8a-4	13274/2	4030.3	11.4	32.8	48.4	80.7
	8a-4	13320.3/2	4044.7	11.6	23.7	27.4	56.6
	8a-4	13437.5/2	4081.0	10.7	29.9	40.8	75.9
	8a-4	13582.7/2	4126.1	5.8	44.7	37.0	76.1

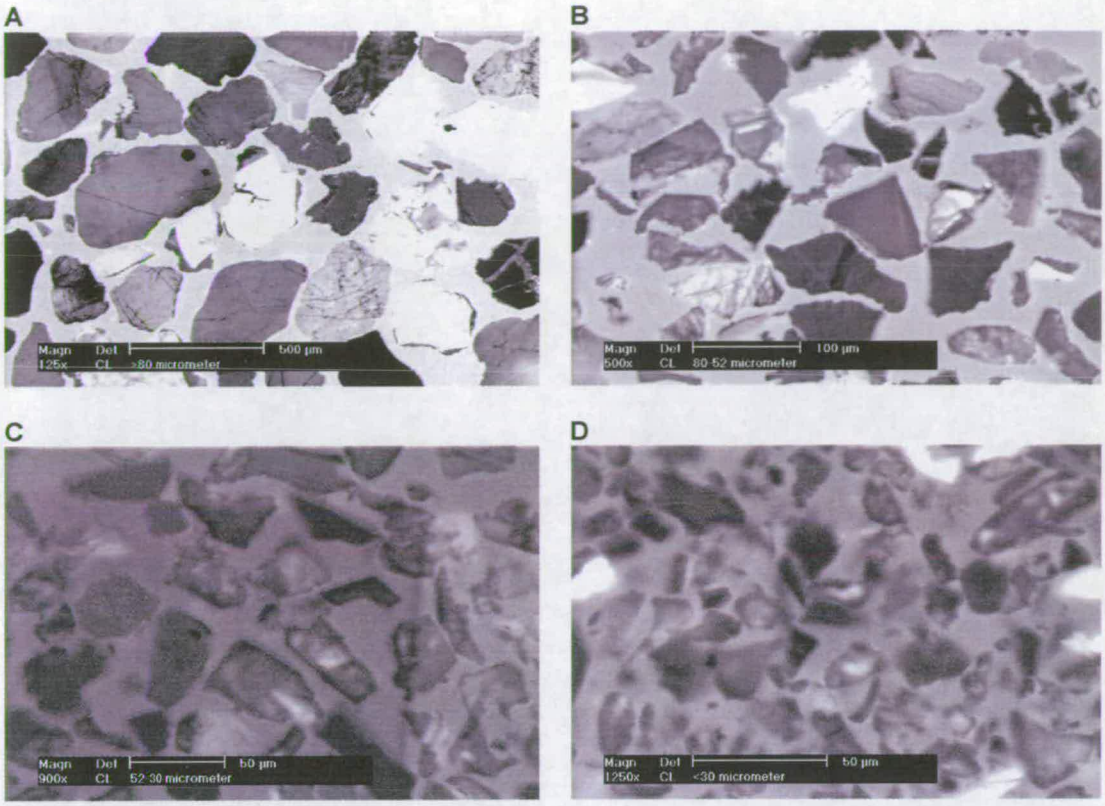

Fig.50 SEM-CL photomicrographs of the four size fractions analysed of sample 13353 (3892 m in Brae Unit 1 reservoir, Kingfisher Field). The thin sections have to be viewed at increasingly higher magnification as size fractions decrease which results in image quality loss. As a result, determination of quartz cement abundance in the two smallest size fractions (C and D) will be subject to large errors.
(**A**) >80 µm, (**B**) 80-52 µm, (**C**) 52-30 µm, (**D**) <30 µm.

Table 21 Extrapolated $\delta^{18}O$ values for pure authigenic (AQ) and detrital (DQ) quartz for each sample analysed by the conventional oxygen isotope technique. The extrapolated $\delta^{18}O$ values were determined for each sample by mass balance of oxygen isotope values and percentages of authigenic quartz measured in all four (column A), three (column B) and two (column C) size fractions. The most likely extrapolated pure authigenic and detrital quartz ^{18}O values for each sample are shaded grey.

Oilfield/ Reservoir	Well	Sample depth (m)	A Extrapolated $\delta^{18}O$ (4 size fractions) AQ (‰)	DQ (‰)	Correlation coefficient	B Extrapolated $\delta^{18}O$ (3 coarsest size fractions) AQ (‰)	DQ (‰)	Correlation coefficient	C Extrapolated $\delta^{18}O$ (2 coarsest size fractions) AQ (‰)	DQ (‰)
Miller	7b-20	4011.7	16.5	14.5	0.38	15.9	14.6	0.16	26.0	13.5
Brae Unit II	7b-20	4019.8	16.3	14.7	0.46	51.8	9.5	1	48.4	9.9
	7b-20	4100.1	19.7	13.8	0.87	20.9	13.6	0.89	27.0	12.7
	7b-24	4045.5	17.7	15.3	0.85	19.4	14.9	0.92	18.7	15.0
	7b-24	4071.9	16.6	14.7	0.99	16.5	14.7	1	19.4	14.1
	8b-3	3993.8	17.8	15.0	0.98	17.4	15.0	0.98	18.3	14.9
	8b-3	3996.9	20.0	12.1	0.95	20.0	12.1	0.94	22.6	11.5
	8b-3	4116.0	17.4	14.4	0.62	19.7	13.8	0.79	24.3	12.9
	8b-3	4039.6	20.6	10.6	0.69	20.1	10.7	0.32	753.4	-46.6
	8b-A06	4065.5	16.6	14.9	0.85	17.1	14.7	0.85	21.3	13.8
	8b-A06	4074.4	16.9	15.2	0.79	17.5	15.1	0.90	19.6	14.7
	8b-A06	4102.2	19.7	11.8	0.96	18.8	12.1	0.98	18.1	12.3
	8b-A06	4110.4	17.9	14.6	0.73	19.9	14.1	0.76	24.5	13.1
Kingfisher	8a-8	3887.5	20.3	12.3	0.68	28.2	10.3	0.98	30.5	10.0
Brae Unit I	8a-8	3892.0	23.1	12.2	0.87	25.5	11.6	0.91	23.2	11.7
	8a-8	3904.2	21.1	12.7	0.80	26.9	11.2	0.98	25.0	11.4
	8a-8	3920.1	22.3	12.9	0.71	27.5	11.4	0.89	25.6	11.2
	8a-8	3938.4	24.4	11.6	0.96	23.6	11.7	0.98	26.5	11.2
Kingfisher	8a-4	3989.7	24.9	10.8	0.98	24.4	10.8	0.98	20.3	11.7
Brae Unit II	8a-4	4015.1	19.6	13.8	0.88	21.5	13.2	0.97	24.1	12.6
	8a-4	4030.3	20.2	14.0	0.84	23.1	13.0	0.94	20.2	13.7
	8a-4	4044.7	21.4	13.8	0.61	24.0	10.7	0.99	31.8	11.1
	8a-4	4081.0	19.9	13.3	0.92	22.0	12.6	0.91	25.0	12.0
	8a-4	4126.1	21.5	13.3	0.75	25.3	12.2	0.86	23.4	12.0

Miller – Brae unit 2 (Fig.51A) Separation of authigenic and detrital quartz appears to have been successful in samples 3996.9 and 4102.2 (Fig.51A). These samples display increasing $\delta^{18}O$ values across decreasing size fractions, with more authigenic quartz determined by SEM-CL and image analysis in the smaller size fractions (Table 20). There is a very good correlation between the datapoints for these samples (0.95 for 3996.9 and 0.96 for 4102.2; Table 21) and extrapolated pure authigenic and detrital quartz $\delta^{18}O$ values are consequently considered to be reliable (Table 21).

There is strong evidence of a problem in estimating the percentage of authigenic quartz in the <30 μm fraction of samples 4100.1 and 4045.5 (Fig.51A). The estimated authigenic quartz percentage in the <30 μm fraction of these samples is higher than the estimated authigenic quartz percentage in the 30-52 μm fraction (Table 20) despite identical (4100.1; Table 19), or very similar (4045.5; Table 19), $\delta^{18}O$ values measured in these smallest two size fractions. For this reason, $\delta^{18}O$ values for pure authigenic and detrital quartz extrapolated from the three coarsest size fractions of these samples are considered to provide a better estimate (Table 21).

In samples 4011.7, 4071.9, 3993.8, 4116, 4065.5, 4074.4 and 4110.4 there is not much difference between the measured $\delta^{18}O$ values of the 80-52 μm, 52-30 μm and <30 μm size fractions (Table 19 and Fig.51A). This indicates that the physical separation of overgrowths from detrital quartz grains was not very successful. However, the percentages of authigenic quartz determined by SEM-CL and image analysis increase significantly from large to smaller size fractions and do not therefore reflect the constancy in measured $\delta^{18}O$ (Tables 19 and 20). For this reason, it was decided to determine $\delta^{18}O$ of pure authigenic and detrital quartz in these samples based on extrapolation of the data from the 2 largest size fractions only (>80 μm and 80-52 μm) (Table 21). The good image quality of these coarsest size fractions means that the extrapolated authigenic and detrital $\delta^{18}O$ values can be considered to reflect good estimates.

There is an obvious problem with sample 4019.8 (Fig.51A). The $\delta^{18}O$ value of the <30 μm size fraction is similar to the $\delta^{18}O$ value of the 52-30 μm size fraction, but the smallest size fraction apparently contains significantly more authigenic quartz (63 % in the <30 μm fraction and 14 % in the 52-30 μm fraction; Table 20)! Also, the slight increase in $\delta^{18}O$ values across the three coarsest size fractions is not

reflected in noticeably increasing authigenic quartz percentages (Tables 19 and 20). The estimated $\delta^{18}O$ values for pure authigenic quartz, based on extrapolation of data from the coarsest size fractions only, are geologically impossible (51.8 ‰ when using the three coarsest size fractions and 48.4 ‰ when using the two coarsest size fractions only; Table 21). Therefore, it was decided to disregard this sample for further interpretation.

The two coarsest size fractions of sample 4039.6 display similar authigenic quartz percentages for different $\delta^{18}O$ values (Fig.51A). Despite this problem, the extrapolated $\delta^{18}O$ values for pure authigenic and detrital quartz (based on all four size fractions) appear reasonable (20.6 ‰ and 10.6 ‰ respectively, Table 21) and are comparable to ion microprobe results available from the same sample (Table 24). For this reason, the extrapolated $\delta^{18}O$ values are considered to be acceptable estimates.

Kingfisher – Brae unit 1 (Fig.51B) Separation of authigenic and detrital quartz appears reasonably successful in samples 3887.5 and 3904.2 (Fig.51B). These samples clearly display increasing $\delta^{18}O$ values across the three coarsest size fractions (Fig.51B and Table 19). The measured $\delta^{18}O$ values are, however, similar in the two smallest size fractions (Table 19). Despite these similar $\delta^{18}O$ values measured in the 52-30 μm and <30 μm fractions, estimated authigenic quartz percentages are significantly higher in the <30 μm fractions than in the 30-52 μm fractions (Table 20). Nevertheless, $\delta^{18}O$ values for pure authigenic and detrital quartz, obtained via extrapolation based on data from all four size fractions analysed, are considered to provide good estimates because these values are comparable to ion microprobe results available from the same samples (Table 24).

There is an obvious problem with samples 3892 and 3920.1; a reversal in the plot is noticeable (Fig.51B). A higher percentage of authigenic quartz was determined by SEM-CL and image analysis in the coarser 80-52 μm size fractions than in the finer 52-30 μm size fractions, despite increasing $\delta^{18}O$ values towards finer size fractions (Fig.51B and Tables 19 and 20). Also here, the good quality of images from the >80 μm and 80-52 μm fractions means that the determination of authigenic quartz percentage was most reliable in these size fractions. Therefore, it was decided to determine $\delta^{18}O$ of pure authigenic and detrital quartz in samples 3892 and 3920.1 based on extrapolation of the data from the 2 largest size fractions only (Table 21).

There is a reversal in the plot of sample 3938.4 (Fig.51B). In this sample, a lower percentage of authigenic quartz was determined by SEM-CL and image analysis in the <30 μm size fraction than in the 52-30 μm size fraction, despite increasing $\delta^{18}O$ values towards the finest size fraction (Fig.51B and Tables 19 and 20). For this reason, $\delta^{18}O$ values for pure authigenic and detrital quartz extrapolated from the three coarsest size fractions only are considered to provide a better estimate (Table 21).

Kingfisher – Brae unit 2 (Fig.51C) Separation of authigenic and detrital quartz appears successful in samples 3989.7 and 4081 (Fig.51C). Sample 4081 displays increasing $\delta^{18}O$ values across decreasing size fractions, with more authigenic quartz determined by SEM-CL and image analysis in the smaller size fractions (Table 20). Despite the reversal in the plot of sample 3989.7, the higher percentage of authigenic quartz in the 52-30 μm size fraction, compared to in the <30 μm size fraction, is consistent with a higher measured $\delta^{18}O$ value in the 52-30 μm size fraction than in the <30 μm size fraction (Table 19 and Fig.51C). There is a good correlation between the datapoints for both samples (0.98 for 3989.7 and 0.92 for 4081; Table 21) and extrapolated pure authigenic and detrital quartz $\delta^{18}O$ values are consequently considered to be reliable (Table 21).

There is strong evidence of a problem in estimating the percentage of authigenic quartz in the <30 μm fraction of samples 4015.1, 4030.3 and 4044.3 (Fig.51C). The estimated authigenic quartz percentage in the <30 μm fraction of these samples is higher than the estimated authigenic quartz percentage in the 30-52 μm fraction (Table 20) despite very similar (Table 19) $\delta^{18}O$ values measured in these smallest two size fractions. For this reason, $\delta^{18}O$ values for pure authigenic and detrital quartz extrapolated from the three coarsest size fractions of these samples are considered to provide a better estimate (Table 21).

There is a reversal in the plot of sample 4126.1 (Fig.51C). A higher percentage of authigenic quartz was determined by SEM-CL and image analysis in the coarser 80-52 μm size fraction than in the finer 52-30 μm size fraction, despite increasing $\delta^{18}O$ values towards finer size fraction (Fig.51C and Tables 19 and 20). In similarity with samples from the Brae Unit 1 reservoir, it was decided to determine $\delta^{18}O$ of pure authigenic and detrital quartz in this sample based on extrapolation of the data from the 2 largest size fractions only (Table 21).

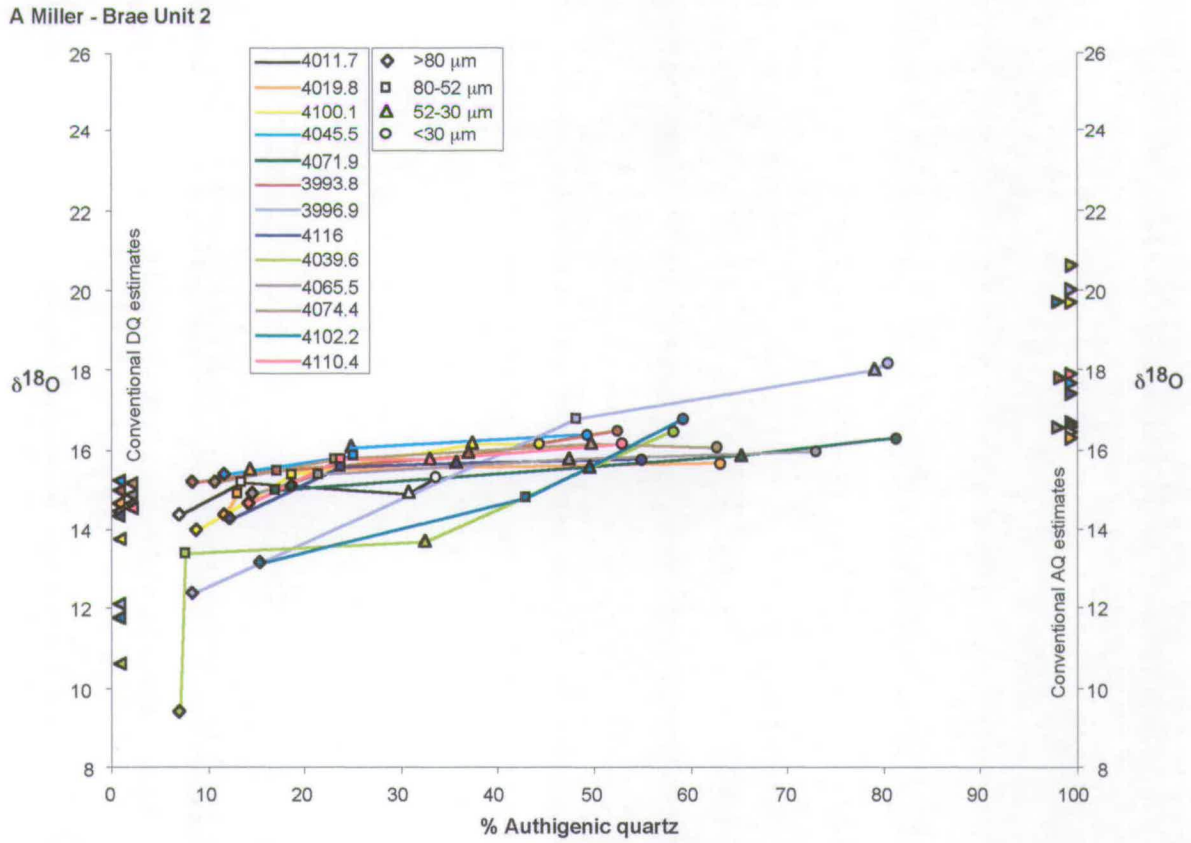

Fig.51 Cross plots of percentage authigenic quartz determined by SEM-CL versus measured quartz $\delta^{18}O$ values in the size fractions of samples analysed by means of the conventional oxygen isotope analysis technique. On each plot, the extrapolated pure authigenic (AQ) and pure detrital quartz (DQ) $\delta^{18}O$ values are indicated for each sample at the 100 % and 0 % authigenic quartz vertical axis respectively. The pure authigenic and detrital quartz $\delta^{18}O$ values were extrapolated from data of all four size fractions in each sample.
A Data from the Brae Unit 2 reservoir in the Miller Field.
B Data from the Brae Unit 1 reservoir in the Kingfisher Field (p.136).
C Data from the Brae Unit 2 reservoir in the Kingfisher Field (p.137).

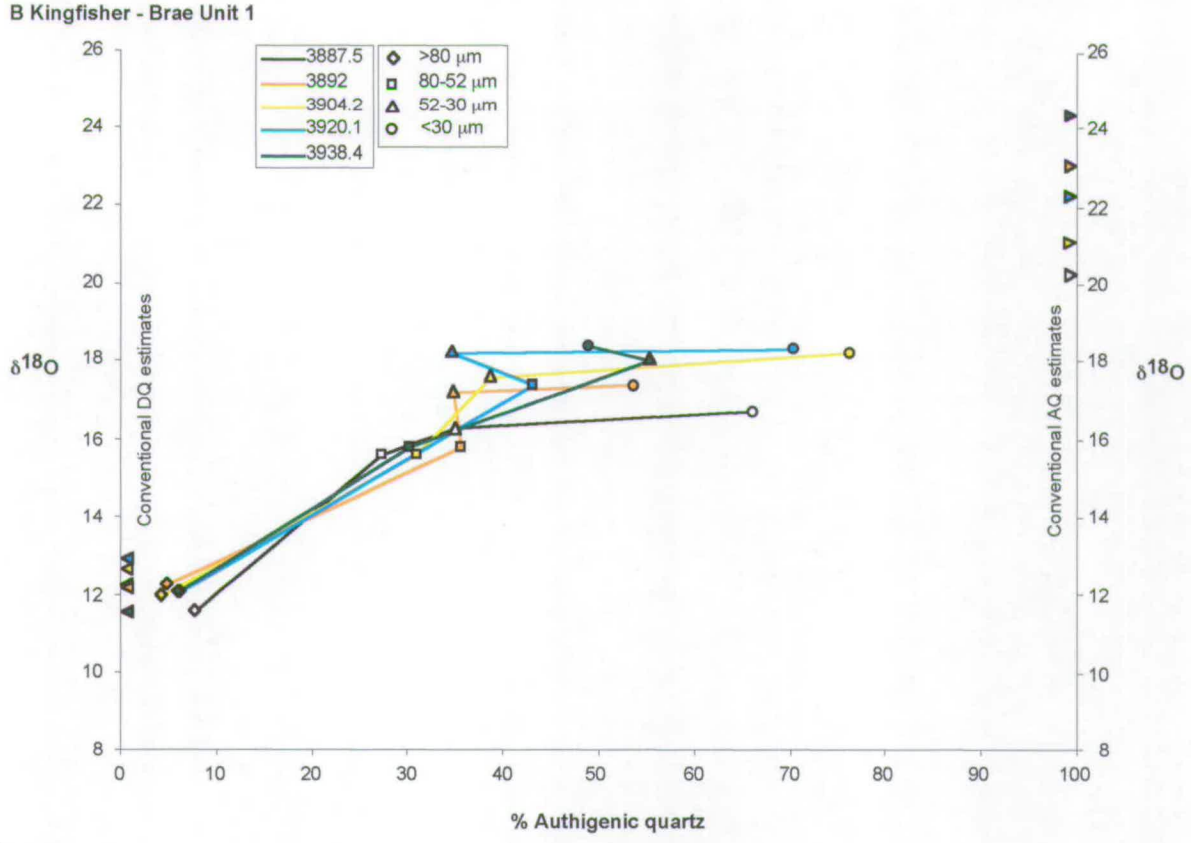

Fig.51 Continued.

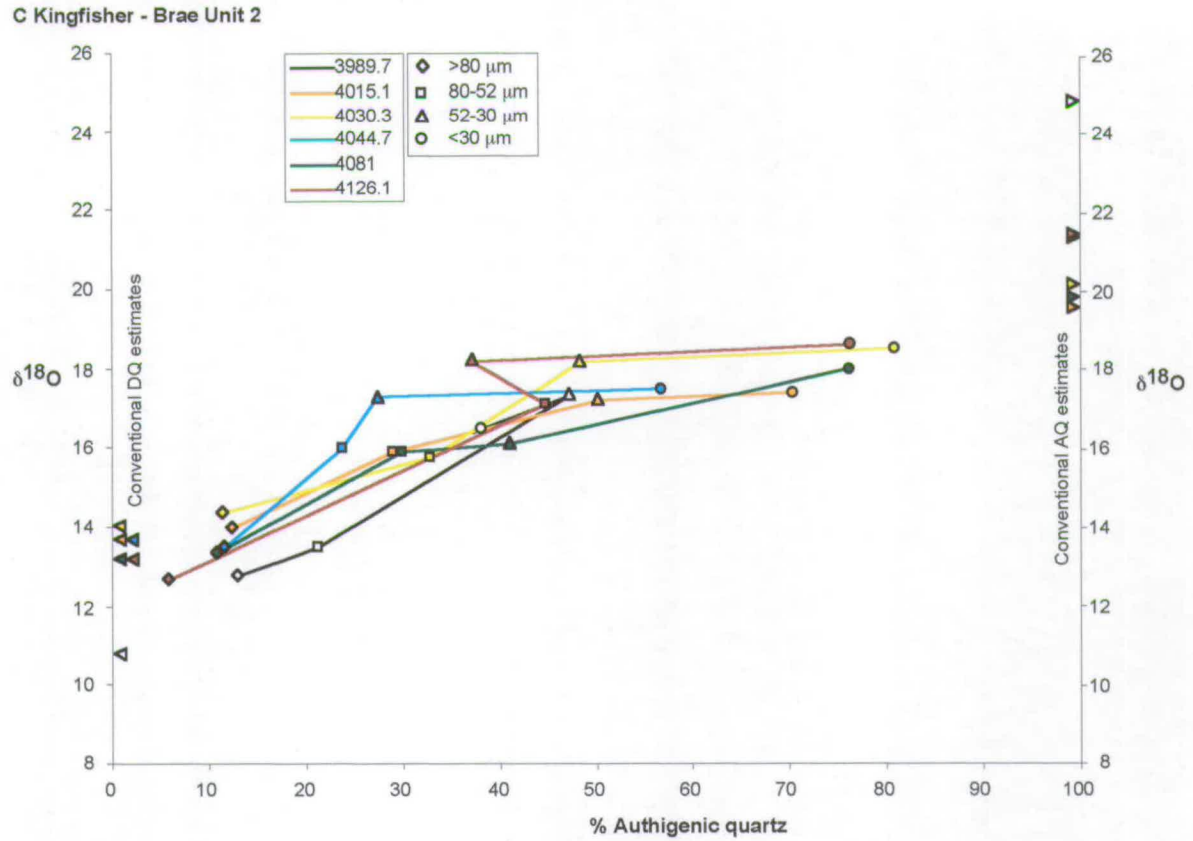

Fig.51 Continued.

Ion microprobe analysis The oxygen isotope data obtained with the ion microprobe are listed in Table 22. Due to the small magnification in the optical microscope (70 x) on the ion microprobe, it is essential to check where the primary ion beam hit the sample before making any data interpretation. Bombardment with the primary ion beam results in a sputter pit on the thin sections. These sputter pits are typically 20-25 μm in diameter (Fig.52). The location of the sputter pits made by analyses in each thin section was checked by SEM (in SE and CL operating mode). In Table 22 an interpretation of the location of the sputter pits (in authigenic quartz, detrital quartz or overlapping both) is inserted in the 'comment' column. The mixed signatures were disregarded for interpretation.

Table 22 Ion microprobe analyses of individual spots in detrital and authigenic quartz in samples from the Brae Formation sandstones. The raw $^{18}O/^{16}O$ data have been dead-time corrected. The reported $\delta^{18}O$ values have been corrected for instrumental mass fractionation by least-squares regression methods based on standard analyses results. An interpretation of which quartz phase (authigenic, detrital or a mix of both) and what quartz cement zone (A or B) was analysed is indicated in the comment column.

Field	Reservoir	Sample depth (m TVD)	Analysis number	Date	Raw $^{18}O/^{16}O$ x1000	Corr. $^{18}O/^{16}O$ x1000	$\delta^{18}O_{SMOW}$ (quartz) (‰)	Error (‰)	Comment/ zone
Miller	Brae II	3993.8	A13163A1	13/06/2000	1.91397	1.888590611	25.8	1.4	authigenic/B
			A13163A2	13/06/2000	1.89158	1.888296716	14.0	1.1	detrital
			A13163A3	13/06/2000	1.9117	1.88800282	24.9	1.3	authigenic/B
			D13163B1	13/06/2000	1.8949	1.892705145	13.4	1.2	detrital
			D13163B2	13/06/2000	1.89482	1.89241125	13.5	1.3	detrital
			A13163B3	13/06/2000	1.90583	1.892117354	19.5	1.4	authigenic/B
			D13163B4	13/06/2000	1.89314	1.891823459	12.9	1.0	detrital
			A13163B5	13/06/2000	1.90076	1.891529564	17.1	1.1	authigenic/A
			A13163B6	13/06/2000	1.90884	1.891235668	21.6	1.3	authigenic/B
			A13163B7	13/06/2000	1.91259	1.890941773	23.8	1.2	authigenic/B
			A13163C1	13/06/2000	1.90868	1.889472297	22.5	1.0	authigenic/B
			A13163C2	13/06/2000	1.89555	1.889178401	15.6	1.0	authigenic/A
			D13163C3	13/06/2000	1.89838	1.888884506	17.3	45.5	mix
		4039.6	A15312A1	14/06/2000	1.88718	1.891309396	10.0	1.1	detrital
			A15312A2	14/06/2000	1.88935	1.890667423	15.5	1.2	authigenic/A
			A15312A3	14/06/2000	1.90226	1.891095405	18.2	1.4	authigenic/A
			A15312A4	14/06/2000	1.89267	1.890881414	16.2	1.1	authigenic/A
			D15312B1	14/06/2000	1.88247	1.888955494	8.7	1.4	detrital
			A15312B2	14/06/2000	1.8926	1.888741503	14.3	1.3	mix
			A15312B3	14/06/2000	1.89727	1.888527511	16.9	1.1	authigenic/B
			A15312B4	14/06/2000	1.90216	1.88831352	19.6	1.2	authigenic/B
			A15312B5	14/06/2000	1.89112	1.888099529	13.8	1.9	mix
			A15312B6	14/06/2000	1.90687	1.887885538	22.4	0.9	authigenic/B
			D15312C1	14/06/2000	1.88418	1.89195137	8.1	1.2	detrital
			A15312C2	14/06/2000	1.87787	1.891737378	4.8	1.3	mix
			A15312C3	14/06/2000	1.88953	1.891523387	11.1	1.3	detrital
			D15312D1	14/06/2000	1.88825	1.89387729	9.2	1.4	detrital
			A15312D2	14/06/2000	1.89915	1.893663299	15.1	1.3	mix
			A15312D3	14/06/2000	1.88504	1.893449307	7.7	1.1	detrital
			A15312D4	14/06/2000	1.8978	1.893235316	14.7	1.3	mix
			A15312D5	14/06/2000	1.90726	1.893021325	19.8	1.2	authigenic/B
			A15312D6	14/06/2000	1.8999	1.892807334	16.0	1.4	authigenic/B
		4110.4	A5939A1	15/06/2000	1.89637	1.891135631	15.0	1.1	detrital
			A5939A2	15/06/2000	1.90683	1.891056191	20.7	1.1	authigenic/B
			A5939A3	15/06/2000	1.91152	1.890976752	23.2	1.2	authigenic/B
			A5939A4	15/06/2000	1.90226	1.890897313	18.3	1.2	mix
			A5939A5	15/06/2000	1.89697	1.890817874	15.5	1.4	authigenic/A
			A5939A6	15/06/2000	1.9137	1.890738434	24.5	1.1	authigenic/B
			A5939B1	15/06/2000	1.89745	1.890102921	16.1	1.1	authigenic/A
			A5939B2	15/06/2000	1.90978	1.890023481	22.8	1.3	authigenic/B
			A5939B3	15/06/2000	1.89858	1.889944042	16.8	1.2	authigenic/B
			A5939B4	15/06/2000	1.90658	1.889387967	21.4	1.1	authigenic/B
			A5939B5	15/06/2000	1.89951	1.889308528	17.7	1.2	mix
			A5939B6	15/06/2000	1.89681	1.889229089	16.3	1.2	mix
			A5939C1	15/06/2000	1.90406	1.890658995	19.4	1.3	authigenic/B
			A5939C2	15/06/2000	1.89614	1.890341238	15.3	1.0	mix
			A5939C3	15/06/2000	1.91249	1.890261799	24.1	1.1	authigenic/B
			A5939C4	15/06/2000	1.90904	1.89018236	22.3	1.2	authigenic/B
			A5939D1	15/06/2000	1.90246	1.889626285	19.1	1.3	authigenic/B
			A5939D2	15/06/2000	1.89574	1.889546846	15.5	1.4	mix
			A5939D3	15/06/2000	1.90777	1.889467407	22.0	1.1	authigenic/B

Table 22 Continued.

Field	Reservoir	Sample depth (m TVD)	Analysis number	Date	Raw $^{18}O/^{16}O$ x1000	Corr. $^{18}O/^{16}O$ x1000	$\delta^{18}O_{SMOW}$ (quartz) (‰)	Error (‰)	Comment/ zone
Kingfisher	Brae I	3887.5	D13337A1	22/06/2000	1.89868	1.888826917	17.5	1.0	detrital
			A13337A2	22/06/2000	1.89295	1.888859235	14.4	1.1	detrital
			A13337A3	22/06/2000	1.88232	1.888891553	8.7	1.0	detrital
			A13337A5	22/06/2000	1.8961	1.88892387	16.1	1.1	authigenic/A
			A13337A6	22/06/2000	1.91048	1.888956188	23.7	1.0	authigenic/B
			D13337C0	21/06/2000	1.89659	1.887011904	17.3	1.2	detrital
			D13337C1	21/06/2000	1.89445	1.887227816	16.1	1.3	detrital
			A13337C2	21/06/2000	1.90976	1.887155846	24.3	1.0	authigenic/B
			A13337C3	21/06/2000	1.90676	1.887083875	22.8	1.2	authigenic/B
			A13337C4	21/06/2000	1.90134	1.886939933	19.9	1.1	mix
			A13337C5	21/06/2000	1.90811	1.886867963	23.6	1.2	authigenic/B
			A13337C6	21/06/2000	1.90085	1.886795992	19.7	1.0	authigenic/B
			D13337C7	22/06/2000	1.88602	1.888988506	10.6	1.1	detrital
			D13337E1	22/06/2000	1.89327	1.889117777	14.4	1.0	detrital
			A13337E2	22/06/2000	1.89799	1.889150095	16.9	1.0	authigenic/A
			A13337E3	22/06/2000	1.89488	1.889182413	15.3	0.9	authigenic/A
			A13337E4	22/06/2000	1.88833	1.88921473	11.7	1.2	detrital
			A13337E5	22/06/2000	1.89177	1.889247048	13.6	1.2	mix
			A13337E6	22/06/2000	1.89928	1.889311684	17.6	1.0	mix
			A13337E7	22/06/2000	1.90209	1.889279366	19.1	1.0	authigenic/B
			A13337E8	22/06/2000	1.90741	1.889020824	22.1	1.0	authigenic/B
		3904.2	D13395A1	21/06/2000	1.88239	1.88852329	8.9	1.2	detrital
			A13395A2	21/06/2000	1.90347	1.888451319	20.3	1.2	authigenic/B
			A13395A3	21/06/2000	1.88708	1.888379349	11.5	1.3	mix
			A13395A4	21/06/2000	1.88374	1.888307378	9.8	1.1	detrital
			A13395A5	21/06/2000	1.90143	1.888235407	19.3	1.3	authigenic/B
			A13395A6	21/06/2000	1.90016	1.888163436	18.6	1.2	authigenic/B
			D13395B1	21/06/2000	1.8834	1.887803583	9.8	1.0	detrital
			A13395B2	21/06/2000	1.90452	1.887731612	21.2	1.1	authigenic/B
			A13395B3	21/06/2000	1.90994	1.887659641	24.2	1.3	authigenic/B
			A13395B4	21/06/2000	1.89526	1.88758767	16.3	1.2	mix
			A13395B5	21/06/2000	1.89234	1.8875157	14.8	1.0	mix
			A13395B6	21/06/2000	1.89838	1.887443729	18.1	1.2	mix
			A13395E1	20/06/2000	1.88962	1.882854535	15.8	1.2	authigenic/A
			A13395E2	20/06/2000	1.87628	1.882748926	8.7	1.2	detrital
			D13395F1	20/06/2000	1.87384	1.883276972	7.1	1.1	detrital
			A13395F2	20/06/2000	1.87329	1.883171363	6.9	1.0	detrital
			A13395F3	20/06/2000	1.90041	1.883065753	21.5	1.1	authigenic/B
			A13395F4	20/06/2000	1.89478	1.882960144	18.6	1.2	authigenic/B
Kingfisher	Brae I	3938.4	D13512A1	23/06/2000	1.88141	1.885070638	10.2	1.1	detrital
			A13512A3	23/06/2000	1.8996	1.885137604	20.0	1.0	authigenic/B
			13512A3	23/06/2000	1.90283	1.88520457	21.7	1.0	authigenic/B
			13512B0	23/06/2000	1.87913	1.885673333	8.7	1.0	detrital
			13512B1	23/06/2000	1.88969	1.885874232	14.3	1.1	mix
			13512B2	23/06/2000	1.90047	1.885941198	20.0	1.0	authigenic/B
			13512B3	23/06/2000	1.90499	1.8857403	22.5	1.1	authigenic/B
			A13512B4	23/06/2000	1.89023	1.886008164	14.5	1.0	mix
			13512B5	23/06/2000	1.89792	1.885807266	18.7	1.0	authigenic/B
			A13512B6	23/06/2000	1.88735	1.88607513	12.9	1.1	detrital
			D13512E1	22/06/2000	1.8803	1.889440955	7.3	0.8	detrital
			A13512E2	22/06/2000	1.90823	1.889473272	22.3	1.0	authigenic/B
			A13512E3	22/06/2000	1.90375	1.88950559	19.8	1.1	authigenic/B
			A13512E4	22/06/2000	1.91081	1.889537908	23.6	1.0	authigenic/B
			A13512E6	22/06/2000	1.90286	1.889570226	19.3	1.0	authigenic/B
			A13512E7	22/06/2000	1.9122	1.889602543	24.3	1.0	authigenic/B
			A13512E8	22/06/2000	1.90701	1.889634861	21.5	0.9	authigenic/B
			A13512F1	23/06/2000	1.90117	1.885405469	20.7	0.9	authigenic/B
			A13512F2	23/06/2000	1.90586	1.885338502	23.2	0.9	authigenic/B
			A13512F3	23/06/2000	1.88765	1.885271536	13.5	1.0	mix
Kingfisher	Brae II	3989.7	A13143A0	16/06/2000	1.90048	1.877550829	24.6	1.1	authigenic/B
			D13143A1	16/06/2000	1.87449	1.877594915	10.5	1.3	detrital
			A13143A2	16/06/2000	1.88972	1.877462655	18.8	1.2	mix
			A13143A3	16/06/2000	1.89478	1.877418569	21.6	1.3	authigenic/B
			A13143A4	16/06/2000	1.89208	1.877374482	20.1	1.2	authigenic/B
			A13143A6	16/06/2000	1.8793	1.877506742	13.2	1.1	mix
			D13143C1	16/06/2000	1.87932	1.878388475	12.7	1.1	detrital
			A13143C2	16/06/2000	1.8772	1.878344388	11.6	1.1	detrital
			A13143C3	16/06/2000	1.88842	1.878300301	17.7	0.9	authigenic/B
			A13143C4	16/06/2000	1.89606	1.878256215	21.8	1.0	authigenic/B
			A13143C5	16/06/2000	1.89142	1.878212128	19.3	0.9	mix
			A13143D1	16/06/2000	1.8872	1.878035782	17.1	1.1	authigenic/B
			A13143D2	16/06/2000	1.90031	1.877991695	24.2	1.1	authigenic/B
			A13143D3	16/06/2000	1.89453	1.877947608	21.2	1.1	authigenic/B
			A13143D4	16/06/2000	1.90128	1.877903522	24.8	1.1	authigenic/B
			A13143D5	16/06/2000	1.89473	1.877859435	21.3	1.0	authigenic/B
			A13143D6	16/06/2000	1.8951	1.877815348	21.5	1.1	authigenic/B
			A13143D7	16/06/2000	1.88595	1.877771262	16.6	1.1	mix
		4030.3	A13274A1	17/06/2000	1.89539	1.879730485	20.6	1.0	authigenic/B
			A13274B1	17/06/2000	1.87733	1.879548792	11.0	1.0	detrital
			A13274B2	17/06/2000	1.9016	1.879609356	24.1	1.0	authigenic/B
			A13274B3	17/06/2000	1.88947	1.87966992	17.5	1.0	authigenic/B
			A13274C1	17/06/2000	1.8978	1.879427663	22.1	1.1	authigenic/B
			A13274C2	17/06/2000	1.89658	1.879488227	21.4	1.1	mix
			A13274D2	17/06/2000	1.90198	1.880154436	24.0	1.1	authigenic/B
			D13274D3	17/06/2000	1.87964	1.880215	11.9	1.1	detrital
			A13274D4	17/06/2000	1.8964	1.880093871	21.0	1.1	authigenic/B
			A13274D5	17/06/2000	1.88199	1.880033307	13.3	1.0	mix
			A13274D7	17/06/2000	1.90117	1.879972742	23.6	1.1	authigenic/B
			A13274D9	17/06/2000	1.88241	1.879912178	13.6	1.1	mix
			D13274E1	17/06/2000	1.88337	1.880699515	13.6	1.2	detrital
			A13274E2	17/06/2000	1.90121	1.880638951	23.3	1.0	authigenic/B
			A13274E3	17/06/2000	1.89141	1.880578386	18.0	1.1	mix
			A13274E4	17/06/2000	1.89621	1.880517822	20.7	1.0	mix
			A13274E5	17/06/2000	1.89272	1.880457258	18.8	1.0	mix
			A13274E6	17/06/2000	1.89714	1.880396693	21.2	1.1	authigenic/B
		4081.0	D13437A1	20/06/2000	1.87754	1.884966716	8.2	1.0	detrital
			A13437A2	20/06/2000	1.89695	1.884861107	18.7	1.1	authigenic/B
			A13437A3	20/06/2000	1.90235	1.884755498	21.7	0.9	authigenic/B
			A13437A4	20/06/2000	1.90080	1.884649889	20.9	0.9	authigenic/B
			A13437A5	20/06/2000	1.89655	1.88454428	18.7	1.1	mix
			A13437A5	20/06/2000	1.90279	1.884438671	22.1	1.0	authigenic/B
			A13437A7	20/06/2000	1.90094	1.884016235	21.3	0.9	mix
			A13437A8	20/06/2000	1.90178	1.883910626	21.8	1.0	authigenic/B
			A13437A9	20/06/2000	1.88878	1.883805017	14.9	1.1	detrital
			A437A10	20/06/2000	1.90091	1.883699408	21.5	1.2	authigenic/B
			A437A11	20/06/2000	1.89785	1.883593799	19.9	1.1	authigenic/B
			D437A14	20/06/2000	1.8823	1.884121844	11.2	1.1	detrital

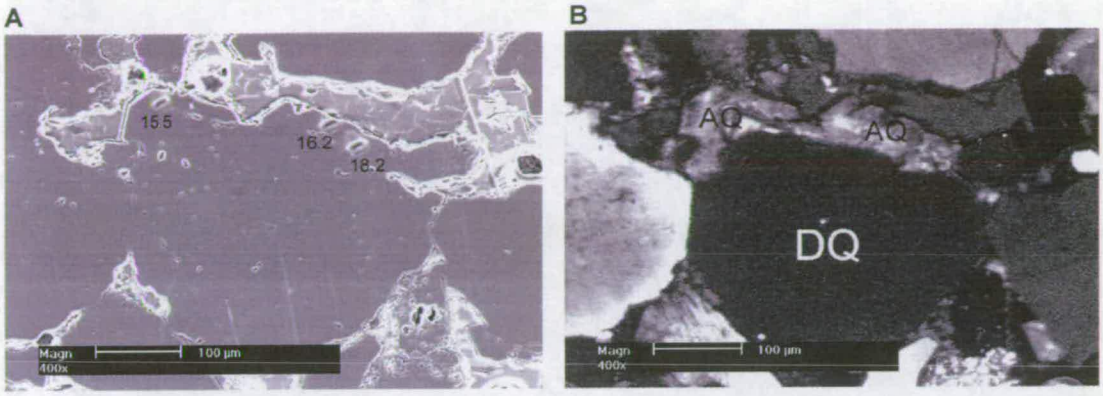

Fig.52 Paired secondary (**A**) and cathodoluminescence (**B**) SEM images of sample 15312 (4039.6 m, Brae Unit 2 reservoir, Miller Field).
(**A**) The ion microprobe analysis pits can easily be seen on this secondary image. Numbers on the image are ion microprobe analysis results ($\delta^{18}O_{SMOW}$).
(**B**) The cathodoluminescence image illustrates that the particular analyses were not contaminated with detrital quartz (DQ) and were carried out in pure authigenic quartz (AQ).

7.5 Ion microprobe results

Detrital quartz The histograms shown in Fig.53 summarize the $\delta^{18}O$ range of the 39 micro-analyses of detrital quartz carried out with the ion microprobe. The $\delta^{18}O$ of detrital quartz grains in the Brae Formation sandstone reservoirs examined ranges from +6.9 to +17.5 ‰ (average 11.4±2.8 ‰). The significant intragrain variations in detrital quartz $\delta^{18}O$ are of comparable magnitude to heterogeneities measured in quartz from granitic rocks (Valley and Graham, 1996). According to Blatt (1987), average $\delta^{18}O$ of quartz in igneous rocks is around +9 ‰, in metamorphic rocks around +13 to +14 ‰ and in sandstones around +11 ‰. The average of all analyses in detrital quartz grains of the Brae Formation sandstones is similar in all three reservoirs examined : 11.4±2.6 ‰ in Brae Unit 2 of the Miller Field, 11.2±3.5 ‰ in Brae Unit 1 of the Kingfisher Field and 11.7±1.9 ‰ in Brae Unit 2 of the Kingfisher Field. These numbers are similar to Blatt's data for sandstones (~11 ‰). The wide range in oxygen isotopic compositions of the detrital quartz grains analysed (+6.9 to +17.5 ‰) is consistent with granitic and/or metamorphic terranes being the predominant source of the detrital quartz in the Brae Formation sandstones. A similar range and average of $\delta^{18}O$ values in each reservoir examined suggests a similar source region for quartz across the whole Brae Formation. The most likely source region, as suggested by McClure and Brown (1990), is the Devonian Fladen Ground Spur (Chapter 2 Fig.1A).

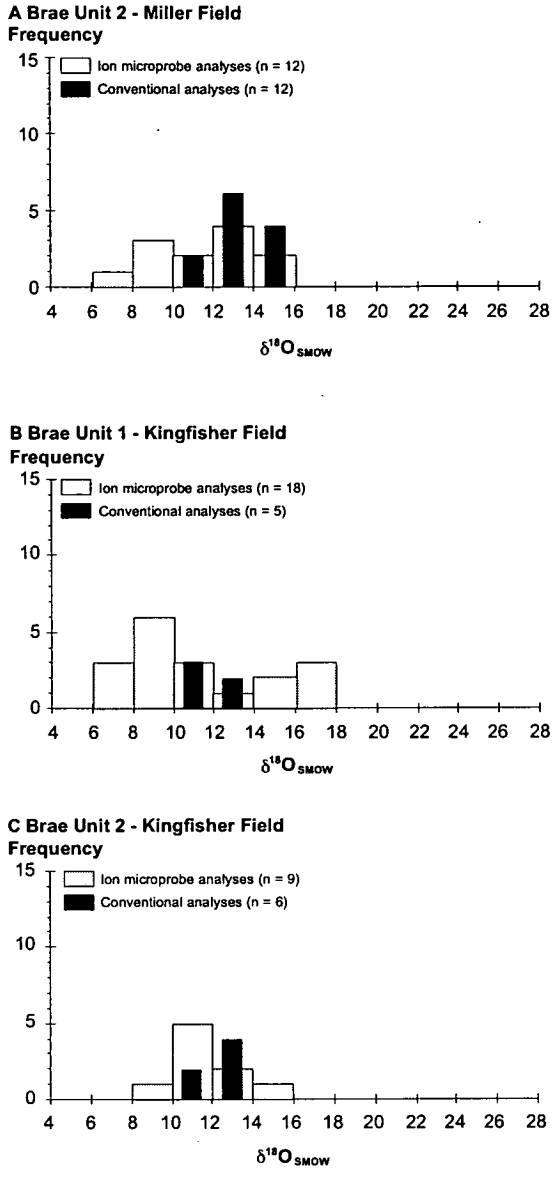

Fig.53 Histograms showing the distribution of detrital quartz oxygen isotope values determined with both the ion microprobe and the conventional analysis technique in the three reservoirs examined.

Authigenic quartz The histograms shown in Fig.54 summarize the $\delta^{18}O$ values of the 86 micro-analyses in authigenic quartz. The $\delta^{18}O$ of authigenic quartz in the Brae Formation sandstone reservoirs examined ranges from +15.3 to +25.8 ‰ (average 20.8±2.7 ‰). There is a wide spread in $\delta^{18}O$ values in all three reservoirs studied (Fig.54). The average oxygen isotopic composition of quartz cements is similar in each reservoir; 20.3±3.2 ‰ in the Brae Unit 2 reservoir in the Miller Field, 20.7±2.6 ‰ in the Brae Unit 1 reservoir in the Kingfisher Field and 21.5±2.1 ‰ in the Brae Unit 2 reservoir in the Kingfisher Field.

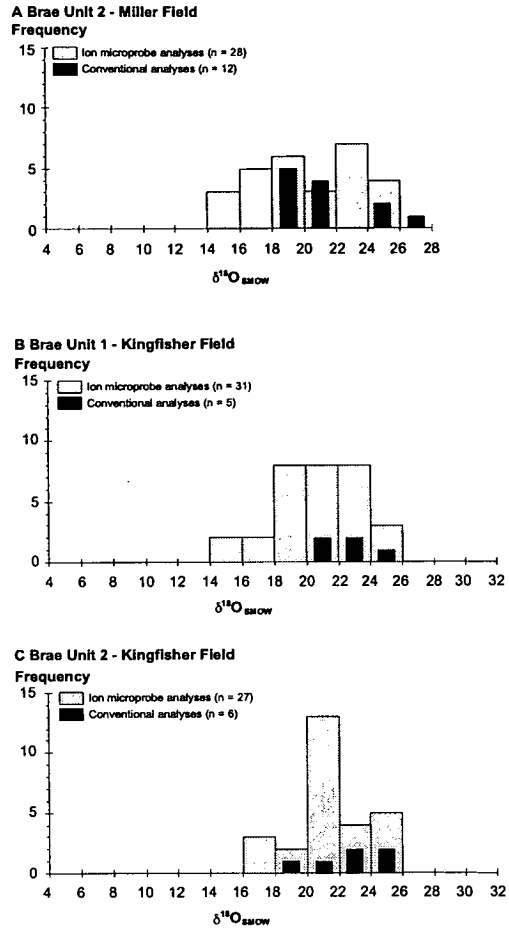

Fig.54 Histograms showing the distribution of authigenic quartz oxygen isotope values determined with both the ion microprobe and the conventional analysis technique in the three reservoirs examined.

CL photomicrographs of quartz overgrowths in the Brae Formation sandstone reservoirs show the presence of two luminescence zones : Zone A quartz cements display a complex CL pattern whereas Zone B quartz cements display a homogeneous CL pattern (Fig.55). Zone A is found always directly bordering detrital grains and is often observed to cement porespace between detrital grains, indicating a possible pre-compactional origin (Fig.55A and B). Zone A is scarce and rarely observed in the quartz cements, and the thickness of this growth zone varies throughout the reservoirs and ranges between <5 to 20 μm. Based on textural observations, two Zone B quartz cement generations can be differentiated. The first generation, Zone B1, occurs in calcite-cemented sandstones (Fig.55C). Therefore, these Zone B1 cements must have precipitated during shallow burial, most likely prior to Zone A cements. Because only small amounts of quartz cement developed

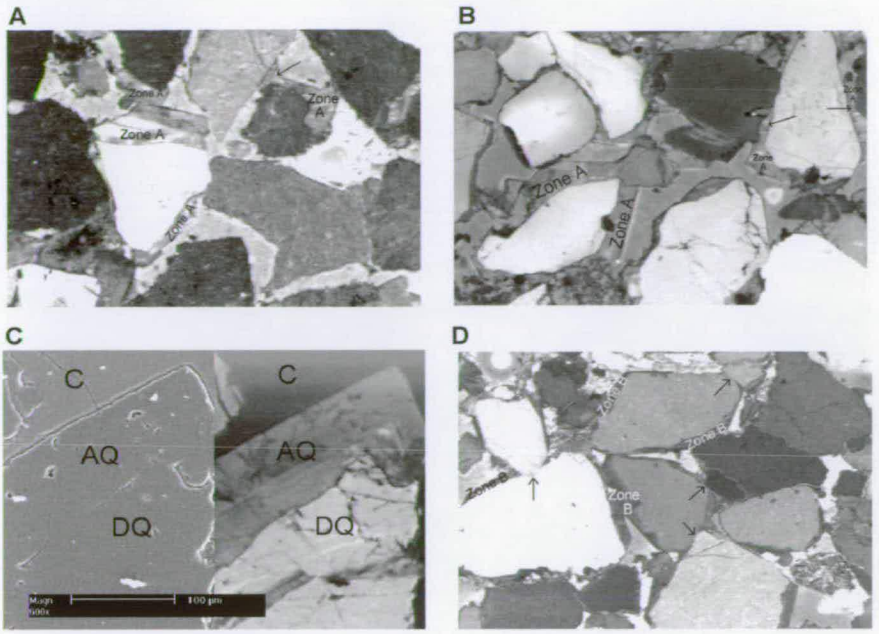

Fig.55 SEM-CL images illustrating the different appearance of Zone A and Zone B quartz cements.
(**A**) and (**B**) Zone A cements display a complex CL pattern. Image A (field of view 625x500 μm) is from the Miller Field (well 7b-A03, 4022.7 m) and image B (field of view 625x500 μm) is from the Kingfisher Field (well 8a-8, 3887.5 m). Arrows indicate cementation in porespace between detrital grains.
(**C**) and (**D**) Zone B cements display a homogeneous CL pattern inside and outside calcite-cemented sandstones. Image C (split SEM secondary and CL picture) is from calcite-cemented sandstone in the Miller Field (well 8b-3, 3992.3 m). C=calcite, DQ=detrital quartz and AQ=authigenic quartz. Image D (field of view 1300x1000 μm) is from the Kingfisher Field (well 8a-4, 4023.6 m). Arrows indicate detrital grains in point-contact with each other.

in the Brae Formation at low temperatures and shallow burial (Chapters 3, 4 and 6), Zone B1 cements can make up only a small volume of the total amount of Zone B cements present in the samples analysed. The second generation of Zone B cements, Zone B2, occurs either on top of Zone A or, where Zone A is absent, directly on detrital grains (Fig.55D). This Zone B2 quartz cement is the most common and makes up the bulk volume of the quartz cements in the Brae Formation. The Zone B2 overgrowths can be up to 50 μm thick and precipitated mainly on grains which are partly in point-contact with each other indicating a post-compactional, and post Zone A cementation, origin (Fig.55D).

Because it is not possible to differentiate petrographically the two generations of Zone B quartz cements in non-calcite cemented samples, I was not able to isotopically distinguish Zone B1 and B2 cements in the ion microprobe analysis results (Table 22). Consequently, the oxygen isotope results below are discussed in terms of Zones A and B only.

Zone A and Zone B quartz cements are distinct in their oxygen isotopic compositions (Table 22). The $\delta^{18}O$ of Zone A ranges from +15.3 to +18.2 ‰. In zone B, $\delta^{18}O$ ranges between +16.0 and +25.8 ‰ (Table 22). The average oxygen isotopic signature of the Zone A cements analysed is similar in the reservoir of the Miller Field (16.3±1.1 ‰) and the Brae Unit 1 reservoir in the Kingfisher Field (16.0±0.7 ‰) (Table 23). No zone A cements were encountered for analysis in the Brae Unit 2 reservoir of the Kingfisher Field. Also, the average oxygen isotopic signature of all Zone B cements analysed is similar in all three reservoirs (Table 23); 21.3±2.7 ‰ in the Brae Unit 2 reservoir of the Miller Field, 21.4±1.9 ‰ and 21.5±2.1 ‰ in the Brae Unit 1 and 2 reservoirs respectively of the Kingfisher Field.

Table 23 Average (± standard deviation) $\delta^{18}O$ values of Zone A and Zone B quartz cements determined by ion microprobe analysis in all three reservoirs examined. No Zone A cements were encountered in the Brae Unit 2 reservoir of the Kingfisher Field.

Field	Reservoir	av. $\delta^{18}O_{SMOW}$ ± st.dev. Zone A (‰)	av. $\delta^{18}O_{SMOW}$ ± st.dev. Zone B (‰)
Miller	Brae II	16.3 ± 1.1	21.3 ± 2.7
Kingfisher	Brae I	16.0 ± 0.7	21.4 ± 1.9
Kingfisher	Brae II		21.5 ± 2.1

Table 24 Comparison of average (± standard deviation) $\delta^{18}O$ value of detrital and authigenic quartz determined in samples by the ion microprobe analysis technique with the $\delta^{18}O$ value obtained in the same sample with the conventional analysis technique.

Field	Reservoir	Sample	Conventional analysis $\delta^{18}O_{SMOW}$ detrital (‰)	Conventional analysis $\delta^{18}O_{SMOW}$ authigenic (‰)	Ion microprobe analysis av. $\delta^{18}O_{SMOW}$ ± st.dev. detrital (‰)	Ion microprobe analysis av. $\delta^{18}O_{SMOW}$ ± st.dev. authigenic (‰)
Miller	Brae II	3993.8	14.9	18.3	13.5 ± 0.5	21.4 ± 3.7
		4039.6	10.6	20.6	9.7±1.9	18.3±2.4
		4110.4	13.1	24.5	15.0	20.6 ± 3.0
Kingfisher	Brae I	3887.5	12.3	20.3	13.8 ± 3.2	20.4 ± 3.4
		3904.2	12.7	21.1	8.5 ± 1.3	19.9 ± 2.5
		3938.4	11.7	23.6	9.8 ± 2.4	21.4 ± 1.8
Kingfisher	Brae II	3989.7	10.8	24.9	11.6 ± 1.1	21.4 ± 2.5
		4030.3	13.0	23.1	12.2 ± 1.3	21.9 ± 2.1
		4081.0	13.3	19.9	11.4 ± 3.4	20.9 ± 1.2

7.6 Comparison of ion microprobe results with conventional analysis data

Detrital quartz The bulk oxygen isotopic compositions of detrital quartz determined with the conventional analysis method are indicated for each reservoir on Fig.53. The $\delta^{18}O$ of detrital quartz grains measured by conventional means in each sample is compared to the average $\delta^{18}O$ of detrital quartz grains measured in the same sample with the ion microprobe in Table 24. In some samples there is good agreement between oxygen isotopic composition determined with the conventional and ion microprobe analysis technique (e.g. samples 4039.6, 3989.7 and 4030.3; Table 24). In other samples, the agreement between $\delta^{18}O$ of detrital quartz determined by conventional analysis and ion microprobe is not so close (Table 24). This is most likely due to the wide range in $\delta^{18}O$ compositions of detrital grains in the

Brae Formation sandstones (Fig.53) and the fact that conventional analysis gives an average result whereas very small parts of grains are analysed by the ion microprobe, which emphasises heterogeneities.

Authigenic quartz The oxygen isotopic compositions of authigenic quartz estimated by the conventional analysis method are indicated for each reservoir on Fig.54. The $\delta^{18}O$ of authigenic quartz obtained by conventional means in each sample is compared to the average $\delta^{18}O$ of authigenic quartz measured in the same sample with the ion microprobe in Table 24.

Again, in some samples there is good agreement between oxygen isotopic compositions determined with the conventional and ion microprobe analysis techniques (e.g. samples 3887.5 and 4081; Table 24). In the other samples, apart from one (3993.8 from the Miller Field), the extrapolated $\delta^{18}O$ values are more positive than the ion microprobe average $\delta^{18}O$ values (Table 24). The reasons for dissimilarity between conventional and ion microprobe results are discussed by Lyon et al. (2000) and apply also to the Brae Formation sandstone samples. Reasons for dissimilarities between results from the two different isotope techniques can be : (1) inaccuracies in the quantification of authigenic quartz abundance in the size fractions; (2) variation in the internal $\delta^{18}O$ composition of the overgrowths or variation in the $\delta^{18}O$ composition of authigenic quartz throughout the reservoirs and (3) the assumption of two endmembers of constant $\delta^{18}O$ values in modelling conventional data.

To bring the conventional and ion microprobe results into parity, around 10 to 30 % more (or less, in the case of sample 3993.8 from the Miller Field) authigenic quartz would need to be present in the size fractions >80 μm and 80-52 μm respectively than was determined by SEM-CL. Due to the high image resolution of the SEM-CL images of those size fractions (Fig.50), it is unlikely that the quantification of authigenic quartz abundance yielded such high inaccuracies.

No ion microprobe traverses were made across quartz overgrowths in the samples analysed. This was because the overgrowths are generally not wide enough to accommodate more than one analysis. The wide range in $\delta^{18}O$ compositions measured with the ion microprobe within each sample, and also between different samples (Table 22), suggests that $\delta^{18}O$ compositions of authigenic quartz are highly variable between grains and possibly also internally within single overgrowths.

Large $\delta^{18}O$ variations within single overgrowths have been measured by other ion microprobe analysts (e.g. Graham et al., 1996, Williams et al., 1997, Lyon et al., 2000). The variability in $\delta^{18}O$ compositions of authigenic quartz in the Brae Formation samples may cause the observed variation between conventional and ion microprobe $\delta^{18}O$ compositions.

The validity of the mass balance technique in modelling conventional isotope data partly depends upon the assumption of two endmembers of constant $\delta^{18}O$. In order for the bulk sample $\delta^{18}O$ value obtained from conventional analysis results to be comparable to ion microprobe data from the same sample, the average $\delta^{18}O$ value of all ion microprobe data needs to reflect a true sample average. Considering the highly variable $\delta^{18}O$ compositions measured in each sample with the ion microprobe, it is unlikely that enough analyses were performed in order to obtain a statistically valid sample average $\delta^{18}O$ value. As a result, discrepancies can occur between conventional bulk isotope data and data from the ion microprobe.

Dissimilarities between the quartz overgrowth conventional and ion microprobe analyses may be partly caused by the fact that conventional analysis gives an average result whereas single overgrowths are analysed by the ion microprobe. The main reason, therefore, for dissimilarities between the quartz overgrowth conventional and ion microprobe analyses is most likely the wide range in $\delta^{18}O$ compositions of quartz overgrowths (either within single overgrowths or between different overgrowths) present in Brae Formation samples. This implies that quartz cementation occurred over a wide range of temperatures from pore-fluids with possibly different $\delta^{18}O$ compositions. This is discussed further in the next paragraph.

7.7 Oxygen isotope compositions of pore-fluids

The oxygen isotope compositions of pore-fluids present in the Brae Formation during diagenetic mineral precipitation can be calculated from the measured $\delta^{18}O$ values of authigenic cements in the sandstones and the estimated precipitation temperatures of those cements. Pore-fluid compositions in a basin change with time and increasing burial, and therefore pore-fluid oxygen isotopic compositions were calculated first for the earliest cements (calcite) precipitated in the sandstones and subsequently for later cements (quartz). In this way, a complete overview of pore-fluid evolution in the Miller and Kingfisher Fields was obtained. The equation

of Friedman & O'Neil (1977) was used to calculate the $\delta^{18}O$ compositions of pore-fluids from which calcite cements precipitated. The equation of Matsuhisa et al. (1979) was used to calculate the $\delta^{18}O$ compositions of pore-fluids from which quartz cements precipitated. For calcite, the equation is presented in Appendix B (eq 2) and for quartz the equation is as follows:

$$\delta^{18}O_{quartz} - \delta^{18}O_{water} = (3.34.10^6 \times T^{-2}) - 3.31 \quad (eq\ 8)$$

where $\delta^{18}O_{quartz}$ is the oxygen isotopic composition of quartz cement (‰), $\delta^{18}O_{water}$ is the oxygen isotopic composition of the pore-fluid (‰) and T is the temperature of quartz precipitation (degrees Kelvin). Table 25 provides an overview of quartz precipitation temperatures and $\delta^{18}O$ values of quartz cements and pore-fluids calculated with eq 8.

Oxygen isotope fractionation curves were constructed to facilitate the interpretation of formation water isotopic composition during diagenesis (Fig.56). The curves were calculated for $\delta^{18}O$ compositions of calcite ranging from +15 to +25 ‰ and for quartz ranging from +10 to +25 ‰ using the equations of Friedman & O'Neil (1977) and Matsuhisa et al. (1979) (eq 2 in Appendix B and eq 8).

Calcite precipitation After deposition of the Brae Formation sands, calcite was the first cement to precipitate (Chapter 3). The oxygen isotopic composition of these calcite cements ranges from +23.8 ‰ in the concretion cores to +15.4 ‰ at the concretion edges (Appendix B). From minus-cement-volumes and burial curves it

Table 25 Quartz precipitation temperatures calculated with the oxygen isotope fractionation equation from Matsuhisa et al. (1979). Temperatures are calculated for the range of quartz cement oxygen isotopic compositions ($\delta^{18}O$) obtained in Brae Formation sandstone samples (+15 to +26 ‰) and a range of possible pore-fluid oxygen isotopic compositions ($\delta^{18}O$) that may have occurred in the Brae Formation sandstones (-7 to +5 ‰). Arrows indicate the range in measured $\delta^{18}O$ values of Zone A and Zone B quartz cements.

$\delta^{18}O_{SMOW}$ PORE FLUID (‰)	$\delta^{18}O_{SMOW}$ Zone A quartz (‰) ← → $\delta^{18}O_{SMOW}$ Zone B quartz (‰)											
	15	16	17	18	19	20	21	22	23	24	25	26
-7	90	83	77	70	65	59	54	49	44	39	35	30
-6	98	90	83	77	70	65	59	54	49	44	39	35
-5	106	98	90	83	77	70	65	59	54	49	44	39
-4	114	106	98	90	83	77	70	65	59	54	49	44
-3	123	114	106	98	90	83	77	70	65	59	54	49
-2	133	123	114	106	98	90	83	77	70	65	59	54
-1	143	133	123	114	106	98	90	83	77	70	65	59
0	154	143	133	123	114	106	98	90	83	77	70	65
1	166	154	143	133	123	114	106	98	90	83	77	70
2	180	166	154	143	133	123	114	106	98	90	83	77
3	194	180	166	154	143	133	123	114	106	98	90	83
4	210	194	180	166	154	143	133	123	114	106	98	90
5	228	210	194	180	166	154	143	133	123	114	106	98

was calculated that calcite cementation started around 15 °C and continued up until ~95 °C (Appendix B). By combining these temperatures with the oxygen isotopic compositions of the cements, it can be calculated (eq 2, Appendix B) that precipitation of the calcite occurred initially from Upper Jurassic meteoric water (~ –7 ‰; Hamilton et al., 1987), with a shift towards more ^{18}O-enriched fluids (~ –3 ‰) with increasing temperature and burial, up to ~95 °C at ~3000 m (Fig.56).

Quartz precipitation In order to derive the oxygen isotopic compositions of the pore-fluids from which quartz cements precipitated in the Brae Formation sandstones, the following information has to be taken into account :

- ✓ Oxygen isotopic compositions of early calcite cements indicate that meteoric fluids were present in the sandstones during shallow burial. Upper Jurassic meteoric water had an oxygen isotopic composition of ~ –7 ‰ (Hamilton et al., 1987). A shift towards more ^{18}O-enriched fluids (~ –3 ‰) had occurred by the time that the reservoirs were buried to ~3000 m (temperature ~95 °C) (see paragraph above).
- ✓ Microthermometric measurements in fluid inclusions in quartz cements indicate that (Chapter 4) : (1) quartz cementation started from at least 70 °C onwards in all three reservoirs; (2) in the Brae Unit 2 reservoir in the Miller Field, quartz growth temperatures are lowest in the crestal areas of the reservoir zones (95-105 °C) and approach present day reservoir temperatures (~120 °C) deeper down in the reservoir zones and in the aquifer; (3) in the Brae Unit 1 reservoir in the Kingfisher Field, quartz cementation occurred until the reservoir was buried to 105 °C; (4) in the Brae Unit 2 reservoir in the Kingfisher Field, quartz growth temperatures in oil zone samples (up to 120 °C) are only slightly lower than in water zone samples (up to 125 °C).
- ✓ CL photomicrographs show the presence of two quartz cementation Zones (A and B; Fig.56). Zone A cements are rarely observed, but always border detrital grains. There are two generations of Zone B quartz cements : Zone B1 occurs in calcite-cemented sandstones and must therefore have precipitated during shallow burial, most likely prior to Zone A cements. Zone B2 makes up the bulk volume of quartz cements and occurs on top of Zone A cements. Therefore, Zone B2 cements precipitated later than Zone A cements.
- ✓ Present day formation water isotopic composition is around +0.6 ‰ in the Miller Field (Smalley & Warren, 1994). Present day reservoir temperatures in the

Miller and Kingfisher Fields are around 115-125 °C (Rooksby, 1991; Shell Internal Report).

Below, pore-fluid evolution is discussed for each reservoir examined separately.

Brae Unit 2 reservoir - Miller Field The $\delta^{18}O$ compositions measured with the ion microprobe of Zone A quartz cements, which are rarely observed, range from +15.5 to +18.2 ‰ (Table 22). The $\delta^{18}O$ compositions measured with the ion microprobe of Zone B quartz cements range from +16.0 to +25.8 ‰ (Table 22). Average bulk quartz cement $\delta^{18}O$ compositions are obtained for a sample with the conventional isotope analysis technique. The range in quartz cement $\delta^{18}O$ compositions obtained with the conventional isotope analysis technique (+18.3 to +26.0 ‰; Table 21) overlaps with the range in Zone B $\delta^{18}O$ compositions measured with the ion microprobe (+16.0 to +25.8 ‰).

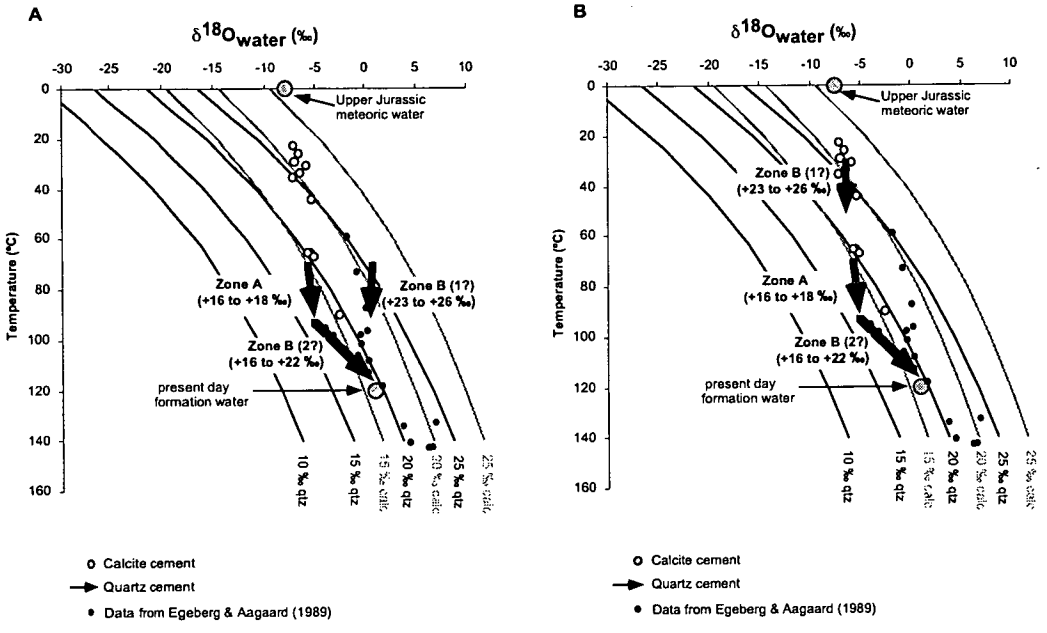

Fig.56 These cross plots of pore-fluid $\delta^{18}O$ values versus temperature show oxygen isotope fractionation curves for calcite cement from +15 to +25 ‰ (grey) and for quartz cement from +10 to +25 ‰ (black). The black arrows represent interpretations of the evolution of pore-fluids in the Brae Formation sandstones since time of deposition until the present day based upon measured quartz cement $\delta^{18}O$ compositions. The grey circles represent measured calcite cement $\delta^{18}O$ compositions. Two pore-fluid evolution models are devloped in order to explain quartz cement $\delta^{18}O$ compositions between +23 and +26 ‰ (A) and (B). Both models are addressed in the text on p. 150-152. The $\delta^{18}O$ evolution of pore-fluids in the Brae Formation complies with other pore-fluid oxygen isotope data from the North Sea. Data from Egeberg & Aagaard (1989) from the Norwegian Continental Shelf are plotted for comparison (black circles).

Zone A quartz cements, with $\delta^{18}O$ compositions between +15.5 and +18.2 ‰, could have been precipitated from meteoric-type fluids (–7 to –6 ‰) around 70 to 80 °C with a shift towards more ^{18}O-enriched fluids (–3 ‰) at temperatures around 90 to 100 °C (Table 25); or could have been precipitated from a more evolved (–1 ‰) or basinal-type fluid (+1 ‰) at higher temperatures (100-130 °C) (Table 25). Considering that Zone A cements precipitated prior to the bulk volume of Zone B cements (i.e. Zone B2), and that cementation in the reservoir started around 70 °C, it seems more likely that Zone A cements precipitated across the temperature range of 70 to 90 °C. The pore-fluids from which the Zone A cements precipitated across this temperature range (meteoric-type fluids with a shift towards more ^{18}O-enriched fluids) also comply with the pore-fluids from which calcite cements precipitated over a similar range of temperatures (Fig.56).

Zone B quartz cements, with $\delta^{18}O$ compositions between +16.0 and +25.8 ‰, were most likely precipitated over a range of temperatures from a range of pore-fluids. As mentioned above, only small amounts of quartz cement developed in the Brae Formation at low temperatures and shallow burial. Therefore, the bulk of the Zone B quartz cements analysed are most likely from the Zone B2 generation. These Zone B2 cements overlie, and are therefore later than, Zone A quartz cements. Consequently, precipitation of Zone B2 cements most likely occurred from ~90 °C onwards. The most plausible fluid evolution in the reservoir is that, with increasing burial depth and temperature, quartz cements progressively precipitated from fluids which evolved in composition from a fluid with $\delta^{18}O$ ~–3 ‰ initially (~90 °C) to an end-member basinal-type fluid with $\delta^{18}O$ similar to the present day formation water oxygen isotope composition (+0.6 ‰) at present day reservoir temperatures (~120 °C) (Fig.56). Such fluid evolution can explain most of the measured quartz cement Zone B $\delta^{18}O$ compositions (+16 to +22 ‰).

The Zone B quartz cement $\delta^{18}O$ compositions between +23 and +26 ‰ are more difficult to explain. Two pore-fluid evolution models can be developed to accommodate $\delta^{18}O$ values of +23 to +26 ‰ (Fig.56) : (1) if the lowest temperatures from fluid inclusions are used (70 to 90 °C), then Zone B quartz cements with $\delta^{18}O$ compositions between +23 and +26 ‰ would have precipitated from pore-fluids with $\delta^{18}O$ compositions between –2 to +1 ‰ (Fig.56A); (2) Zone B quartz cements with $\delta^{18}O$ compositions between +23 and +26 ‰ could have precipitated from a

meteoric-type fluid (–7 to –6 ‰) at temperatures around 30-50 °C (Fig.56B). There are two arguments against the first model :

- if Zone B quartz cements with $\delta^{18}O$ values of +23 to +26 ‰ precipitated across a temperature range of 70 to 90 °C, then precipitation of Zone B cements overlaps in time with precipitation of Zone A cements despite precipitating from isotopically different pore-fluids (Fig.56A).
- the pore-fluid composition derived for Zone B quartz cements in this model (–2 to +1 ‰) is not in agreement with measured calcite cement $\delta^{18}O$ compositions across the 70 to 90 °C temperature range (Fig.56A).

For these reasons, the pore-fluid evolution model in Fig.56A seems unlikely. Although no low temperatures (<50 °C) have been measured in fluid inclusions in quartz cements, the second model (Fig.56B) is more plausible for the following reasons :

- there is evidence of early quartz cementation (Zone B1) in the calcite cemented sandstones (Fig.55C). These Zone B1 overgrowths suggest precipitation of quartz cements at shallow burial depths (<1500 m) and low temperatures (<60 °C). The lack of low temperature inclusions in quartz cement can be explained by the fact that it takes a long time to grow sufficient quartz to enclose an inclusion at temperatures <70 °C (Chapter 4). Therefore, the likelihood of finding low temperature inclusions in quartz cement is small.
- the pore-fluid composition derived for Zone B quartz cements in this model (–7 to –6 ‰) is in agreement with measured calcite cement $\delta^{18}O$ compositions across the 30 to 50 °C temperature range (Fig.56B).
- pore-fluid evolution in reservoir sandstones from the Middle Jurassic Garn Formation located in the Haltenbanken region (offshore Norway) is identical to the model presented for the Brae Formation sandstones in Fig.56B. Williams et al. (1997) found three isotopically distinct generations of quartz cement present in the Garn Formation sandstones : the first generation of quartz cement has $\delta^{18}O$ compositions between +23 and +26 ‰, the second generation of quartz cement has $\delta^{18}O$ compositions between +14 and +19 ‰ and the third generation of quartz cement has $\delta^{18}O$ compositions between +20 and +22 ‰. Williams et al. (1997) suggest that these generations of quartz cements precipitated consecutively from pore-waters which evolved in

composition from meteoric-type fluids ($\delta^{18}O$ between –10 to –5 ‰) during shallow burial (<50 °C), to ^{18}O-enriched fluids during burial to temperatures up to 120 °C, and finally to basinal-type fluids (~+3 ‰) at present day temperatures (120 to 140 °C).

The model presented in Fig.56B implies that the $\delta^{18}O$ values between +23 and +26 ‰ measured in quartz cements in Brae Formation samples correspond to early Zone B1 cementation. If oxygen isotope analysis results of the early Zone B1 generation of quartz cements in calcite-cemented sandstones was to provide $\delta^{18}O$ values between +23 and +26 ‰, then it would strongly support the pore-fluid model in Fig.56B. Unfortunately, no Zone B1 quartz overgrowths in calcite-cemented sandstone samples were analyzed in this study. However, based on the arguments above, the pore-fluid model in Fig.56B seems much more likely than the one presented in Fig.56A.

Brae Unit 1 reservoir - Kingfisher Field The $\delta^{18}O$ compositions measured with the ion microprobe of Zone A quartz cements in the Brae Unit 1 reservoir of the Kingfisher Field range from +15.3 to +16.9 ‰ (Table 22). The $\delta^{18}O$ compositions measured in Zone B quartz cements range from +18.6 to +24.3 ‰ (Table 22). Bulk quartz cement $\delta^{18}O$ compositions, obtained with the conventional isotope analysis technique, overlap largely (+20.3 to +25.6 ‰; Table 21) with the range in Zone B $\delta^{18}O$ compositions measured with the ion microprobe (+18.6 to +24.3 ‰).

By analogy with the Brae Unit 2 reservoir of the Miller Field, Zone A quartz cements, with $\delta^{18}O$ compositions between +15.3 and +16.9 ‰, could have been precipitated from a meteoric to a more ^{18}O-enriched-type fluid (–7 to –5 ‰) at temperatures around 70-90 °C (Table 25). From fluid inclusion data, it was clear that quartz cementation had ceased in the reservoir around ~105 °C. Consequently, Zone B quartz cements, with $\delta^{18}O$ compositions between +19 and +22 ‰, will have precipitated until temperatures of around 105 °C were reached in the reservoir (Chapter 4). This precipitation could have occurred from an ^{18}O-enriched fluid with $\delta^{18}O$ composition between –3 and +1 ‰ (Table 25). A few $\delta^{18}O$ compositions between +23 and +24 ‰ were measured in quartz cements also in this reservoir. By analogy with the Brae Unit 2 reservoir of the Miller Field, these signatures are best explained by quartz cement precipitation from a meteoric-type fluid (–7 to –6 ‰) at temperatures around 30-50 °C.

Brae Unit 2 reservoir - Kingfisher Field In this reservoir, no Zone A quartz cements were encountered. The $\delta^{18}O$ compositions measured in Zone B quartz cements range from +17.1 to +24.8 ‰ (Table 22). Bulk quartz cement $\delta^{18}O$ compositions, obtained with the conventional isotope analysis technique, range from +19.9 to +24.9 ‰ (Table 21). The range in quartz cement $\delta^{18}O$ compositions obtained with the conventional isotope analysis technique is similar to the range in Zone B $\delta^{18}O$ compositions measured with the ion microprobe. Assuming that precipitation of Zone B quartz cements occurred also in this reservoir from around 90 °C onwards, the measured quartz cement $\delta^{18}O$ compositions are best explained by precipitation from fluids which became increasingly ^{18}O-enriched (from ~–4 to +1 ‰) during burial (~90 to 120 °C). The end-member fluid composition here is also, most likely, a basinal-type fluid with $\delta^{18}O$ ~ +1 ‰.

7.8 Discussion

Based on the $\delta^{18}O$ compositions of calcite and quartz cements, a similar pore-fluid evolution was derived for all three reservoirs studied. This indicates that hydrogeologic evolution was similar across the whole Brae Formation sandstone. Three isotopically distinct fluid phases, which most probably correspond with the three generations of quartz cements observed (Zone B1, Zone A and Zone B2), can be differentiated :

(1) The $\delta^{18}O$ compositions of diagenetic early calcite cements in the Brae Formation suggest that meteoric pore-waters (Upper Jurassic –7 ‰; Hamilton et al., 1987) were present in the sandstones at shallow burial depth (<1500 m) (Fig.56B). This burial depth corresponds with temperatures up to 60 to 70 °C (Appendix D, Table D.3). Quartz overgrowths (Zone B1) in the calcite concretions indicate also that quartz cementation may have occurred over this range of depths and temperatures in the sandstones. Measured oxygen isotopic compositions of quartz cements between +23 and +26 ‰ comply with such low temperature precipitation (30-50 °C) from meteoric-type fluids (–7 to –6 ‰) (Fig.56B). Considering the marine depositional environment of the sandstones studied, the presence of waters with oxygen isotopic composition similar to meteoric water in the Brae Formation implies that the sandstones were open to surface water recharge. The high initial porosities (~35 to 40 %), and also permeabilities, in the sandstones during shallow burial are

likely to have permitted advective flow of meteoric fluids from the graben margin during the early stages of diagenesis (<1500 m and <60-70 °C).

(2) During burial between ~1500-3000 m, and temperatures between 70 and 95 °C, a shift in pore-fluid isotopic compositions occurred from meteoric-type fluids (–7 to –6 ‰) to more ^{18}O-enriched fluids (–5 to –2 ‰). This is reflected in the oxygen isotopic compositions of calcite cements (Appendix B) and also in Zone A quartz cements with oxygen isotopic compositions of +15 to +18 ‰ (Fig.56B). The estimated porewater oxygen isotope signatures of ~–5 to –2 ‰ may be explained by mixing of the meteoric-type fluids (–7 ‰; Hamilton et al., 1987) with basinal-type fluids (+2 to +5 ‰; Egeberg & Aagaard, 1989, Wilkinson et al., 1992) originating from deeper in the basin. A mixing of meteoric fluids with a significant component of deep basinal saline fluids may also explain the high salinity of fluid inclusions (15-25 wt% NaCl eq) measured in quartz cements which formed between 75-95 °C (Chapter 4). As mentioned in Chapter 4, the origin of the high salinity fluids may be attributed to dissolution of salts occurring in deeper parts of the basin.

(3) In previous chapters it was concluded that a change in reservoir hydrology occurred around 90 to 95 °C (~3000 m) because of decreasing porosities at greater depths, and also petroleum emplacement in the Brae Unit 2 reservoir in the Miller Field and the Brae Unit 1 reservoir in the Kingfisher Field. During burial from ~3000 m to present day burial depths (~4000 m), porewater oxygen isotope composition in the sandstones evolved from around ~–2 ‰ to present day formation water oxygen isotope composition (+0.6 ‰; Smalley & Warren, 1994). Quartz cement oxygen isotopic compositions between +16 to +22 ‰ (Zone B2) may be explained by precipitation from such fluids ($\delta^{18}O$ between –1 to +1 ‰) at temperatures around 100-120 °C (Fig.56B). The increasing enrichment of ^{18}O in the porewaters indicates an increasing rock-water ratio (Longstaffe, 1989). A high rock-water ratio indicates that the oxygen isotopic composition of the pore-fluid is rock-buffered. Rock-water reactions which are generally cited to explain the increase in $\delta^{18}O$ values of pore-fluids include illitisation and/or chloritisation of kaolinite and smectite clays formed by low temperature weathering (Wilkinson et al., 1992), and/or recrystallisation of early formed carbonates (Saigal & Bjørlykke, 1987). As mentioned in Chapter 4, clay mineral reactions also generate H_2O-rich porewaters which may have diluted the high salinity pore-fluids present in the sandstones at burial depths >3000 m.

Present day formation water $\delta^{18}O$-data from the Norwegian continental shelf (Egeberg & Aagaard, 1989) show that pore-fluids become progressively enriched in ^{18}O relative to surface waters with increasing burial depth. When these present day data from the Norwegian continental shelf are plotted on Fig.56, together with the Brae Formation sandstone data, then it can be seen that the calculated $\delta^{18}O$ values of pore-fluids in the Brae Formation sandstones fit in the present day regional North Sea trend of ^{18}O-enrichment of fluids with increasing temperature (and burial depth). The fact that the pore-fluid $\delta^{18}O$ evolution derived for the Brae Formation sandstones displays a similar trend with temperature (and consequently also burial depth) to that seen in present day formation water data from different depths on the Norwegian continental shelf (Fig.56) suggests that porewater evolution may have occurred through similar subsurface processes on both sides of the North Sea.

7.9 Conclusions

1 The ion microprobe allows in-situ oxygen isotope analysis of quartz cements in polished thin sections. A wide range of authigenic quartz $\delta^{18}O$ compositions was obtained with this analysis technique in Brae Formation sandstone samples. Conventional isotope analysis results are, however, a valuable asset for the interpretation of ion microprobe results. Because the $\delta^{18}O$ composition obtained for a sample by the conventional analysis technique represents an average oxygen isotope composition for the bulk volume of quartz cements present in that sample, conventional analysis results indicate which ion microprobe $\delta^{18}O$ values are likely to be volumetrically more important than others.

2 Care needs to be taken when interpreting isotope analysis results. For the ion microprobe, it is essential to check with SEM-CL where the ion beam hit the sample before making any data interpretation. A problem inherent in the method of conventional analysis is that each analyzed size fraction is composed of mixtures of detrital and authigenic quartz. The validity of the conventional isotope modelling technique therefore depends upon the accuracy of the percentage of authigenic quartz determined by SEM-CL and image analysis. Cross plots of percentage of authigenic quartz versus measured $\delta^{18}O$ in each size fraction need to be constructed and assessed to provide the most reasonable estimate of extrapolated pure authigenic and detrital quartz $\delta^{18}O$ values of a sample.

3 The oxygen isotopic compositions of detrital quartz grains in the Brae Formation sandstones, determined with the ion microprobe, range between +6.9 and +17.5 ‰. The average $\delta^{18}O$ values of detrital grains are similar in all three Brae Formation reservoirs examined (~ +11 ‰). Despite the smaller range in $\delta^{18}O$ values of detrital quartz determined with the conventional analysis technique (+10.6 to +14.9 ‰), the average $\delta^{18}O$ values of detrital quartz (+12 ‰) are similar to average $\delta^{18}O$ values determined with the ion microprobe in all three reservoirs examined (+11 ‰). The wide range in detrital quartz $\delta^{18}O$ values indicates that the grains in the sandstones are a mixture of quartz from different origins (e.g. igneous quartz, metamorphic quartz).

4 Despite the wide range in oxygen isotopic compositions of authigenic quartz (+15.3 to +25.8 ‰), the average $\delta^{18}O$ values of authigenic quartz determined with the ion microprobe are similar (+20 to +21 ‰) in all three reservoirs examined. In most samples, the extrapolated $\delta^{18}O$ values obtained from the conventional analysis technique (+18 to +26 ‰) are more positive than the ion microprobe average $\delta^{18}O$ values (+20 to +21 ‰). The dissimilarity in ion microprobe and conventional results can be mainly attributed to the wide range in $\delta^{18}O$ compositions of quartz overgrowths present in the Brae Formation sandstone samples.

5 Two quartz cement phases can be distinguished under SEM-CL : Zone A quartz cements display a complex CL pattern and Zone B cements display a homogeneous CL pattern. Based on textural observations, two generations can be distinguished in the Zone B cements : Zone B1 cements precipitated during shallow burial, prior to Zone A cements, and are present in early calcite-cemented sandstones; Zone B2 cements make up the bulk of the quartz cements in the Brae Formation sandstones and precipitated after Zone A cements during deeper burial.

6 Based on measured $\delta^{18}O$ compositions of calcite and quartz cements, the following pore-fluid evolution in the Brae Formation sandstones seems most likely :

- Early calcite cements, and Zone B1 quartz cements ($\delta^{18}O$ between +23 and +16 ‰), precipitated from a meteoric-type fluid (~–7 ‰) during shallow burial. The initial presence of meteoric fluids in the marine Brae Formation sands implies that the sandstones were open to surface water recharge during

shallow burial (<1500 m and <60-70 °C) when porosities and permeabilities were high.

- Subsequent precipitation of Zone A quartz cements ($\delta^{18}O$ between +14 and +19 ‰) during burial from ~1500 to ~3000 m (70 to 90 °C) occurred from fluids with oxygen isotope signatures between –5 and –2 ‰. The shift in oxygen isotope composition of pore-fluid can be explained by mixing of the meteoric-type fluids (~–7 ‰) with basinal-type fluids (+2 to +5 ‰) originating from deeper in the basin. A mixing of the initial shallow burial meteoric fluids with deep basinal saline fluids may also explain the high salinity of fluid inclusions (15-25 wt% NaCl eq) measured in quartz cements which formed between 75-95 °C (Chapter 4). As mentioned in Chapter 4, the high salinity of the basinal fluids may be attributed to dissolution of salts occurring in deeper parts of the basin.
- Most quartz overgrowths, Zone B2, precipitated during burial from ~3000 m to present day reservoir depths (~4000 m) from porewaters which evolved in oxygen isotope composition from ~–2 ‰ to present day formation water oxygen isotope composition (+0.6 ‰). The increasing enrichment of ^{18}O in the porewaters can be explained by increasing rock-water ratio. Increasing quartz cement abundances and petroleum emplacement in the reservoirs will have decreased porosities and permeabilities in the Brae Formation at depths >3000 m. Consequently, the oxygen isotopic composition of the pore-fluids may become rock-buffered. Rock-water reactions which are generally cited to explain the increase in $\delta^{18}O$ values of pore-fluids include illitisation and/or chloritisation of kaolinite and smectite clays formed by low temperature weathering, and/or recrystallisation of early formed carbonates. Clay mineral reactions also generate H_2O-rich porewaters which may have diluted the high salinity pore-fluids present in the sandstones at burial depths between 1500 and 3000 m. Salinities measured in fluid inclusions which formed between 90 and 120 °C are comparable to present day formation water salinties (5-10 wt% NaCl eq).

CHAPTER VIII

SOURCES OF SILICA FOR QUARTZ CEMENTATION

In this chapter :

- *Which sources of silica can be identified to explain the quartz cement volumes present in the Brae Formation sandstone reservoirs examined ?*
- *Can silicon isotopes be used as a tracer for silica sources in sandstones ?*

8.1 Introduction

In order to understand, and predict, the extent of quartz cementation in actual and potential reservoirs, it is important to constrain the source(s) of silica for quartz cementation. At least 23 possible sources of silica have been proposed by McBride (1989). Sources of silica within the quartz cemented sandstones are usually referred to as "internal sources", as opposed to "external sources" which refer to silica sources outside the quartz cemented sandstones.

In this Chapter, I will use a combination of petrographic and geochemical techniques in order to identify the most likely sources of silica for quartz cementation in the Brae Formation sandstones. The following internal silica sources will be considered for quartz cementation in the sandstones studied : dissolution of K-feldspars, dissolution of biogenic silica (sponge spicules) and pressure dissolution of quartz at grain contacts or stylolites. Illitisation of kaolinite also releases silica to the porewaters in sandstones (Bjørlykke & Egeberg, 1993). However, the studied sandstones do not show any significant illitisation of kaolinite. Silica precipitated

from meteoric water and silica released from interbedded shales during compaction will be considered as potential external silica sources.

I will use petrographic point-count results reported in Chapter 3 to elicit the importance of K-feldspar and sponge spicule dissolution as silica sources for quartz cementation. I have also looked with the optical microscope for stylolites and evidence of grain-to-grain pressure dissolution in sandstone thin sections. External silica sources, such as meteoric water and silica released from mudrocks, are difficult to constrain. This does not mean, however, that these sources should be automatically discounted.

I have carried out silicon isotope analyses of detrital and authigenic quartz with the ion microprobe. Based on the similarities between the means and spreads of $\delta^{30}Si$ of dissolved silicon and quartz deposited from solution above 50 °C, Douthitt (1982) concluded that no silicon isotope fractionation occurs above that temperature and therefore $\alpha^{30}Si_{QTZ\text{-}Si(aq)} \sim 1.0000$. The consequence of an equilibrium between silicates and solution is that authigenic quartz, precipitated at temperatures >50 °C, should yield a similar silicon isotope composition as the silica present in the pore-fluid. Therefore, if dissolution of detrital quartz is an important silica source for precipitation of authigenic quartz in the Brae Formation sandstones, then the silicon isotopic compositions of detrital and authigenic quartz are expected to be similar. I have also carried out some silicon isotope analyses of sponge spicules in the Brae Formation sandstones. If sponge spicules are an important silica source, then the silicon isotopic compositions of authigenic quartz and spicules are expected to be similar.

Rather than providing a definite answer as to the sources of silica for quartz cementation in the Brae Formation sandstones, I am aim to assess which silica sources are likely to be volumetrically more significant than others.

8.2 Petrographic observations

K-feldspar dissolution Dissolution of feldspars in the Brae Formation sandstones resulted in the creation of small amounts of secondary porosity (average 1.7±1.2 %; Chapter 3, Table 5). The occurrence of authigenic clay in the sandstones examined is also low (average 1.2±0.8 %; Chapter 3, Table 5). The observation that authigenic kaolinite occurs in secondary pore spaces suggests that feldspar dissolution follows the reaction :

$$2KAlSi_3O_8 + 2H^+ + H_2O \rightarrow Al_2Si_2O_5(OH)_4 + 2K^+ + 4SiO_2$$

molar volume : 217.4 90.8

(Robie & Hemingway, 1995)

volume ratio : 1 0.42

For every mole of K-feldspar altered to kaolinite, two moles of silica are released and made available for quartz cementation (Siever, 1957). When following the approach of Hartmann et al. (2000), and assuming that all the dissolved K-feldspar has been altered to kaolinite, then it can be calculated that 0 to 6.2 vol% secondary porosity in the Brae Formation sandstones (Chapter 3, Table 5) can account for 0 to 2.6 vol% quartz cement. Fig.57 demonstrates that, in all three reservoirs examined, only a fraction of the total quartz cement observed in the samples could have been sourced by the dissolution reaction of feldspars. In samples with low quartz cement abundance (<6 %; e.g. top of the reservoir zones in the Brae Unit 2 sands of the Miller Field, Brae Unit 1 reservoir in the Kingfisher Field), dissolution of K-feldspars could have provided 10 to 50 % of the silica necessary for the observed quartz cement abundances. In samples with higher quartz cement abundances (6-15 %; e.g. lower areas of the Brae Unit 2 reservoir in the Miller Field, Brae Unit 2 reservoir in the Kingfisher Field), dissolution of K-feldspars provided only up to 10 % of the silica necessary for the observed quartz cement abundances.

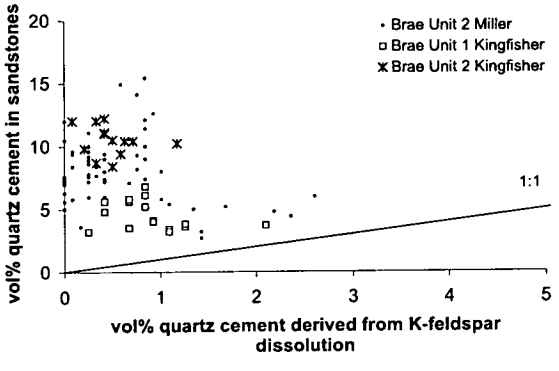

Fig.57 Cross-plot of percentage of quartz cement derived from K-feldspar dissolution versus actual percentage of quartz cement present in thin section samples from the Brae Formation sandstones (data from Chapter 3). Two areas on the plot are separated by a diagonal line : if samples plot on the line (1:1) then silica released from K-feldspar dissolution mass-balances with quartz cement volumes in the samples; if samples plot in the top area then insufficient K-feldspar dissolution occurred in those samples to explain their quartz cement volumes; if samples plot in the bottom area then ions released by the K-feldspar dissolution reactions were not consumed for the precipitation of quartz cements. All samples from the Brae Formation plot in the top area. This indicates that other processes, apart from K-feldspar dissolution, must contribute to the silica budget in the sandstones in order to explain quartz cement volumes in the samples.

Sponge spicule dissolution Sponge spicules occur in very small quantities in the Brae Formation reservoirs in the Miller and Kingfisher Fields (Table 26, Fig.58). The spicules are composed of silica in an opaline form, have an axial canal and are several 100 μm up to 1 mm in size (Figs. 58 and 59). Although the spicules are not numerous, they are exceptional in North Sea oil reservoirs both in quality of preservation and in variety of forms present (Figs. 58 and 59). Because the concretions in the Brae Formation sandstones formed soon after deposition of the sediments (Appendix B), it can be assumed that they preserve both depositional fabric and composition of the sands. In order to assess the extent of sponge spicule dissolution in the Brae Formation sandstones, spicule abundances in and outside calcite cemented intervals are compared. The method of comparing sandstone composition in and outside concretions in order to reveal silica fluxes was described by Gluyas & Coleman (1992). There is a very small difference (<1 %) in sponge spicule abundance in and outside the carbonate cemented sands in all three reservoirs (Table 26). Consequently, only a small fraction of the quartz cement observed in the samples may be sourced by the dissolution of biogenic silica.

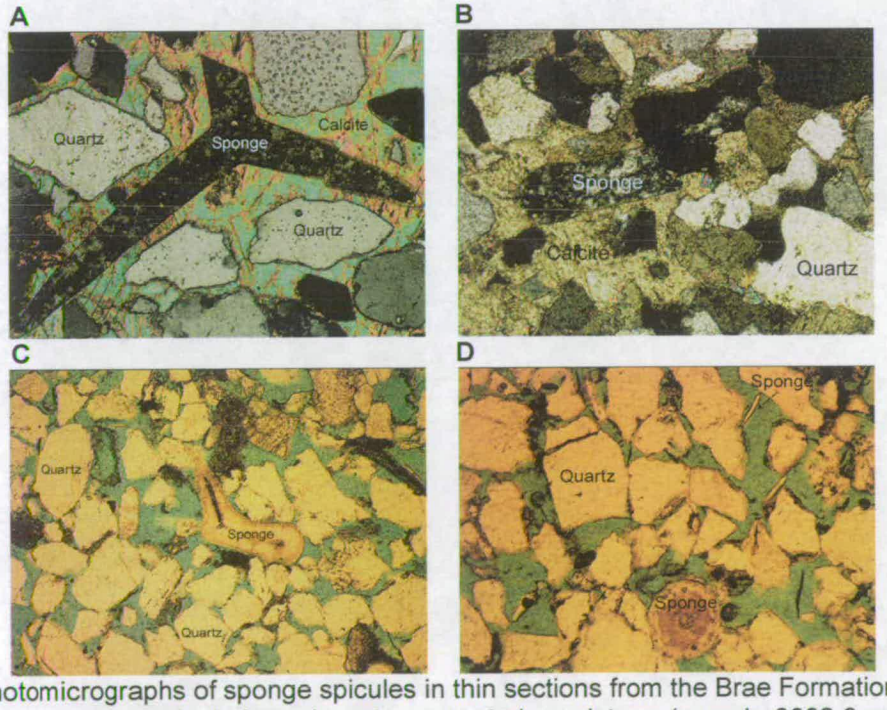

Fig.58 Photomicrographs of sponge spicules in thin sections from the Brae Formation.
(**A**) Siliceous sponge spicule in carbonate cemented sandstone (sample 3992.3 m, well 8b-3, Brae Unit 2, Miller Field, field of view 1280x1000 μm).
(**B**) Siliceous sponge spicule in carbonate cemented sandstone (sample 3914.1 m, well 8a-8, Brae Unit 1, Kingfisher Field, field of view 1350x1050 μm).
(**C**) Sponge spicule in porous sandstones sample (3929.5 m, well 8a-8) in the Brae Unit 1 reservoir of the Kingfisher Field, field of view 1400x1100 μm).
(**D**) Sponge spicule in porous sandstones sample (3887.5 m, well 8a-8) in the Brae Unit 1 reservoir of the Kingfisher Field, field of view 1350x1050 μm).

Table 26 Average (± standard deviation) percentages (in the detrital mineral assemblages) of sponge spicules in and outside calcite cemented sandstones in the Brae Formation sandstone reservoirs in the Miller and Kingfisher Fields. The calcite cemented sandstones, which can be considered to represent initial depositional sandstone compositions, contain slightly more spicules than the porous sandstones. This may indicate that dissolution of minor amounts of sponge spicules (<1 %) occurred during burial.

Field	Reservoir	Outside concretions % sponge spicules in detrital assemblage	Inside concretions % sponge spicules in detrital assemblage
Miller	Brae II	0.0 ± 0.0 (n=59)	0.2 ± 0.2 (n=15)
Kingfisher	Brae I	0.8 ± 0.5 (n=16)	1.8 ± 1.1 (n=11)
Kingfisher	Brae II	0.1 ± 0.2 (n=13)	0.2 ± 0.2 (n=3)

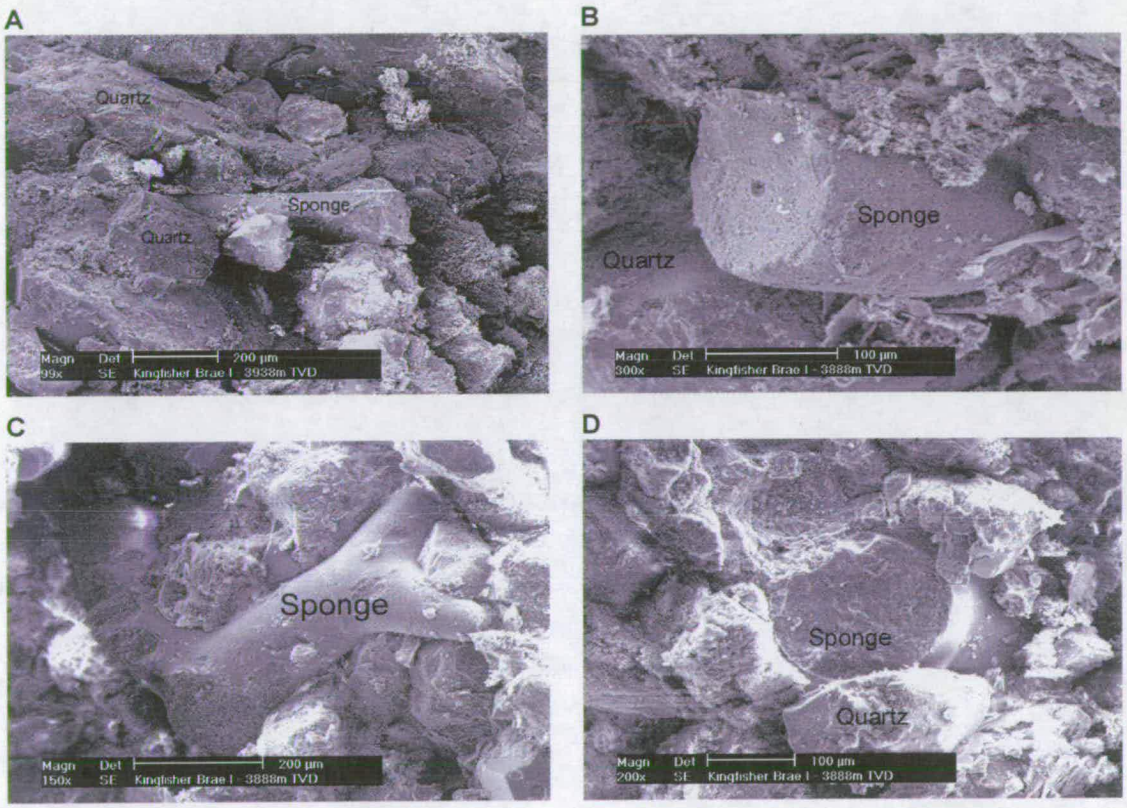

Fig.59 SEM images of sponge spicules in rock pieces of Brae Formation sandstones.
(**A**) Sample 3938 m, well 8a-8, Brae Unit 1, Kingfisher Field.
(**B**), (**C**) and (**D**) Sample 3888 m, well 8a-8, Brae Unit 1, Kingfisher Field.

Pressure dissolution Dissolution of quartz at stylolites and grain contacts is a long-recognised source of quartz cement (e.g. Heald, 1955; Sibley & Blatt, 1976). Dissolution of quartz at stylolites and grain contacts is observed in all the studied sandstone reservoirs (Figs. 60 and 61). Fine-grained sandstones are usually more susceptible to pressure dissolution than coarse-grained sandstones (Porter & James, 1986). Also in the Brae Formation sandstones, laminae of interbedded

highly argillaceous sandstones display signs of extensive quartz pressure dissolution (Fig.60). Silica dissolved in these fine-grained laminae may diffuse (centimeter to meter scale) to precipitation sites in the nearby medium-grained sandstones. As mentioned in Chapter 1, there is controversy surrounding pressure solution as to whether it is initiated by lithostatic pressure, temperature, or the presence of clay minerals along grain interfaces or by a combination of these (Worden & Morad, 2000). Both temperature and pressure increase silica solubility and are therefore both considered to be important in the quartz dissolution process. The fact that large-scale pressure dissolution and stylolite formation is observed in interbedded laminae of fine-grained sands also indicates that clay and micas act as catalysts in inducing pressure solution.

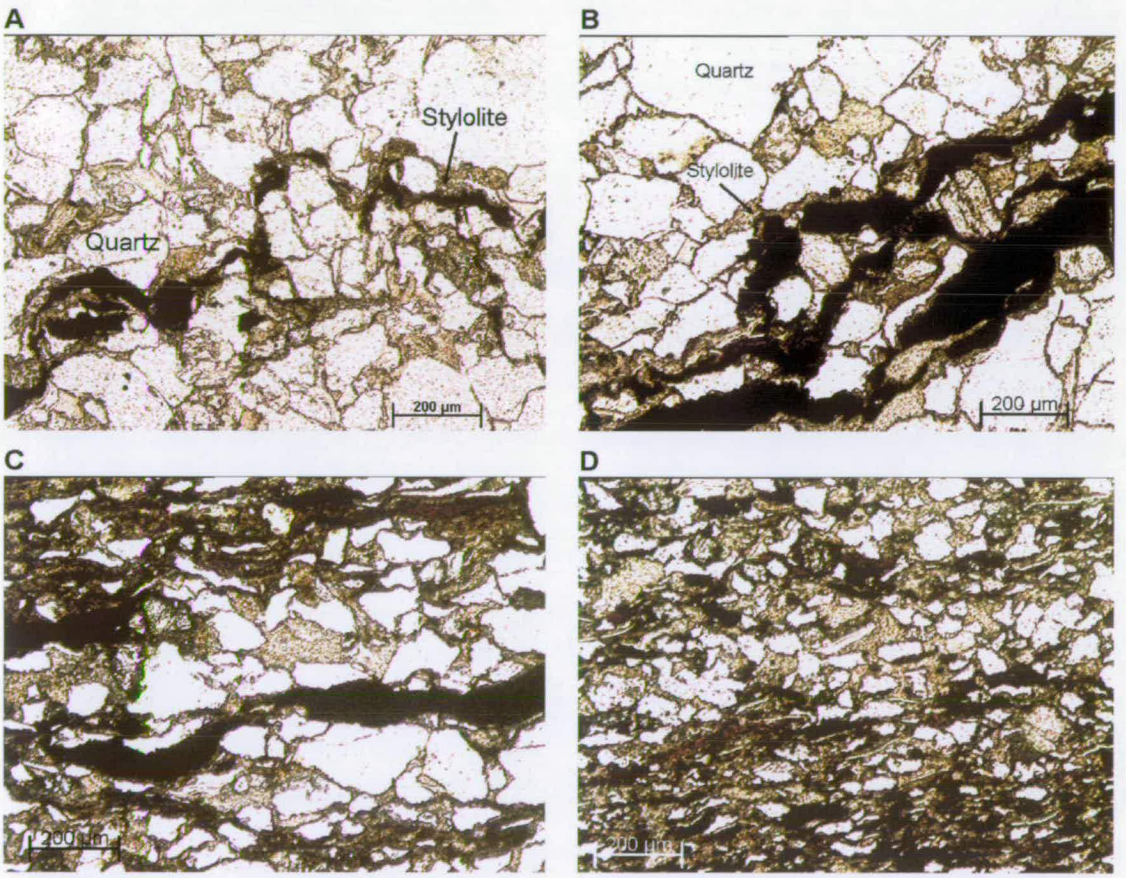

Fig.60 Optical microscopy photomicrographs of stylolite seams and pressure solution of quartz grains in the Brae Formation sandstones.
(**A**) and (**B**) Stylolite seams in Brae Formation sandstone samples. Quartz grains adjacent to the stylolite are irregular-shaped and smaller in size compared to quartz grains further away from the stylolite. This suggests solution of detrital quartz at the stylolite interface.
(**C**) and (**D**) Pressure solution of quartz grains embedded in argillaceous matrix (black). Silica dissolved in these fine-grained laminae may diffuse to precipitation sites in the nearby medium-grained sandstones and precipitate as quartz cement.
Photomicrographs are all of samples from the Brae Unit 2 reservoir in the Miller Field. Sample depths : 4037 m (**A**), 4067 m (**B**), 4066 m (**C**), 4043 m (**D**).

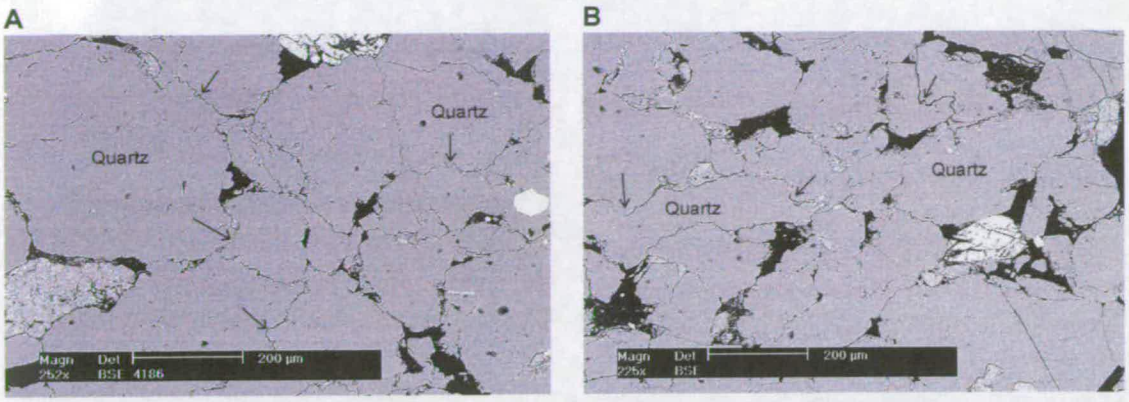

Fig.61 Backscatter SEM images of solution of detrital quartz at points of contact between grains. In some places this process has produced sutured grain-contacts (arrows) in the Brae Formation sandstone samples.
(**A**) Sample 4186 m, well 7b-26, Brae Unit 2, Miller Field.
(**B**) Sample 4081 m, well 8a-4, Brae Unit 2, Kingfisher Field.

8.3 Silicon isotope analysis

Methodology All samples were analysed for silicon isotope ratios with a Cameca ims-4f ion microprobe equipped with a Charles Evans & Associates control system at the University of Edinburgh. The samples were bombarded in the ion microprobe with a focused (20-30 µm) primary beam of $^{16}O^{+}$. An initial burn in time of 1 minute was used to burn through the gold coat and to stabilize the secondary ion current prior to each analysis. Negative high energy (offset 120 V) secondary ions ($^{30}Si^{+}$ and $^{28}Si^{+}$) were accelerated and focused into a mass spectrometer where the isotopes are separated and subsequently counted with an electron multiplier. For each analysis of $^{30}Si/^{28}Si$ in quartz, secondary $^{30}Si^{+}$ and $^{28}Si^{+}$ ions were collected with total counting times of 120 and 40 s respectively. The total counting times were made up of 40 cycles of counting for 3 s on ^{30}Si and 1 s on ^{28}Si yielding a theoretical precision of ±0.6 ‰.

Standards All analyses were standardised against NBS28 ($\delta^{30}Si$ = 0 ‰). At the start and end of the day, at least 3 standard analyses were made. Also, 2 to 3 standard analyses were made after every 6 to 8 unknown analyses. Fig.62 shows the measured $\delta^{30}Si$ compositions in NBS28 throughout the analytical session. As described in Chapter 7, the standard analyses were used for correcting the data for the effect of instrumental mass fractionation.

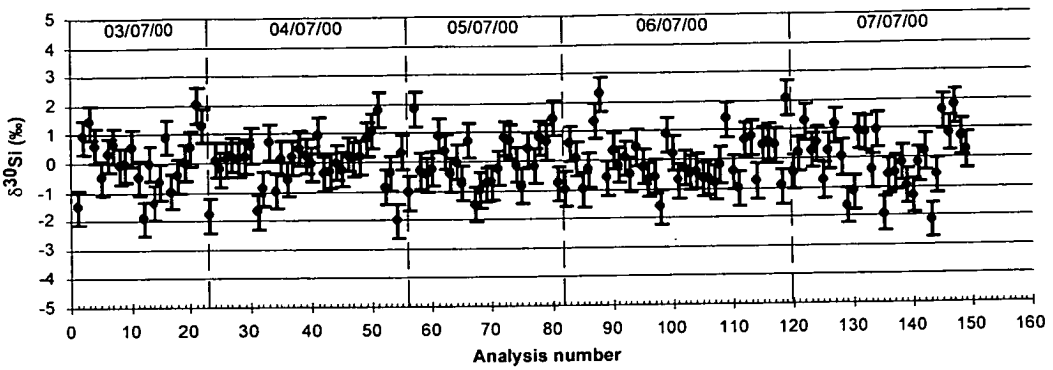

Fig.62 Ion microprobe analysis results of the $\delta^{30}Si$ values of the NBS28 standard throughout the analytical session (July 3th to 7th 2000). The error bars are the internal reproducibility of individual ion microprobe analyses (±0.6 ‰).

Samples Three samples were selected for analysis : 1 oil zone sample from the Brae Formation Unit 2 reservoir in the Miller Field (4039.6 m); 1 oil zone sample from the Brae Formation Unit 1 reservoir in the Kingfisher Field (3904.2 m) and 1 oil zone sample from the Brae Formation Unit 2 reservoir in the Kingfisher Field (3989.7 m). All samples were analysed during a 1 week period from July 3rd to July 7th 2000.

Sample preparation The samples used for silicon isotope analysis were used initially for oxygen isotope analysis. Sample preparation is therefore as described in Chapter 7.

Data quality control The silicon isotope data obtained with the ion microprobe are listed in Table 27. As described in Chapter 7 for oxygen isotope analysis, it is essential to check where the primary ion beam hit the sample before making any data interpretation. Also, the location of the sputter pits made by analyses in each thin section was checked by SEM-CL. In Table 27 an interpretation of the location of the sputter pits (in sponge spicules, authigenic quartz, detrital quartz or overlapping both) is inserted in the 'comment' column. The mixed signatures were disregarded for interpretation.

Table 27 (p.166-167) Results of in-situ ion microprobe analyses in detrital and authigenic quartz and sponge spicules in samples from the Brae Formation sandstones. The raw $^{30}Si/^{28}Si$ data have been dead-time corrected. The reported $\delta^{30}Si$ values have been corrected for instrumental mass fractionation by least-squares regression methods on standard analyses results. An interpretation of which quartz phase (authigenic, detrital or a mix of both, sponges) was analysed is indicated in the comment column.

Field	Reservoir	Sample depth (m TVD)	Analysis number	Date	Raw $^{30}Si/^{28}Si$ x1000	Corr. $^{30}Si/^{28}Si$ x1000	$\delta^{30}Si$ (‰)	Error (‰)	Comment
Miller	Brae II	4039.6	A:15312A1.DAT	5/ 07/2000	3.1790E-02	0.031826805	-1.1	0.7	authigenic
			A:15312A2.DAT	5/ 07/2000	3.1781E-02	0.031825737	-1.4	0.7	authigenic
			A:15312A3.DAT	5/ 07/2000	3.1835E-02	0.03182467	0.3	0.9	mix
			A:15312A4.DAT	5/ 07/2000	3.1754E-02	0.031824136	-2.2	0.7	mix
			A:15312A5.DAT	7/ 07/2000	3.1792E-02	0.03181651	-0.8	0.9	authigenic
			A:15312A6.DAT	7/ 07/2000	3.1797E-02	0.031817324	-0.6	0.9	authigenic
			A:15312A7.DAT	7/ 07/2000	3.1781E-02	0.031818138	-1.2	0.9	authigenic
			A:15312A8.DAT	7/ 07/2000	3.1809E-02	0.031818951	-0.3	0.9	authigenic
			A:15312A9.DAT	7/ 07/2000	3.1823E-02	0.031819765	0.1	0.8	authigenic
			A:15312A10.DAT	7/ 07/2000	3.1809E-02	0.031821393	-0.4	0.7	authigenic
			A:15312A11.DAT	7/ 07/2000	3.1846E-02	0.031826275	0.6	0.9	mix
			A:15312A12.DAT	7/ 07/2000	3.1813E-02	0.031827089	-0.4	1.0	authigenic
			A:15312A13.DAT	7/ 07/2000	3.1783E-02	0.031827902	-1.4	1.0	mix
			A:15312A14.DAT	7/ 07/2000	3.1793E-02	0.031828716	-1.1	1.0	authigenic
			A:15312A15.DAT	7/ 07/2000	3.1794E-02	0.031830343	-1.1	0.8	authigenic
			A:15312A16.DAT	7/ 07/2000	3.1806E-02	0.031831971	-0.8	1.1	authigenic
			A:15312A17.DAT	7/ 07/2000	3.1797E-02	0.031840922	-1.4	0.9	authigenic
			A:15312A18.DAT	7/ 07/2000	3.1847E-02	0.031841735	0.2	1.1	authigenic
			A:15312A19.DAT	7/ 07/2000	3.1861E-02	0.031842549	0.6	1.0	authigenic
			A:15312A20.DAT	7/ 07/2000	3.1871E-02	0.031844176	0.8	1.1	authigenic
			A:15312A21.DAT	7/ 07/2000	3.1764E-02	0.031845804	-2.6	1.3	mix
			A:15312D1.DAT	5/ 07/2000	3.1798E-02	0.031827873	-0.9	0.7	detrital
			A:15312D2.DAT	5/ 07/2000	3.1805E-02	0.031827339	-0.7	0.7	detrital
			A:15312D3.DAT	5/ 07/2000	3.1858E-02	0.031826271	1.0	0.8	detrital
			A:15312D4.DAT	5/ 07/2000	3.1859E-02	0.031825204	1.1	0.8	detrital
			A:15312D5.DAT	5/ 07/2000	3.1839E-02	0.031820934	0.6	0.8	detrital
			A:15312D6.DAT	5/ 07/2000	3.1792E-02	0.0318204	-0.9	0.6	detrital
			A:15312D7.DAT	5/ 07/2000	3.1752E-02	0.031819866	-2.1	0.8	detrital
			A:15312D8.DAT	5/ 07/2000	3.1831E-02	0.031819332	0.4	0.9	detrital
			A:15312D9.DAT	5/ 07/2000	3.1781E-02	0.031818798	-1.2	0.8	detrital
			A:15312D10.DAT	5/ 07/2000	3.1761E-02	0.031818265	-1.8	0.8	detrital
			A:15312D11.DAT	5/ 07/2000	3.1761E-02	0.031817731	-1.8	0.8	detrital
			A:15312D12.DAT	5/ 07/2000	3.1801E-02	0.031817197	-0.5	0.8	detrital
			A:15312D13.DAT	7/ 07/2000	3.1775E-02	0.031815697	-1.3	0.7	detrital
			A:15312D14.DAT	7/ 07/2000	3.1803E-02	0.031820579	-0.5	1.0	detrital
			A:15312D15.DAT	7/ 07/2000	3.1840E-02	0.03182953	0.3	1.0	detrital
			A:15312D16.DAT	7/ 07/2000	3.1790E-02	0.031831157	-1.3	1.0	detrital
			A:15312D17.DAT	7/ 07/2000	3.1814E-02	0.031832784	-0.6	0.8	detrital
			A:15312D18.DAT	7/ 07/2000	3.1872E-02	0.031840108	1.0	1.0	detrital
			A:15312D19.DAT	7/ 07/2000	3.1819E-02	0.031843363	-0.8	0.8	detrital
			A:15312D20.DAT	7/ 07/2000	3.1821E-02	0.03184499	-0.8	0.9	detrital
Kingfisher	Brae I	3904.2	A:13195A1.DAT	3/ 07/2000	3.1797E-02	0.031833312	-1.1	1.1	mix
			A:13195A2.DAT	3/ 07/2000	3.1818E-02	0.031833551	-0.5	0.9	mix
			A:13195A3.DAT	3/ 07/2000	3.1820E-02	0.03183379	-0.4	1.1	authigenic
			A:13195A4.DAT	3/ 07/2000	3.1854E-02	0.031834028	0.6	1.0	authigenic
			A:13195A5.DAT	3/ 07/2000	3.1788E-02	0.031834267	-1.4	0.8	authigenic
			A:13195A6.DAT	3/ 07/2000	3.1762E-02	0.031834506	-2.3	1.1	authigenic
			A:13195A7.DAT	3/ 07/2000	3.1867E-02	0.031834744	1.0	1.1	authigenic
			A:13195A8.DAT	3/ 07/2000	3.1816E-02	0.031836653	-0.6	1.2	authigenic
			A:13195A9.DAT	3/ 07/2000	3.1927E-02	0.031836892	2.8	1.2	authigenic
			A:13195A10.DAT	3/ 07/2000	3.1836E-02	0.031837131	0.0	0.9	authigenic
			A:13195A11.DAT	3/ 07/2000	3.1833E-02	0.031837369	-0.1	1.1	authigenic
			A:13195A12.DAT	3/ 07/2000	3.1842E-02	0.031837608	0.1	1.0	authigenic
			A:13195A13.DAT	3/ 07/2000	3.1797E-02	0.031837847	-1.3	1.0	authigenic
			A:13195A14.DAT	4/ 07/2000	3.1779E-02	0.031811627	-1.0	0.6	mix
			A:13195A15.DAT	4/ 07/2000	3.1819E-02	0.031811535	0.2	0.8	authigenic
			A:13195A16.DAT	4/ 07/2000	3.1795E-02	0.031811443	-0.5	0.8	authigenic
			A:13195A17.DAT	4/ 07/2000	3.1817E-02	0.031811351	0.2	0.9	authigenic
			A:13195A18.DAT	4/ 07/2000	3.1751E-02	0.031811259	-1.9	0.7	authigenic
			A:13195A19.DAT	4/ 07/2000	3.1753E-02	0.031811167	-1.8	0.8	authigenic
			A:13195A20.DAT	4/ 07/2000	3.1814E-02	0.031811075	0.1	0.7	authigenic
			A:13195D1.DAT	3/ 07/2000	3.1753E-02	0.031829733	-2.4	0.9	detrital
			A:13195D2.DAT	3/ 07/2000	3.1815E-02	0.031829972	-0.5	0.9	detrital
			A:13195D3.DAT	3/ 07/2000	3.1768E-02	0.03183021	-2.0	0.8	detrital
			A:13195D4.DAT	3/ 07/2000	3.1791E-02	0.031830449	-1.3	1.0	detrital
			A:13195D5.DAT	3/ 07/2000	3.1771E-02	0.031830687	-1.9	0.8	detrital
			A:13195D6.DAT	3/ 07/2000	3.1811E-02	0.031830926	-0.6	0.9	detrital
			A:13195D7.DAT	3/ 07/2000	3.1857E-02	0.031831165	0.8	1.0	detrital
			A:13195D8.DAT	3/ 07/2000	3.1764E-02	0.031831403	-2.1	0.7	detrital
			A:13195D9.DAT	3/ 07/2000	3.1857E-02	0.031833074	0.8	1.1	detrital
			A:13195D10.DAT	3/ 07/2000	3.1795E-02	0.031836415	-1.3	0.9	detrital
			A:13195D11.DAT	3/ 07/2000	3.1783E-02	0.031838085	-1.7	1.4	detrital
			A:13195D12.DAT	4/ 07/2000	3.1845E-02	0.031811811	1.0	0.8	detrital
			A:13195D13.DAT	4/ 07/2000	3.1809E-02	0.031811719	-0.1	0.7	detrital
			A:13195D14.DAT	4/ 07/2000	3.1798E-02	0.031810246	-0.4	0.8	detrital
			A:13195D15.DAT	4/ 07/2000	3.1775E-02	0.031810154	-1.1	0.9	detrital
			A:13195D16.DAT	4/ 07/2000	3.1827E-02	0.031810062	0.5	1.1	detrital
			A:13195D17.DAT	4/ 07/2000	3.1807E-02	0.03180997	-0.1	0.9	detrital
			A:13195D18.DAT	4/ 07/2000	3.1828E-02	0.031809878	0.6	0.8	detrital
			A:13195D19.DAT	4/ 07/2000	3.1824E-02	0.031809786	0.4	0.9	detrital
			A:13195D20.DAT	4/ 07/2000	3.1803E-02	0.031809694	-0.2	0.9	detrital
			A:13195S1.DAT	4/ 07/2000	3.1879E-02	0.031809602	2.2	0.7	detrital
			A:13195S2.DAT	4/ 07/2000	3.1861E-02	0.03180905	1.6	0.6	detrital
			A:13195S3.DAT	4/ 07/2000	3.1801E-02	0.031808958	-0.3	0.8	detrital
			A:13195S4.DAT	4/ 07/2000	3.1782E-02	0.031808866	-0.8	0.6	detrital
			A:13195S5.DAT	4/ 07/2000	3.1789E-02	0.031808774	-0.6	0.7	sponge
			A:13195S6.DAT	4/ 07/2000	3.1785E-02	0.031808682	-0.7	0.9	sponge
			A:13195S7.DAT	4/ 07/2000	3.1898E-02	0.03180859	2.8	0.9	sponge
			A:13195S8.DAT	4/ 07/2000	3.1920E-02	0.031808498	3.5	0.7	sponge
			A:13195S9.DAT	4/ 07/2000	3.1967E-02	0.031808406	5.0	0.7	sponge
			A:13195S10.DAT	4/ 07/2000	3.1894E-02	0.031807854	2.7	1.2	sponge
			A:13195S11.DAT	4/ 07/2000	3.1845E-02	0.031807762	1.2	0.8	sponge
			A:13195S12.DAT	4/ 07/2000	3.1915E-02	0.03180767	3.4	0.9	sponge
			A:13195S13.DAT	4/ 07/2000	3.1851E-02	0.031807578	1.4	0.7	sponge
			A:13195S14.DAT	4/ 07/2000	3.1855E-02	0.031807486	1.5	0.7	sponge
			A:13195S15.DAT	4/ 07/2000	3.1795E-02	0.031807394	-0.4	0.9	sponge
			A:13195S16.DAT	4/ 07/2000	3.1773E-02	0.031807302	-1.1	0.8	sponge
			A:13195S17.DAT	4/ 07/2000	3.1842E-02	0.03180721	1.1	0.8	sponge
			A:13195S18.DAT	4/ 07/2000	3.1821E-02	0.031806841	0.4	0.7	sponge
			A:13195S19.DAT	4/ 07/2000	3.1851E-02	0.031806749	1.4	0.9	sponge
			A:13195S20.DAT	4/ 07/2000	3.1964E-02	0.031806657	4.9	0.9	sponge

Table 27 Continued.

Field	Reservoir	Sample depth (m TVD)	Analysis number	Date	Raw $^{30}Si/^{28}Si$ x1000	Corr. $^{30}Si/^{28}Si$ x1000	$\delta^{30}Si$ (‰)	Error (‰)	Comment
Kingfisher	Brae II	3989.7	A:13143A1.DAT	6/ 07/2000	3.1740E-02	0.031826638	-2.7	0.9	authigenic
			A:13143A2.DAT	6/ 07/2000	3.1758E-02	0.03182621	-2.1	0.7	mix
			A:13143A3.DAT	6/ 07/2000	3.1760E-02	0.031825782	-2.1	0.9	authigenic
			A:13143A4.DAT	6/ 07/2000	3.1738E-02	0.031825355	-2.8	0.8	authigenic
			A:13143A5.DAT	6/ 07/2000	3.1753E-02	0.031824927	-2.2	0.9	authigenic
			A:13143A6.DAT	6/ 07/2000	3.1808E-02	0.031824499	-0.5	0.7	authigenic
			A:13143A7.DAT	6/ 07/2000	3.1790E-02	0.031824071	-1.1	0.8	mix
			A:13143A8.DAT	6/ 07/2000	3.1799E-02	0.031814661	-0.5	0.7	authigenic
			A:13143A9.DAT	6/ 07/2000	3.1827E-02	0.031812094	0.5	0.8	authigenic
			A:13143A10.DAT	6/ 07/2000	3.1785E-02	0.031811666	-0.8	0.8	authigenic
			A:13143A11.DAT	6/ 07/2000	3.1807E-02	0.031811238	-0.1	0.7	mix
			A:13143A12.DAT	6/ 07/2000	3.1804E-02	0.031810811	-0.2	0.9	authigenic
			A:13143A13.DAT	6/ 07/2000	3.1762E-02	0.031810383	-1.5	0.8	authigenic
			A:13143A14.DAT	6/ 07/2000	3.1811E-02	0.031809955	0.0	0.8	mix
			A:13143A15.DAT	6/ 07/2000	3.1746E-02	0.031803539	-1.8	0.7	authigenic
			A:13143A16.DAT	6/ 07/2000	3.1791E-02	0.0318014	-0.3	0.8	authigenic
			A:13143A17.DAT	6/ 07/2000	3.1795E-02	0.031800972	-0.2	0.8	authigenic
			A:13143A18.DAT	6/ 07/2000	3.1750E-02	0.031800544	-1.6	1.0	authigenic
			A:13143A19.DAT	6/ 07/2000	3.1746E-02	0.031800117	-1.7	0.6	authigenic
			A:13143A20.DAT	6/ 07/2000	3.1763E-02	0.031799689	-1.2	0.7	authigenic
			A:13143A21.DAT	7/ 07/2000	3.1755E-02	0.0318515	-3.0	1.1	authigenic
			A:13143D1.DAT	6/ 07/2000	3.1833E-02	0.031827066	0.2	0.8	detrital
			A:13143D2.DAT	6/ 07/2000	3.1846E-02	0.03182236	0.7	0.8	detrital
			A:13143D3.DAT	6/ 07/2000	3.1815E-02	0.031821932	-0.2	0.8	detrital
			A:13143D4.DAT	6/ 07/2000	3.1769E-02	0.031821505	-1.7	0.8	detrital
			A:13143D5.DAT	6/ 07/2000	3.1767E-02	0.031821077	-1.7	0.8	detrital
			A:13143D6.DAT	6/ 07/2000	3.1766E-02	0.031820649	-1.7	0.7	detrital
			A:13143D7.DAT	6/ 07/2000	3.1760E-02	0.031820221	-1.9	0.9	detrital
			A:13143D8.DAT	6/ 07/2000	3.1775E-02	0.031819794	-1.4	0.7	detrital
			A:13143D9.DAT	6/ 07/2000	3.1749E-02	0.031819366	-2.2	0.7	detrital
			A:13143D10.DAT	6/ 07/2000	3.1799E-02	0.031817655	-0.6	0.7	detrital
			A:13143D11.DAT	6/ 07/2000	3.1802E-02	0.031815516	-0.4	0.9	detrital
			A:13143D12.DAT	6/ 07/2000	3.1804E-02	0.031815088	-0.3	0.7	detrital
			A:13143D14.DAT	6/ 07/2000	3.1793E-02	0.031809527	-0.5	0.7	detrital
			A:13143D15.DAT	6/ 07/2000	3.1801E-02	0.0318091	-0.2	0.8	detrital
			A:13143D16.DAT	6/ 07/2000	3.1763E-02	0.031801828	-1.2	0.9	detrital
			A:13143D17.DAT	6/ 07/2000	3.1807E-02	0.031799261	0.2	0.8	detrital
			A:13143D18.DAT	6/ 07/2000	3.1731E-02	0.031797978	-2.1	1.0	detrital
			A:13143D19.DAT	7/ 07/2000	3.1830E-02	0.031849059	-0.6	1.1	detrital
			A:13143D20.DAT	7/ 07/2000	3.1786E-02	0.031849872	-2.0	1.1	detrital
			A:13143D21.DAT	7/ 07/2000	3.1831E-02	0.031850686	-0.6	0.9	detrital
			A:13143S1.DAT	6/ 07/2000	3.2021E-02	0.031817227	6.4	0.8	sponge
			A:13143S2.DAT	6/ 07/2000	3.1984E-02	0.031816799	5.3	0.8	sponge
			A:13143S3.DAT	6/ 07/2000	3.1965E-02	0.031816372	4.7	1.0	sponge
			A:13143S4.DAT	6/ 07/2000	3.1995E-02	0.031815944	5.6	0.8	sponge
			A:13143S5.DAT	6/ 07/2000	3.2019E-02	0.031807389	6.7	0.9	sponge
			A:13143S6.DAT	6/ 07/2000	3.2036E-02	0.031806961	7.2	0.7	sponge
			A:13143S7.DAT	6/ 07/2000	3.1993E-02	0.031806533	5.8	0.7	sponge
			A:13143S8.DAT	6/ 07/2000	3.2022E-02	0.031806105	6.8	0.7	sponge
			A:13143S9.DAT	6/ 07/2000	3.1931E-02	0.031805678	3.9	0.8	sponge
			A:13143S10.DAT	6/ 07/2000	3.1928E-02	0.03180525	3.9	0.9	sponge
			A:13143S11.DAT	6/ 07/2000	3.1997E-02	0.031804822	6.1	0.9	sponge
			A:13143S12.DAT	6/ 07/2000	3.1944E-02	0.031804394	4.4	0.8	sponge
			A:13143S13.DAT	6/ 07/2000	3.1964E-02	0.031803967	5.0	0.9	sponge
			A:13143S14.DAT	6/ 07/2000	3.1898E-02	0.031798833	3.1	1.1	sponge
			A:13143S15.DAT	6/ 07/2000	3.1962E-02	0.031798406	5.1	1.2	sponge

Results The histograms shown in Fig.63 summarize the $\delta^{30}Si$ range of the micro-analyses of detrital (64 analyses) and authigenic quartz (50 analyses) carried out with the ion microprobe. The data from all three reservoirs display a similar range in values (Fig.63). In general, silicon isotopic compositions of both detrital and authigenic quartz range between –3 to +3 ‰ (Fig.63). The average $\delta^{30}Si$ of detrital and authigenic quartz is similar in all three reservoirs (Table 28) : –0.5±1.0 ‰ and –0.6±0.8 ‰ respectively in the Brae Unit 2 reservoir in the Miller Field; –0.4±1.2 ‰ and –0.3±1.2 ‰ respectively in the Brae Unit 1 reservoir in the Kingfisher Field; –0.9±0.9 ‰ and –1.3±1.0 ‰ respectively in the Brae Unit 2 reservoir in the Kingfisher Field. Silicon isotope analyses were also carried out in sponge spicules in the Brae Unit 1 (16 analyses) and Brae Unit 2 (15 analyses) reservoirs in the Kingfisher Field (Table 27). The silicon isotopic compositions of the sponge spicules are in both reservoirs very different from the silicon isotopic

compositions of detrital and authigenic quartz (Table 28). Average spicule $\delta^{30}Si$ in the Brae Unit 1 reservoir in the Kingfisher Field is 1.7±1.9 ‰ (Table 28). Average spicule $\delta^{30}Si$ in the Brae Unit 2 reservoir in the Kingfisher Field is 5.3±1.2 ‰ (Table 28). The range in measured $\delta^{30}Si$ values of sponge spicules is also different in the two samples analysed (Fig.64). Sponge spicules have a more positive silicon isotopic composition in the Brae Unit 2 reservoir in the Kingfisher Field (+3.1 to +7.2 ‰) than in the Brae Unit 1 reservoir in the Kingfisher Field (–1.1 to +5.0 ‰) (Fig.64).

Table 28 Average (± standard deviation) $\delta^{30}Si$ values in detrital quartz, authigenic quartz and sponge spicules in each reservoir examined.

Field	Reservoir	Sample depth (m TVD)	average $\delta^{30}Si$ ± st.dev. (‰) detrital quartz	average $\delta^{30}Si$ ± st.dev. (‰) authigenic quartz	average $\delta^{30}Si$ ± st.dev. (‰) sponges
Miller	Brae II	4039.6	-0.5 ± 1.0	-0.6 ± 0.8	no data
Kingfisher	Brae I	3904.2	-0.4 ± 1.2	-0.3 ± 1.2	1.7 ± 1.9
Kingfisher	Brae II	3989.7	-0.9 ± 0.9	-1.3 ± 1.0	5.3 ± 1.2

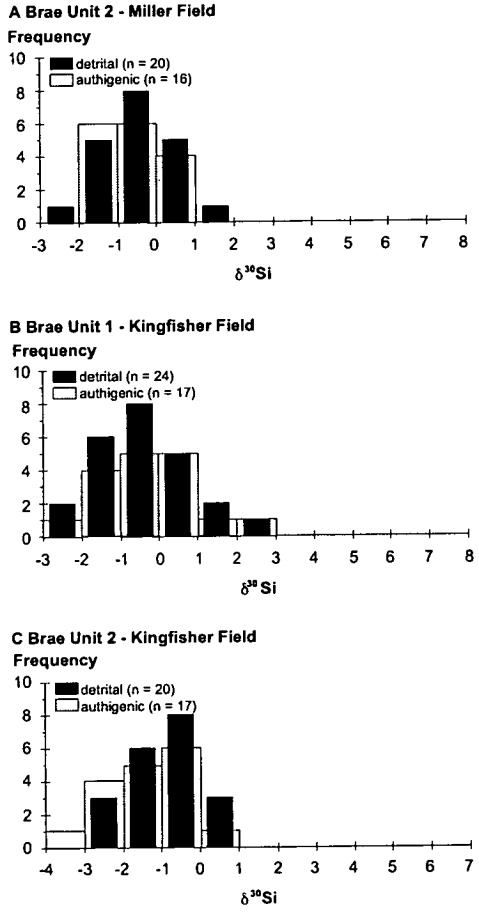

Fig.63 Histograms showing the distribution of silicon isotopic compositions of detrital and authigenic quartz in samples from the Brae Formation sandstones. Silicon isotopic compositions of detrital and authigenic quartz overlap in all three reservoirs.

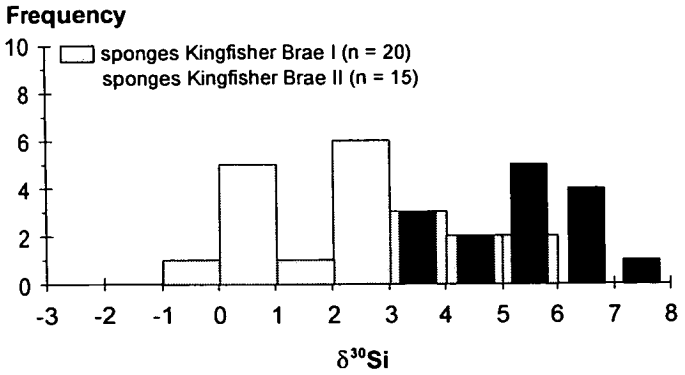

Fig.64 Histogram showing the distribution of silicon isotopic compositions of sponge spicules in samples from the Brae Formation sandstones. Silicon isotopic compositions of sponges from the Brae Unit 1 reservoir are different than the silicon isotopic compositions of sponges from the Brae Unit 2 reservoir in the Kingfisher Field.

Interpretation of results Silicon isotope analysis results of igneous and volcanic rocks, published by Douthitt (1982), display a range in values from –0.7 to +0.3 ‰ (mean –0.4±0.2 ‰) and from –0.7 to +0.2 ‰ (mean –0.1±0.2 ‰) respectively. No silicon isotope compositions for metamorphic rocks were found in the literature. The range of silicon isotope compositions in detrital quartz from the Brae Formation sandstones is interpreted to reflect the variability of $\delta^{30}Si$ for quartz in source materials. The mean $\delta^{30}Si$ detrital quartz value in the Brae Unit 2 reservoir in the Miller Field (–0.5±1.0 ‰) is similar to the mean $\delta^{30}Si$ detrital quartz value in the Brae Unit 1 reservoir in the Kingfisher Field (–0.4±1.2 ‰). The mean $\delta^{30}Si$ detrital quartz value in the Brae Unit 2 reservoir in the Kingfisher Field is slightly lower (–0.9±0.9 ‰) in comparison to the mean $\delta^{30}Si$ detrital quartz values in the other two reservoirs. However, the spread in measured $\delta^{30}Si$ in detrital quartz is similar in all three reservoirs studied (Fig.63). Therefore, the mean $\delta^{30}Si$ detrital quartz value in the Brae Unit 2 reservoir in the Kingfisher Field most likely appears different due to the small number of analyses.

Statistical t-tests indicate there is 65 to 60 % confidence that the $\delta^{30}Si$ of detrital quartz is similar to the $\delta^{30}Si$ of authigenic quartz in the Brae Unit 2 and Brae Unit 1 reservoirs in the Miller and Kingfisher Fields respectively (Table 29). The similarity in silicon isotope composition of detrital and authigenic quartz indicates that dissolved detrital quartz in pore-fluids most likely was the silica source for quartz cementation in these reservoirs. The degree of confidence that the $\delta^{30}Si$ of detrital quartz is similar to the $\delta^{30}Si$ of authigenic quartz in the Brae Unit 2 reservoir in Kingfisher is lower (29 %; Table 29). The mean $\delta^{30}Si$ authigenic quartz value

(–1.3±1.0 ‰) in this reservoir is lower than the mean δ^{30}Si detrital quartz value (–0.9±0.9 ‰). However, the spread in measured δ^{30}Si in authigenic quartz is similar to the spread in measured δ^{30}Si in detrital quartz (Fig.63C). Therefore, the different mean δ^{30}Si values for detrital and authigenic quartz in this reservoir may simply be due to the limited number of analyses.

In the literature, relatively large fractionations of silicon isotopes are reported to occur in low temperature (<50 °C) opaline sinters and biogenic opal such as sponge spicules, diatoms and cherts (Reynolds & Verhoogen, 1953; Allenby, 1954; Tilles, 1961; Douthitt, 1982; De La Rocha et al., 2000). Published silicon isotope values of opaline sinter (–0.8±1.1 ‰; Douthitt, 1982) and sponge spicules (–2.1±1.0 ‰; Douthitt, 1982) both show moderately variable but consistently negative δ^{30}Si values and are interpreted to be indicative of a kinetic fractionation upon precipitation of opal from dissolved silicon (Tilles, 1961; Douthitt, 1982). Silicon isotope compositions of sponge spicules in the Brae Formation sandstones are, on the contrary, consistently ^{30}Si-enriched (mean values of 1.7±1.9 ‰ and 5.3±1.2 ‰ in the Brae Unit 1 and Brae Unit 2 reservoirs in the Kingfisher Field respectively). The sputter pits in the spicules were double-checked under the optical microscope and with the SEM in order to find out if possibly any contamination with underlying glass or resin had occurred during analysis. However, the ion probe pits look normal (Fig.65). Analysis of a pure glass slide, carried out by Dr. Craven, gave δ^{30}Si values of –4.9±0.3 ‰ confirming that no contamination with glass occurred. Douthitt (1982) noted that different taxa of sponges have distinct δ^{30}Si values. Considering the small amount of δ^{30}Si values of sponge spicules available in the literature, it is perhaps not surprising that silicon isotope values of sponge spicules in the Brae Formation sandstones, which come from a different area and are probably from different taxa than the sponges discussed in the literature, are different. Silicon isotope compositions of sponge spicules in the Brae Formation sandstones are, in any case, very different to the measured δ^{30}Si values of authigenic quartz. Statistical t-tests indicate there is 100 % confidence that the δ^{30}Si of authigenic quartz is different to the δ^{30}Si of sponges in the Brae Unit 1 and Brae Unit 2 reservoirs in the Kingfisher Field (Table 29). This confirms petrographic observations that sponge spicules are not a significant source for quartz cement in the Brae Formation sandstones.

Table 29 Statistical t-test results on silicon isotope data. There is 65 and 60 % confidence for the silicon isotope signatures of authigenic and detrital quartz to be similar in the Brae Formation Unit 2 and Unit 1 reservoirs in the Miller and Kingfisher Fields respectively (blue colour). In the Brae Formation Unit 2 reservoir in the Kingfisher Field, there is only 29 % confidence for the silicon isotope signatures of authigenic and detrital quartz to be similar (blue colour). The degree of confidence that the silicon isotope signatures of authigenic quartz and sponge spicules is similar, is zero (green colour).

Statistics	Miller Brae Unit 2 DQ	Miller Brae Unit 2 AQ	Miller Brae Unit 2 S	Kingfisher Brae Unit 1 DQ	Kingfisher Brae Unit 1 AQ	Kingfisher Brae Unit 1 S	Kingfisher Brae Unit 2 DQ	Kingfisher Brae Unit 2 AQ	Kingfisher Brae Unit 2 S
Mean	-0.5	-0.6	no	-0.4	-0.3	1.7	-0.9	-1.3	5.3
Standard deviation	1.0	0.8	data	1.2	1.2	1.9	0.9	1.0	1.2
Number of analyses	20	16		24	17	16	20	17	15
t-stat significance DQ and AQ	65%			60%			29%		
t-stat significance AQ and S	no data			0%			0%		

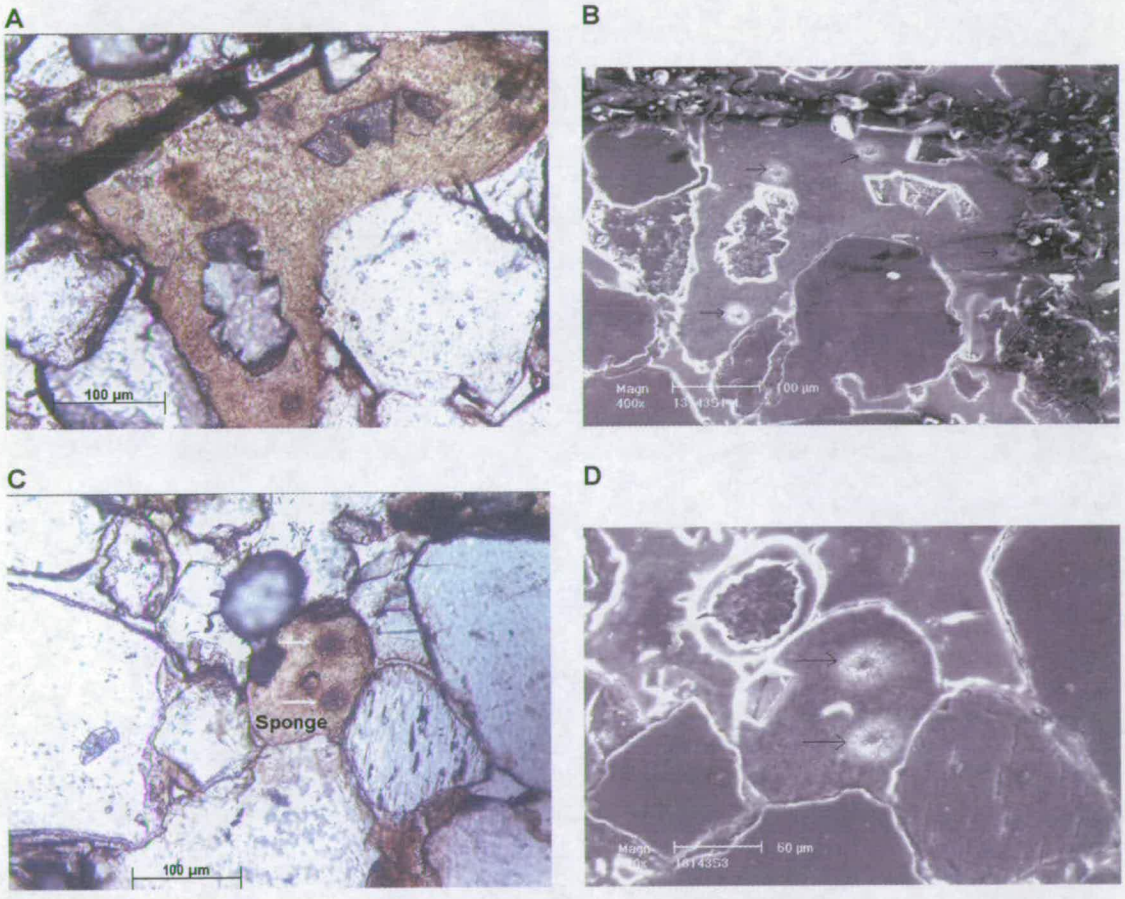

Fig.65 Paired optical microscopy and SEM photomicrographs of ion microprobe pits in sponge spicules.
(**A** and **B**) Four ion microprobe pits (arrows) are visible in the spicule in sample 13143 (3989.7 m, Brae Unit 2 reservoir, Kingfisher Field). The $\delta^{30}Si$ values range between +4.7 and +6.4 ‰.
(**C** and **D**) Two ion microprobe pits (arrows) are visible in the spicule in sample 13143 (3989.7 m, Brae Unit 2 reservoir, Kingfisher Field). The $\delta^{30}Si$ values are +5.8 and +6.8 ‰.

8.4 Discussion

In this Chapter, the following internal silica sources were considered for quartz cementation in the Brae Formation sandstones : dissolution of K-feldspars, dissolution of biogenic silica (sponge spicules) and pressure dissolution of quartz at grain contacts or stylolites. In this discussion, silica dissolved in meteoric water and silica released from interbedded shales during compaction will also be considered (external silica sources).

I concluded in Chapter 7, based on oxygen isotope analyses of early calcite and quartz cements, that meteoric-type fluids were present during shallow burial (<1500 m) in the Brae Formation. This burial depth corresponds with temperatures up to 60 to 70 °C (Appendix D). According to Blatt (1979), meteoric water is normally supersaturated with silica. However, according to Bjørlykke & Egeberg (1993), temperatures are generally too low for quartz cementation at depths where meteoric water flushing is significant. As mentioned in Chapter 3, early circulation of meteoric water in sandstones can result in feldspar dissolution during shallow burial (temperatures between 20-55 °C) (Glasmann, 1992). Also the dissolution of biogenic silica may occur at relatively low temperature (<60 °C) (Vagle et al., 1994). The early diagenetic dissolution of K-feldspar and biogenic spicules by meteoric water may have caused supersaturation of silica in the pore-fluids. This could in turn have led to the precipitation of the small amounts of early quartz cements observed in the Brae Formation sandstones. According to the results of quartz cementation modelling in the Brae Formation sandstones (Chapter 6), the amounts of quartz cement precipitated at burial depths <1500 m (<70 °C) are low (<1 %). Considering the small contribution of dissolved sponge spicules to the overall silica budget needed to explain total quartz cement abundances in the Brae Formation sandstones, it is not surprising that statistical t-tests indicate no correlation between $\delta^{30}Si$ of authigenic quartz and $\delta^{30}Si$ of the sponge spicules (Table 29).

With increasing burial depth and temperature (>1500 m and >70 °C), quartz cements progressively precipitated from fluids which became more ^{18}O-enriched relative to meteoric-type fluids (Chapter 7). The bulk of the quartz cements observed in the Brae Formation sandstone reservoirs were precipitated during deeper burial and temperatures >90 °C. Petrographic observations of quartz dissolution in the sandstones and in small laminae of fine-grained argillaceous sandstones interbedded with the reservoir rocks (Figs. 60 and 61) indicate that silica for quartz cementation could have been sourced from quartz dissolution internally in

the Brae Formation. Because of the limited number of thin sections available from fine-grained argillaceous sandstones in the Brae Formation, and because quantifying pressure solution is problematic, no attempt was made to mass-balance silica derived from internal pressure solution with quartz cement abundances in the thin sections examined. However, silicon isotope analysis results indicate that the $\delta^{30}Si$ of detrital quartz is similar to the $\delta^{30}Si$ of authigenic quartz (65 and 60 % confidence for the Brae Unit 2 and Brae Unit 1 reservoirs in the Miller and Kingfisher Fields respectively, 29 % confidence for the Brae Unit 2 reservoir in the Kingfisher Field; Table 29). The confidence degrees, obtained from statistical t-tests, indicate that detrital quartz is a very likely, but perhaps not the only, source of silica for quartz cementation. Porosity and permeability in the Brae Formation sandstones at deeper burial are not likely to permit advective fluid flow and, therefore, the transport mechanism of silica is considered to be diffusion. These findings are in agreement with theoretical models (e.g. Oelkers et al., 1996; Walderhaug, 1996; Bjørkum et al., 1998) that most of the silica for quartz cementation is derived mainly on a local scale (pressure dissolution). In these theoretical models, silica diffuses from the site of dissolution to nearby precipitation sites.

Another potential silica source during burial diagenesis is the transformation of smectite to illite (at temperatures >90 to 100 °C). This transformation releases silica according to the reaction (Boles & Franks, 1979) :

$$\text{smectite} + K^{+} \rightarrow \text{illite} + H_4SiO_4 + \text{cations (Ca, Mg, Na, Fe)}$$

This reaction could occur within the sandstones themselves or within adjacent mudrocks. Within the Brae Formation sandstones there is hardly any illite (<1 %) observed. Silica released from clay mineral reactions in adjacent mudstones could be transported into the sandstones via localised diffusion or advection (e.g. Sullivan & McBride, 1991) and provide an additional silica source. Gluyas et al. (2000) concluded, based on geochemical analyses of mudrocks, that the mudstones that are interbedded with the Brae Formation sandstones in the Miller Field contain less silica than mudstones that occur above the Brae Formation. Gluyas et al. (2000) infer this to indicate that the Kimmeridge Clay mudstones interbedded in the reservoir exported silica into the sandstones during diagenesis. Because no stylolites or grain-to-grain pressure dissolution were observed in the Brae Formation sandstones of the Miller Field by Gluyas et al. (2000), these authors attributed all silica exported from the mudrocks into the sandstones to clay mineral reactions in the mudrocks. This is clearly in contradiction with observations of pressure

dissolution features, in the sandstones as well as in interbedded argillaceous sandstones (Figs. 60 and 61), and silicon isotope results documented in this thesis. Therefore, it seems more plausible to regard silica supplied from clay transformation reactions in the mudrocks interbedded with the Brae Formation sandstones as an additional (rather than only) source of silica for quartz cementation. Because the Brae Unit 2 reservoir in the Kingfisher Field has a lower net:gross ratio (0.48; Chapter 2) than the other 2 reservoirs examined (~0.75; Chapter 2), clay mineral reactions may have been a more important source for silica in this reservoir than in the other two Brae Formation reservoirs (Brae Unit 2 in the Miller Field and Brae Unit 1 in the Kingfisher Field). This could explain why statistical t-tests of silicon isotope results indicate a lower degree of confidence (29 %) in the similarity of the $\delta^{30}Si$ of detrital quartz to the $\delta^{30}Si$ of authigenic quartz in this reservoir than in the other two reservoirs examined (60 to 65 %; Table 29).

8.5 Conclusions

1 The following sources of silica are considered for quartz cementation in the Brae Formation sandstone reservoirs : K-feldspar and sponge spicule dissolution and pressure dissolution of quartz at grain contacts or stylolites as internal sources; meteoric water and silica released from interbedded shales during compaction as external sources.

2 Petrographic observations and mass balance calculations indicate that only a small proportion of the quartz cements can be sourced from K-feldspar and sponge spicule dissolution. This dissolution occurred most likely during shallow burial when the sandstones were open to meteoric water through-flow. Because meteoric water is usually supersaturated with silica, the silica released from K-feldspar and sponge spicule dissolution may have been sufficient to explain precipitation of the small amounts of quartz cements (<1 %) in the reservoirs during shallow burial (<1.5 km).

3 The bulk of the quartz cements in the Brae Formation sandstones were precipitated during deeper burial and temperatures >90 °C. There is abundant evidence in the sandstones, and in small laminae of interbedded argillaceous sandstones, of grain-to-grain pressure dissolution and stylolites. Consequently, the quartz cements observed in the reservoirs studied are thought to be sourced from these mechanisms. Clay mineral reactions in

mudstones interbedded with the reservoir rocks are also considered to have attributed to the silica budget in the sandstones.

4 Statistical t-tests of silicon isotope results indicate that the $\delta^{30}Si$ of detrital quartz is similar to the $\delta^{30}Si$ of authigenic quartz in the Brae Unit 2 and Brae Unit 1 reservoirs in the Miller and Kingfisher Fields respectively (65 and 60 % confidence respectively). The similarity in silicon isotope compositions of detrital and authigenic quartz confirms that dissolved detrital quartz in pore-fluids is a very likely source of silica for quartz cementation during deeper burial (>2500 m) in these reservoirs. The lower degree of confidence (29 %) in the similarity of the $\delta^{30}Si$ of detrital quartz to the $\delta^{30}Si$ of authigenic quartz in the Brae Unit 2 reservoir in the Kingfisher Field indicates that quartz dissolution is perhaps not the main silica supplying process in this reservoir. Considering the low net:gross ratio of the Brae Unit 2 reservoir in the Kingfisher Field (0.48), clay mineral reactions in the interbedded mudrocks are very likely to be an important source of silica for quartz cementation in the sandstones. Because porosity and permeability in the Brae Formation sandstones at deeper burial (>2500 m) are not likely to permit advective fluid flow, the most likely transport mechanism of silica is via diffusion.

5 It should be emphasized that, due to the small number of samples analyzed, the silicon isotope results presented in this Chapter are not conclusive. However, these initial results do indicate that silicon isotopes have potential to contribute useful information to questions such as origins of silica for quartz cementation. However, more analyses of different possible source materials are needed (e.g. clay minerals, meteoric waters, biogenic silica).

CHAPTER IX

DIAGENESIS AND POROSITY PRESERVATION IN DEEPWATER OILFIELD SANDSTONES

The Miller and Kingfisher Fields are producing hydrocarbon fields with combined estimated reserves of around 300 MMbbl. Both fields are located along the western margin of the South Viking Graben in blocks 16/7 and 16/8 of the North Sea (Fig.1B). The hydrocarbon reservoirs are located in the Upper Jurassic Brae Formation sandstones, which interbed with Kimmeridge Clay source rocks. The Brae Formation sandstones were deposited as a complex of submarine fans (Fig.3). The oil reservoirs in the Miller and Kingfisher Fields are located in the Brae Unit 2 sandstones, which were deposited during Early to Middle Volgian times. Despite sharing a communal reservoir (Brae Unit 2), the oil accumulations in the Miller and Kingfisher Fields are structurally separated from each other by a syncline (Fig.7). A gas condensate reservoir also occurs in the Kingfisher Field; this is located in the younger Brae Unit 1 sandstones, which were deposited during the Middle Volgian. The Brae Unit 1 gas condensate reservoir is separated from the Brae Unit 2 oil reservoir in the Kingfisher Field by interbedded Kimmeridge Clay Formation mudstones (Fig.8).

The Miller Field is situated in mid-fan deposits and net:gross in the oil-bearing reservoir is typically greater than 0.75. The reservoirs in the Kingfisher Field are located in distal fan deposits. The net:gross ratios in the oil and gas condensate reservoirs in this field are 0.48 and 0.75 respectively.

All Brae Formation samples examined in this study are from the lithofacies which makes up the actual reservoir rock. This lithofacies is, in both fields, composed of clean, fine- to medium-grained sandstone beds of up to 30 m in thickness. The thin sections examined plot within the arenite, subarkose or sublith-arenite area of McBride's sandstone classification system (1963) (Fig.14). Samples from all three reservoirs are mineralogically and texturally homogeneous regardless their position in the reservoir (oil or water zone). The sandstones are mainly composed of quartz (84.2±9.0 %), detrital clay (4.6±4.5 %), K-feldspar (2.8±1.0 %), rock fragments (3.5±1.7 %), organic material (3.3±2.6 %) and minor amounts of mica (0.9±0.7 %). The sands are generally medium-grained (323±66 μm) and moderately sorted.

The Brae Formation sandstones underwent continuous burial, since time of deposition until the present, in both the Miller and Kingfisher Fields (Fig.36). The oil-bearing Brae Unit 2 reservoirs in the Miller and Kingfisher Fields are buried to similar depths and temperatures (~4 km and ~120 °C). The oil in those reservoirs was locally sourced from interbedded Kimmeridge Clay layers (MacKenzie et al., 1987). Maturity calculations for the Kimmeridge Clay source rocks in the Miller and Kingfisher Fields indicate oil generation from around 40 and 15 Ma respectively (Fig.38). Because migration distances are short, the timing of source rock maturity can be used as an indication of the timing of hydrocarbon emplacement in the Brae Unit 2 reservoirs. The Brae Unit 1 gas condensate reservoir in the Kingfisher Field is presently buried to ~3.8 km (~115 °C). The hydrocarbons in this reservoir are thought to have migrated from source rocks deeper in the graben (MacKenzie et al., 1987; Reitsema, 1983). Due to lack of information about this kitchen area it was not possible to calculate source rock maturity. However, petrographic and fluid inclusion data suggest that hydrocarbon emplacement in the Brae Unit 1 reservoir took place around 40 to 30 Ma.

Apart from localized early diagenetic calcite cementation, compaction and quartz cementation were the main causes of porosity loss during burial in the Brae Formation reservoirs. Mechanical compaction was active from the time of deposition of the sands until stable packing configuration of detrital grains was achieved. This stabilization of grain configuration occurred when porosities were ~25-30 % at around 1500-2000 m burial depth (~70 °C) (Tables D4 and D5). Small quantities of early quartz cements (<70 °C) may have aided stabilization of the sandstone framework and reduction of porosity-loss by mechanical compaction.

Microcrystalline quartz, which occurs as polynuclear coatings on the surfaces of detrital quartz grains, represents the earliest stage of nucleation of quartz crystals in the Brae Formation sandstones. Intergrowth of microquartz crystals led subsequently to formation of bigger overgrowths (Fig.26). Other evidence of early quartz cementation is the presence of overgrowths on detrital quartz grains in calcite cemented sandstones (Zone B2; Fig.55C). Measured $\delta^{18}O$ compositions between +23 and +26 ‰ (Fig.54) in quartz cements are compatible with precipitation from meteoric-type fluids (~–7 ‰; Hamilton et al., 1987) at temperatures <70 °C (Fig.56B). Also, the oxygen isotope compositions of early calcite cement ($\delta^{18}O$ ~+20 ‰; Appendix B) point to the presence of meteoric-type fluids (~–7 ‰; Hamilton et al., 1987) at temperatures <70 °C (Appendix B). Considering the marine depositional environment of the sandstones studied, the presence of waters with oxygen isotopic composition similar to meteoric water in the Brae Formation implies that the sandstones were open to surface water recharge. The high porosities (~25 to 30 %), and also permeabilities, in the sandstones during shallow burial (<1500 m) are likely to have permitted advective flow of meteoric fluids from the graben margin during the early stages of diagenesis (<70 °C).

The lowest homogenization temperatures measured in fluid inclusions in quartz cements are around 70 °C in all three reservoirs examined (Fig.30). This indicates that the initiation of the main phase of quartz cementation occurred around burial depths of ~1500 m. Because only a few measurements in fluid inclusions yielded temperatures around 70 °C it is most likely that, initially, only small amounts of quartz cements were precipitated. The early overgrowths are usually thin (<20 μm) and display heterogeneous cathodoluminescence patterns (Zone A cements) (Fig.55). Oxygen isotopic compositions of Zone A quartz cements (+15 to +18 ‰; Table 22) are best explained by precipitation from pore-fluids which evolved in composition from meteoric-type fluids (~–7 ‰; Hamilton et al., 1987) to more ^{18}O-enriched fluids (–5 to –2 ‰) during burial from 1500 to 3000 m (70-95 °C). Such a shift in pore-fluid isotopic composition is also reflected in calcite cement $\delta^{18}O$ compositions (~+16 ‰; Appendix B). The shift in estimated porewater oxygen isotope signatures, from ~–7 to ~–2 ‰, during burial of the sandstones from ~1500 to ~3000 m may be explained by mixing of the meteoric-type fluids (–7 ‰; Hamilton et al., 1987) with basinal-type fluids (+2 to +5 ‰; Egeberg & Aagaard, 1989, Wilkinson et al., 1992) originating from deeper in the basin. A mixing of meteoric fluids with deep basinal saline fluids may also explain the high salinity of fluid

inclusions (15-25 wt% NaCl eq) measured in quartz cements which formed between 70-95 °C (Fig.33). As mentioned in Chapter 4, the origin of the high salinity fluids may be attributed to dissolution of salts occurring in deeper parts of the basin.

In all the Brae Formation reservoirs studied, the bulk of the quartz cements precipitated from around 90-95 °C onwards. These overgrowths (Zone B2) have homogeneous cathodoluminescence patterns and can be up to 50 μm thick (Fig.55D). There are no distinct fluid inclusion temperature populations (Fig.30), which could potentially distinguish the two different cathodoluminescence zones (A and B) as different episodes of quartz cementation, and so it is thought that quartz cementation in the Brae Formation sandstones was more or less a continuous process. The different luminescence patterns of Zone A and Zone B quartz cements are thought to be caused by fluid compositional changes during burial. A change in reservoir hydrogeology around 90-95 °C is recorded in the oxygen isotope compositions of the quartz cements (Fig.56) and in the fluid inclusion salinities (Fig.33). Measured $\delta^{18}O$ compositions between +16 and +22 ‰ (Table 22) in Zone B quartz cements (>95 °C) are best explained by precipitation from fluids which became increasingly ^{18}O-enriched during progressive burial and increasing temperatures up to 120 °C (i.e. from ~–3 ‰ around 3000 m burial to ~+1 ‰ at present day burial ~4000 m). The progressive enrichment of ^{18}O in the porewaters indicates an increase in rock-water interaction. Decreasing porosities at greater depths, and also petroleum emplacement in the Brae Unit 2 reservoir in the Miller Field and the Brae Unit 1 reservoir in the Kingfisher Field, will cause the oxygen isotopic composition of the pore-fluids to become rock-buffered. Rock-water interactions which are generally cited to explain the increase in $\delta^{18}O$ values of pore-fluids include illitisation and/or chloritisation of kaolinite and smectite clays formed by low temperature weathering (Wilkinson et al., 1992), and/or recrystallisation of early formed carbonates (Saigal & Bjørlykke, 1987). The shale dehydration reactions may also have diluted the high salinity fluids initially present in the reservoirs and may have caused the salinity of fluid inclusions incorporated in quartz cement to drop to values comparable to present day formation water (5-10 wt% NaCl eq).

Petrographic mass-balance calculations indicate that only a fraction of the total quartz cements observed in Brae Formation sandstone samples could be sourced from feldspar and sponge spicule dissolution (Fig.57 and Table 26). Dissolution of

feldspar and sponges is reported to take place at temperatures <60 °C (Glasmann, 1992; Vagle et al., 1994). The Brae Formation sandstones were open to meteoric water through-flow during shallow burial (<1500 m) and temperatures <70 °C (Chapter 7). Considering that meteoric waters are usually supersaturated with silica themselves (Blatt, 1979), the additional silica released into the pore-fluids from dissolution of K-feldspars and spicules may have caused small amounts of quartz cement (<1 %) to precipitate.

The bulk of the quartz cements in the Brae Formation sandstones were precipitated during deeper burial and temperatures >90 °C. Petrographic observations of grain-to-grain pressure dissolution and stylolites in all three reservoirs studied, as well as in argillaceous sandstones interbedded with the reservoir sandstones, indicate that quartz dissolution processes were the main sources of silica for quartz cementation during deeper burial (Figs. 60 and 61). Statistical t-tests indicate there is 65 to 60 % confidence that the δ^{30}Si of detrital quartz is similar to the δ^{30}Si of authigenic quartz in the Brae Unit 2 and Brae Unit 1 reservoirs in the Miller and Kingfisher Fields respectively (Table 29). The degree of confidence that the δ^{30}Si of detrital quartz is similar to the δ^{30}Si of authigenic quartz in the Brae Unit 2 reservoir in the Kingfisher Field is considerably less (29 %) (Table 29). Because this reservoir contains a considerable amount of interbedded shale layers (net:gross ratio 0.48), it is possible that clay mineral reactions provided an additional source of silica in this reservoir.

Quartz cementation in sandstones during burial is usually viewed as being composed of three linked steps : A) dissolution of a silica source; B) silica transportation by diffusion to the site of precipitation; C) quartz cement precipitation. Whichever of these steps is the slowest will be rate-limiting, dictating the overall rate of quartz cementation (Lasaga and Kirkpatrick, 1981). Worden et al. (1998) hypothesized that in water-filled sands, quartz cementation will probably be precipitation-rate controlled. If the water in the pore-space within a sandstone becomes gradually replaced by oil, through which silica transport rates by diffusion are negligible, a critical point will be reached where silica diffusion is so slow that the quartz cementation reaction will become transport-rate controlled (Worden et al., 1998). At high oil saturations, quartz cementation could be virtually halted.

Petrographic and fluid inclusion data from the reservoirs in the Miller and Kingfisher Fields provide excellent empirical evidence for the retarding effect of hydrocarbons on quartz cementation. In the crestal areas of the Brae Unit 2 reservoir in the Miller

Field and throughout the oil zone of the Brae Unit 1 reservoir in the Kingfisher Field, which both charged with oil around 40-30 Ma, porosities are high (25-30 %) and quartz cement abundances low (<5 %) (Figs. 23 and 24). Maximum fluid inclusion temperatures measured in samples from these areas are around 95-105 °C (Figs. 30 and 31). This temperature was reached around 40 to 45 Ma in the reservoirs (Fig.39), and coincides with the oil emplacement times. Increasing quartz cement abundances (up to 10 %), and fluid inclusion temperatures which approach present day reservoir temperature (~120 °C), in the reservoir oil zone suggest a gradual oil-fill over a prolonged period of time in the Miller Field (Figs. 24 and 30). Oil emplacement in the Brae Unit 2 reservoir in the Kingfisher Field was a more recent event (~15 Ma) (Fig.38). As a result, quartz cement is abundant throughout this reservoir (~12 %) and measured fluid inclusion temperatures (up to 118 °C) approach present day reservoir temperatures (~120 °C) (Figs. 24 and 30). The aquifers of the Brae Unit 2 reservoirs in both the Miller and Kingfisher Fields, which remained hydrocarbon-free throughout their burial history, consistently display the highest quartz cement abundances (up to 15 %) (Fig.24). Fluid inclusion temperatures which equal present day reservoir temperatures confirm unhindered cementation until present day burial depths in the reservoir aquifers (Fig.30).

Some researchers have inferred that oil emplacement has little or no effect on quartz cementation (Oelkers et al., 1992; Walderhaug, 1996; Bjørkum et al., 1998). This is a view based on examples of reservoirs which do not show a significant difference in volumes of cement between oil and water zones and on the occurrence of oil-bearing fluid inclusions entrapped in quartz cement. The first of these arguments can be dismissed because the timing of oil emplacement is crucial. If oil emplacement was a recent event in a reservoir, as is the case in the Brae Unit 2 reservoir in the Kingfisher Field, there is no reason why rocks in the oil and water zones should have different quantities of quartz cement. The second argument, the occurrence of petroleum fluid inclusions in quartz cements, is proof that some oil was present at the time that quartz cement was growing but is not conclusive evidence that cement can grow at irreducible water saturations (Worden & Morad, 2000). In the Brae Formation sandstones, petroleum inclusions are rare and occur either as single inclusions in detrital quartz grains or as lines of inclusions in microfractures (Fig.35). The lack of primary oil inclusions in quartz overgrowths in the samples examined indicates that the entrapment of petroleum inclusions was

not contemporaneous with extensive quartz cementation. This agrees with the hypothesis of Worden et al. (1998) that entrapment of petroleum in inclusions in quartz cements most likely occurs when water saturation in the reservoirs is high and silica diffusion rates are not significantly reduced by the presence of hydrocarbons (e.g. during the earlier stages of oil emplacement or on migration routes). The relationship between quartz cement abundance and petroleum emplacement times (Fig.40) in the Brae Formation reservoirs indicates that, with rising oil saturation, quartz cementation in the oil zone sandstones was strongly inhibited by oil emplacement compared to the underlying aquifer sandstones.

Quartz cementation is considered to have been a more or less continuous process in the Brae Formation sandstones. Therefore, it should be straightforward to quantitatively model the cementation process with software such as Exemplar™. However, because the software does not incorporate the retarding effect of hydrocarbon emplacement on quartz cementation, quartz cement abundances are over-predicted (and porosities under-predicted) in areas of reservoirs which have been filled with hydrocarbons for a considerable period of time (i.e. crestal areas of the Brae Unit 2 reservoir in the Miller Field and the Brae Unit 1 reservoir in the Kingfisher Field) (Fig.42). Kinetic modelling of the quartz cementation process in the Brae Formation sandstones suggests that progressive oil charge has slowed quartz cement growth rates by at least 2 orders of magnitude. Average quartz precipitation rates are in the order of magnitude of 10^{-22} moles/cm^2.s in areas which had high oil saturations (80 %) over a prolonged period of time such as the oil zones of the Brae Unit 2 and Brae Unit 1 reservoirs in the Miller and Kingfisher Fields respectively (Fig.45). In reservoir aquifers, or areas with low oil saturation (e.g. transition zones), average quartz precipitation rates are in the order of magnitude of 10^{-20} moles/cm^2.s (Fig.45). In the most extreme cases, e.g. in the crestal areas of the Brae Unit 2 reservoir in the Miller Field where oil charged earliest, quartz cementation was halted completely (zero precipitation rates) (Fig.45). These modelling results are extremely valuable for improving the capacity of software packages such as Exemplar™ to predict porosity in deeply buried structures, and to predict porosity differences between oil and water zones within individual fields.

Results presented in this thesis offer a valuable petrographic and geochemical dataset from the Brae Formation sandstone reservoirs in the Miller and Kingfisher Fields. In these sandstones, occlusion of sandstone porosity by quartz cementation occurred gradually over a long period of time during continuous burial, except where quartz cementation was hindered by oil emplacement. The Brae Formation sandstones initially were open to external advective through-flow of meteoric water. The silica source for early quartz cementation was dissolution of K-feldspars and sponge spicules, or silica dissolved in the meteoric waters themselves. During the later stages of burial (>2.5 to 3 km), closed-system conditions prevailed and fluids evolved towards a basinal-type fluid oxygen isotope composition. Petrographic observations and silicon isotope analyses are consistent with theoretical models (e.g. Oelkers et al., 1996; Walderhaug, 1996; Bjørkum et al., 1998) that most of the silica for quartz cementation was derived on a local scale mainly from mud-rich parts of the same formation (pressure dissolution and clay mineral reactions). In these theoretical models, silica diffuses from the site of dissolution to nearby precipitation sites. Oil emplacement can slow down the rate of quartz cementation by at least two orders of magnitude. The insights into oil zone quartz precipitation rates derived from this study improve the prospect for more accurate oil zone reservoir quality predictions.

REFERENCES

Aase N.E., Bjorkum P.A. & Nadeau P.H. (1996) The effect of grain-coating microquartz on preservation of reservoir porosity. AAPG Bulletin, v.80, p.1654-1673.

Allenby R.J. (1954) Determination of the isotopic ratios of silicon in rocks. Geochimica et Cosmochimica Acta, v.5, p.40-48.

Aplin A.C. & Warren E.A. (1994) Oxygen isotopic indications of the mechanisms of silica transport and quartz cementation in deeply buried sandstones. Geology, v.22, p.847-850.

Atkins J.E. & McBride E.F. (1992) Porosity and packing of Holocene river, dune and beach sands. AAPG Bulletin, v.76, p.339-355.

Baldwin B. & Butler C.O. (1985) Compaction curves. AAPG Bulletin, v.69, p.622-626.

Barclay S.A. & Worden R.H. (2000) Geochemical modelling of diagenetic reactions in a sub-arkosic sandstone. Clay Minerals, v.35, p.57-67.

Barclay S.A. & Worden R.H. (2000bis) Effects of reservoir wettability on quartz cementation in oil fields. In: Quartz cementation in sandstones (Worden R.H. & Morad S., Eds.), Spec. Publ. International Association of Sedimentologists, no.29, p.103-117.

Basin modelling system software manual. Platte River Associates, Inc., Denver, USA.

Beard D.C. & Weyl P.K. (1973) Influence of texture on porosity and permeability of unconsolidated sand. AAPG Bulletin, v.57, no.2, p.349-369.

Bjørkum P.A., Walderhaug O. & Aase N.E. (1993) A model for the effect of illitisation on porosity and quartz cementation of sandstones. Journal of Sedimentary Research, v.A63, no.6, p.1089-1091.

Bjørkum P.A. (1996) How important is pressure in causing dissolution of quartz in sandstones? Journal of Sedimentary Research, v.66, no.1, p.147-154.

Bjørkum P.A., Oelkers E.H., Nadeau P.H., Walderhaug, O. & Murphy W.M. (1998) Porosity prediction in quartzose sandstones as a function of time, temperature, depth, stylolite frequency, and hydrocarbon saturation. AAPG Bulletin, v.82, no.4, p.637-648.

Bjørlykke K., Aagaard P., Dypvik H., Hastings D.S. & Harper A.S. (1986) Diagenesis and reservoir properties of Jurassic sandstones from the Haltenbanken area, offshore mid-Norway. In: Habitat of hydrocarbons on the Norwegian continental shelf (Spencer A.M., Holter E., Campell C.J., Hanslien S.H., Nelson

P.H.H., Nysaether E. & Ormaasen E.G., Eds.), Graham and Trotman, London, p.275-286.

Bjørlykke K., Ramm M. & Saigal G. (1989) Sandstone diagenesis and porosity modification during basin evolution. Geologisches Rundschau, v.78, p.243-268.

Bjørlykke K., Nedkvitne T., Ramm M. & Saigal G.C. (1992) Diagenetic processes in the Brent Group (Middle Jurassic) reservoirs of the North Sea: an overview. In: Geology of the Brent Group (Morton A.C., Haszeldine R.S., Giles M.R. & Brown S., Eds.), Geological Society of London Spec. Publ., no.61, p.263-287.

Bjørlykke K. (1993) Fluid flow in sedimentary basins. Sedimentary Geology, v.86, p.137-158.

Bjørlykke K. & Egeberg P.K. (1993) Quartz cementation in sedimentary basins. AAPG Bulletin, v.77, no.9, p.1538-1548.

Bjørlykke K. (1994) Pore-water flow and mass transfer of solids in solution in sedimentary basins. In: Quantitative Diagenesis – Recent Developments and Applications to Reservoir Geology (Parker A. & Sellwood B.W., Eds.), Kluwer Academic Publishers, Netherlands, p.189-221.

Bjørlykke K., Aagaard P., Egeberg P.K. & Simmons S.P. (1995) Geochemical constraints from formation water analyses from the North Sea and the Gulf Coast Basins on quartz, feldspar and illite precipitation in reservoir rocks. In: The Geochemistry of Reservoirs (Cubitt J.M. & England W.A., Eds.), Geological Society Special Publication, no.86, p.33-50.

Blatt H. (1979) Diagenetic processes in sandstones. SEPM Spec. Publ., no.26, p.141-157.

Blatt H. (1987) Oxygen isotopes and the origin of quartz. Journal of Sedimentary Petrology, v.57, no.2, p.373-377.

Bloch S., McGowen J.H., Duncan J.R. & Brizzolara D.W. (1990) Porosity prediction, prior to drilling, in sandstones of the Kekiktuk Formation (Mississippian), North slope of Alaska. AAPG Bulletin, v.74, p.1371-1385.

Bloch S. (1991) Empirical prediction of porosity and permeability in sandstones. AAPG Bulletin, v.75, p.1145-1160.

Bodnar R.J. & Bethke P.M. (1984) Systematics of stretching of fluid inclusions I: fluorite and sphalerite at 1 atmosphere confining pressure. Economic Geology, v.78, p.535-542.

Bodnar R.J. (1990) Petroleum migration in the Miocene Monterey Formation, California, USA: constraints from fluid inclusion studies. Mineralogical Magazine, v. 54, p.295-304.

Bodnar R.J. (1992) Current research on fluid inclusions – a brief introduction. Geochimica et Cosmochimica Acta, v.56, no.1, p.3-3.

Boles J.R. & Franks S.G. (1979) Clay diagenesis in Wilcox sandstones of Southwest Texas: implications of smectite diagenesis on sandstone cementation. Journal of Sedimentary Petrology, v.49, p.55-70.

Brigaud F. & Vasseur G. (1989) Mineralogy, porosity and fluid control on thermal conductivity of sedimentary rocks. Geophysical Journal, v.98, p.525-542.

Brint J.F., Hamilton P.J., Haszeldine R.S., Fallick A.E. & Brown S. (1991) Oxygen isotopic analysis of diagenetic quartz overgrowths from the Brent sands : a comparison of two preparation methods. Journal of Sedimentary Petrology, v.61, no.4, p.527-533.

Burley S.D., Mullis J. & Matter A. (1989) Timing diagenesis in the Tartan reservoir (UK North Sea): constraints from combined cathodoluminescence microscopy and fluid inclusion studies. Marine and Petroleum Geology, v.6, p.98-120.

Burley S.D. (1993) Models of burial diagenesis for deep exploration plays in Jurassic fault traps of the Central and Northern North Sea. In: Petroleum Geology of Northwest Europe: Proceedings of the 4th Conference (Parker J.R., Ed.), Geological Society of London, p.1353-1375.

Burruss R.C. (1987) Diagenetic palaeotemperatures from aqueous fluid inclusions: reequilibration of inclusions in carbonate cements by burial heating. Mineralogical Magazine, v.51, p.477-481.

Canals M. & Meunier J.D. (1995) A model for porosity reduction in quartzite reservoirs by quartz cementation. Geochimica et Cosmochimica Acta, v.59, no.4, p.699-709.

Cornford C., Morrow J.A., Turrington A., Miles J.A. & Brooks J. (1983) Some geological controls on oil composition in the UK North Sea. In: Petroleum Geochemistry and Exploration of Europe (Brooks J., Ed.), Geological Society of London Spec. Publ., no.12, p.175-194.

Deegan C.E. & Scull B.J. (1977) A standard lithostratigraphic nomenclature for the central and northern North Sea. Bulletin of the Norwegian Petroleum Directorate, v.1, p.1-36.

De La Rocha C.L., Brzezinski M.A. & DeNiro M.J. (2000) A first look at the distribution of the stable isotopes of silicon in natural waters. Geochimica et Cosmochimica Acta, v.64, no.14, p.2467-2477.

Dixon S.A., Summers D.M. & Surdam R.C. (1989) Diagenesis and preservation of porosity in Norphlet Formation (Upper Jurassic), Southern Alabama. AAPG Bulletin, v.73, p.707-728.

Douthitt C.B. (1982) The geochemistry of the stable isotopes of silicon. Geochimica et Cosmochimica Acta, v.46, p.1449-1458.

Egeberg P.K. & Aagaard P. (1989) Origin and evolution of formation waters from oil fields on the Norwegian shelf. Applied Geochemistry, v.4, p.131-142.

Ehrenberg S.N. (1990) Relationship between diagenesis and reservoir quality in sandstones of the Garn Formation, Haltenbanken, mid-Norwegian continental shelf. AAPG Bulletin, v. 74, p.1538-1558.

Ehrenberg S.N. (1993) Preservation of anomalously high porosity in deeply buried sandstones by grain-coating chlorite: examples from the Norwegian continental shelf. AAPG Bulletin, v.77, no.7, p.1260-1286.

Eiler J.M., Valley J.W., Graham C.M. & Baumgartner L.P. (1995) Ion microprobe evidence for the mechanisms of stable isotope retrogression in high grade metamorphic rocks. Contributions to Mineralogy and Petrology, v.118, p.365-378.

ElectroScan Corporation (1996) Environmental Scanning Electron Microscopy – an introduction to ESEM. Robert Johnson Associates, El Dorado Hills, 55p.

Elsenheimer D. & Valley J.W. (1993) Submillimeter zonation of $\delta^{18}O$ in quartz and feldspar, Isle of Skye, Scotland. Geochimica et Cosmochimica Acta, v.57, p.3669-3676.

Emery D., Smalley P.C. & Oxtoby N.H. (1993) Synchronous oil migration and cementation in sandstone reservoirs demonstrated by quantitative description of diagenesis. Phil. Trans. R. Soc. London , v.344, p.115-125.

Evans J., Hogg A.J.C., Hopkins M.S. & Howarth R.J. (1994) Quantification of quartz cements using SEM, CL, and image analysis. Journal of Sedimentary Research, v.A64, no.2, p.334-338.

Folk R.L (1966) A review of grain-size parameters. Sedimentology, v.6, p.73-93.

Friedman M. (1954) Miocene orthoquartzite from New Jersey. Journal of Sedimentary Petrology, v.24, p.235-241.

Friedman I. & O'Neil J.R. (1977) Compilation of stable isotope fractionation factors of geochemical interest. In: Data of Geochemistry 6th Edition (Fleischer M., Ed.), United States Geological Survey Professional Paper, v.440-kk, 12p.

Galloway W.E. (1984) Hydrogeologic regimes of sandstone diagenesis. In: Clastic Diagenesis (McDonald D.A. & Surdam R.C., Eds.), AAPG Memoir, no.37, p.3-13.

Garland C.R. (1993) Miller Field: reservoir stratigraphy and its impact on development. In: Petroleum Geology of Northwest Europe: Proceedings of the 4th Conference (Parker J.R., Ed.), p.401-414.

Garland C.R., Haughton P., King R.F. & Moulds T.P. (1999) Capturing reservoir heterogeneity in a sand-rich submarine fan, Miller Field. In: Petroleum Geology of Northwest Europe: Proceedings of the 5th Conference (Fleet A.J. & Boldy S.A.R., Eds.), p.1199-1208.

Giles M.R., Stevenson S., Martin S.V., Cannon S.J.C., Hamilton P.J., Marshall J.D. & Samways G.M. (1992) The reservoir properties and diagenesis of the Brent Group: a regional perspective. In: Geology of the Brent Group (Morton A.C.,

Haszeldine R.S., Giles M.R. & Brown S., Eds.), Geological Society of London Spec. Publ., no.61, p.289-327.

Giles M.R., Indrelid S.L., Beynon G.V. & Amthor J. (2000) The origin of large-scale quartz cementation: evidence from large data sets and coupled heat-fluid mass transport modelling. In: Quartz Cementation in Sandstones (Worden R.H. & Morad S., Eds.), Spec. Publ. International Association of Sedimentologists, no.29, p.21-38.

Glassman J.R. (1992) The fate of feldspar in the Brent Group reservoirs, North Sea: a regional synthesis of diagenesis in shallow, intermediate and deep burial environments. In: Geology of the Brent Group (Morton A.C., Haszeldine R.S., Giles M.R. & Brown S., Eds.), Geological Society of London Special Publication, no.61, p.329-350.

Glennie K.W. (1984) Structural framework and pre-Permian history of the North Sea area. In: Introduction to the Petroleum Geology of the North Sea (Glennie K.W., Ed.), Blackwell Oxford, p.17-39.

Gluyas J. & Coleman M. (1992) Material flux and porosity changes during sediment diagenesis. Nature, v.356, p.52-54.

Gluyas J.G., Robinson A.G., Emery D., Grant S.M. & Oxtoby N.H. (1993) The link between petroleum emplacement and sandstone cementation. In: Petroleum Geology of NW-Europe (Parker J.R., Ed.), Geological Society of London, p.1395-1402.

Gluyas J.& Cade C.A. (1997) Prediction of porosity in compacted sands. In: Reservoir Quality Prediction in Sandstones and Carbonates (Kupecz, J.A., Gluyas J. & Bloch S., Eds.), AAPG Memoir, no.69, p.19-28.

Gluyas J., Garland C., Oxtoby N.H. & Hogg A.J.C. (2000) Quartz cement : the Miller's tale. In: Quartz cementation in sandstones (Worden R.H. & Morad S., Eds.), Spec. Publ. International Association of Sedimentologists, no.29, p.199-218.

Goldstein R.H. (1986) Reequilibration of fluid inclusions in low-temperature calcium-carbonate cement. Geology, v.14, p.792-795.

Goldstein R.H. & Reynolds T.J. (1992) Systematics of fluid inclusions in diagenetic minerals – notes for a short course. Short Course on Fluid Inclusions in Sedimentary Rocks, Newcastle Research Group, August 17-20, p.64.

Graham C.M., Valley J.W. & Winter B.L. (1996) Ion microprobe analysis of $^{18}O/^{16}O$ in authigenic and detrital quartz in the St. Peter Sandstone, Michigan Basin and Wisconsin Arch, USA : Contrasting diagenetic histories. Geochimica et Cosmochimica Acta, v.60, no.24, p.5101-5116.

Hagemann H.W. & Hollerbach A. (1985) The fluorescence behaviour of crude oils with respect to their thermal maturation & degradation. Organic Geochemistry, v.10, p.473-480.

Hamilton P.J., Fallick A.E., Macintyre R.M. & Elliott S. (1987) Isotopic tracing of the provenance and diagenesis of Lower Brent Group Sands, North Sea. In: Petroleum

Geology of Northwest Europe (Brooks J. & Glennie K., Eds.), Graham & Trotman, London, p.939-949.

Hanor J.S. (1980) Dissolved methane in sedimentary brines : potential effect on the PVT properties of fluid inclusions. Economic Geology, v.75, p.603-609.

Hardy J.A. & Hart R.G. (1994) The North Brae Field. In: North Sea Formation Water Atlas (Warren E.A. & Smalley P.C., Eds.), Geological Society Memoir, no.15, p.54.

Harms J.C., Tackenberg P., Pickles E. & Pollock R.E. (1981) The Brae oilfield area. In: Petroleum Geology of the Continental Shelf of north-west Europe (Illing L.V. & Hobson G.D., Eds.), Heyden London, p.352-357.

Harrison W.J. & Tempel R.N. (1993) Diagenetic pathways in sedimentary basins. In: Diagenesis and Basin Development (Horbury A. & Robinson A., Eds.), AAPG Studies in Geology, v.36. p.69-86.

Hartmann B.H., Juhasz-Bodnar, K., Ramseyer K. & Matter A. (2000) Polyphased quartz cementation and its sources: a case study from the Upper Palaeozoic Haushi Group sandstones, Sultanate of Oman. In: Quartz cementation in sandstones (Worden R.H. & Morad S., Eds.), Spec. Publ. International Association of Sedimentologists, no.29, p.253-270.

Haszeldine R.S., Samson I.M. & Cornford C. (1984) Dating diagenesis in a petroleum basin, a new fluid inclusion method. Nature, v.307, p.354-357.

Haszeldine R.S., Samson I.M. & Cornford C. (1984bis) Quartz diagenesis and convective fluid movement; Beatrice Oilfield, UK North Sea. Clay Minerals, v.19, p.391-402.

Haszeldine R.S., Brint J.F., Fallick A.E., Hamilton P.J. & Brown S. (1992) Open and restricted hydrologies in Brent Group diagenesis : North Sea. In: Geology of the Brent Group (Morton A.C., Haszeldine R.S., Giles M.R. & Brown S., Eds.), Geological Society of London Special Publication, v.61, p.401-419.

Hayes J.B. (1979) Sandstone diagenesis – the hole truth. SEPM Spec. Publ., no.26, p.127-139.

Heald M.T. (1955) Stylolites in sandstones. Journal of Geology, v.63, no.2, p.101-114.

Heald M.T. (1959) Significance of stylolites in permeable sandstones. Journal of Sedimentary Petrology, v.29, p.251-253.

Heald M.T. & Larese R.E. (1974) Influence of coatings on quartz cementation. Journal of Sedimentary Petrology, v.44, no.4, p.1269-1274.

Hendry J.P. & Trewin N.H. (1995) Authigenic quartz microfabrics in Cretaceous turbidites: evidence for silica transformation processes in sandstones. Journal of Sedimentary Research, v.65, p.380-392.

Hodgson N.A., Farnsworth J. & Fraser A.J. (1992) Salt-related tectonics, sedimentation and hydrocarbon plays in the Central Graben, North Sea, UKCS. In: Exploration Britain : Geological Insights for the Next Decade (Hardman R.F.P., Ed.), Geological Society of London Special Publication, v.67, p.31-63.

Hogg A.J.C., Sellier E. & Jourdan A.J. (1992) Cathodoluminescence of quartz cements in Brent Group sandstones, Alwyn South, UK North Sea. In: Geology of the Brent Group (Morton A.C., Haszeldine R.S., Giles M.R. & Brown S., Eds.), Geological Society of London Special Publication, v.61, p.421-440.

Hogg A.J.C., Garland C.R. & Oxtoby N.H. (1993) The origin and distribution of high permeability sandstones in the Miller Field reservoir (UKCS Blocks 16/7b and 16/8b). BP internal report RDB/31/92.

Houseknecht D.W. (1987) Assessing the relative importance of compaction processes and cementation to reduction of porosity in sandstones. AAPG Bulletin, v.71, no.6, p.633-642.

Houseknecht D.W. (1988) Intergranular pressure solution in four quartzose sandstones. Journal of Sedimentary Petrology, v.58, no.2, p.228-246.

Iliffe J.E. & Dawson M.R. (1996) Basin modelling history and predictions. In: NW Europe's Hydrocarbon Industry (Glennie K. & Hurst A., Eds.), Geological Society of London, p.83-105.

Jourdan A., Thomas M. & Brevart O. (1987) Diagenesis as the control of the Brent sandstone reservoir properties in the Greater Alwyn area (East Shetland Basin). In: Petroleum Geology of Northwest Europe (Brooks J. & Glennie K.W., Eds.), Graham & Trotman, London, p.951-961.

Kerlogue A., Cherry S., Davies H., Quine M. & Spotti G. (1994) The Tiffany and Toni oil fields, Upper Jurassic submarine fan reservoirs, South Viking Graben, UK North Sea. Petroleum Geoscience, v.1, p.279-285.

Land L.S. & Dutton S.P. (1978) Cementation of Pennsylvanian deltaic sandstone: isotopic data. Journal of Sedimentary Petrology, v.48, p.1167-1176.

Land L.S. & Fisher R.S. (1987) Wilcox sandstone diagenesis, Texas Gulf coast : a regional isotopic comparison with the Frio Formation. In: Diagenesis of Sedimentary Sequences (Marshall J.D., Ed.), Geological Society of London Spec. Publ., no.36, p.219-235.

Lander R.H. & Walderhaug O. (1999) Predicting porosity through simulating sandstone compaction and quartz cementation. AAPG Bulletin, v.83, no.3, p.433-449.

Lasaga A. & Kirkpatrick R.J. (1981) Kinetics of geochemical processes. Reviews in Mineralogy, v.8, Mineralogical Society of America.

Leder F. & Park W.C. (1986) Porosity reduction in sandstones by quartz overgrowth. AAPG Bulletin, v.70, p.1713-1728.

Lee M. & Savin S.M. (1985) Isolation of diagenetic overgrowths on sand grains for oxygen isotope analysis. Geochimica et Cosmochimica Acta, v.49, p.664-669.

Lemée C. & Guéguen Y. (1996) Modelling porosity loss during compaction and cementation of sandstones. Geology, v.24, no.10, p.875-878.

Lewis S. (1999) Metamorphic fluid flow and stable isotope modification in marble : an example from Naxos, Greece. PhD thesis, Department of Geology and Geophysics , University of Edinburgh, 350p.

Lisk M., Eadington P.J. & O'Brien G.W. (1998) Unravelling complex filling histories by constraining the timing of events which modify oil fields after initial charge. In: Dating and Duration of Fluid Flow and Fluid-Rock Interaction (Parnell J., Ed.), Geological Society of London, Special Publication, v.144, p.189-203.

Longstaffe F.J. (1989) Stable isotopes as tracers in clastic diagenesis. In: Short Course in Burial Diagenesis (Hutcheon I.E., Ed.), Mineralogical Association of Canada Short Course Series, v.15, p.201-277.

Lopatin N.V. (1971) Temperature and geologic time as factors in coalification. Izvestiya Akademii Nauk. SSSR (Ser. Geol.), v.3, p.95-106.

Lyon I.C., Burley S.D., McKeever P.J., Saxton J.M. & Macaulay C. (2000) Oxygen isotope analysis of authigenic quartz in sandstones : a comparison of ion microprobe and conventional analytical techniques. In: Quartz cementation in sandstones (Worden R.H. & Morad S., Eds.), Spec. Publ. International Association of Sedimentologists, no.29, p.299-316.

Macaulay C.I., Haszeldine R.S. & Fallick A.E. (1992) Diagenetic pore waters stratified for at least 35 million years: Magnus Oilfield, North Sea. AAPG Bulletin, v.76, no.10, p.1625-1634.

Macaulay C.I., Haszeldine R.S. & Fallick A.E. (1993) Textural and isotopic variations in diagenetic kaolinite from the Magnus Oilfield sandstones. Clay Minerals, v.28, p.625-639.

Macaulay C.I., Boyce A.J., Fallick A.E. & Haszeldine R.S. (1997) Quartz veins record vertical flow at a graben edge : Fulmar Oil Field, Central North Sea. AAPG Bulletin, v.81, no.12, p.2024-2035.

Macaulay C.I., Fallick A.E., Haszeldine R.S. & Graham C.M. (2000) Methods of laser-based stable isotope measurement applied to diagenetic cements and hydrocarbon reservoir quality. Clay Minerals, v.35, p.313-322.

MacKenzie A.S., Price, I., Leythaeuser D., Muller P., Radke M. & Schaefer R.G. (1987) The expulsion of petroleum from Kimmeridge Clay source-rocks in the area of the Brae Oilfield, UK continental shelf. In: Petroleum Geology of North West Europe (Brooks J. & Glennie K., Eds.), Graham & Trotman, p.865-877.

Marchand A.M.E., Haszeldine R.S., Macaulay C.I., Swennen R. & Fallick A.E. (2000) Quartz cementation inhibited by crestal oil charge: Miller deep water sandstone, UK North Sea. Clay Minerals, v.35, p.205-214.

Matsuhisa Y., Goldsmith J.R. & Clayton R.N. (1979) Oxygen isotopic fractionation in the system quartz-albite-anorthite-water. Geochimica et Cosmochimica Acta, v.43, p.1131-1140.

McAulay G.E., Burley S.D., Fallick A.E. & Kusznir N.J. (1994) Palaeohydrodynamic fluid flow regimes during diagenesis of the Brent Group in the Hutton-NW Hutton reservoirs : constraints from oxygen isotope studies of authigenic kaolin and reverse flexural modelling. Clay Minerals, v.29, p.609-626.

McBride E.F. (1963) A classification of common sandstones. Journal of Sedimentary Petrology, v.33, p.664-669.

McBride E.F. (1989) Quartz cement in sandstones : a review. Earth Science Reviews, v.26, p.69-112.

McBride E.F., Diggs T.N. & Wilson J.C. (1990) Compaction of Wilcox and Carrizo sandstones (Paleocene-Eocene) to 4420 m, Texas Gulf Coast. Journal of Sedimentary Petrology, v.61, p.73-85.

McClure N.M. & Brown A.A. (1990) Miller Field : a subtle Upper Jurassic submarine fan trap in the South Viking Graben, UK Sector North Sea. In: Giant Oil and Gas Fields of the Decade 1978-1988 (Halburty M.T., Ed.), AAPG Memoir, no.54, p.307-322.

McCrea J.M. (1950) On the isotope chemistry of carbonates and a paleotemperature scale. Journal of Chemical Physics, v.18, p.849-857.

McLaughlin O.M. (1992) Isotopic and textural evidence for diagenetic fluid mixing in the South Brae oilfield, North Sea. PhD thesis, Department of Geology and Applied Geology, University of Glasgow, 298p.

McLaughlin O.M., Haszeldine R.S., Fallick A.E. & Rogers G. (1994) The case of the missing clay, aluminium loss and secondary porosity, South Brae oilfield, North Sea. Clay Minerals, v.29, p.651-663.

McLaughlin O.M., Haszeldine R.S. & Fallick A.E. (1996) Quartz diagenesis in layered fluids in the South Brae oilfield, North Sea. SEPM Spec. Publ., no.55, p.103-113.

McLimans R.K. (1987) The application of fluid inclusions in migration of oil and diagenesis in petroleum reservoirs. Applied Geochemistry, v.2, p.585-603.

Midtbø R.E.A., Rykkje J.M. & Ramm M. (2000) Deep burial diagenesis and reservoir quality along the eastern flank of the Viking Graben. Evidence for illitisation and quartz cementation after hydrocarbon emplacement. Clay Minerals, v.35, p.227-237.

Milliken K.L., Land L.S. & Loucks R.G. (1981) History of burial diagenesis determined from isotopic geochemistry, Frio Formation, Brazoria County, Texas. AAPG Bulletin, v.65, p.1397-1413.

Milliken K.L., McBride E.F. & Land L.S. (1989) Numerical assessment of dissolution versus replacement in the subsurface destruction of detrital feldspars, Oligocene Frio Formation, South Texas. Journal of Sedimentary Petrology, v.59, p.740-757.

Mullis A.M. (1993) Determination of the rate-limiting mechanism for quartz pressure dissolution. Geochimica et Cosmochimica Acta, v.57, p.1499-1503.

Munz I.A., Johansen H., Holm K. & Lacharpagne J.-C. (1999) The petroleum characteristics and filling history of the Frøy field and the Rind discovery, Norwegian North Sea. Marine and Petroleum Geology, v.16, p.633-651.

Murphy W.M., Oelkers E.H. & Lichtner P.C. (1989) Surface reaction versus diffusion control of mineral dissolution and growth rates in geochemical processes. Chemical Geology, v. 78, p.357-380.

Oelkers E.H., Bjørkum P.A. & Murphy W.M. (1992) The mechanisms of porosity reduction, stylolite development and quartz cementation in North Sea sandstones. In: Water-Rock Interactions (Kharaka Y.K. & Maest A.S., Eds.), Balkema Rotterdam, p.1183-1186.

Oelkers E.H., Bjørkum P.A. & Murphy W.M. (1996) A petrographic and computational investigation of quartz cementation and porosity reduction in North Sea sandstones. American Journal of Science, v.296, p.420-452.

Oelkers E.H., Bjørkum P.A., Walderhaug, O., Nadeau, P.H. & Murphy W.M. (2000) Making diagenesis obey thermodynamics and kinetics: the case of quartz cementation in sandstones from offshore mid-Norway. Applied Geochemistry, v.15, p.295-309.

Olsen E., Jahren J. & Bjørlykke K. (1996) Preservation of anomalously high porosity in deeply buried sandstones by grain-coating chlorite. Abstract Volume of the Rosenqvist Symposium on Clay Minerals in the Modern Society, Oslo, p.44.

Osborne M. & Haszeldine R.S. (1993) Evidence for resetting of fluid inclusion temperatures from quartz cement in oilfields. Marine and Petroleum Geology, v.10, p.271-278.

Oxtoby N.H., Mitchell A.W. & Gluyas J.G. (1995) The filling and emptying of the Ula oilfields: fluid inclusion constraints. In: The geochemistry of reservoirs (Cubitt J.M. & England W.A., Eds.), Geological Society Special Publication, no.86, p.141-157.

Paxton S.T., Szabo, J.O., Calvert C.S. & Ajdukiewicz, J.M. (1990) Preservation of primary porosity in deeply buried sandstones: a new play concept from the Cretaceous Tuscaloosa Sandstone of Louisiana (Abs.). AAPG Bulletin, v.74, p.737.

Pittman E.D. & Larese R.E. (1991) Compaction of lithic sands: experimental results and applications. AAPG Bulletin, v.75, no.8, p.1279-1299.

Porter E.W. & James W.C. (1986) Influence of pressure, salinity, temperature and grain size on silica diagenesis in quartzose sandstones. Chemical Geology, v.57, p.359-369.

Prezbindowski D.R. & Larese R.E. (1987) Experimental stretching of fluid inclusions in calcite – Implications for diagenetic studies. Geology, v.15, p.333-336.

Primmer T.J., Cade C.A., Evans J., Gluyas J.G., Hopkins M.S., Oxtoby N.H., Smalley P.C., Warren E.A. & Worden R.H. (1997) Global patterns in sandstone diagenesis: their application to reservoir quality prediction for petroleum exploration. In: Reservoir Quality Prediction in Sandstones and Carbonates (Kupecz J.A., Gluyas J. & Bloch S., Eds.), AAPG Memoir, no.69, p.61-78.

Prosser D.J., McKeever M.E., Hogg A.J.C. & Hurst A. (1995) Permeability heterogeneity within massive Jurassic submarine fan sandstones from the Miller Field, northern North Sea, UK. In: Characterisation of Deep Marine Clastic Systems (Hartley A.J. & Prosser D.J., Eds.), Geological Society of London Spec. Publ., no.94, p.201-219.

Ramm M. (1992) Porosity-depth trends in reservoir sandstones : theoretical models related to Jurassic sandstones, offshore Norway. Marine and Petroleum Geology, v.9, p.553-567.

Ramm M. & Bjørlykke K. (1994) Porosity-depth trends in reservoir sandstones: assessing the quantitative effects of varying pore-pressure, temperature history and mineralogy, Norwegian shelf data. Clay Minerals, v.29, p.475-490.

Ramm M., Forsberg A.W. & Jahren J.S. (1997) Porosity-depth trends in deeply buried Upper Jurassic reservoirs in the Norwegian Central Graben: an example of porosity preservation beneath the normal economic basement by grain-coating microquartz. In: Reservoir quality prediction in sandstones and carbonates (J.A. Kupecs, J. Gluyas, and S. Bloch, eds.), AAPG Memoir, no.69, p. 177-199.

Ramseyer K., Baumann J., Matter A. & Mullis J. (1988) Cathodoluminescence colours of a-quartz. Mineralogical Magazine, v.52, p.669-677.

Reitsema R.H. (1983) Geochemistry of North and South Brae areas, North Sea. In: Petroleum Geochemistry and Exploration of Europe (Brooks J., Ed.), Geological Society of London Spec. Publ., no.12, p.203-212.

Renard F., Brosse E. & Gratier J.P. (2000) The different processes involved in the mechanism of pressure solution in quartz-rich rocks and their interactions. In: Quartz cementation in sandstones (Worden R.H. & Morad S., Eds.), Spec. Publ. International Association of Sedimentologists, no.29, p.67-78.

Reynolds J.H. & Verhoogen J. (1953) Natural variations in the isotopic constitution of silicon. Geochimica et Cosmochimica Acta, v.3, p.224-234.

Roberts M.J. (1991) The South Brae Field, Block 16/7a, UK North Sea. In: United Kingdom Oil and Gas Fields, 25 Years Commemorative Volume (Abbotts I.L., Ed.), Geological Society Memoir, no.14, p.55-62.

Robie R.A.& Hemingway B.S. (1995) Thermodynamic properties of minerals and related substances at 298.15K and 1 bar (10^5 Pascals) pressure and higher temperatures. US Geological Survey Bulletin, v.2131, p.461.

Robinson A. & Gluyas J. (1992) Model calculations of loss of porosity in sandstones as a result of compaction and quartz cementation. Marine and Petroleum Geology, v.9, p.319-323.

Robinson A., Grant S. & Oxtoby N. (1992) Evidence against natural deformation of fluid inclusions in diagenetic quartz. Marine and Petroleum Geology, v.9, p.568-572.

Roedder E. (1979) Fluid inclusion evidence on the environments of sedimentary diagenesis, a review. SEPM Special Publication, no.26, p.89-107.

Roedder E. (1984) Fluid Inclusions. In: Reviews in Mineralogy v.12 (Ribbe P.H., Ed.), Mineralogical Society of America.

Rooksby S.K. (1991) The Miller Field, Blocks 16/7b, 16/8b, UK North Sea. In: United Kingdom Oil and Gas Fields, 25 Years Commemorative Volume (Abbotts I.L., Ed.), Geological Society Memoir, no.14, p.159-164.

Rutter E.H. (1976) The kinetics of rock deformation by pressure solution. Philosophical Transactions of the Royal Society of London, v.A283, p.203-220.

Saigal G.C. & Bjørlykke K. (1987) Carbonate cements in clastic reservoir rocks from offshore Norway – relationships between isotopic composition, textural developments and burial depth. In: Diagenesis of Sedimentary Sequences (Marshal J.D., Ed.), Geological Society Special Publication, no.36, p.313-324.

Saigal G.C., Morad S., Bjørlykke K., Egeberg P.K. & Aagaard P. (1988) Diagenetic albitisation of detrital K-feldspar in Jurassic, Lower Cretaceous, and Tertiary clastic reservoir rocks from offshore Norway, 1.Textures and origin. Journal of Sedimentary Petrology, v.58, p.1003-1013.

Saigal G.C., Bjørlykke K. & Larter S. (1992) The effects of oil emplacement on diagenetic processes – examples from the Fulmar reservoir sandstones, Central North Sea. AAPG Bulletin, v.76, no.7, p.1024-1033.

Scherer M. (1987) Parameters influencing porosity in sandstones: a model for sandstone porosity prediction. AAPG Bulletin, v.71, p.485-491.

Schmoker J.W. & Gautier D.L. (1988) Sandstone porosity as a function of thermal maturity. Geology, v.16, p.1007-1010.

Sclater J.G. & Christie P.A.F. (1980) Continental stretching: an explanation of the post-mid-Cretaceous subsidence of the Central North Sea Basin. Journal of Geophysical Research, v.85(B7), p.3711-3739.

Scotchman I., Johnnes L.H. & Miller R.S. (1989) Clay diagenesis and oil migration in Brent Group sandstones of NW Hutton Field, UK North Sea. Clay Minerals, v.24, p.339-374.

Selley R.C. (1978) Porosity gradients in the North Sea oil-bearing sandstones. Journal of the Geological Society of London, v.135, p.119-132.

Shackleton N.J. & Kennett J.P. (1975) Paleotemperature history of the Cenozoic and the initiation of Antarctic glaciation : oxygen and carbon analyses in DSDP sites 277, 279 and 281. In: Initial report DSDP 24 (Kennett J.P. & Howtz R.E., Eds.), Washington, p.653-659.

Sharp Z.D. (1990) A laser-based microanalytical method for the in situ determination of oxygen isotope ratios in silicates and oxides. Geochimica et Cosmochimica Acta, v.54, p.1353-1357.

Sibley D.F. & Blatt H. (1976) Intergranular pressure solution and cementation of the Tuscarora orthoquartzite. Journal of Sedimentary Petrology, v.46, p.881-896.

Siever R. (1957) Pennsylvanian sandstones of the Eastern Interior Coal Basin. Journal of Sedimentary Petrology, no.27, p.227-250.

Smalley P.C., Primmer T., Garland C., Oxtoby N. & Hopkins M. (1993) Miller Field: reservoir fluid communication and reservoir quality. BP internal report SST/16/93.

Smalley P.C. & Warren E.A. (1994) The Miller Field. In: North Sea Formation Water Atlas (Warren E.A. & Smalley P.C., Eds.), Geological Society Memoir, no.15, p.52.

Souza R.S. & McBride E.F. (2000) Diagenetic modelling and reservoir quality assessment and prediction : an integrated approach. AAPG Bulletin, v.84, no.9, p.1495.

Stephenson M.A. (1991) The North Brae Field, Block 16/7a, UK North Sea. In: United Kingdom Oil and Gas Fields, 25 Years Commemorative Volume (Abbotts I.L., Ed.), Geological Society Memoir, no.14, p.43-48.

Stoker S.J. & Brown S. (1986) Coarse clastic sediments of the Brae Field and adjacent areas, North Sea : a core workshop. British Geological Survey, Edinburgh.

Stow D.A.V., Bishop C.D. & Mills S.J. (1982) Sedimentology of the Brae oilfield, North Sea, fan models and controls. Journal of Petroleum Geology, v.5, no.2, p.129-148.

Sullivan M.D., Haszeldine R.S. & Fallick A.E. (1990) Linear coupling of carbon and strontium isotopes in Rotliegend Sandstone, North Sea : Evidence for cross-formational fluid flow. Geology, v.18, p.1215-1218.

Sullivan K.B. & McBride E.F. (1991) Diagenesis of sandstones at shale contacts and diagenetic heterogeneity, Frio Formation, Texas. AAPG Bulletin, v.75, no.1, p.121-138.

Tada R. & Seiver R. (1989) Pressure solution during diagenesis. Annual Reviews of Earth and Planetary Sciences, v.17, p.89-118.

Thomas D.W. & Coward M.P. (1996) Mezosoic regional tectonics and South Viking Graben formation : evidence for localised thin-skinned detachments during rift developments and inversion. Marine and Petroleum Geology, v.13, no.2, p.149-177.

Tilles D. (1961) Natural variations in isotopic abundances of silicon. Journal of Geophysical Research, v.66, no.9, p.3003-3013.

Turner C.C., Cohen J.M., Connell E.R. & Cooper D.M. (1987) A depositional model for the South Brae oilfield. In: Petroleum Geology of Northwest Europe (Brooks J. & Glennie K., Eds.), Graham and Trotman, p.853-864.

Turner C.C. & Allen Ph.J. (1991) The Central Brae Field, Block 16/7a, UK North Sea. In: United Kingdom Oil and Gas Fields, 25 Years Commemorative Volume (Abbotts I.L., Ed.), Geological Society Memoir, no.14, p.49-54.

Turner C.C. & Connell E.R. (1991) Stratigraphic relationships between Upper Jurassic submarine fan sequences in the Brae area, UK North Sea : the implications for reservoir distribution. In: Proceedings of the 23rd Annual Offshore Technology Conference, OTC 6508, Houston, Texas.

Vagle G.B., Hurst A. & Dypvik H. (1994) Origin of quartz cements in some sandstones from the Jurassic of the Inner Moray Firth (UK). Sedimentology, v.41, p.363-377.

Valley J.W. & Graham C.M. (1991) Ion microprobe analysis of oxygen isotope ratios in granulite facies magnetites : diffusive exchange as a guide to cooling history. Contributions to Mineralogy and Petrology, v.109, p.38-52.

Valley J.W. & Graham C.M. (1996) Ion microprobe analysis of oxygen isotope ratios in quartz from Skye granite : healed microcracks, fluid flow, and hydrothermal exchange. Contributions to Mineralogy and Petrology, v.124, p.225-234.

van der Plas L. & Tobi A.C. (1965) A chart for judging the reliability of point counting results. American Journal of Science, v.263, p.87-90.

Walderhaug O. (1990) A fluid inclusion study of quartz cemented sandstones from offshore Mid-Norway – possible evidence for continued quartz cementation during oil emplacement. Journal of Sedimentary Research, v.60, no.2, p.203-210.

Walderhaug O. (1994) Temperatures of quartz cementation in Jurassic sandstones from the Norwegian continental shelf - evidence from fluid inclusions. Journal of Sedimentary Research, v.A64, p.311-323.

Walderhaug O. (1996) Kinetic modelling of quartz cementation and porosity loss in deeply buried sandstone reservoirs. AAPG Bulletin, v.80, no.5, p.731-745.

Walderhaug O. (2000) Modelling quartz cementation and porosity in Middle Jurassic Brent Group sandstones of the Kvitebjørn Field, Northern North Sea. AAPG Bulletin, v.84, no.9, p.1325-1339.

Walderhaug O., Lander R.H., Bjørkum P.A., Oelkers E.H., Bjørlykke K. & Nadeau P.H. (2000) Modelling quartz cementation and porosity in reservoir sandstones : examples from the Norwegian continental shelf. In: Quartz cementation in sandstones (Worden R.H. & Morad S., Eds.), Spec. Publ. International Association of Sedimentologists, no.29, p.39-49.

Walther J.V. & Orville P.M. (1983) The extraction quench technique for determination of the thermodynamic porperties of solute complexes – application to quartz solubility in fluid mixtures. American Mineralogist, v.68, no.7-8, p.731-741.

Wangen M. (1998) Modelling porosity evolution and cementation of sandstones. Marine and Petroleum Geology, v.15, p.453-465.

Waples D.W. (1980) Time and temperature in petroleum formation – application of Lopatin's method to petroleum exploration. AAPG Bulletin, v.64, p.916-926.

Wilkinson M., Crowley S.F. & Marshall J.D. (1992) Model for the evolution of oxygen isotope ratios in the pore fluids of mudrocks during burial. Marine and Petroleum Geology, v.9, p.98-105.

Wilkinson J.J., Lonergan L., Fairs T. & Herrington R.J. (1998) Fluid inclusion constraints on conditions and timing of hydrocarbon migration and quartz cementation in Brent Group reservoir sandstones, Columba Terrace, northern North Sea. In: Dating and Duration of Fluid Flow and Fluid-Rock Interaction (Parnell J., Ed.), Geological Society of London Special Publication, no.144, p.69-89.

Williams L.B., Hervig R.L. & Bjørlykke K. (1997) New evidence for the origin of quartz cements in hydrocarbon reservoirs revealed by oxygen isotope microanalyses. Geochimica et Cosmochimica Acta, v.61, no.12, p.2529-2538.

Wilson M.D. & Stanton P.T. (1994) Diagenetic mechanisms of porosity and permeability reduction and enhancement. In: Reservoir Quality Assessment and Prediction in Clastic Rocks (Wilson M.D., Ed.), SEPM Short Course, no.30, p.59-119.

Wood J.R. & Hewett T.A. (1984) Reservoir diagenesis and convective fluid flow. In: Clastic Diagenesis (McDonald D.A. & Surdam R.C., Eds.), AAPG Memoir, no.37, p.99-111.

Worden R.H. (1996) Controls on halogen concentrations in sedimentary formation waters. Mineralogical Magazine, v.60, p.259-274.

Worden R.H., Oxtoby N.H. & Smalley P.C. (1998). Can oil emplacement prevent quartz cementation in sandstones? Petroleum Geoscience, v.4, p.129-137.

Worden R.H., Mayall M. & Evans I.J. (2000) The effect of ductile-lithic sand grains and quartz cement on porosity and permeability in Oligocene and Lower Miocene clastics, South China Sea: prediction of reservoir quality. AAPG Bulletin, v.84, no.3, p.345-359.

Worden R.H. & Morad S. (2000) Quartz cementation in oil field sandstones: a review of the key controversies. In: Quartz cementation in sandstones (Worden R.H. & Morad S., Eds.), Spec. Publ. International Association of Sedimentologists, no.29, p.1-20.

Zinkernagel U. (1978) Cathodoluminescence of quartz and its application to sandstone petrology. Contributions to Sedimentology 8, Amsterdam, Elsevier, 69p.

APPENDIX A

USE OF BACKSCATTER AND CATHODOLUMINESCENCE MODE SEM

A1 Introduction to SEM

The primary function of SEM (Scanning Electron Microscopy) is to facilitate examination of objects at high magnifications (x20 to x100 000). Since the first commercial SEM was produced in 1965, a whole range of additional techniques and applications have become available to complement standard high magnification microscopy. These include backscatter electron imaging and SEM-CL. The SEM type used in this study is a Philips XL Series 30CP.

The basic operation of the SEM is illustrated in Fig.A1. An electron gun produces a stream of electrons in a vacuum, across which an accelerating voltage is applied. Electromagnetic lenses in the column produce a small demagnified image of the electron source which is scanned or 'rastered' across the surface of the sample. The electrons in an SEM never form a real image of the sample. Instead, the SEM constructs a virtual image from the signals emitted by the sample. On striking the sample, two types of electrons are emitted : high energy backscattered electrons and low energy secondary electrons. Some of the secondary electrons may be completely absorbed at certain depths within the specimen. Cathodoluminenscence (CL) and X-rays will also be generated during electron scanning. To create an image, the electron beam scan is synchronized with that of a cathode ray tube (CRT) and a picture built of the scanned area. SEM operation can be carried out in three modes, each of which yields different types of information. The microscope is generally operated in emission mode (SE), in which secondary and backscattered electrons are collected, providing a high magnification image. The second mode of operation is backscattered mode (BSE) in which only the backscattered electrons are captured. Backscatter mode operation requires a backscattered electron

collector. The third mode is cathodoluminescence (CL). The SEM-CL device comprises a luminescence detector attached to the SEM. Visible CL light is emitted as a part of the process of bombarding the sample with electrons. Capturing the luminescence is achieved with a CL detector.

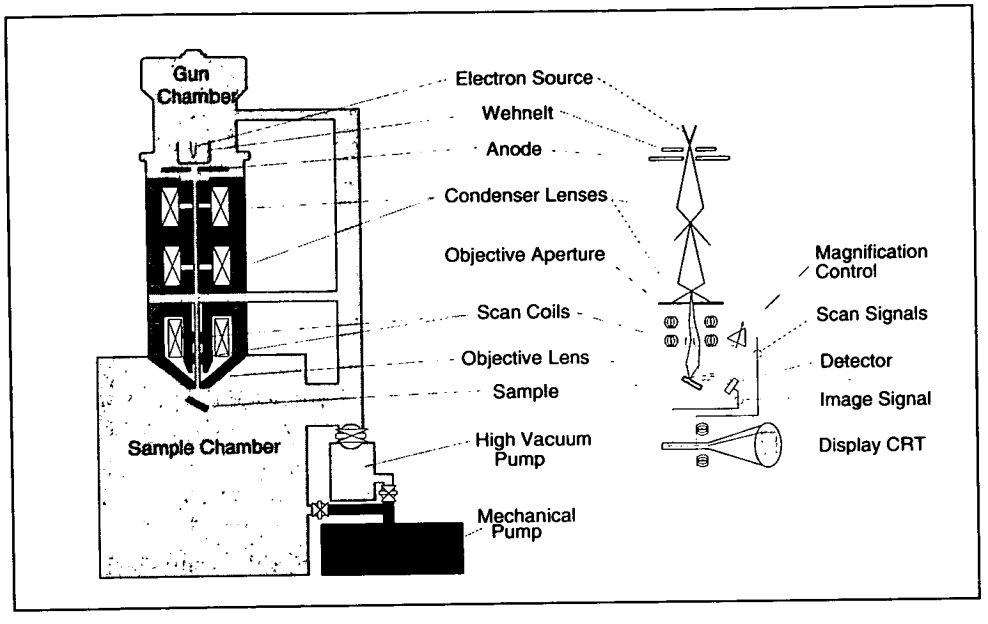

Fig.A1 The basic features of a scanning electron microscope (SEM). The electron column accelerates and focuses a beam of electrons onto the sample surface. Interactions between the sample and the beam electrons cause a variety of signal emissions. The signals are detected and reconstructed into a virtual image displayed on a CRT. (From : ElectroScan Corporation, 1996)

A2 Use of SEM backscatter for quantification of K-feldspar

Untwinned feldspars with no clear cleavage and unaffected by dissolution could be mistaken for quartz under an ordinary optical light microscope. Because the abundance of K-feldspar in the Brae Formation sandstone thin sections is important in terms of a potential silica source, it was important to quantify feldspar occurrence correctly. This was done by means of SEM backscatter in combination with an image analysis package called Optimas.

The efficiency of electron backscatter from the surface of a mineral depends on its mean atomic number. Mineral identification with BSE relies on the increase in efficiency of electron scattering as the atomic number of the mineral increases. Quartz, with a lower average atomic number than K-feldspar, will reflect electrons less efficiently and give a duller grey image (Fig.A2a). K-feldspar, with a higher average atomic number, will reflect electrons more efficiently than quartz and

produce a brighter image (Fig.A2a). Image analysis software packages such as Optimas can digitally highlight selected greylevels from an image in different colours (Fig.A2b). Subsequently, the number of pixels for each colour can be quantified and converted into percentages.

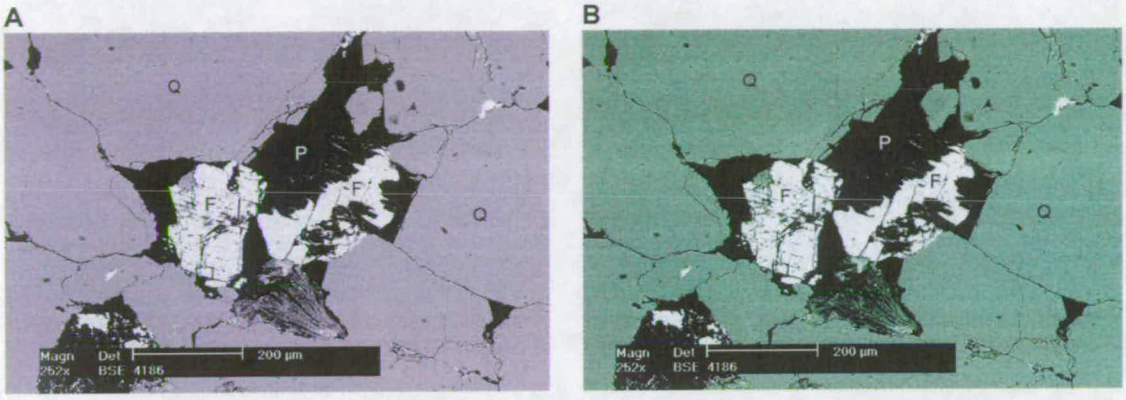

Fig.A2 Sequence of steps in image acquisition and processing to delimit K-feldspar. **(A)** BSE image of a thin section from the Miller Field (well 7b-26, depth 4186 m) where black = porespace (P), grey = quartz (Q) and light grey = K-feldspar (F). **(B)** With Optimas, the grey-levels in which quartz, K-feldspar and porespace occur are determined via a grey-level histogram and each grey-level groups is assigned a colour : green for quartz (Q), white for K-feldspar (F) and black for porespace (P). From this image, the percentage of K-feldspar can be readily quantified (8 %).

A3 Use of SEM-CL for quantification of authigenic quartz

Recognising and quantifying quartz cement using optical microscopy is often unreliable due to the difficulty in distinguishing between detrital and authigenic quartz (Evans et al., 1994). Previous work has shown the value of SEM-CL in differentiating between quartz cement and detrital grains in clastic reservoir rocks (e.g. Hogg et al., 1992; Evans et al., 1994). In this study, quartz cement abundance in the Brae Formation sandstone thin sections was determined by combined SEM-CL and an image analysis package called Scion.

Cathodoluminescence is the emission of light from crystals when excited by high-energy electrons. The colour and intensity of CL are governed by the presence of trace element impurities and defects in the crystal lattice, which may relate to the environment of mineral formation (Zinkernagel, 1978; Ramseyer et al., 1988). A problem with SEM-CL is that images are, in many cases, noisy and their interpretation is therefore difficult. Image problems include smearing owing to beam rastering and swamping of weak quartz luminescence by bright luminescence from adjacent minerals (e.g. calcite) (Evans et al., 1994). The latter of these problems

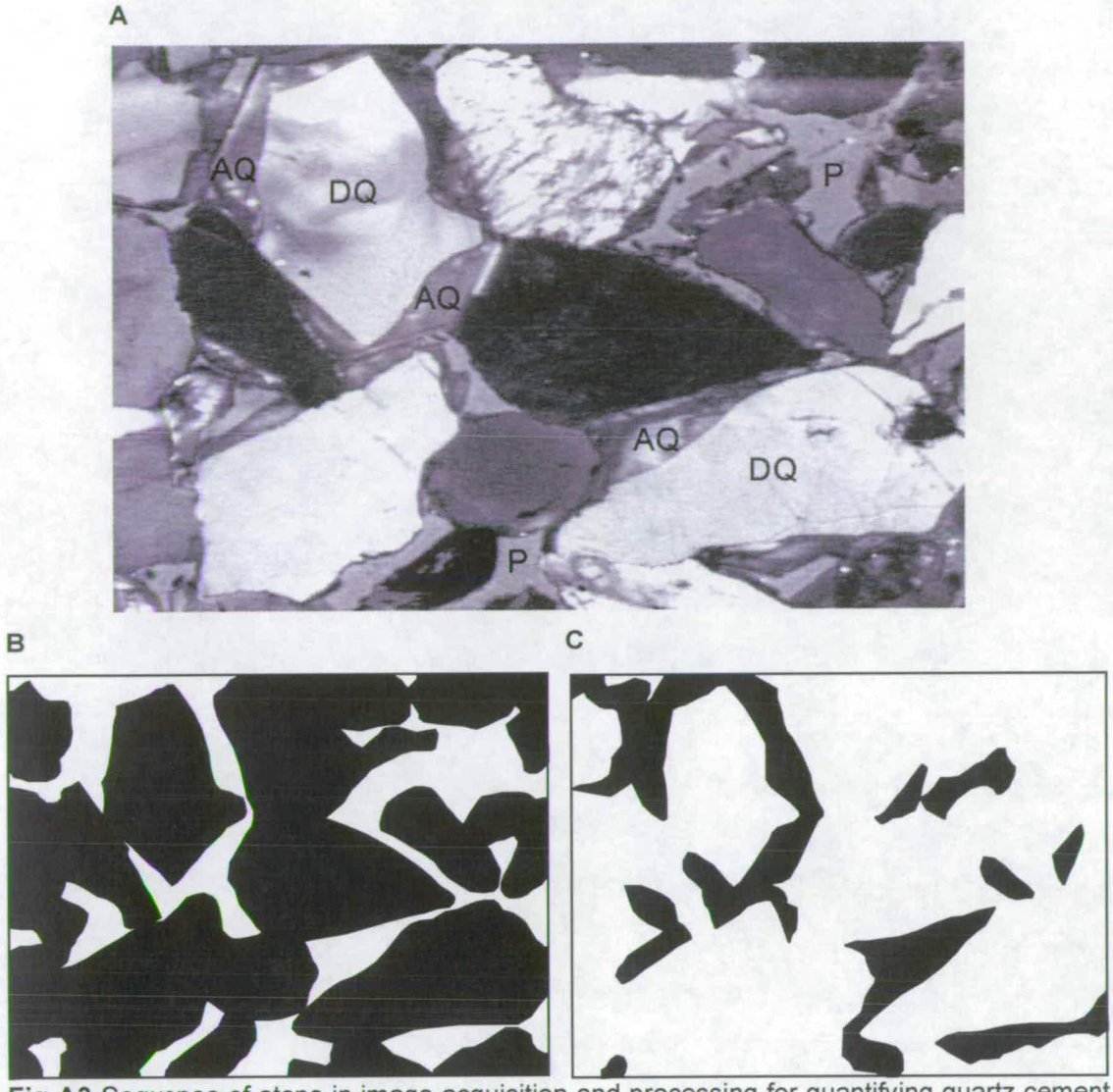

Fig.A3 Sequence of steps in image acquisition and processing for quantifying quartz cement in thin section.
(A) SEM-CL image of a thin section from the Miller Field (well 7b-A03, depth 4053 m). The field of view of the image is 950x680 µm. Detrital (DQ) and authigenic quartz (AQ) display different luminescence colours. P stands for porosity.
(B) Binary picture of the SEM-CL image in (A) showing detrital quartz in black and all other phases in white. The total amount of pixels (black + white) in this image is 8 932 650. The amount of black pixels is 6 592 296. The percentage of detrital quartz in this image is 73.8 %.
(C) Binary picture of the SEM-CL image in A showing authigenic quartz in black and all other phases in white. The total amount of pixels (black + white) in this image is 8 932 650. The amount of black pixels is 1 018 664. The percentage of detrital quartz in this image is 11.4 %.

was overcome in this study by avoiding areas in which calcite was present. This was not difficult considering the low abundance (<2 %) of authigenic calcite cement in the thin sections examined. The former problem, image smearing, was eliminated by combining the CL detector with a digital image analyser. This

analyser allows many images from the same field of view to be "averaged" during collection and consequently reduces noise in this way. For this study, 16 frames were averaged during acquisition, giving a total acquisition time of around 5 minutes per image.

Detrital quartz luminescence with SEM-CL may range from bright to dull grey to dark colours (Fig.A3a). Authigenic quartz has a characteristic dull grey colour (Fig.A3a). Because detrital quartz displays a wide range in grey level luminescence colours, it is not uncommon that some of those grey levels overlap with authigenic quartz grey level luminescence colours. Therefore, quantification of detrital and authigenic quartz with image analysis software directly from the collected images is impossible. The approach to solving this problem was to make hand-drawn pictures of each image. These pictures were subsequently scanned and digitised. With the image analysis package Scion, the pictures were made binary (Fig.A3b and c). Using Scion it was then possible to determine the amount of black and white pixels in each picture and to calculate the exact amount of detrital and authigenic quartz for each SEM-CL image.

A4 Results

In order to produce a reliable estimate of the percentage of K-feldspar and quartz cement present in a sample, several fields of view must be analyzed and the results averaged. The number of fields of view that must be analyzed to give a statistically meaningful result depend on the inhomogeneity of the sample and the image magnification used (Evans et al., 1994). For the quantification of quartz cement, it is easier to use images collected at higher magnifications because the CL-image resolution is better. Because the Brae Formation sandstones are fairly homogeneous on the thin section scale, collection of ten BSE and CL images, at magnifications of x100 and x250 respectively, were considered sufficient. The theoretical accuracy of the point-count results, for ~5% K-feldspar and ~10% quartz cement, is ±2% and ±2.5% respectively for 500 point counts (van der Plas and Tobi, 1965). Because the SEM imaging method applied in this study was adopted from Evans et al. (1994), it is believed that the results presented in this thesis yield a similar accuracy as reported by those authors (±1%). Hence, the percentages of K-feldspar and quartz cement determined by SEM imaging are considered more accurate than point-count results. A comparison of K-feldspar and quartz cement percentages obtained with SEM imaging and point-counting methods is presented in

Fig.A4. From Fig.A4a it is clear that K-feldspar abundance is mainly overestimated (in 83% of all analysed thin sections) by the traditional point-count method. Quartz cement abundance, on the other hand, is mainly underestimated (in 70% of all analysed thin sections) by point-counting (Fig.A4b).

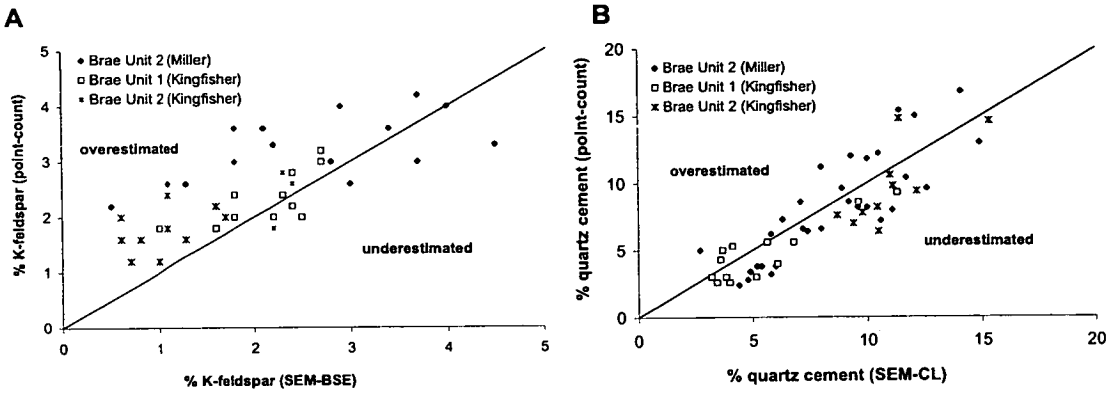

Fig.A4 Comparison of K-feldspar and quartz cement percentages obtained with SEM imaging and point-counting methods.
A K-feldspar abundance is in 83% of all analysed samples overestimated by the traditional point-count method.
B Quartz cement abundance is in 70% of all analysed samples underestimated by the traditional point-count method.

APPENDIX B

OXYGEN ISOTOPE ANALYSIS OF CALCITE CEMENTS

B1 Introduction

The Brae Formation reservoir sandstones in the Miller and Kingfisher Fields are locally cemented by calcite. The calcite cemented areas are up to 11 m thick and are interpreted to be concretions. Within these concretions practically all porosity is filled with carbonate cement (up to 40% whole rock) and permeability is insignificant. Therefore, the concretions are potential barriers to vertical fluid flow during hydrocarbon migration and production. Consequently, it is important to understand the processes controlling the formation of these concretions. Because the oxygen isotopic composition of diagenetic minerals can provide valuable information about the fluid type, temperature and depth at which mineral precipitation occurred, I carried out such analyses of the carbonate cement. This was done as part of a research project funded by the Flemish government (VIS 95-4) and conducted at the Katholieke Universiteit Leuven (Belgium). The oxygen isotope analyses were carried out by myself at the Scottish Universities Research and Reactor Centre (East-Kilbride) during a one month work stay in May 1997.

B2 Samples & methodology

Analysis was carried out on concretion samples from the Miller Field only. Three concretions were sampled in three different wells; 16/7b-24, 16/7b-28 and 16/8b-A10 (Table B1). Three to four samples (~50 mg) of carbonate cement were drilled out of the sandstone core with a dentist drill. The sample positions in the concretions are illustrated in Fig.B1.

Oxygen extractions for calcite were performed using the method outlined by McCrea (1950). Samples (~30 mg) were reacted with 5 ml phosphoric acid (100 %) for three hours in a water bath kept at a constant temperature of 25 °C. The evolved CO_2 gas was dried, purified and analysed on a VG SIRA 10 mass spectrometer. The oxygen isotope values are shown in δ notation as parts per thousand relative to SMOW (Standard Mean Ocean Water). A fractionation factor α of 1.01025 (Friedman & O'Neil, 1977) was used to correct the raw values for the $\delta^{18}O$ compositions of the samples :

$$\alpha = \{(^{18}O/^{16}O)_{CO2}\} / \{(^{18}O/^{16}O)_{Carbonate}\} \quad (eq.b1)$$

Replicate analyses of inter-laboratory standard MBL1 produced an average $\delta^{18}O_{SMOW}$ value of 28.7 ‰ with a precision of ±0.2 ‰.

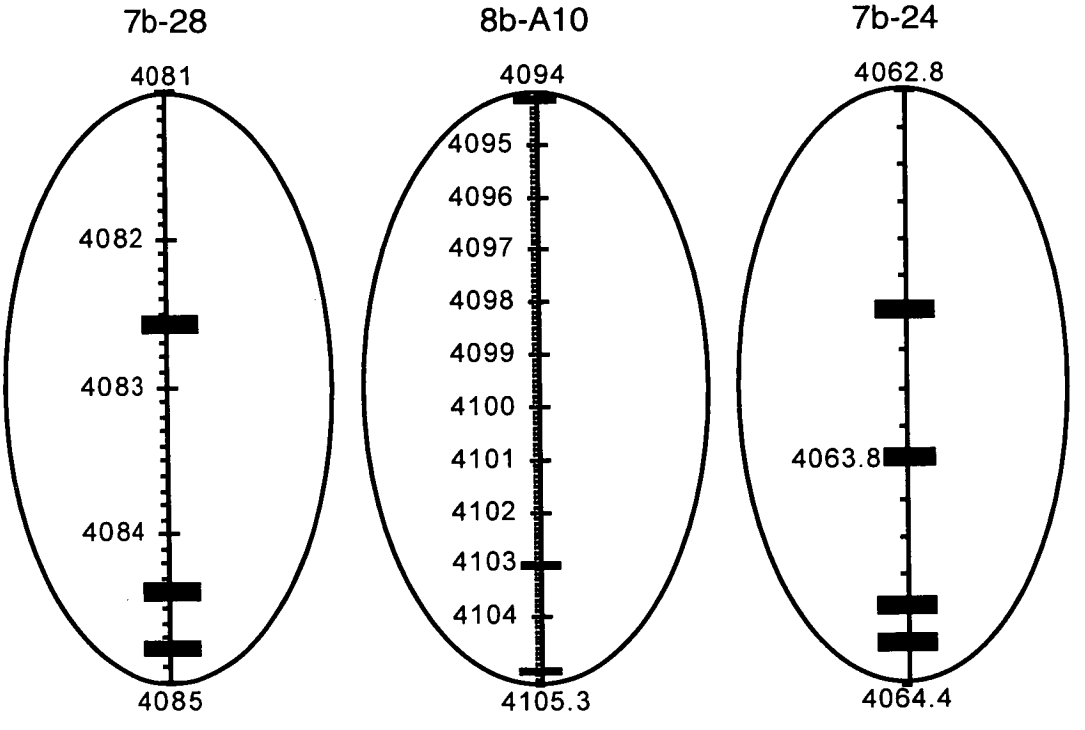

Fig.B1 Schematic overview of samples taken for oxygen isotope analysis from concretions in wells 7b-28, 8b-A10 and 7b-24 in the Miller Field. All numbers are depths expressed as meters. The black boxes represent sample positions.

B3 Oxygen isotope results & interpretation

The $\delta^{18}O$ values of the calcite cement in the concretions from wells 7b-28 and 8b-A10 range from +19.0 ‰ to +23.8 ‰ SMOW (Table B1). In these concretions, there is a trend of decreasing $\delta^{18}O$ from the centres to the margins (Table B1). Calcite cements in the concretion from well 7b-24 display overall lower $\delta^{18}O$ values (+15.4

to +16.9 ‰). The different isotopic signatures can originate from precipitation of the cements at different temperatures and/or from different pore-fluids. The measured $\delta^{18}O$ composition of the calcite can be used to calculate the calcite concretion formation temperature by using the equation of Friedman & O'Neil (1977) :

$$\delta^{18}O_{calcite} - \delta^{18}O_{water} = 2.78 \times 10^6 T^{-2} - 2.89 \quad (eq.b2)$$

where $\delta^{18}O_{calcite}$ is the measured oxygen isotope composition of the calcite cement (‰), $\delta^{18}O_{water}$ is the oxygen isotope composition of the porewater from which the calcite precipitated (‰) and T is the temperature (Kelvin). Various possible concretion formation temperatures were calculated assuming calcite precipitation from Upper Jurassic meteoric ($\delta^{18}O$ = -7.0 ‰; Hamilton et al., 1987) and marine ($\delta^{18}O$ = -1.2 ‰; Shackleton & Kennett, 1975) water. Results are presented in Table B1.

Table B1 Results of oxygen isotope analyses on calcite cements from concretions in the Miller Field. Calcite precipitation temperatures, assuming precipitation from meteoric and marine water, were calculated with the equation of Friedman & O'Neil (1977).

Well	Depth (m)	Calcite (%)	$\delta^{18}O_{SMOW}$ (‰)	Calculated T (°C) from Jurassic meteoric water	Calculated T (°C) from Jurassic marine water
7b-28	4082.6	39.0	23.8	15.5	44.4
	4084.4	37.2	23.0	19.0	49.1
	4084.8	24.2	20.9	28.4	62.5
	4084.8	24.2	19.9	33.5	68.8
8b-A10	4094.2	31.8	19.6	35.0	70.9
	4103.1	38.4	22.1	22.7	54.6
	4105.1	33.6	19.0	38.2	75.4
7b-24	4063.4	11.4	16.9	49.7	93.5
	4063.8	25.2	16.7	50.9	93.5
	4064.2	19.4	15.4	59.1	106.5
	4064.3	19.2	16.4	52.7	96.2

From the calculations (Table B1) it was clear that if the calcite was precipitated from meteoric water, the concretion formation temperatures range from 16 to 23 °C in the concretion centres up to 38-59 °C at the concretion margins (wells 7b-28 and 8b-A10). If those same concretions were precipitated from marine water, formation temperatures are higher (44 to 55 °C in the centres and 69 to 75 °C at the margins) (Table B1). The concretion in well 7b-24 appears to have precipitated at a slightly higher temperature than the other two concretions examined; between 50 and 60 °C if precipitated from meteoric water and between 94 and 107 °C if precipitated from marine water (Table B1). To estimate from which of these porewaters the calcite cement is more likely to have precipitated, I estimated the depth range over which the concretions grew. This was done by using the minus cement porosity (MCP)

volume pointcount values and the equation for calculating compaction curves of Baldwin & Butler (1985). This crude method, which was employed also by McLaughlin (1992) for estimating the depth of calcite cementation for concretions in the South Brae Field, provides by no means an exact answer but merely gives an indication which porewater $\delta^{18}O$ is more likely. The equation used is :

$$D = 3.7 \ln (0.49 / 1\text{-}S) \quad (eq.b3)$$

Where D is burial depth [km] and S is solidity defined as the volume of solid grains as a percent of total volume of sediment (Baldwin & Butler, 1985). Solidity can be calculated as substracting MCP from one hundred percent. The burial depths calculated for concretion formation are presented in Table B2.

Table B2 Burial depths calculated for concretion growth by using the minus cement porosity (MCP) pointcount values and the equation for calculating compaction curves of Baldwin & Butler (1985). Temperatures corresponding to the burial depths are calculated by assuming a temperature gradient of 30 °C/km.

Well	Depth (m)	MCP (%)	S (%)	Calculated Depth (m)	Calculated T (°C)
7b-28	4082.6	40.6	59.4	696	21
	4084.4	37.6	62.4	979	29
	4084.8	25.0	75.0	2490	75
	4084.8	25.0	75.0	2490	75
8b-A10	4094.2	33.6	66.4	1395	42
	4103.1	39.2	60.8	826	25
	4105.1	35.2	64.8	1224	37
7b-24	4063.4	27.0	73.0	2206	66
	4063.8	27.2	72.8	2177	65
	4064.2	21.4	78.6	3066	92
	4064.3	27.4	72.6	2150	65

Results indicate that calcite precipitated when the Brae Formation sandstones were buried from ~700 to ~3000 m (Table B2). By using the present day temperature gradient of 30 °C/km (see Chapter 4) in the Miller Field, it is possible to calculate also a corresponding temperature interval for concretion growth. In Table B2 it can be seen that calculated temperatures range from 21 to 75 °C for precipitation of the concretions in wells 7b-28 and 8b-A10, and between 65 and 92 °C for the concretion in well 7b-24. When comparing these estimated calcite precipitation temperatures with the temperatures presented in Table B1, it becomes obvious that the earliest formed calcite cement (concretion centres) is more likely to have precipitated from a meteoric-derived fluid. As the concretion grows (from the centre outward), the fluid from which the calcite precipitated becomes more evolved (^{18}O enriched) and some of the temperatures are more compatible with precipitation from a marine-type or

isotopically evolved fluid. The bulk of the data, however, indicate an early diagenetic origin for the concretions with calcite precipitation from a meteoric-type fluid, starting at burial depths around 700 m (~ 20 °C).

B4 Calcite cement in the Kingfisher Field

Calcite cement oxygen isotope analyses (paragraph B3), and also Zone quartz cement $\delta^{18}O$ compositions (Chapter 7) from samples in the Miller Field indicate the presence of meteoric water in the reservoir sandstones during shallow burial. Oxygen isotope compositions of Zone A quartz cements, which indicate precipitation of quartz from meteoric-type fluids, were also analysed from the Brae Unit 1 reservoir in the Kingfisher Field (Chapter 7). In the Brae Unit 2 reservoir in the Kingfisher Field, however, no Zone A quartz cements were encountered for analysis. In order to verify the presence of meteoric-type fluids during shallow burial in this reservoir, I decided to perform some oxygen isotope analyses on carbonate concretion samples. Three samples from different concretions in well 16/8a-4 were analysed at the Department of Geology and Geophysics (Edinburgh University) during the week of January 8th 2001. Results of these analyses are presented in Table B3. The $\delta^{18}O$ compositions of the calcite cement in the concretions centres (>30 % calcite cement) from well 8a-4 are ranging between +20.5 and +20.9 ‰ SMOW (Table B3). The sample from the concretion edge (4141.4) has a $\delta^{18}O$ composition of +16.5 ‰ SMOW (Table B3). These results are similar to oxygen isotope values measured in calcite cements from the Miller Field (Table B1). In analogy with analysis results from the Miller Field, it can be calculated from the fractionation equation of Friedman & O'Neil (1977) (eq.b2) and from minus cement porosity values that the calcite cements in the concretion centres precipitated from meteoric-type fluids at low temperatures (~28 to 35 °C) and shallow burial depths (~950 to 1200 m) (Table B4). As in the Miller Field, the sample from the concretion edge precipitated from a more evolved fluid at higher temperature (~100 °C) and deeper burial (~3600 m) (Table B4). These results indicate that the Brae Unit 2 reservoir in the Kingfisher Field was also open to surface water recharge during shallow burial.

Table B3 Results of oxygen isotope analyses on calcite cements from concretions in the Kingfisher Field. Calcite precipitation temperatures, assuming precipitation from meteoric and marine water, were calculated with the equation of Friedman & O'Neil (1977).

Well	Depth (m)	Calcite (%)	$\delta^{18}O_{SMOW}$ (‰)	Calculated T (°C) from Jurassic meteoric water	Calculated T (°C) from Jurassic marine water
8a-4	4022.1	32.4	20.6	29.0	62.6
			20.5	29.5	63.2
	4094.5	34.6	20.9	27.5	60.5
			20.8	28.0	61.2
	4141.4	11.2	16.5	51.6	94.4
			16.4	52.2	95.3

Table B4 Burial depths calculated for concretion growth by using the minus cement porosity (MCP) pointcount values and the equation for calculating compaction curves of Baldwin & Butler (1985). Temperatures corresponding to the burial depths are calculated by assuming a temperature gradient of 30 °C/km.

Well	Depth (m)	MCP (%)	S (%)	Calculated Depth (m)	Calculated T (°C)
8a-4	4022.1	34.2	65.8	1176	35
	4094.5	36.4	63.6	946	28
	4141.4	17.4	82.6	3677	110

APPENDIX C

Fluid Inclusion T_H AND SALINITY DATA

Table C1 All T_h and salinity data measured in aqueous fluid inclusions in quartz cements in Brae Formation sandstones in the Miller and Kingfisher Fields. Salinity data are converted from T_m values measured in the aqueous inclusions by using the conversion table from Bodnar (1992) (Table 8; Chapter 4). Salinity is expressed as weight % NaCl equivalent.
(*) Data from Hogg et al. (1993)
(**) Data from Dr. C.I. Macaulay
(***) Data from A. Marchand

Field	Well	Sample Depth (m)	T_h	Salinity
Miller	8b-A10	4080.1 (*)	98.4	11.62
			99.6	9.62
			102.7	11.01
			103.6	10.77
			105.5	9.62
			106.6	10.64
			108.4	10.64
			108.5	10.52
			108.7	10.77
			108.9	10.52
			108.9	10.52
			109.4	10.52
			109.4	10.52
			109.9	11.5
			110.3	10.26
			110.4	10.01
			110.8	10.64
			112.9	
			113.5	10.14
			114.1	10.64
			115.1	9.75
			117.1	9.75
			117.9	10.14
			119.2	8.96
			121.0	8.96
			121.1	8.69

Table C.1 Continued.

Field	Well	Sample Depth (m)	T_h	Salinity
Miller	8b-A10	4093.4 (*)	102.1	11.14
			102.2	10.39
			102.3	10.52
			106.6	10.77
			107.2	10.64
			107.4	10.77
			107.4	10.64
			109.9	9.75
			110.0	10.77
			110.2	11.26
			110.4	
			110.8	10.52
			111.5	10.52
			112.6	
			113.3	9.09
			114.7	10.77
			115.0	8.82
			115.6	10.89
			117.8	9.09
			117.8	10.64
			121.5	
			123.7	10.52
			126.3	8.96
			127.2	8.82
			127.4	9.62
			129.0	10.77
			131.8	8.69
Miller	8b-A11	4088.8 (*)	88.8	20.59
			94.9	10.52
			99.5	10.77
			99.8	10.77
			104.1	9.36
			104.8	
			105.2	9.09
			105.2	9.88
			106.7	6.73
			107.2	10.64
			107.4	6.73
			108.4	10.64
			108.5	9.62
			108.8	8.69
			109.0	7.87

Table C.1 Continued.

Field	Well	Sample Depth (m)	T_h	Salinity
Miller	*8b-A11*	*4088.8 (*)*	*109.0*	*9.23*
			109.4	7.73
			109.5	8.28
			110.1	7.59
			110.4	7.16
			110.8	8.01
			110.8	10.26
			110.9	9.09
			111.3	
			111.6	7.3
			111.9	8.96
			112.8	8.69
			113.5	8.01
			113.9	9.75
			114.0	9.09
			114.6	6.59
			115.2	7.87
			115.7	8.28
			116.0	8.28
			116.8	8.82
			117.9	8.55
			120.7	10.77
			121.7	7.3
Miller	8b-A11	4096.3 (*)	100.6	10.64
			106.4	11.14
			107.8	10.77
			108.9	11.01
			108.9	10.52
			109.5	11.01
			110.3	11.01
			110.5	10.64
			110.8	11.14
			111.7	7.73
			111.9	11.01
			113.6	7.87
			113.7	10.77
			113.9	10.77
			115.8	10.64
			115.9	10.89
			116.8	8.01
			117.1	9.88

Table C.1 Continued.

Field	Well	Sample Depth (m)	T_h	Salinity
Miller	*8b-A11*	*4096.3 (*)*	*118.2*	*10.52*
			118.6	7.87
			118.7	11.14
			120.8	11.14
			121.2	8.01
			121.3	7.73
			121.4	7.45
			122.0	8.82
			122.2	8.14
			128.1	8.28
Miller	8b-A11	4100.6 (*)	99.3	11.26
			101.4	11.38
			102.2	11.01
			102.2	9.49
			102.6	9.23
			103.2	12.33
			103.3	10.77
			103.6	10.77
			104.4	11.01
			106.7	8.42
			106.8	10.89
			107.1	10.26
			107.4	10.89
			107.7	8.55
			108.5	10.01
			108.6	11.74
			109.4	11.26
			109.9	9.49
			110.6	9.75
			111.1	7.87
			111.5	10.14
			111.8	8.82
			112.1	8.96
			113.8	8.01
			115.7	9.36
			118.8	9.09
			119.2	7.73
			123.7	8.82
			124.5	8.42
Miller	8b-A11	4141.8 (*)	84.6	22.02
			86.5	22.02

Table C.1 Continued.

Field	Well	Sample Depth (m)	T_h	Salinity
Miller	*8b-A11*	*4141.8 (*)*	*89.4*	*20.67*
			96.6	20.52
			98.0	21.05
			103.3	10.52
			106.7	10.64
			108.3	11.01
			109.7	10.01
			109.9	10.77
			111.2	10.52
			112.9	10.77
			113.6	10.26
			114.5	9.75
			115.7	10.64
			115.7	10.26
			115.9	11.38
			116.1	11.14
			116.2	10.77
			116.3	10.77
			116.8	10.64
			117.2	10.52
			117.8	10.14
			118.3	10.77
			118.8	10.01
			119.0	9.75
			119.5	10.77
			120.3	10.52
			121.1	10.89
			121.4	9.88
			122.3	9.88
			123.2	10.14
			123.5	11.01
			126.3	8.96
			128.3	7.87
			129.0	8.14
			130.3	10.64
Miller	7b-25	4062.1 (*)	95.2	8.01
			95.7	
			95.9	2.23
			104.6	12.67
			107.1	8.42
			107.5	

Table C.1 Continued.

Field	Well	Sample Depth (m)	T_h	Salinity
Miller	*7b-25*	*4062.1 (*)*	*109.5*	
			109.8	8.01
			113.9	7.59
Miller	7b-25	4063.9 (*)	91.7	10.64
			94	8.14
			96.3	7.73
			98.3	7.73
			102.1	8.14
			102.7	
			103.6	
			104.6	8.42
			106.6	8.28
			109.5	7.87
			111.5	
Miller	7b-25	4065.5 (*)	95.2	7.02
			98.5	9.36
			104.7	9.62
			107.4	7.02
			107.6	9.23
			111.3	7.59
Miller	7b-25	4067.5 (*)	99.9	
			99.9	
			103.7	8.82
Miller	7b-25	4068.7 (*)	102.1	6.73
			102.8	
			103.7	6.88
			104.7	
			106.1	6.15
			115.7	6.59
				10.77
Miller	7b-25	4084.4 (*)	99.4	9.62
			102	9.09
			104.2	8.69
			104.7	8.82
			104.9	9.75
			105	
			105.3	9.23
			106.6	
			107.1	9.09
			107.3	8.69
			110.9	10.26

Table C.1 Continued.

Field	Well	Sample Depth (m)	T_h	Salinity
Miller	*7b-25*	*4084.4 (*)*	*111.6*	*9.36*
			111.9	8.96
			114.7	9.75
			120.9	8.82
			131.7	8.42
Miller	8b-3	3993 (*)	84.5	6.88
			87.9	16.3
			91.2	
			108.5	
			109.4	3.85
			110.8	9.36
			112	6.73
			112.9	9.23
Miller	8b-3	3998.2 (*)	69	26.62
			79.2	
			91.2	
			92.3	
			108.5	
			109.4	3.85
			110.8	9.36
			112	6.73
			112.9	9.23
Miller	8b-3	4009.1 (*)	101.3	
			102	7.73
			102.3	9.75
			102.5	7.02
			104.1	
			105.8	
			109	7.59
			118.6	8.28
			118.9	8.42
			119.9	
			123.1	
			123.5	
			124	6.73
			125	10.26
			126.7	7.87
			127.3	7.02
Miller	8b-3	4012.7 (*)	104.6	9.09
			107.4	6.15

Table C.1 Continued.

Field	Well	Sample Depth (m)	T_h	Salinity
Miller	*8b-3*	*4012.7 (*)*	*108.5*	*5.25*
			108.7	6.73
			108.9	5.55
			108.9	7.59
			109.2	4.94
			109.8	4.94
			110.4	6.44
			111.4	5.85
			113.7	6.29
			118.9	7.02
Miller	8b-3	4021.3 (*)	105.4	7.87
			106.2	7.59
			106.6	7.16
			106.8	6.88
			108	8.14
			110.1	7.02
			110.8	7.73
			112.6	8.14
			113.1	
			115	3.85
			115.9	8.55
			117.7	8.42
			118.9	7.59
			119	7.16
			121.7	6.88
			125.4	8.42
				6.59
				3.69
Miller	7b-26	4101.3 (**)	97.5	9.3
			103.7	
			105.3	
			109.6	
			112	
			115.3	9.2
			115.5	
			116.6	
			117.7	10.9
			117.7	
			118	
			118.1	
			118.4	10.6

Table C.1 Continued.

Field	Well	Sample Depth (m)	T_h	Salinity
Miller	*7b-26*	*4101.3 (**)*	*118.5*	
			118.5	3.6
			118.6	4.5
			119.4	3.9
			120.7	
			137.1	3.4
			137.2	
			142	3.6
Miller	7b-26	4186.4 (**)	92.8	
			96.3	
			96.9	
			103.3	
			104.1	
			104.5	
			106.3	
			109.4	
			109.6	9
			111.3	
			111.4	
			113.3	
			114.3	
			114.4	
			116.1	9.5
			117.9	10.5
			117.9	
			119.4	
			119.6	9.2
Miller	7b-A03	4024.8 (***)	97.4	9.34
			97.7	9.60
			106.7	9.08
			107.8	
Miller	7b-A03	4036.4 (***)	98.5	
			104.3	
			105.2	
			106.1	
			106.2	4.80
			111.1	6.74
Miller	7b-A03	4057.2 (***)	104.9	
Miller	7b-A03	4064.2 (***)	97.0	9.60
			97.6	
			98.0	

Table C.1 Continued.

Field	Well	Sample Depth (m)	T_h	Salinity
Miller	*7b-A03*	*4064.2 (***)*	*98.5*	
			102.7	
			104.2	5.86
			105.2	5.56
			105.4	
			105.8	
			106.0	
			106.1	
			106.4	9.60
			108.0	
			108.6	
			108.8	
			108.9	9.21
			112.7	
			116.8	4.65
Miller	7b-A03	4068.9 (***)	96.5	
			97.3	
			97.8	
			98.7	
			101.1	
			101.4	
			101.7	0.71
			102.7	
			103.4	
			104.2	
			104.4	0.53
			104.6	
			104.9	
			108.4	
			109.7	
Kingfisher	8a-8	3887.3 (***)	77.5	25.21
			77.7	
			82.0	
			82.1	
			87.2	
			88.3	
			89.0	
			89.7	
			89.8	22.03
			90.4	
			91.1	19.21

Table C.1 Continued.

Field	Well	Sample Depth (m)	T_h	Salinity
Kingfisher	*8a-8*	*3887.3 (***)*	*92.4*	*2.90*
			95.5	
Kingfisher	8a-8	3904.2 (***)	*97.8*	
			97.9	8.68
			99.7	
			99.8	1.23
			100.0	
			103.1	8.81
			104.1	9.60
Kingfisher	8a-8	3915.5 (***)	83.2	
			89.5	
			94.5	
			99.5	6.45
			101.1	16.62
			101.4	
			135.2	
Kingfisher	8a-8	3955.1 (***)	74.1	
			76.7	
			92.8	
			94.4	
			95.0	
			96.5	0.53
			98.1	
			98.5	
			99.5	6.88
			100.7	
			103.2	
Kingfisher	8a-4	3989.7 (***)	94.0	
			103.4	
			106.5	
			109.7	
			112.3	
			120.0	
Kingfisher	8a-4	4015.1 (***)	88.2	1.57
			98.1	
			100.5	5.11
			102.0	
			104.0	
			106.5	0.88
			106.9	3.71
			109.7	

Table C.1 Continued.

Field	Well	Sample Depth (m)	T_h	Salinity
Kingfisher	*8a-4*	*4015.1 (***)*	*110.0*	*5.56*
			117.1	
Kingfisher	8a-4	4028.8 (***)	81.2	
			88.6	
			92.6	
			93.2	6.59
			93.7	
			97.0	
			98.1	
			100.2	
			102.8	12.51
			103.2	
			105.2	
			105.8	
			108.8	
			109.4	
			110.0	
			110.3	
			110.3	8.68
			111.0	
			111.5	
			111.7	
			111.8	
			112.8	
			118.3	
			132.3	
Kingfisher	8a-4	4033.7 (***)	74.1	
			89.4	
			91.9	
			101.6	
			102.7	
			104.7	
			107.5	
			107.7	
			108.8	
			116.3	
			117.1	
			118.3	
Kingfisher	8a-4	4081 (***)	95.6	
			96.4	
			103.8	

Table C.1 Continued.

Field	Well	Sample Depth (m)	T_h	Salinity
Kingfisher	*8a-4*	*4081 (***)*	*110.3*	
			120.0	
			132.1	
Kingfisher	8a-4	4126.1 (***)	67.4	
			91.0	
			93.1	
			98.5	1.05
			101.5	1.23
			101.7	
			102.4	3.39
			104.3	10.11
			108.5	6.59
			109.7	3.23
			111.0	12.73
			114.2	
			115.2	12.51
			116.1	7.59
			117.4	0.53
			121.1	
			123.7	
			131.7	

APPENDIX D

EXEMPLAR™ : A NUMERICAL MODEL FOR RESERVOIR QUALITY PREDICTION

D1 Introduction

Exemplar™ is a numerical model which uses mathematically simple algorithms for calculating compaction and quartz cementation in order to provide a general method suited to porosity prediction in quartzose and ductile grain-rich sandstones (Lander & Walderhaug, 1999). The diagenetic history of sandstones is modelled in the software from the time of deposition to the present. In the current software, reservoir quality prediction is aimed especially at quartz-rich sandstones (Lander & Walderhaug, 1999). This is because quartzose sandstones are a common sandstone reservoir type and because their porosity is typically controlled by two diagenetic processes : compaction and quartz cementation (Lander & Walderhaug, 1999). In this Appendix, I give an overview of the algorithms used in the software for modelling compaction and quartz cementation, and how the equations were derived. All information below is extracted from Walderhaug (1994 and 1996) and from Lander & Walderhaug (1999).

D2 The compaction algorithm

There is no known direct measure of the extent of compaction in sandstones (Wilson & Stanton, 1994). Therefore, intergranular volume (IGV) is used in Exemplar™ as an indirect measure of compaction. The compaction function incorporated in the software is :

$$IGV = IGV_f + (\phi_0 + m_0 - IGV_f).e^{-\beta.\sigma} \qquad (eq.d1)$$

where IGV is the sum of pore space, cements and matrix material [volume fraction], IGV_f is the stable packing configuration [volume fraction], ϕ_0 is the depositional porosity [volume fraction], m_0 is the initial proportion of matrix material [volume

fraction], β is the exponential rate of IGV decline with effective stress [MPa^{-1}], and σ is the maximum effective stress [MPa].

IGV is defined as the sum of intergranular porosity, cements and matrix material. Matrix material is included because matrix material generally has little or no compressive strength. It is also assumed that matrix material in grain-supported sandstones does not compact significantly, and that no cements occur at the time of deposition of the sand when the effective stress is zero. IGV, and also m_0, can be determined from standard point count data.

Values for ϕ_0 are taken from measurements of near-surface sandstone porosities or artificially mixed and packed sandstones published by Atkins & McBride (1992) and Beard & Weyl (1973) respectively. These depositional porosities are largely independent of sandstone composition, but are strongly controlled by texture.

IGV_f (stable packing configuration) and β (exponential rate of compaction with effective stress) are obtained through empirical calibration. IGV_f is calibrated for rigid grain-rich rocks by using 218 well to moderately sorted samples with less than 10% non-quartz cements. The samples are all from the Jurassic and Cretaceous Norwegian continental shelf. The samples show present day IGV values of 28.0±5.6% and show no significant variation with estimated maximum effective stress values over a range of from around 25 to 55 Mpa. This lack of variation suggests that all samples are at or near their minimum compacted IGV values. As a result, the values can be used to define the IGV_f term in the compaction function. The term β was constrained by using samples that have not achieved stable packing configurations. For the calibration of β for rigid grain-rich rocks, the data of McBride et al. (1990) for Texas Eocene sandstones were used. These sandstones have been exposed to maximum effective stresses ranging from about 10 to 50 Mpa. A value of 0.06 Mpa^{-1} for β provides a good correspondence between model predictions and measurements (Fig.D1).

The frame of reference for the compaction model is a 1 cm^3 volume defined by uncompacted sediment at the depositional interface. This reference frame is comparable in scale to thin sections and core plugs, the basic sources for evaluating and calibrating simulation results. Although the model conserves the volumes and densities of detrital materials, it does not attempt to maintain mass balance of pore fluids or cements. Through the course of a simulation, the net volume of pore fluid is typically reduced, whereas the net volume of solids increases. Because

sandstones exhibit negligible decompaction with unloading at the model scale of observation, compaction is not reversible in the model even in cases where effective stress decreases, such as after uplift and erosion. Compaction will also terminate when a specified amount of quartz cement has precipitated, strengthening the sandstone framework.

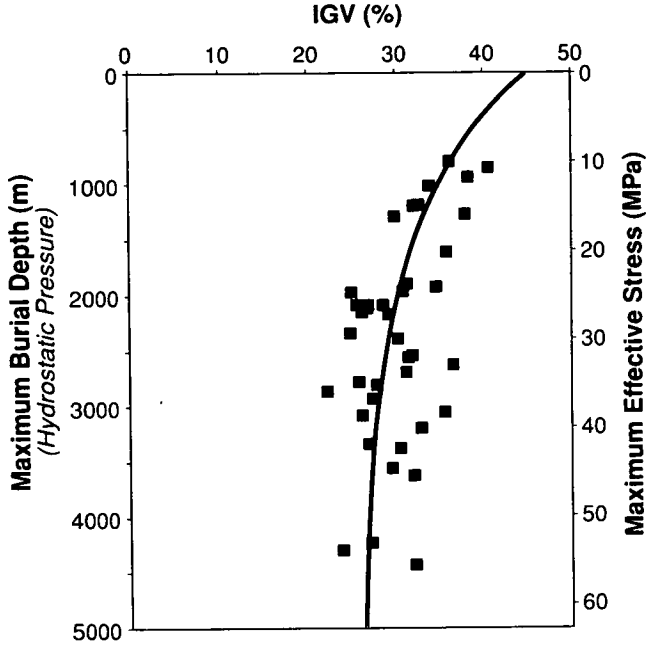

Fig.D1 Calibration of the Exemplar™ compaction model for well sorted to moderately sorted rigid grain-rich sandstones. The petrographic data are from McBride et al. (1990). IGV = intergranular volume. (From : Lander & Walderhaug, 1999)

D3 The quartz cementation algorithm

Exemplar™ incorporates a model of quartz cementation that assumes that 1) the quartz cement is derived from nearby stylolites; 2) of the three steps that control the quartz cementation process: silica dissolution, diffusion, and precipitation - silica precipitation is the rate-limiting or controlling step; 3) the surface area available for quartz cement precipitation is a function of the grainsize, fraction and extent of coating of quartz grains, as well as of the overall rock porosity.

In Exemplar™ software, quartz cement volumes are calculated as the sum of a series of integrals with small time steps :

$$m = \int_{t_o}^{t_1} A_1 r(t)\, dt + \int_{t_1}^{t_2} A_2 r(t)\, dt + \ldots + \int_{t_{n-1}}^{t_n} A_n r(t)\, dt \quad (eq.d2)$$

where m is moles of quartz cement precipitated per cm^3 sandstone, A is the surface area in cm^2 per cm^3 sandstone, t is the time in seconds (t_0 and t_n the time when

quartz cementation starts and terminates), and r is the rate of quartz cementation in moles/cm^2.s.

The surface area of quartz grains at the start of quartz precipitation is estimated as the cumulative surface area of spheres with a diameter equal to the grain size of the sandstone, and with a total volume equal to the fraction of detrital quartz in a unit volume of the sandstone. The number of quartz grains in a unit volume V of sandstone can be obtained from the equation :

$$\frac{N.\pi.D^3}{6} = V.f \quad (eq.d3)$$

where N is the number of quartz grains per unit volume of sandstone, D is the grain diameter [cm], and f is the fraction of unit volume composed of quartz grains. The total surface area A of quartz grains in a unit volume of rock is equal to the number of quartz grains times the surface area of each grain :

$$A = N.\pi.D^2 \quad (eq.d4)$$

or, combining eqs. d3 and d4 :

$$A = \frac{6.f.V}{D} \quad (eq.d5)$$

The reduction of surface area during cementation is taken into account by assuming that the decrease is linear and proportional to the concomitant porosity reduction caused by the precipitation of quartz cement. The mean surface area during quartz precipitation can therefore be expressed as :

$$A = \frac{6.f.V}{D} . ((\phi_0 + \phi) / 2\phi_0) \quad (eq.d6)$$

where ϕ_0 is the porosity at the onset of quartz cementation and ϕ is the present porosity. In sandstones which lack significant percentages of other late-diagenetic minerals ϕ_0 has been estimated as equal to the sum of present porosity and the fraction of quartz cement in the sample, on the assumption that porosity loss since the onset of quartz cementation is equal to the volume of quartz cement precipitated. By expressing ϕ_0 as the sum of present porosity and the fraction of quartz cement in a unit rock volume, eq.d6 can be written as :

$$A = \frac{6.f.V}{D} ((q + 2\phi) / 2(q + \phi)) \quad (eq.d7)$$

Quartz cementation rates in the software are expressed by a logarithmic function of temperature which was empirically derived using data from the Norwegian continental shelf (Fig.D2). This temperature dependence of quartz cementation rates can be expressed by Arrhenius law :

$$ln\ r = ln\ B - E_a/R.T \qquad (eq.d8)$$

where r is the quartz cementation rate [moles/cm^2.s], parameter B is the pre-exponential or frequency factor, E_a is the activation energy [J/mol], R is the gas constant [J/K.mol] and T is temperature [K]. Default reaction kinetics, derived using data from the Norwegian continental shelf, are E_a=58 J/mol and B=5x10^{-12}.

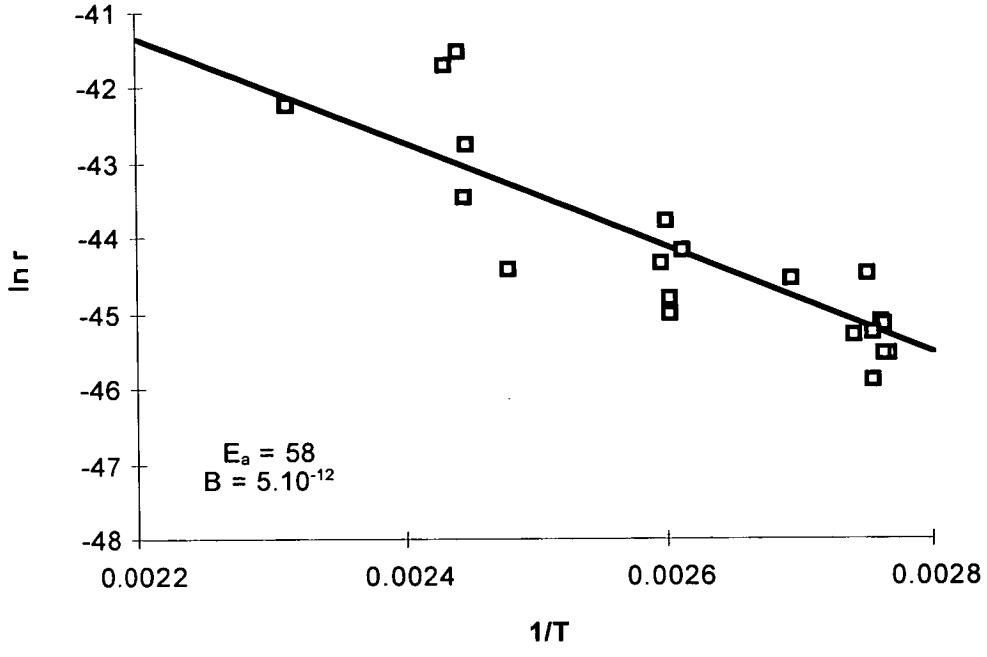

Fig.D2 Quartz precipitation rate r expressed as a function of temperature [K]. The data presented are from Jurassic sandstones of the Norwegian continental shelf (Walderhaug, 1994). This dataset was used to calibrate the kinetic parameters E_a and B for the Arrhenius equation in the Exemplar™ software. (After : Walderhaug, 1994)

Exemplar™ starts modelling from the time of deposition of the sand until the present day. The model steps forward through time by using time-step durations that are selected by the user. The calculations for a given time step are done in the following sequence : compaction, precipitation or dissolution of non-quartz cements, quartz surface area calculation, and quartz cement volume.

D4 Exemplar™ input data

Input data needed to conduct a simulation include texture and composition of the sandstone, burial history information and parameter values for the compaction and quartz cementation algorithms.

Sandstone texture and composition Sandstone texture and compositional data are derived from standard petrographic analyses as described in Chapter 3. All this information is entered into a master spreadsheet in the computer program. A copy of the data entered for the samples selected from the Miller and Kingfisher Fields is given in Table D1.

Table D1 Textural and compositional data of samples from the Brae Formation sandstones in the Miller and Kingfisher Fields used in Exemplar™ simulations. All data were derived from standard petrographic methods as described in Chapter 3.

		Sample info				Matrix		Detrital minerals				Authigenic minerals			
Field	Reservoir	Sample	Grain size	Trask	Porosity	Clay	Organics	Quartz	Feldspar	RF	Others	Calcite	Clay	Pyrite	Quartz
Miller	Brae II	4022.7	226	1.7	22.2	2.6	0.4	61.0	2.6	3.2	0.8	0.4	1.6	0.4	4.8
Miller	Brae II	4029.4	370	1.7	12.4	2.0	1.0	74.0	2.4	1.6	0.2		0.6		5.8
Miller	Brae II	4043.6	352	1.7	15.4	2.2	1.2	67.0	2.0	0.4	0.2	1.0	2.6	0.2	7.8
Miller	Brae II	4057.2	316	1.7	17.0	1.6	0.6	65.0	2.2	2.2	0.2	0.2	3.0		8.0
Miller	Brae II	4068.2	338	1.7	17.2	8.2		60.1	2.4	1.0	1.0		1.2		8.9
Miller	Brae II	4101.3	421	1.7	13.6	1.6	0.2	66.9	1.4	1.8	1.0		0.8	0.6	12.1
Miller	Brae II	4141.3	356	1.7	14.6	1.6	1.0	60.4	1.8	2.2	1.4		1.2	0.4	15.4
Miller	Brae II	4186.4	437	1.7	12.4	2.2	0.6	61.7	2.2	2.8	1.4		2.4	0.2	14.1
Miller	Brae II	4045.5	372	1.7	18.6	2.4	1.6	62.8	2.2	3.8	0.6	0.6	1.4	0.2	5.8
Miller	Brae II	4062.7	331	1.7	15.0	2.6	1.0	69.0	3.0	2.0	0.6		0.6	0.2	6.0
Miller	Brae II	4064.5	257	1.7	14.6	3.6	1.6	65.0	2.0	3.0	0.6	0.4	0.2	0.4	8.6
Miller	Brae II	4071.9	358	1.7	14.8	1.4	1.2	66.6	2.2	2.8	0.4		1.6		9.0
Miller	Brae II	4112.9	294	1.7	14.2	1.8	1.0	62.2	2.4	3.8	0.6		1.2	0.2	12.6
Miller	Brae II	3989.9	228	1.7	23.2	1.4	1.8	60.3	2.8	6.0	0.6		1.2		2.7
Miller	Brae II	3993.8	309	1.7	21.6	2.0	2.2	62.0	2.6	3.4	0.2		0.8	0.2	5.0
Miller	Brae II	3996.9	273	1.7	22.6	2.2	4.2	60.4	2.0	3.0	1.6		0.6	0.2	3.2
Miller	Brae II	4039.6	416	1.7	13.2	1.2	2.0	71.5	0.4	3.0	0.2	0.4	0.4	0.6	7.1
Miller	Brae II	4116.0	354	1.7	13.4	1.2	1.6	66.4	2.2	3.4	0.2	0.2	0.8		10.6
Miller	Brae II	4102.2	382	1.7	14.0	1.2	1.0	64.8	1.6	4.8			1.0	0.2	11.4
Miller	Brae II	4110.4	252	1.3	13.8	1.0	1.0	65.4	1.8	2.8	0.6	0.2	1.4	0.6	11.4
Kingfisher	Brae I	3887.5	268	1.7	25.4	5.0	0.8	55.0	2.1	2.6	3.4	1.0	0.6		4.1
Kingfisher	Brae I	3890.6	312	1.7	26.6	4.0	0.2	57.2	2.2	2.2	1.8	1.2	1.0	0.2	3.4
Kingfisher	Brae I	3894.6	291	1.7	26.2	2.6	0.2	58.0	2.3	2.0	1.8	2.2	1.2		3.5
Kingfisher	Brae I	3900.0	326	1.7	25.4	4.0	0.6	55.4	2.2	3.0	2.4	2.6	0.6	0.2	3.6
Kingfisher	Brae I	3904.2	301	1.7	22.8	6.2	1.6	49.0	2.0	5.0	2.8	4.2	1.0	0.2	5.2
Kingfisher	Brae I	3913.3	337	1.7	29.0	1.2	1.8	59.3	1.3	1.6	1.4	0.2	0.2	0.2	3.8
Kingfisher	Brae I	3929.5	308	1.7	20.6	5.0	1.6	58.9	1.8	2.6	0.8	1.6	0.0	1.0	6.1
Kingfisher	Brae I	3938.4	265	1.7	24.6	5.0	1.6	55.8	1.2	1.2	1.4	2.6	1.0		5.6
Kingfisher	Brae I	3947.2	194	1.7	18.0	7.2	0.2	57.8	2.2	3.0	2.4	1.2	2.0	0.2	5.8
Kingfisher	Brae I	3955.1	304	1.7	19.6	7.2	2.2	57.3	1.9	3.0	1.4	2.0	0.6	0.2	4.8
Kingfisher	Brae II	3989.7	312	1.7	17.0	3.2	4.0	58.8	0.8	2.6	1.8	0.4	0.8	0.2	10.4
Kingfisher	Brae II	4004.7	286	1.7	13.2	4.4	4.8	61.2	0.8	3.0	1.0	0.2	0.6	0.4	10.4
Kingfisher	Brae II	4019.0	325	1.7	13.0	5.4	7.0	58.7	0.7	1.2	0.6		0.6	0.6	12.2
Kingfisher	Brae II	4023.6	333	1.7	14.0	6.2	5.2	58.2	1.8	1.8	0.4	0.6	1.2	0.4	10.2
Kingfisher	Brae II	4028.8	337	1.7	16.2	6.2	2.6	59.8	1.1	1.8	0.6	0.2	0.8	0.2	10.5
Kingfisher	Brae II	4030.3	251	1.7	13.0	4.0	2.2	61.6	1.7	3.0	1.2	0.4	1.0	0.8	11.1
Kingfisher	Brae II	4033.7	308	1.7	13.6	7.8	1.6	62.1	1.3	1.6	0.4	1.4	0.2	0.6	9.4
Kingfisher	Brae II	4053.9	344	1.7	13.2	4.8	3.4	61.4	1.0	2.4	0.8	0.4	0.2	0.4	12.0
Kingfisher	Brae II	4081.0	348	1.7	14.0	6.2	2.6	58.6	1.6	3.2	1.4		0.4		12.0
Kingfisher	Brae II	4126.1	352	1.7	12.4	7.2	2.2	61.2	1.0	3.2	1.0	0.2	0.4	0.2	11.0

Burial history information Burial history information (depth-time-temperature) also needs to be entered in a spreadsheet in the software program. For the Brae Formation samples, the reconstructed burial and thermal histories discussed in Chapter 5 were used. In order to obtain as accurate as possible modelling results, a method was worked out to enter in the program a sample-specific burial and

temperature history. For this method, the burial history curves of the top of the Brae Unit 2 reservoirs in Miller and Kingfisher (Fig.39, Chapter 5), and also the top of the Brae Unit 1 reservoir in Kingfisher (Fig.39B), were divided into linear segments. For the start and end point of each segment, the burial depth, time and temperature are tabled (Table D2). By using simple regression, it was then possible to extrapolate burial depths and temperatures from these formation tops to the modelled sample depths. Burial and temperature histories entered in the program for all modelled samples are given in Table D3. Table D3 can be found on the PC-formatted disc enclosed in the pocket attached to the inside of the back cover.

Table D2 Burial and thermal history information of the formation tops from the Brae Unit 1 and Unit 2 reservoirs in the Miller and Kingfisher Fields (see Chapter 5). The unknown burial and thermal information of all samples studied needed in Exemplar™ for the simulations was extrapolated from the information tabled below.

Miller-Unit 2 reservoir			Kingfisher-Unit 1 reservoir			Kingfisher-Unit 2 reservoir		
Time (My)	T (°C)	Depth (m)	Time (My)	T (°C)	Depth (m)	Time (My)	T (°C)	Depth (m)
150	5	0	150	5	0	150	5	0
144	10	200	143	8	100	67	67	1950
68	70	1750	66	63	1850	58	73	2500
58	78	2350	58	70	2300	35	89	3000
40	102	3050	50	79	2500	23	100	3400
38	104	3150	37	87	2900	15	108	3530
5	114	3620	24	98	3400	5	109	3700
0	120	3990	5	106	3580	0	114	3986
			0	112	3850			

Algorithm parameters Values for depositional porosity ϕ_0, stable packing configuration IGV_f and exponential rate of compaction with effective stress β were designated by Exemplar™ to each sample according to the sample's mineralogical composition and texture. Finally, the program also offers the option to enter a value for the minimum temperature necessary for the onset of quartz precipitation. The lowest fluid inclusion homogenization temperature measured in quartz cements in Brae Formation sandstone samples is around 67 °C (Appendix C). In Chapter 4 it was concluded that quartz cementation actually starts at temperatures lower than the minimum measured T_h. This is because a certain amount of quartz cement needs to be precipitated first before inclusions can be surrounded and trapped by quartz (Chapter 4). For this reason, the minimum temperature for onset of quartz cementation in the Brae Formation sandstones was set at 60 °C in the software program.

D5 Exemplar™ output data

For this study, the output data selected to save in a data spreadsheet were predicted amounts of quartz cement (%) and porosity (%) for each time step (calculated every 1 My), and the quartz cement precipitation rate (moles/cm^2.s). All output data (Tables D4 to D7) needed for the construction of graphs in Chapter 6 can be found on the PC-formatted disc enclosed in the pocket attached to the inside of the back cover.